



BRNO UNIVERSITY OF TECHNOLOGY
VYSOKÉ UČENÍ TECHNICKÉ V BRNĚ

FACULTY OF MECHANICAL ENGINEERING
FAKULTA STROJNÍHO INŽENÝRSTVÍ

INSTITUTE OF MACHINE AND INDUSTRIAL DESIGN
ÚSTAV KONSTRUOVÁNÍ

**TRIBOLOGY OF THE WHEEL-RAIL
INTERFACE**
TRIBOLOGIE ROZHŘANÍ KOLO-KOLEJNICE

HABILITATION THESIS
HABILITAČNÍ PRÁCE

AUTHOR
AUTOR

Ing. Milan Omasta, Ph.D.

BRNO 2024

ABSTRACT

The tribology of the wheel-rail interface is essential for ensuring optimal traction, reducing wear and energy consumption, and improving the overall safety and efficiency of railway systems. This habilitation thesis examines critical aspects of the wheel-rail interface from a tribological perspective, addressing friction-related challenges caused by contamination in this open system, exploring friction control techniques such as wheel-rail sanding and top-of-rail lubrication, and discussing the challenges in the experimental simulation of the wheel-rail interface. The findings of this research are documented in nine papers published in scientific journals and a book.

KEYWORDS

wheel-rail interface, tribology, top-of-rail conditioning, lubrication, traction, adhesion

ABSTRAKT

Tribologie rozhraní kola a kolejnice je zásadní pro zajištění optimální trakce, snížení opotřebení a spotřeby energie a zlepšení celkové bezpečnosti a účinnosti kolejové dopravy. Tato habilitační práce zkoumá kritické aspekty rozhraní kola a kolejnice z tribologického hlediska, řeší problémy související s třením způsobené kontaminací v tomto otevřeném tribologickém systému, zkoumá techniky řízení tření, jako je pískování kol a kolejnic a mazání temene kolejnice, a diskutuje výzvy v experimentální simulaci rozhraní kola a kolejnice. Výsledky tohoto výzkumu jsou shrnuty v devíti článcích publikovaných ve vědeckých časopisech a knize.

KLÍČOVÁ SLOVA

rozhraní kolo-kolejnice, tribology, úprava temene kolejnice, mazání, trakce, adheze

ACKNOWLEDGEMENT

I would like to express my deepest gratitude to my advisors, Professor Martin Hartl and Professor Ivan Křupka, for their support and motivation to write this habilitation thesis.

I am also immensely grateful to the members of our Wheel-rail research group for their responsible and dedicated work.

Lastly, I must express my heartfelt appreciation to my family for their encouragement and understanding. Special thanks to my wife and my children for their patience and tolerance during the nights spent at work.

AUTHOR'S DECLARATION OF ORIGINALITY

I hereby declare that this habilitation thesis titled "TRIBOLOGY OF THE WHEEL-RAIL INTERFACE" and the work presented herein is entirely my own creation and original effort, except where clearly indicated and properly cited.

.....

Author's signature

1	INTRODUCTION	1
2	WHEEL-RAIL INTERFACE AS AN OPEN TRIBOLOGY SYSTEM	3
2.1	Introduction	3
2.2	Water in the wheel-rail contact	4
2.3	Leaf contamination	6
2.4	Humidity and oxidation	7
2.5	Research gaps	7
2.6	Author's contribution	8
2.6.1	Wheel-rail interface under extreme conditions [1]	9
2.6.2	Asperity-based model for prediction of traction in water-contaminated wheel-rail contact [62]	10
2.6.3	The low adhesion problem: The effect of environmental conditions on adhesion in rolling-sliding contact [63]	11
2.6.4	The performance of top-of-rail products under water contamination [64]	11
3	WHEEL-RAIL INTERFACE AND FRICTION MANAGEMENT	13
3.1	Introduction	13
3.2	Traction enhancement	14
3.3	Top-of-rail conditioning	14
3.4	Research gaps	15
3.5	Author's contribution	16
3.5.1	Influence of sanding parameters on adhesion recovery in contaminated wheel–rail contact [117]	17
3.5.2	Development of an adaptive top-of-rail friction modification system [118]	18
3.5.3	Case Study: the influence of oil-based friction modifier quantity on tram braking distance and noise [99]	19
4	EXPERIMENTAL FACILITY TO STUDY THE WHEEL-RAIL INTERFACE	20
4.1	Introduction	20
4.2	Lab-scale experimental facility	20
4.3	Field-test facility	21
4.4	Research gaps	21
4.5	Author's contribution	22
4.5.1	Design and development of a twin disc test rig for the study of squeal noise from the wheel – rail interface [147]	23
4.5.2	An approach for the creep-curve assessment using a new rail tribometer [148]	24
5	CONCLUSIONS AND FUTURE WORK	26
6	REFERENCES	28
7	LIST OF FIGURES AND GRAPHS	40

1

INTRODUCTION

Rail transport holds a key role in the global transportation infrastructure, offering a highly efficient, reliable, and sustainable mode of moving both goods and passengers over various distances. Its significance lies in its capacity to facilitate mass transit, thereby reducing congestion on roads, lowering greenhouse gas emissions, and contributing significantly to environmental sustainability. Railways' energy efficiency and lower carbon footprint, compared to road and air transport, align well with global efforts to combat climate change. Moreover, rail networks serve as a crucial mode of transportation for trade and the development of the global economy, connecting ports, industrial hubs, and urban centres across countries and continents.

The wheel-rail interface is essential for the safety and operational performance of rail transport. The contact between the steel wheel and steel rail occurs on a small area of approximately 1 - 2 cm² and this contact zone is responsible for the transfer of nearly all the forces between the train and the track. It affects everything from how much energy the train needs to move, to how quickly it can stop, to how comfortable the ride feels. Keeping this interface in good shape helps prevent accidents, reduces wear on the track and wheels, and makes train travel more reliable and less noisy.

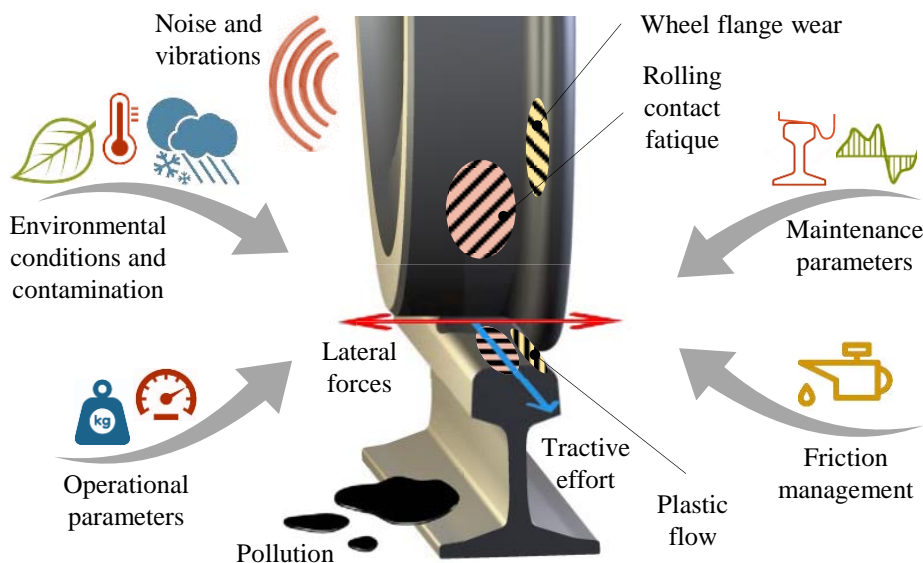


Fig. 1 Issues related to the wheel-rail interface [1]

The wheel-rail interface is a very complex tribological system, as shown in Fig. 1 [1]. An extensive array of factors gives its functionality. These factors mainly include operational conditions such as speed and the vertical load exerted by the wheels, together with the dynamic interactions between the rail vehicle and the track [2, 3]. Maintenance considerations, covering the profiles of both the wheel and rail head, their surface roughness, and the materials, play a significant role as well [4].

The tribological interactions within this interface determine its behaviour. The most important aspect is the ability to transfer traction and braking forces in the longitudinal direction and lateral forces in the perpendicular direction. The high contact pressures and shear stresses experienced at this interface cause a variety of wear and damage mechanisms. Notably, the rail head and wheel tread are susceptible to rolling contact fatigue [5, 6], the wheel flange to pronounced sliding wear [7, 8], and the materials of both wheel and rail to cyclic plastic deformation [9, 10]. This interface is also the source of most of the negative effects of rail transport such as rolling and squealing noise [11, 12] and ground-borne vibration.

WHEEL-RAIL INTERFACE AS AN OPEN TRIBOLOGY SYSTEM

2.1 Introduction

The wheel-rail interface represents an open tribological system, contrasted with the stable and well-defined conditions of closed systems like gearboxes. The wheel-rail contact is affected by several environmental factors, notably weather conditions such as temperature, humidity, and precipitation [13]. These variables constantly change with the day-to-night cycle, seasonal changes, and as trains move through different environments.

Fig. 2 classifies the various substances and materials found at the wheel-rail interface into several groups [1]. The first consists of substances naturally produced by tribological processes, including wear particles from both the wheel and rail, and iron oxides and hydroxides resulting from chemical reactions with water and oxygen. The second group encompasses external contaminants, with a particular focus on natural environmental sources like water, snow, and fallen leaves. Water can enter the contact area through different means such as rainfall, condensation, snowmelt, and flooding. Fallen leaves, particularly prevalent along tracks with nearby vegetation, are a primary cause of reduced adhesion during autumn [14–17]. The environment also contributes to contaminants like soil and sand, often wind-transported in dry and desert regions [18], and rock salt or grit applied for winter weather road and platform treatment [19]. Artificial contaminants mainly originate from the rail vehicles themselves, with operational fluids like grease, fuel, and transformer oils posing significant risks to traction and braking. Additionally, other train components, such as brake pads and discs, generate contamination particles [20]. The sand in this category is used by rolling stock to enhance wheel-rail adhesion. Rail infrastructure contributes to contamination through dust from ballast and concrete sleepers, wear particles from overhead wires, and lubricants from wayside lubri-

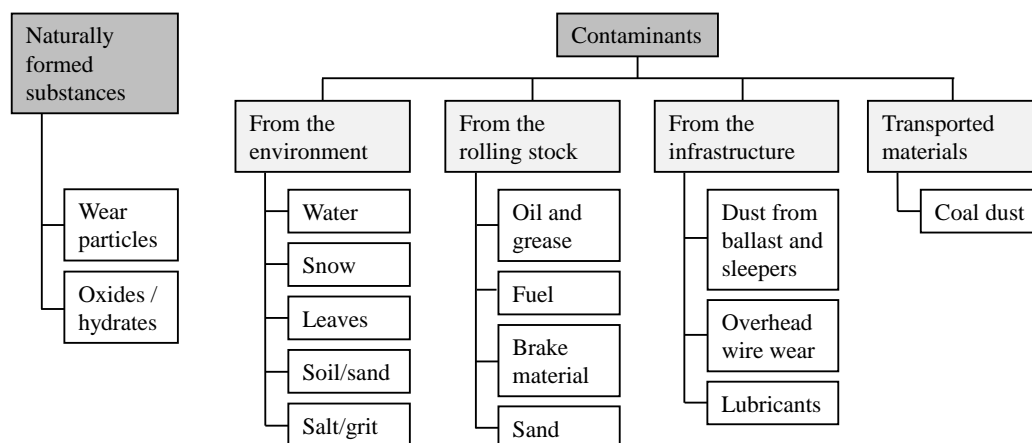


Fig. 2 Classification of various wheel-rail interface contaminants [1]

cators. An example of transported-material contamination includes coal dust from uncovered coal-carrying trains [21]. Identifying and understanding the various contamination sources and their impacts remains a major challenge in wheel-rail interface research.

The most adverse effect of the contamination is a critical decrease in the coefficient of adhesion (CoA) in the wheel-rail contact. The minimum required coefficient of adhesion for braking typically falls between 0.07 and 0.15, varying by railroad. For traction purposes, this value is approximately 0.2. A lack of sufficient adhesion often leads to delays, platform overruns, and incidents such as Signals Passed at Danger (SPADs) [22, 23]. In severe cases, insufficient adhesion can cause wheel burns during acceleration and the development of wheel flats due to abrupt braking. Poor friction conditions are often termed "the wet-rail" phenomenon [24]. This phenomenon was first systematically studied by Beagley [25, 26] who showed that a small amount of water and oxide debris significantly reduces coefficient of friction (CoF), as summarized in Fig. 3. The authors hypothesized that the decrease of COF is caused by the presence of a non-Newtonian viscous paste (wear debris mixed with small quantities of water), which completely separates the contact surfaces. Similar results were subsequently observed on the train track contaminated by an artificially created silica paste [26]. Moreover, the latest studies [27–29] have shown that the decline in COF can be even more dramatic than was found by Beagley.

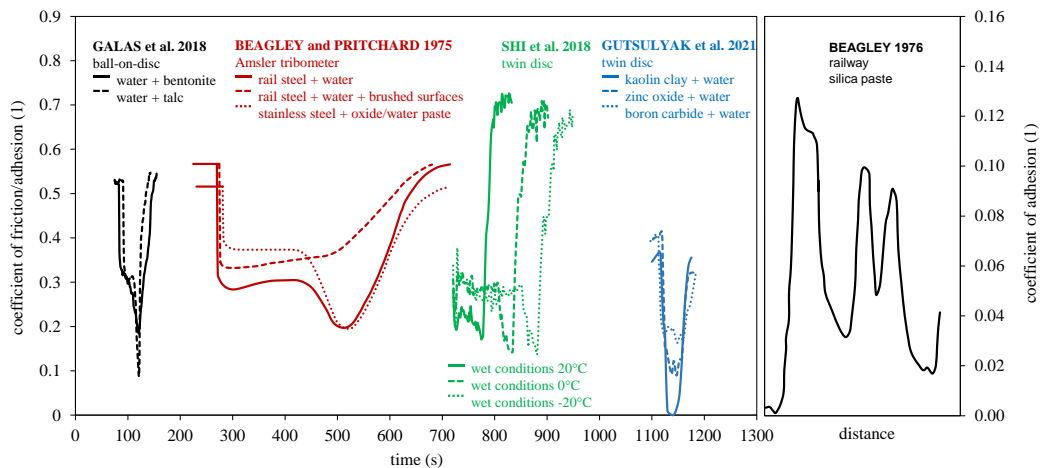


Fig. 3 Summary of experimental reports of sudden friction drop in concentrated contacts contaminated with liquid-solid suspension [25–29].

On the other hand, the openness of the wheel-rail tribology system allows substances generated at the interface or applied to the contact area to disperse into the environment. The artificially applied substances include lubricants for wheel-flange lubrication, top-of-rail friction modifiers and traction enhancers. Those products are gradually dispersed into the environment. This type of lubrication is referred to as “total loss lubrication” – “total loss” from a lubrication system perspective, but not from nature's point of view!

2.2 Water in the wheel-rail contact

The most important natural contaminant affecting the wheel-rail interface is water, occurring typically due to rainfall or morning dew. In extreme scenarios, such as heavy rainstorms, particularly in areas prone to poor drainage, railway lines can experience flooding, posing a significant risk even to underground rail systems [30]. Water's presence significantly impacts the adhesion between the rails and the wheels, influencing the train's operational safety and efficiency [25, 31].

The impact of water on adhesion at the contact point relates to the lubrication regime under which the interface operates. These regimes are depicted in Stribeck's curve (see Fig. 4), which qualitatively illustrates the relationship between the COF and the lubricant film thickness as functions of a dimensionless parameter that includes velocity, lubricant viscosity, and load. The degree of surface separation defines the specific lubrication regime. In the boundary lubrication regime, the surfaces are primarily separated by a thin layer of material, which naturally forms in open environments like rail tracks. As velocity increases and a sufficient quantity of water or another fluid lubricant is introduced to the interface, hydrodynamic forces begin to separate the surfaces. In the mixed lubrication regime, this separation occurs locally, while other areas of contact, maintained by surface asperities, continue to operate within the boundary lubrication regime. With further increases in velocity, the hydrodynamic forces lead to a complete separation of the surfaces by a full fluid film, known as the fluid-film lubrication regime. The effect of water at the contact interface, therefore, depends on the prevailing lubrication regime.

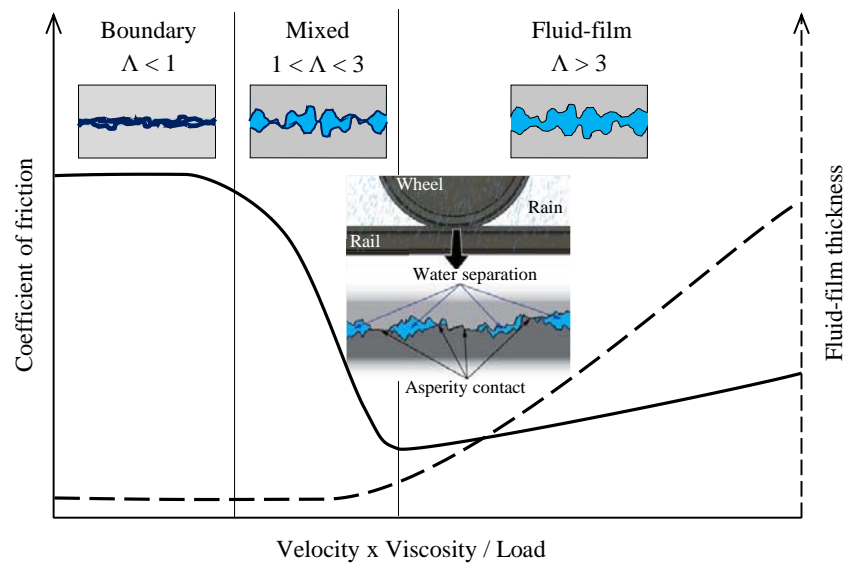


Fig. 4 Stribeck curve describing various lubricating regimes in water-contaminated contact [1]

In the boundary regime, water mainly forms the so-called 3rd body layer with other contaminants [32, 33]. The 3rd body concept, introduced by Godet in 1984 [34] is frequently applied in wheel-rail tribology to explain the behavior of a layer formed between the wheel and rail, focusing on its rheological properties [35–38]. This layer arises from the mechanical, chemical, and thermal interactions between the contacting surfaces and various contaminants under the conditions of high-pressure rolling-sliding contact. In addition to water and wear particles, natural contaminants such as leaves also play a significant role in the formation of this layer.

In the fluid-film regime, the thickness of water films can be approximated through the application of Elastohydrodynamic Lubrication (EHL) theory. Over recent decades, a comprehensive array of film thickness formulas and factors has been developed to accommodate a variety of operational regimes and conditions [39]. Typically, these formulas are derived from least-squares fitting of outcomes obtained from numerical analyses under specific conditions. Initially, these formulas were designed and tested for scenarios involving oil-lubricated contacts, where the oil's viscosity significantly changes with pressure. However, water's piezo viscosity, i.e. its change in viscosity under pressure, is not as strong. Thus, one approach involves adopting the isoviscous-elastic lubrication regime. This regime is defined by the significant impact of the contacting bodies' elastic deformation on the lubricant film formation, without causing a notable increase in the lubricant's viscosity due to the

pressure in the contact zone. The widely used equation by Esfahanian [40] can be applied, as shown in Tab. 1, with non-dimensional parameters provided as follows: $H_{min} = \frac{h_{min}}{R_x}$; $U = \frac{\eta_0 v}{ER_x}$; $W = \frac{F}{ER_x^2}$ for point contact and $W = \frac{F_l}{ER_x}$ for elliptical contact; $G = \alpha E$; $k = 1.03 \left(\frac{R_y}{R_x}\right)^{0.64}$. Considering water as a piezo-viscous fluid offers an alternative approach. To incorporate the piezo viscosity of fluids into film thickness calculations, the pressure-viscosity coefficient α is used. However, a straightforward application of this coefficient is inappropriate for water due to its unique behaviour under varying conditions. The study summarizes equivalent values for the pressure-viscosity coefficient of water as a function of contact pressure and temperature. Then, the lubricant film thickness in the piezo-viscous elastic regime for elliptical contacts can be calculated using the formula outlined by Hamrock and Dowson [41], Chen et al. [42] or a recently published model expanded into three-dimensional simulations by Wu et al. [43]. The predicted film thickness represents the potential film that could form under ideal lubrication conditions.

Tab. 1 Empirical equations for the lubricant-film thickness prediction

Author	Regime and contact	Lubricant-film thickness equation
Esfahanian [40]	Iso-viscous elastic, elliptical	$H_{min} = 8.70U^{0.66}W^{-0.21}(1 - 0.85e^{-31k})$
Hamrock and Dowson [41]	Piezo-viscous elastic, elliptical	$H_{min} = 3.63U^{0.67}W^{-0.073}G^{0.49}(1 - e^{-68k})$
Chen, et al. [42]	Piezo-viscous elastic, line	$H_{min} = 2.578U^{0.59}W^{-0.211}G^{0.002}$
Wu, et al. [43]	Piezo-viscous elastic, elliptical	$H_{min} = 9.36U^{0.72}W^{-0.29}G^{0.007}(1 - e^{-68k})$

The effect of water in the fluid-film regime is strongly affected by train speed, surface roughness and even water temperature. Extensive studies were made towards the water-film separation and wheel-rail adhesion prediction for high-speed trains [40, 42–45].

2.3 Leaf contamination

Leaf contamination in the wheel-rail interface presents a significant challenge for rail operations, particularly during the autumn months when falling leaves accumulate on the tracks. This problem has complex effects on train safety, efficiency, and time scheduling, especially in Great Britain and northern Europe [16, 17, 44]. When leaves fall onto the railway tracks and are run over by passing trains, they are crushed and compressed into a compact, sticky layer. This layer adheres to the rails and the wheels of the trains, having a huge impact on the behaviour of the resulting 3rd body layer [14]. Research into the leaf-contaminated wheel-rail interface focuses on understanding, mitigating, and solving the problems associated with the leaf layer on railway tracks, which significantly affect traction and safety. The scope of this research covers testing methodologies [16, 45], description of leaf layer-formation mechanisms [17, 44, 46, 47], modelling [37, 38, 48], mitigation strategies [49, 50] and field tests [51, 52].

Many incidents of low adhesion in real operation are not solely due to leaf contamination. The problem intensifies when the leaves are wet, either from rain or morning dew, which further enhances

their adhesiveness and creates a slippery, greasy film on the rail tracks [24]. Particularly the effect of humidity on friction properties of the leaf-contaminated layer, has to be addressed accordingly.

2.4 Humidity and oxidation

Water influences the wheel-rail interface even in the form of humid air. One of the mechanisms relates to surface oxidation. The interplay between humid air, temperature, and surface oxidation is complex, making it challenging to distinguish the individual factors clearly. Iron oxides emerge as the principal natural contaminants within the wheel-rail interface, encompassing a variety of chemical compounds differentiated by their content of Fe cations, oxygen, hydroxyl groups, and water [53–55]. In-situ analysis has identified five predominant types of oxides on rail heads: magnetite (Fe_3O_4), hematite (Fe_2O_3), goethite ($\alpha\text{-FeOOH}$), lepidocrocite ($\gamma\text{-FeOOH}$), and akaganeite ($\beta\text{-FeOOHCl}$) [56]. Each oxide type influences wheel-rail adhesion differently, though typically, multiple oxides are present and act concurrently [55]. For instance, magnetite, known as "black oxide", tends to reduce friction, whereas hematite tends to increase it. It is posited that high humidity levels can hinder normal atmospheric oxidation due to the presence of water molecules in the air, leading to the formation of a protective layer [57]. When surfaces are encrusted and covered with a thick layer of hydrates, or rust, friction levels tend to remain constant, regardless of whether liquid water is present [58].

The daily variations in relative humidity and temperature significantly affect the coefficient of adhesion. Studies have shown that adhesion coefficients can drop from 0.55 to 0.22 as relative humidity increases, whereas temperature changes have a comparatively minor effect [25]. These observations have been validated by pin-on-disc experiments, further underscoring the predominant influence of humidity over temperature on adhesion [45, 54, 58]. Significant efforts have been made to better understand low adhesion issues in wheel/rail contact areas, leading to the development of more accurate prediction models and effective mitigation strategies. Nevertheless, field validation of the trends is still challenging due to a broad spectrum of contaminants and conditions that contribute to various low-adhesion mechanisms [59]

2.5 Research gaps

Although a lot of work was done in the area of the wheel-rail interface as an open tribology system. However, the following research questions were not addressed correspondingly.

- i. Climate changes and the increasing intensity and occurrence of extreme weather events raise critical questions about the key factors impacting the wheel-rail interface. There is a need for a comprehensive overview of these influential elements and their effects on the behaviour of the wheel-rail interface, with a particular focus on adhesion.
- ii. Water contamination can be viewed from the perspective of the wheel-rail contact separation due to the hydrodynamic action of water. Several studies dealt with the problem of water contamination and model prediction were published [42, 60, 61] taking into account empirical prediction of water-film separation. However, there is still a missing experimental validation of the prediction under pure water lubrication.
- iii. It is evident that the low-adhesion problem is activated by water [55, 60]. Particularly, the effect of air humidity, possible condensation and interaction with other contaminants under rolling-sliding conditions was studied only to a limited extent. Particularly, the question of

how the combination of leaf contamination, temperature, humidity and related risk of water condensation influences wheel-rail adhesion needs to be addressed.

- iv. Water interacts with other contaminants and lubricants. One of the important questions is what is the effect of water contamination when top-of-rail conditioning using top-of-rail lubricants is used. Particularly critical is the assessment of the potential risk of very low adhesion in the wheel-rail contact.

2.6 Author’s contribution

In the last 5 years, the author has focused on the problems of various influences affecting friction in the wheel-rail contact.

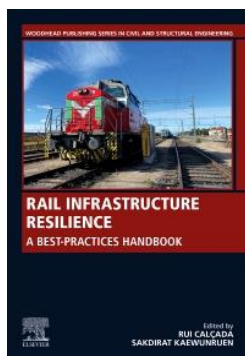
The first study **i.** includes a summary of research activities made under the *RISEN - Rail Infrastructure Systems Engineering Network* Horizon 2020 project aimed to improve rail infrastructure systems resilience towards future demand, extreme events, and climate change. The author’s contribution is in a comprehensive assessment of external factors influencing wheel-rail interface concerning extreme weather events.

The second work **ii.** deals with the problem of water contamination and model prediction. Thanks to the advanced experimental and measurement methods used, this work overcomes difficulties in the measurement of film thickness of pure water in EHL contact. The approach used allowed to validation of lubricant film thickness prediction and its validity for water to be considered as iso-viscous liquid.

The third work **iii.** is focused on the so-called “low-adhesion problem” caused by a complex action of air humidity, temperature and leaf contamination. This lab-scale work, led by the author, provides systematic insights into the effects under rolling-sliding conditions. Previous works under lab-controlled conditions were made mostly under pure-sliding conditions, which affects the results [45, 54, 58]. An important contribution is the establishment of adhesion prediction equations for a relevant range of relative humidity and temperature.

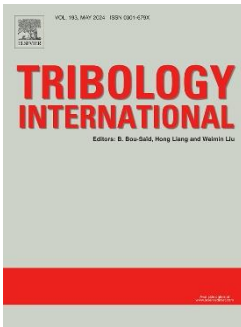
The openness of the wheel-rail system raises questions about the resilience of friction-management techniques to external factors. The last work **iv.** concerns the effect of water contamination on wheel-rail adhesion when liquid friction modifiers are used to optimize frictional properties (these products are described in Chapter 3 in more detail). The author’s contribution to the topic is a comprehensive discussion of mechanisms that are responsible for friction and surface separation in rolling-sliding contacts under the joint action of water and oil-based products.

The author has contributed to the following papers/book chapter:



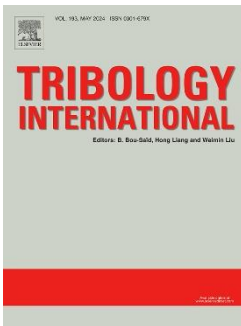
[1] **OMASTA, M.** and H. CHEN. Wheel-rail interface under extreme conditions. In book: *Rail Infrastructure Resilience: A Best-Practices Handbook*, 2022, s. 137–160. ISBN 978-0-12-821042-0. DOI:10.1016/B978-0-12-821042-0.00005-8

Author’s contribution (BUT)	100 %
Journal impact factor	not relevant
JIF Quartile	not relevant
Citations (Scopus)	0



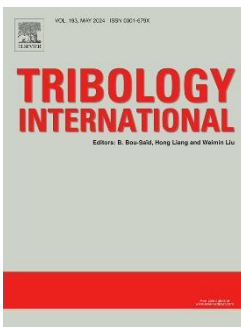
[62] KVARDA, D., R. GALAS, **M. OMASTA**, L.B. SHI, H. DING, W.J. WANG, I. KRUPKA and M. HARTL. Asperity-based model for prediction of traction in water-contaminated wheel-rail contact. *Tribology International*, 2021, **157**, 106900, ISSN 0301679X. DOI:10.1016/j.triboint.2021.106900

Author's contribution (BUT)	15 %
Journal impact factor (2021)	5.620
JIF Quartile	Q1
Citations (WoS)	14



[63] GALAS, R., **M. OMASTA**, L.B. SHI, H. DING, W.J. WANG, I. KRUPKA and M. HARTL. The low adhesion problem: the effect of environmental conditions on adhesion in rolling-sliding contact. *Tribology International*, 2020, **151**, 106521. ISSN 0301679X. DOI:10.1016/j.triboint.2020.106521

Author's contribution (BUT)	44 %
Journal impact factor (2020)	4.872
JIF Quartile	Q1
Citations (WoS)	17



[64] SKURKA, S., R. GALAS, **M. OMASTA**, B. WU, H. DING, W.J. WANG, I. KRUPKA and M. HARTL. The performance of top-of-rail products under water contamination. *Tribology International*, 2023, **188**, 108872. ISSN 0301-679X. DOI:10.1016/J.TRIBOINT.2023.108872

Author's contribution (BUT)	25 %
Journal impact factor (2022)	6.200
JIF Quartile	Q1
Citations (WoS)	0

2.6.1 Wheel-rail interface under extreme conditions [1]

The *Rail Infrastructure Resilience: A Best-Practices Handbook* offers a collection of refined strategies aimed at enhancing the resilience of rail infrastructure systems against extreme conditions. This guide demonstrates the most effective ways to apply recent insights into the engineering, maintenance, construction, and renewal of rail infrastructure. The book chapter brings a wider perspective on the impact of climate changes or extreme weather conditions on railway transport. Although some relevant studies were published [65–69], they broadly deal with the impact on the entire railway infrastructure, rolling stock, and asset management. This chapter focuses on the specific effects of predicted climatic changes and events on the wheel-rail interface and their implications for railway service and operations. The consequences are largely influenced by how particular contaminants or climatic conditions change the behaviour of the wheel-rail interface, especially friction-related phenomena. This survey based on recent studies elucidates the impact of water, weather conditions, particulate contamination, and other hazards associated with extreme conditions.

One of the important contributions is a critical comparison of various models estimating water lubrication in a fluid-film regime. The thickness of water films can be approximated through the EHL theory considering the isoviscous elastic or piezo-viscous elastic lubrication regime. Those models were not validated under the ideal conditions, which was the purpose of the following author’s study.

2.6.2 Asperity-based model for prediction of traction in water-contaminated wheel-rail contact [62]

This work deals with the implementation of a numerical model for the evaluation of friction in water-contaminated contact. The model utilizes the Greenwood and Tripp theory to calculate the load carried by asperities and liquid film. Kalker’s simplified theory with an implemented third body layer was used to determine the frictional values of asperity contact and elastohydrodynamic theory for friction generated by liquid.

Lubricant film thickness prediction was made using a film thickness formula by Esfahanian and Hamrock [40] assuming the iso-viscous behaviour of water, so having Newtonian behaviour to shear rate and presuming no change in viscosity with the change of pressure. This formula is very often used in simulations of wheel-rail contact contaminated with water; however, there is no validation of the prediction for water-lubricated contact with a low film thickness.

Thin-film colorimetric interferometry method implemented on the ball-on-disc tribometer was used to measure the film thickness of very thin water film formed between the steel ball and glass disc under pure rolling conditions. The resulting interferograms are depicted in Fig. 5. Because of the very low thickness of several nanometres, only grey shades are relevant for the evaluation. The lubricant film thickness measurement compared with the prediction is shown in Fig. 6.

These results show the change difference in calculated film thickness compared to the analytical prediction by Esfahanian and Hamrock [14]. This study brings the unique experimental validation of the model to predict water film thickness under the conditions relevant for wheel-rail water contamination.

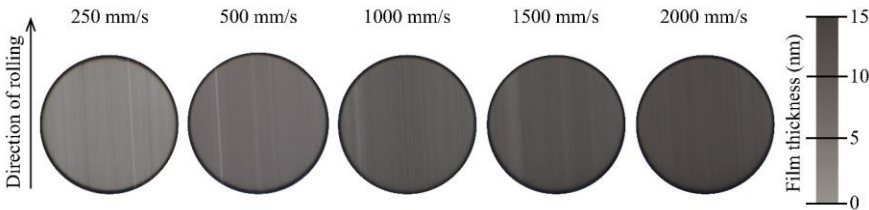


Fig. 5 Water film thickness interferograms [62]

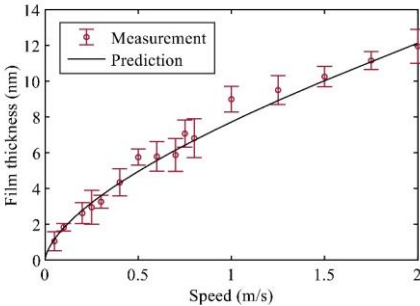


Fig. 6 Water film thickness measurement compared with prediction [62]

2.6.3 The low adhesion problem: The effect of environmental conditions on adhesion in rolling-sliding contact [63]

One of the most important contributions is the investigation of the effects of humidity and temperature on CoA in the rolling-sliding contact under clean and leaf-contaminated conditions. Such contact was simulated using the ball-on-disc tribometer (Mini-traction-Machine, PCS Instruments), while the air temperature (1 to 50 °C) and relative humidity (RH, 6 to 100%) in the test chamber were controlled. Leaf contamination was prepared according to the procedure shown in Fig. 7.

Experimental results shown in Fig. 8 indicate that under clean conditions, the effect of RH becomes important for temperatures of 24°C and below. For these temperatures, the coefficient of adhesion decreases in the whole tested RH range. If water condenses, further adhesion decrease occurs and problems with traction and braking can be expected. In leaf-contaminated conditions, the effect of RH is much more significant. The combination of water condensation and disc contamination results in critically low adhesion, even below 0.05. The following analytical models for adhesion prediction under different temperatures and RH were proposed for both clean and leaf-contaminated contact:

$$\mu_{clean} = 0,5461 + 0,003029 \cdot T - 0,002844 \cdot RH - 3,346 \cdot 10^{-5} \cdot T^2 + 5,401 \cdot 10^{-5} \cdot T \cdot RH$$

$$\mu_{contaminated} = 0,4153 + 0,001587 \cdot T - 0,001662 \cdot RH$$



Fig. 7 Preparation of leaf-contaminated condition on test sample [63]

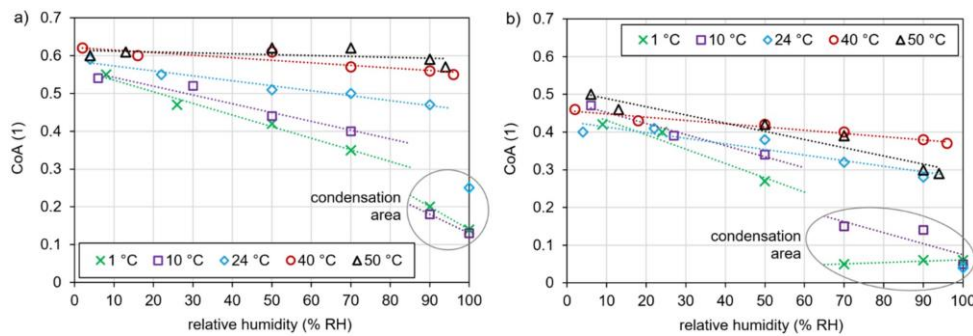


Fig. 8 Effect of RH and temperature on CoA for clean disc (a) and contaminated disc (b) [63]

2.6.4 The performance of top-of-rail products under water contamination [64]

This work has provided a series of experiments under well-controlled conditions when a small amount of top-of-rail lubricants and various amounts of water were applied to the contact. The ball-on-disc tribometer (Mini-traction-Machine, PCS Instruments) was used to simulate wheel-rail rolling-sliding contact. The results show that water influences the coefficient of traction (CoT) substantially. In most cases, a combination of a small amount of water and oil-based lubricant caused lower CoT than the water of the lubricant itself.

The mechanisms behind the behaviour depend on the lubrication regime, as indicated in Fig. 9. The discussion is based on theories generally accepted in EHL grease-lubricated contacts. At low speeds and fluid-film regime, plate-out theory [70, 71], theory of energy displacement [72] and dynamic concentration theory [73] predict well the increasing concentration of oil in the inlet zone as water is gradually excluded from the gap. As the speed increases, the oil pool becomes unstable in accordance with a starvation theory [74–76]. Under the starved fluid-film regime, water influences an apparent viscosity of the fluid [77], which affects the ability of the lubricant to replenish the contact [78, 79]. With increasing starvation severity, a mixed lubrication regime becomes dominant [80]. The results and discussion are very important as they indicate possible problems with low adhesion. Water compatibility should be a part of TOR product’s benchmarking and the application should be avoided under wet conditions.

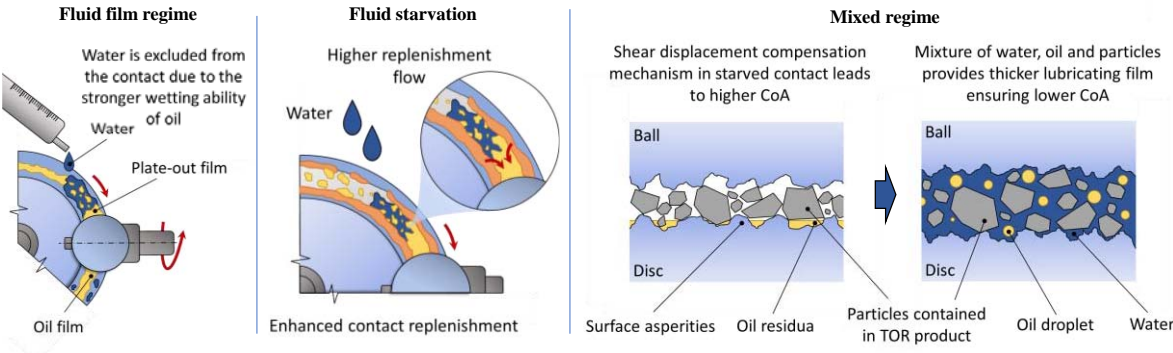


Fig. 9 Discussed mechanisms: a) Fluid-film regime, b) Starved fluid-film regime, c) Mixed regime. Modified from [64]

WHEEL-RAIL INTERFACE AND FRICTION MANAGEMENT

3.1 Introduction

So-called “friction management” is a group of techniques that involves the targeted application of lubricants, friction modifiers or traction enhancers to maintain the friction level between the wheel and the rail at the desired level. As shown in Fig. 10, there are three main groups of friction management techniques. This practice is essential for maintaining the balance between too much and too little friction, each of which can lead to different operational problems. Each technique has its purpose. The first group aims to improve traction when low-adhesion conditions occur. The most traditional is sanding, where sand particles are applied directly to the rails in front of the wheel through a sanding system. The sand particles increase the roughness of the rail surface, thereby improving friction and preventing wheel slip, especially under wet or slippery conditions [49, 81].

On the other side, wheel-flange lubrication is used to decrease friction between the rail gauge and wheel flange as much as possible. This contact is important for guiding the train along the track, particularly through curves, without derailment. This interaction results in significant friction and wear, so the proper friction management of this contact area is essential for safe, smooth, and cost-efficient railway operations, minimizing maintenance costs and extending the life of both rails and train wheels [82].

Besides the conventional wheel-flange lubrication protecting the wheel edges and rail sides in curving scenarios, top-of-rail (TOR) conditioning is a progressively developing strategy where some



Fig. 10 Wheel-rail interface and relevant friction management techniques

liquid and semi-liquid TOR products are applied directly to the top surface of the rails. This technique aims to achieve the balance of friction in the contact area responsible for the traction and braking for better performance and wear characteristics [83, 84]. TOR products include a wide range of solid, liquid and semi-liquid lubricants and friction modifiers containing solid particles to provide a coefficient of traction in an optimal range of 0.25 to 0.4 [85, 86].

3.2 Traction enhancement

Sanding is a common method used to enhance traction in railway systems, particularly in low-adhesion conditions. While using sand as a traction enhancer in rail systems is effective, it does pose several challenges. The abrasiveness of sand can lead to surface damage on both wheels and rails, which increases [83, 84]. Additionally, the use of sand can lead to insulation issues between the wheel and rail, negatively impacting track circuits and raising safety concerns [84–86]. There are also health concerns; fine sand particles can become airborne, posing respiratory risks, particularly in urban rail transport [87].

Over recent decades, significant research has focused on optimizing the sanding process [88] and exploring alternative materials and techniques [49, 81]. In the wheel-rail interactions, sand particles are first broken down into finer fragments at the contact zone [89]. Using smaller sand particles can reduce wear and improve material use efficiency [84, 90]. Studies have shown that micro-fragments can decrease wear and surface damage while maintaining their ability to enhance adhesion, similar to standard sand particles [91]. Additionally, alternatives like mineral and ceramic particles have been used, demonstrating superior adhesion properties compared to traditional sand [92, 93]. The crushing strength of these particles is crucial for both adhesion and minimizing damage to wheels and rails [94], indicating promising developments in low-energy granular materials.

Furthermore, semi-liquid materials, including high-positive-friction modifiers and traction gels, have been developed [50, 95]. These materials typically combine sand and metal particles in a water-based or hybrid liquid, ensuring better adherence to the rail surface to boost traction [96]. This increases the efficiency of both adhesion recovery and material usage. The advantage of these semi-liquid and liquid substances is their applicability via stationary track units, providing repeated traction enhancement at critical points such as car departures at stops or junctions—a notable challenge in urban rail transport.

3.3 Top-of-rail conditioning

Top-of-rail conditioning using TOR product is essential for optimizing the wheel-rail interface friction and related phenomena like wear, noise, rolling stock driving stability, etc. TOR products are specialized solutions used in the rail industry to manage friction at the wheel-rail interface [96]. This large group of products include so-called solid sticks that are pushed against the wheel using a train-borne system [97] and water-based friction modifiers [4, 6, 12, 27] and a range of oil- or grease-based products [98, 99] usually sprayed on top of the rail from rolling stock.

Over the past decade, there has been considerable advancement in the technology of TOR conditioning. Numerous field studies have demonstrated the benefits of employing TOR products, particularly with water-based products applied on critical track curves in North America, Australia, Europe and China. These studies have primarily focused on enhancing fuel efficiency within heavy

haul networks, as evidenced by several studies [95, 100–102]. Additionally, the use of TOR FM has been explored in metro and tram systems across Europe [12, 103, 104]. Currently, the TOR concept is increasingly receiving recognition and support from rail network owners and train operators. On-board applications are becoming more prevalent, especially in mainland Europe, often involving oil-based FMs.

Current research is mainly focused on the description of mechanisms how the products works in the wheel-rail interface. Most research questions deal with the performance characteristics of TOR products [105–109], the effect on wear and development of rolling contact fatigue (RCF) [6, 97, 110, 111] and the study of the rheological parameters [105, 112, 113]. For the practical deployment of the technology, questions on the product transfer mechanisms between the wheel and the rail [37, 114] and carry distance of the products along the track [102, 115, 116] play an important role.

3.4 Research gaps

Some friction management methods are very traditional, e.g. sanding is nearly as old as the rolling stock itself. On the other hand, TOR conditioning is a new and dynamically developing area. Nevertheless, challenges and research gaps can be found in each of these areas:

- v. The sanding rate is a critical parameter in rail operations when the technique is used to overcome low-adhesion problems. While numerous studies have explored the impact of sanding, only a few have specifically examined how different sanding parameters affect its performance. As indicated in Fig. 11, general questions arise on what are adhesion curves for different contact contamination and conditions and what is the necessary sand quantity to restore the adhesion coefficient to the required level?

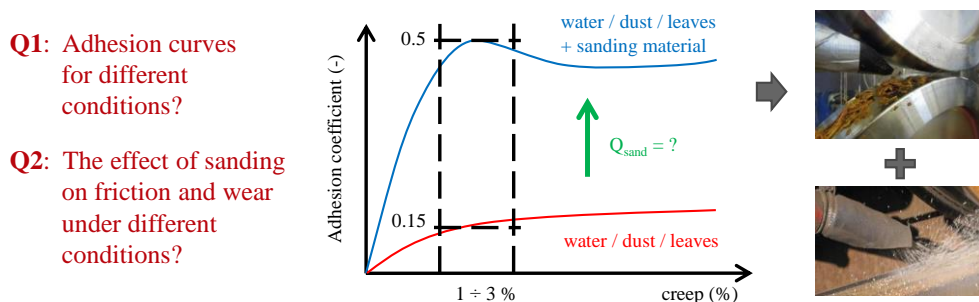


Fig. 11 Research questions in optimization of wheel-rail sanding parameters

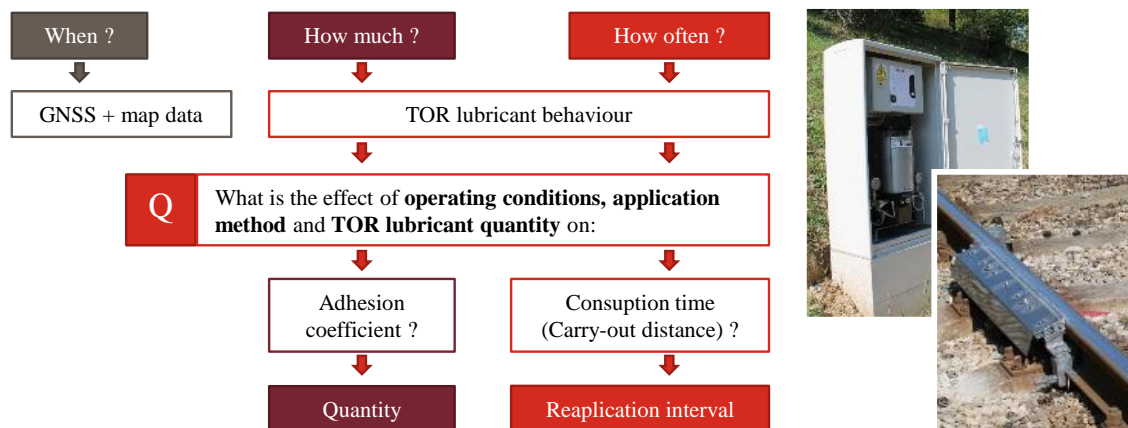


Fig. 12 Main questions connected with application of TOR lubricants

- vi. Proper application parameters and strategy are crucial also in the field of TOR conditioning, where insufficient application leads to unfulfilled expectations in noise mitigation and wear reduction, while the product overdosing causes unacceptably low friction on top of the rail. Fig. 12 summarizes the main questions connected with the application of TOR lubricants. To answer the questions When?, How much? and How often?, an investigation of the effect of operating conditions, application parameters and TOR product quantity has to be done.
- vii. Application parameters need field validation. There is no methodology suitable for the determination of optimal TOR product quantity under the field.

3.5 Author's contribution

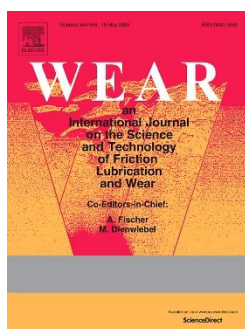
The author's research into friction management techniques during the last 10 years includes all the most important techniques. Particular research progress was made in wheel-rail sanding and top-of-rail conditioning using friction modifiers and lubricants.

The first study in this field v. focuses on a lab-scale experimental study of the sanding process within a simulated wheel-rail contact. The primary objective was to assess how different sanding rates influence adhesion recovery in wheel/rail contact under specific contamination and a range of contact conditions. Common contaminants such as water, grease, and leaves have been considered in these experiments.

The second work vi. covers experimental research done within the development and implementation of control algorithms for the on-board top-of-rail lubrication system. The experimental approach provides a comprehensive methodology for the design of application parameters.

The third work vii. is focused on the field validation of application parameters of TOR lubricant and its effect on tram braking distance. This is especially important for oil-based TOR products that are highly amount-dependent with a possible risk of low adhesion.

The author has contributed to the following papers:



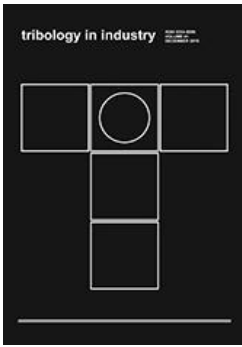
[117] **OMASTA, M., M. MACHATKA, D. SMEJKAL, M. HARTL and I. KRUPKA.** Influence of sanding parameters on adhesion recovery in contaminated wheel–rail contact. *Wear*, 2015, **322–323**, 218–225. ISSN 00431648. DOI:10.1016/j.wear.2014.11.017

Author's contribution (BUT)	60 %
Journal impact factor (2021)	2.323
JIF Quartile	Q1
Citations (WoS)	34



[118] **OMASTA, M., R. GALAS, J. KNAPEK, M. HARTL a I. KRUPKA.** Development of an adaptive top-of-rail friction modification system. In: *Institution of Mechanical Engineers - Stephenson Conference: Research for Railways 2017*. 2017, 325–332. ISBN 978-1-5108-8295-9

Author's contribution (BUT)	50 %
Journal impact factor	not relevant
JIF Quartile	not relevant
Citations (Scopus)	1



[99] GALAS, R., M. OMASTA, M. KLAPKA, S. KAEWUNRUEN, I. KRUPKA a M. HARTL. Case study: The influence of oil-based friction modifier quantity on tram braking distance and noise. *Tribology in Industry*, 2017, **39(2)**, 198–206. ISSN 0354-8996. DOI:10.24874/ti.2017.39.02.06

Author's contribution (BUT)	20 %
Journal impact factor	not relevant
JIF Quartile	not relevant
Citations (Scopus)	18

3.5.1 Influence of sanding parameters on adhesion recovery in contaminated wheel–rail contact [117]

The largest contribution to the wheel-rail sanding was made through the study aimed to investigate the effect of sanding parameters on the adhesion recovery in the contaminated wheel-rail contact. For this purpose, a new twin-disc machine in scale 1:3 allowing the application of real sanding material into the wheel-rail contact was developed. Fig. 13 depicts the methodology and typical results indicating adhesion recovery under various speed, slip and sand quantities in the contact contaminated with leaves.

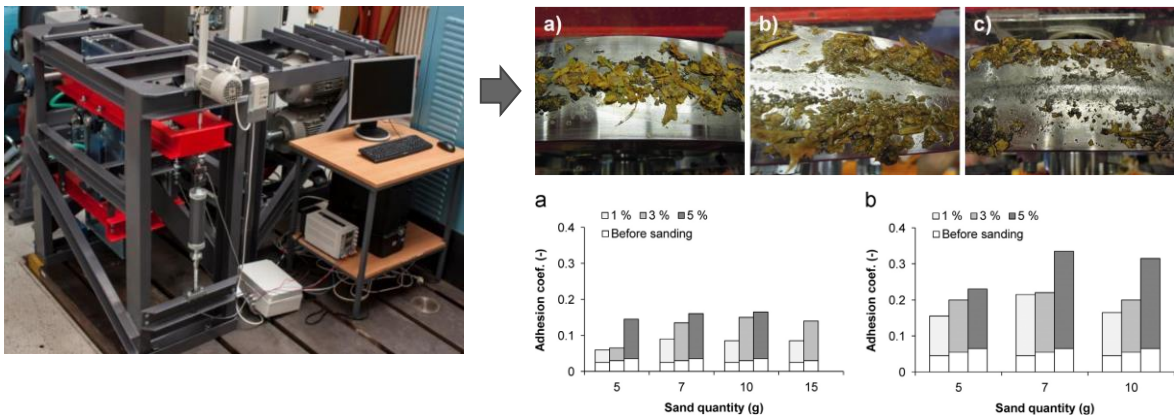


Fig. 13 Investigation of sanding parameters in the leaf-contaminated wheel-rail contact using twin-disc approach; (a) 1 m/s; (b) 3 m/s, modified from [117]

The main findings from this study are that sanding under dry and slightly wet conditions leads to an immediate decrease in adhesion, while the extent of the reduction and the duration of reduced adhesion are amplified by increasing the sanding rate. Although the adhesion coefficient decreases with rolling speed under wet conditions, adhesion recovery improves with increased speed during sanding. Notably, higher adhesion coefficients can be achieved compared to those in dry conditions.

Under wet, leaf and grease contamination, the amount of sand significantly influenced adhesion recovery, but only at low wheel slip and low rolling speeds. In contaminated contacts, the effectiveness of sanding in improving adhesion recovery grows with both wheel slip and rolling speed. Contacts contaminated with wet leaves exhibited the lowest adhesion coefficient, around 0.05. Although the passing sand temporarily enhanced adhesion, it subsequently declines again due to the formation of a hard-to-remove layer left by the leaves on the disc surfaces.

3.5.2 Development of an adaptive top-of-rail friction modification system [118]

This paper outlines the development of a control system designed for top-of-rail friction modification, utilizing an onboard application method. This work involves an experimental methodology to assess the optimal amount of oil-based TOR lubricant and the frequency of its application, tailored to different operating conditions. To achieve this, laboratory-scale twin-disc test rigs have been employed in the study. This experimental approach is illustrated in Fig. 14. Application of a small amount of TOR lubricant leads to a decrease in CoA and the formation of 3rd body layer on disc surfaces. During the following period, CoA gradually increases as the friction layer wears off. The increase in CoA over time was used to calculate the CoA rate, shown in Fig. 14.

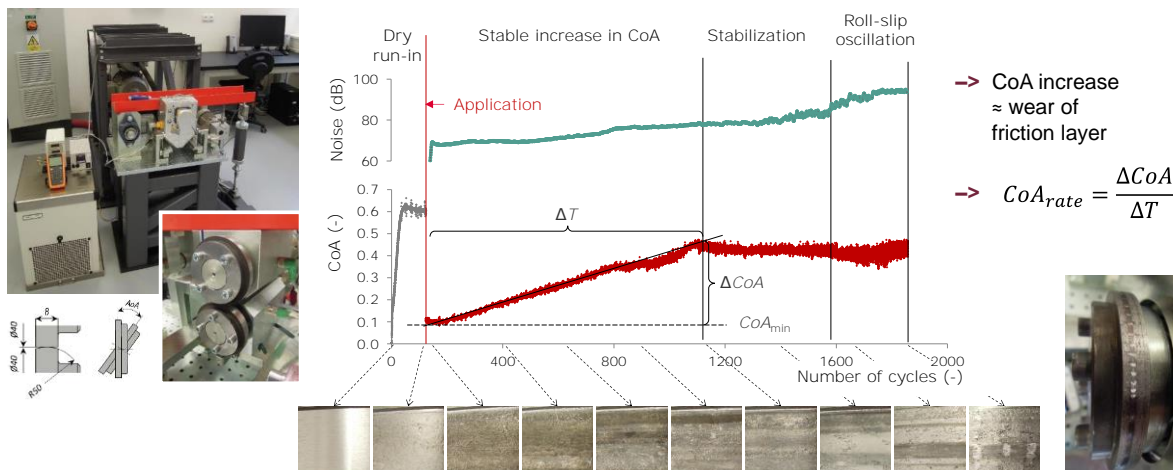


Fig. 14 Evolution of CoA and disc surface after the application of TOR lubricant, modified from [118]

Such experiments were conducted under various conditions to quantify the effect of applied TOR lubricant amount, rolling speed and slip in the contact, as shown in Fig. 15. Based on experimental results for various TOR lubricants, CoA rate was fitted with 3D exponential curve as a function of the amount and sliding speed. CoA rate quantifies how fast the resulting 3rd body layer wears off and could be seen as a suitable parameter for benchmarking the TOR products.

Based on the experimental results, the slip velocity is identified as the key parameter for real-time estimation of TOR lubricant consumption time. This prediction was implemented into control algorithms of the developed adaptive system that determines the suitable amount and application interval based on the train's location using GPS data and considering actual operating and weather conditions (Fig. 16).

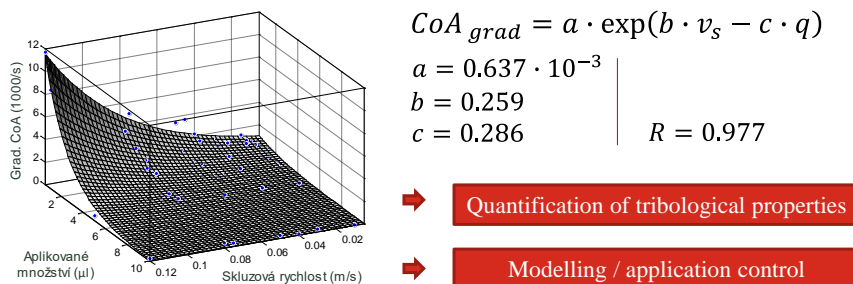


Fig. 15 CoA rate as a function of sliding speed and applied TOR lubricant quantity, modified from [118]

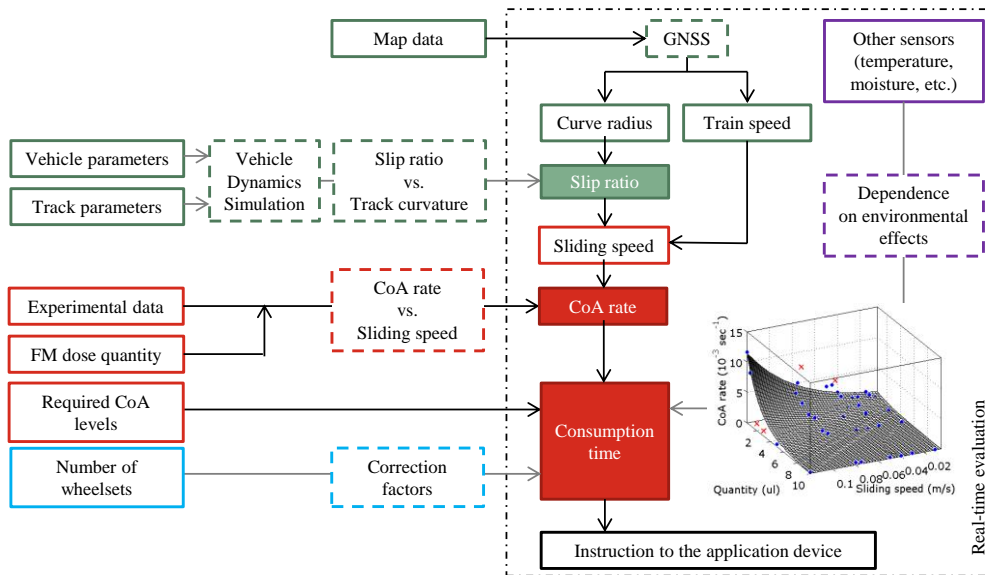


Fig. 16 Scheme of algorithms of a developed control system for TOR products application, modified from [118]

3.5.3 Case Study: the influence of oil-based friction modifier quantity on tram braking distance and noise [99]

The necessary step in the implementation of TOR lubrication control algorithms is to validate the applied amount in the field. The most convenient is a braking test, where rolling stock starts to brake under given conditions and total braking distance, activation of wheel-slide protection (WSP) system and/or sliding between vehicle and track are evaluated. Such a study was conducted by employing a light-rail system in Brno, Czech Republic. Fig. 17 depicts an application of TOR lubricant using a wayside applicator and results of braking tests. It is evident, that tram braking distance strongly depends on an applied quantity. For the higher quantity (4 g), the braking distance is up to 20 meters longer, while the low quantity (1 g) provides a nearly unchanged braking distance. This approach is suitable for field validation, mainly from rail transport operators, however the positive effect of such a low amount of TOR lubricant is questionable.

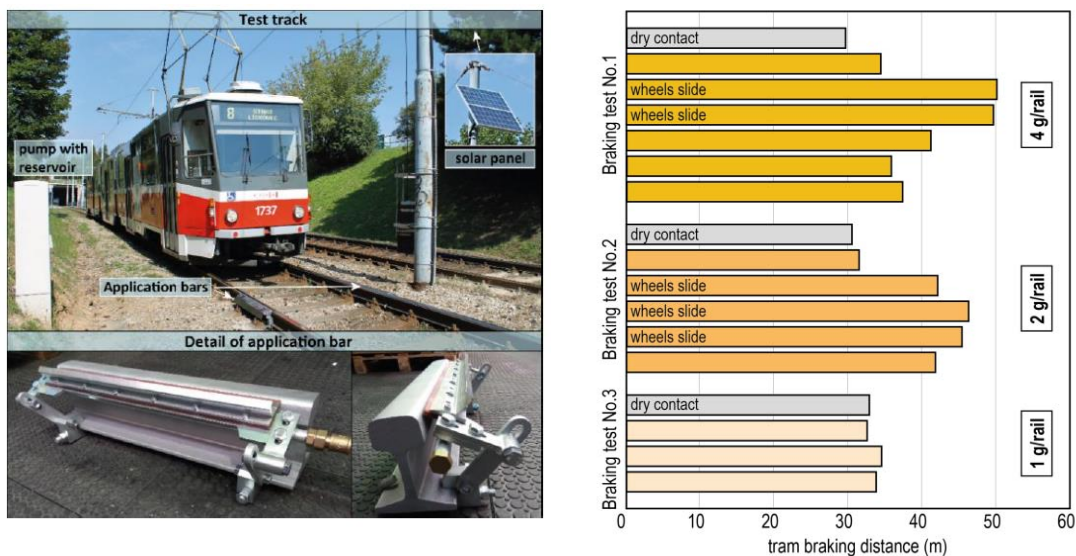


Fig. 17 Field tests towards the optimization of application amount to prevent extension in braking distance [99]

4

EXPERIMENTAL FACILITY TO STUDY THE WHEEL-RAIL INTERFACE

4.1 Introduction

Experimental research into wheel-rail tribology is essential for understanding and improving the interactions between train wheels and rails, which are critical for the safety and efficiency of rail transport. This research relies on various specialized tribometers and laboratory devices to simulate the wheel-rail contact in both, the laboratory and field. These instruments are essential to evaluate the effects of different materials, lubricants, and environmental conditions on friction and wear behaviour at the interface. One of the focuses of such research is to optimize the formulation of TOR products and lubricants that can enhance frictional properties and reduce wear even under adverse weather conditions. Another important aspect is the study of wear mechanisms and material degradation under varying loads and speeds and other adverse effects. Experimental research in wheel-rail tribology advances our understanding of fundamental tribological principles and drives innovations in rail technology, leading to more durable materials, more effective lubrication systems, and more reliable and efficient railway operations.

4.2 Lab-scale experimental facility

The laboratory provides controlled conditions for experiments, offering a significant advantage over field measurements, though with somewhat reduced representativeness. Lab-scale setups often incorporate environmental simulation chambers to replicate different climatic conditions, enabling researchers to study how factors like moisture, temperature, and contaminants such as leaves affect the wheel-rail interaction.

Various laboratory test rigs and tribometers are available to study the wheel-rail contact. Rheological characterisation under the real wheel-rail pressure is allowed by a High-Pressure Torsion (HPT) concept [55, 60, 112, 119, 120]. Simple pure-sliding tribometers allow to study the wheel-rail contact behaviour on a more fundamental level [45, 58, 107] or in a well-insulated environmental chamber [121]. To simulate rolling-sliding contacts, ball-on-disc tribometers are available. The most widely used device is the Mini-Traction Machine (MTM), utilized to determine the creep curve in the simulated wheel-rail contact [17, 63, 64, 98, 122, 123].

Among the various testing setups, the small-scale twin-disc concept is particularly favoured in wheel-rail research due to its cost-effectiveness and a good level of representativeness of actual contact conditions. This setup can simulate rolling-sliding contact with precise control over slip [54, 99, 124–126] or torque [127, 128]. Additionally, smaller-scale test rigs often feature a rotating disc on a circular rail setup, which is beneficial for specific studies focusing on wear and stress distribution

[129, 130]. The most realistic experimental configuration provides full-scale tribometers that utilize an actual train wheel paired either with another disc representing the rail [3, 109, 131] or with the rail itself [50, 132, 133]. These full-scale setups are particularly valuable for simulating and studying complex conditions. This broad spectrum of testing equipment in the laboratory helps bridge the gap between theoretical research and practical applications.

4.3 Field-test facility

For some purposes or the final implementation and validation of technologies like TOR conditioning, field tests play an indispensable role. Some options are summarised in Fig. 18. The most comprehensive method involves using a locomotive equipped with a measuring system that captures the traction forces and sliding velocities of all bogies during instances of sliding [14, 102, 134]. However, these experiments are very costly. A more affordable alternative is to conduct brake testing on rolling stock, particularly when combined with materials promoting low adhesion conditions [50, 51]. The other side on the graph in Fig. 18 represents the Pendulum that evaluates the coefficient of friction under pure sliding based on the energy loss principle [135, 136].



Fig. 18 Various approaches for field measurement of wheel-rail coefficient of adhesion.

Between these extremes, there exists a range of track tribometers designed to allow fast measurements with acceptable model bias. For example, The TriboRailer is a car-pushed tribometer that induces creep by rotating the measuring wheel around the yaw axis [137]. Another common tool is the hand-pushed tribometer from Salient Systems [102, 138] or the TriboMetro FR 101 hand-pushed tribometer [139], inducing wheel slip by applying a ramped braking force via an electromagnetic brake. Another group of field tribometers induces lateral creep by rotating the measuring wheel at a specified angle of attack (AoA). The most relevant is the Hand-operated (HO) tribometer, also known as OnTrak [140–142].

4.4 Research gaps

From a tribological perspective, the challenges in the experimental simulation of wheel-rail contact include accurately replicating the specific wear mechanisms and lubrication conditions that occur at the interface under varying loads and environmental influences. Some research gaps were identified in both, lab-scale and field approaches:

- viii. One of the tasks for full-scale test rigs is the study of dynamic-related phenomena like squealing noise [143, 144]. For the experimental validation of models describing the noise-excitation mechanisms, appropriate test rigs are essential [145, 146]. The dynamics captured by the experimental model are crucial to understanding the effects being studied.
- ix. Fast assessment of the frictional properties on the rail head presents significant challenges. The use of instrumented trains is time-demanding and costly, sophisticated track tribometers are complex to operate, and simpler portable devices often lack representativeness. Traditional hand-pushed tribometers typically give an average friction coefficient over a longer track section and tend to overestimate the coefficient of friction [102]. The Hand-operated tribometer allows for evaluating the creep curve in a single pass thanks to the adjustable AoA; however, employing controlled lateral slip to generate a traction curve may not be as representative of typical operating conditions.

4.5 Author's contribution

The author deals with the development and implementation of appropriate experimental devices for more than 10 years. During this time, a complex experimental facility was exploited allowing comprehensive research into various tasks in wheel-rail tribology. An overview of self-developed as well as commercial tribometers used for the research in the author's research group is shown in Fig. 19. The development was mainly related to the following devices/papers:

The first study **viii.** was focused on the design of a twin-disc test rig specifically developed for investigating wheel-squeal phenomena. This rig incorporates a dynamic model that simulates the interaction between the track and train, employing an actual train wheel to more accurately represent the noise produced.

The second work **ix.** was aimed to introduce a new portable rail tribometer, which features a controlled traction force, to assess the creep curve. By fitting a creep force model to the experimental data, this approach enables a straightforward and fast evaluation of the tribological properties of the 3rd body layer that forms on the rail. This method is versatile, applicable in both laboratory and field studies of the wheel-rail interface, and useful in the deployment of friction-management strategies.

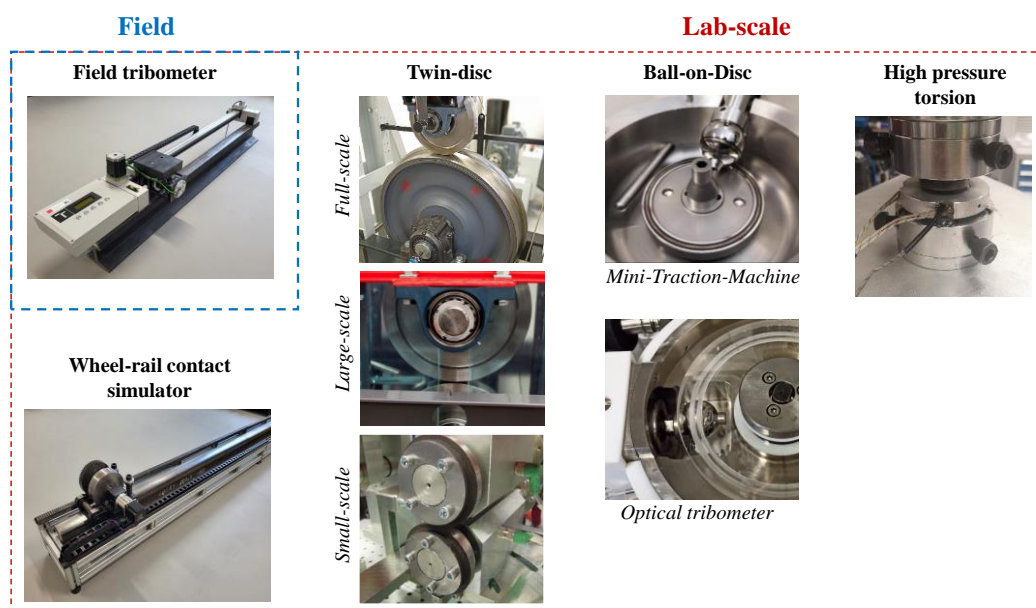
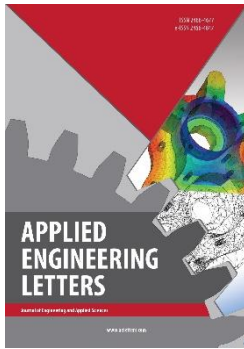


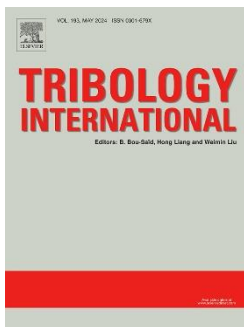
Fig. 19 Experimental facility for the research into wheel-rail tribology

The author has contributed to the following papers:



[147] **OMASTA, Milan**, Václav NAVRÁTIL, Tomáš GABRIEL, Radovan GALAS a Milan KLAPKA. Design and development of a twin disc test rig for the study of squeal noise from the wheel – rail interface. *Applied Engineering Letters*. 2022, **7(1)**, 10–16. ISSN 24664847. DOI:10.18485/AELETTERS.2022.7.1.2

Author’s contribution (BUT)	60 %
Journal impact factor	not relevant
JIF Quartile	not relevant
Citations (Scopus)	1



[148] VALENA, Martin, **Milan OMASTA**, Daniel KVARDA, Radovan GALAS, Ivan KRUPKA a Martin HARTL. An approach for the creep-curve assessment using a new rail tribometer. *Tribology International*, 2024, **191**, 109153. ISSN 0301679X. DOI:10.1016/j.triboint.2023.109153

Author’s contribution (BUT)	24 %
Journal impact factor (2022)	6.200
JIF Quartile	Q1
Citations (WoS)	0

4.5.1 Design and development of a twin disc test rig for the study of squeal noise from the wheel – rail interface [147]

The developed twin-disc test rig with a real tram wheel was intended for the study of squealing noise, especially under the mode-coupling mechanism [145]. The design parameters of the test rig were tailored to meet specific dynamic requirements. The dynamic characteristics of the wheel and disc suspension were achieved by optimizing the stiffness of select support frame elements, as illustrated in Fig. 20. By measuring the loading force, lateral reaction acting on the disc and torque on the driven wheel, traction curves in longitudinal and transversal directions can be evaluated. During the experiments, sound pressure level (SPL) is recorded to be compared with the adhesion characteristics. The results are used to validate wheel-squeal prediction models and to investigate the influence of weather conditions and the presence of various friction layers. Possible noise mitigation techniques, like top-of-rail conditioning, can be assessed. See the implemented test rig in Fig. 21.

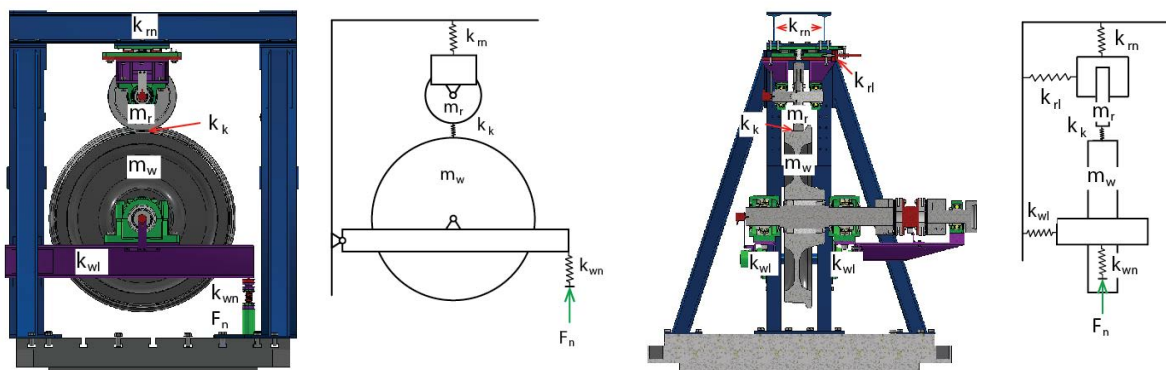


Fig. 20 Implementation of the dynamic model [147]

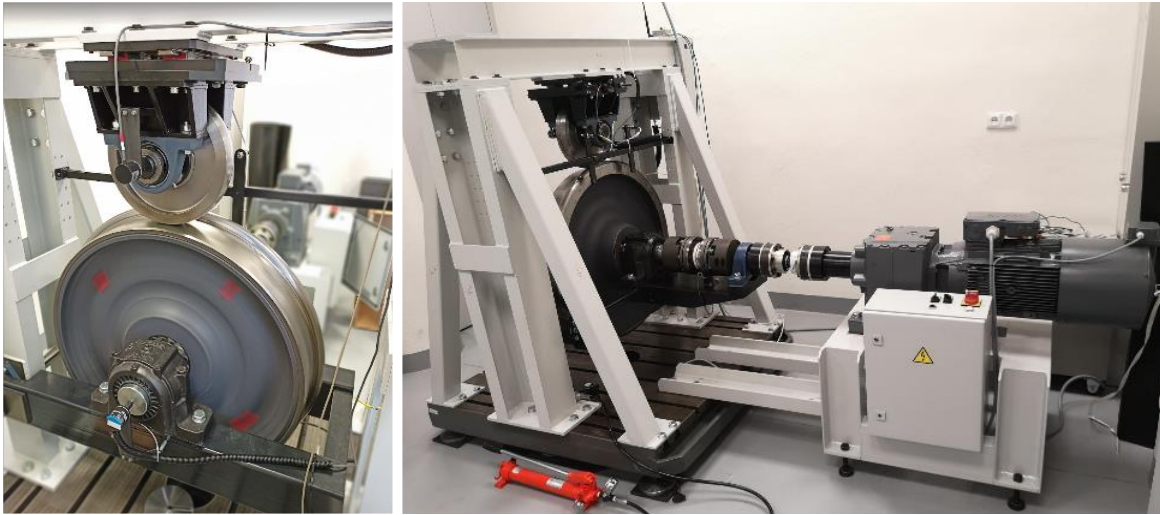


Fig. 21 Twin-disc test rig with a real tram wheel to study squealing noise

4.5.2 An approach for the creep-curve assessment using a new rail tribometer [148]

The new tribometer called “BUT rail tribometer” (Fig. 22) and the corresponding experimental approach represents a significant advance on previous solutions. The controlled traction force method was selected to replicate the real conditions of wheel-rail contact. Well-designed braking and control system allow an evaluation a whole traction curve during one pass along app. 700 mm rail. Precise measurement enables to determine CoT as low as 0.02. Multiple methods were utilized to assess the parameters of the creep curve based on measured data. Typical experimental results under various contact conditions are in Fig. 23. Traction curves were fitted using Polach’s analytical model and the modified FASTSIM model. Although these methods vary in complexity, the coefficient of traction (CoT) results show a variation of only 2% compared to models that describe the entire creep curve.

This method serves as an effective tool for analyzing TOR product characteristics, including redistribution, carry distance and retentivity. The high creep generated by the tribometer, coupled with its capability to capture the full traction curve in one pass, enables its use in studying the wear resistance of the friction layer. This is particularly crucial for developing models of friction layers, implementing friction management techniques and other related applications.



Fig. 22 BUT rail tribometer

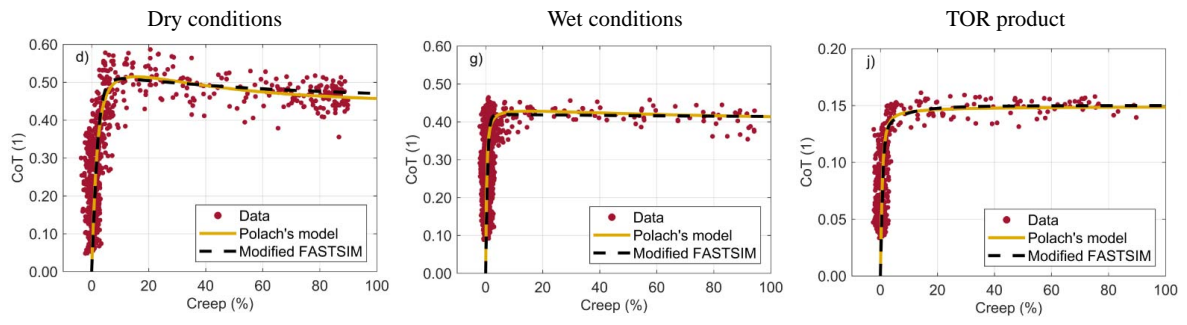


Fig. 23 Typical experimental results and theoretical fits under various contact conditions, modified from [148]

CONCLUSIONS AND FUTURE WORK

This habilitation thesis includes the most important work of the author in the field of tribology of the wheel-rail interface. It should be noted, that the author's fields of interest include a variety of other problems in tribology, like thin-film and elastohydrodynamic lubrication, journal and rolling-element bearings, implementation of experimental techniques in tribology, etc. The field of wheel-rail tribology began to dominate in the author's work in the last 10 years, following the establishment of the research subgroup under the Department of Tribology.

The work covers significant aspects and up-to-date problems in the tribology of the wheel-rail interface. Namely:

Wheel-rail interface as an open tribology system

- This topic is of increasing interest because the “openness” of the wheel-rail interface is a source of many problems, stemming especially from the wheel and rail contamination by natural contaminants.
- The most important contribution is the study of the effect of humidity and water contamination [63]. The tests in rolling-sliding configuration and under well-controlled conditions have provided valuable insights and made it possible to quantify these effects by prediction formulas.
- The effect of humidity and water contamination is connected with a wide range of low-adhesion problems in rail transport. Especially its interaction with biological contaminants or solid particles brings research challenges. The author's team has unique equipment [62, 148] that is a prerequisite for achieving further new knowledge in this field.

Friction management in the wheel-rail interface

- The author's team has a very good position in the research of top-of-rail conditioning. A range of papers is focused on both, more fundamental research into the mechanism of how those products behave in the wheel-rail interface [64, 98, 113, 120, 123], as well as the development of application strategies and control algorithms [99, 118].
- The most important contribution is in the study of possible low-adhesion conditions as a result of the interaction of water and TOR products [64]. Development activities [99, 118] have a strong practical impact and are still going towards implementation in rail transport operations. Practical applications of the research findings should provide more effective top-of-rail conditioning solutions with the impact on reducing maintenance costs and extending the life of rail infrastructure.
- An important aspect of friction management becoming increasingly urgent is an “openness” of the system. All the traditional friction management techniques, especially lubrication and TOR conditioning, can be referred to as “total loss systems” – “total loss” from the application system perspective, but not from nature's point of view! We need to change the way we look at this problem.

Experimental facility to study the wheel-rail interface

- As already mentioned, the developed BUT rail tribometer [148] represents a unique device that has proven to be very effective in the assessment of adhesion curves on the real rail. The author is not aware of any other similar solution that is comparable to this device in terms of practicality, simplicity and speed of measurement. This device is very useful not only in the field but also in laboratory conditions, where it makes it possible to study the contact under a well-controlled environment.

REFERENCES

- [1] OMASTA, Milan a Hua CHEN. Wheel-rail interface under extreme conditions. *Rail Infrastructure Resilience* [online]. 2022, 137–160. doi:10.1016/B978-0-12-821042-0.00005-8
- [2] VOLLEBREGT, Edwin, Klaus SIX a Oldrich POLACH. Vehicle System Dynamics International Journal of Vehicle Mechanics and Mobility ISSN: (Print) (Challenges and progress in the understanding and modelling of the wheel-rail creep forces Challenges and progress in the understanding and modelling of the wheel-rail creep forces [online]. 2021, **59**(7), 1026–1068. doi:10.1080/00423114.2021.1912367
- [3] VOLTR, Petr a Michael LATA. Transient wheel–rail adhesion characteristics under the cleaning effect of sliding. *Vehicle System Dynamics* [online]. 2015, **53**(5), 605–618. ISSN 0042-3114. doi:10.1080/00423114.2014.961488
- [4] LI, J. X., B. N. WU, H. H. DING, R. GALAS, M. OMASTA, Z. F. WEN, J. GUO a W. J. WANG. Wear and damage behaviours of wheel and rail materials: Effects of friction modifier and environmental temperature. *Wear* [online]. 2023, **523**. ISSN 00431648. doi:10.1016/j.wear.2023.204796
- [5] EKBERG, Anders a Elena KABO. Fatigue of railway wheels and rails under rolling contact and thermal loading—an overview. *Wear* [online]. 2005, **258**(7–8), 1288–1300. ISSN 00431648. doi:10.1016/j.wear.2004.03.039
- [6] EADIE, Donald T., Dave ELVIDGE, Kevin OLDKNOW, Richard STOCK, Peter POINTNER, Joe KALOUSEK a Peter KLAUSER. The effects of top of rail friction modifier on wear and rolling contact fatigue: Full-scale rail–wheel test rig evaluation, analysis and modelling. *Wear* [online]. 2008, **265**(9–10), 1222–1230. ISSN 00431648. doi:10.1016/j.wear.2008.02.029
- [7] BOLTON, P. J., P. CLAYTON a I. J. MCEWEN. Wear of Rail and Tire Steels Under Rolling/Sliding Conditions. *A S L E Transactions* [online]. 2008, **25**(1), 17–24. ISSN 0569-8197. doi:10.1080/05698198208983059
- [8] SUNDH, Jon a Ulf OLOFSSON. Seizure mechanisms of wheel–rail contacts under lubricated conditions using a transient ball-on-disc test method. *Tribology International* [online]. 2008, **41**(9–10), 867–874. ISSN 0301679x. doi:10.1016/j.triboint.2007.12.011
- [9] LI, Yifei, Yiping WU, Peter MUTTON, Cong QIU a Wenyi YAN. A ratcheting mechanism-based numerical model to predict damage initiation in twin-disc tests of premium rail steels. *Engineering Failure Analysis* [online]. 2023, **146**, 107066. ISSN 1350-6307. doi:10.1016/j.engfailanal.2023.107066
- [10] MAZZÙ, Angelo, Davide BATTINI a Nicola ZANI. Computational assessment of ratcheting in rail-wheel contact with solid contaminant. *Wear* [online]. 2024, **546–547**, 205346. ISSN 0043-1648. doi:10.1016/j.wear.2024.205346
- [11] BEER, F. G. de, M. H. A. JANSSENS a P. P. KOOIJMAN. Squeal noise of rail-bound vehicles influenced by lateral contact position. *Journal of Sound and Vibration* [online]. 2003, **267**(3), 497–507. ISSN 0022460X. doi:10.1016/S0022-460X(03)00710-7

- [12] EADIE, Donald T., Marco SANTORO a Joe KALOUSEK. Railway noise and the effect of top of rail liquid friction modifiers: changes in sound and vibration spectral distributions in curves. *Wear* [online]. 2005, **258**(7–8), 1148–1155. ISSN 00431648. doi:10.1016/j.wear.2004.03.061
- [13] LYU, Yezhe, Ellen BERGSETH a Ulf OLOFSSON. Open System Tribology and Influence of Weather Condition. *Scientific Reports* [online]. 2016, **6**(1). ISSN 2045-2322. doi:10.1038/srep32455
- [14] MEIERHOFER, Alexander, Gerald TRUMMER, Christof BERNSTEINER a Klaus SIX. Vehicle tests showing how the weather in autumn influences the wheel–rail traction characteristics. *Proceedings of the Institution of Mechanical Engineers, Part F: Journal of Rail and Rapid Transit* [online]. 2020, **234**(4), 426–435. ISSN 0954-4097. doi:10.1177/0954409719863643
- [15] CHEN, H., T. FURUYA, S. FUKAGAI, S. SAGA, J. IKOMA, K. KIMURA a J. SUZUMURA. Wheel slip/Slide and low adhesion caused by fallen leaves. *Wear* [online]. 2020, **446–447**. ISSN 00431648. doi:10.1016/j.wear.2020.203187
- [16] LEWIS, R., G. TRUMMER, K. SIX, J. STOW, H. ALTURBEH, B. BRYCE, P. SHACKLETON a L. Buckley JOHNSTONE. Leaves on the line: Characterising leaf based low adhesion on railway rails. *Tribology International* [online]. 2023, **185**, 108529. ISSN 0301-679X. doi:10.1016/J.TRIBOINT.2023.108529
- [17] CANN, P. M. The “leaves on the line” problem—a study of leaf residue film formation and lubricity under laboratory test conditions. *Tribology Letters* [online]. 2006, **24**(2), 151–158. ISSN 10238883. doi:10.1007/s11249-006-9152-2
- [18] BRUNO, Luca, Marko HORVAT a Lorenzo RAFFAELE. Windblown sand along railway infrastructures: A review of challenges and mitigation measures. *Journal of Wind Engineering and Industrial Aerodynamics* [online]. 2018, **177**, 340–365. ISSN 01676105. doi:10.1016/j.jweia.2018.04.021
- [19] HARDWICK, Christopher, Roger LEWIS a Ulf OLOFSSON. Low adhesion due to oxide formation in the presence of salt. *Proceedings of the Institution of Mechanical Engineers, Part F: Journal of Rail and Rapid Transit* [online]. 2014, **228**(8), 887–897. ISSN 0954-4097. doi:10.1177/0954409713495666
- [20] ABBASI, S., L. OLANDER, C. LARSSON, U. OLOFSSON, A. JANSSON a U. SELLGREN. A field test study of airborne wear particles from a running regional train. *Proceedings of the Institution of Mechanical Engineers, Part F: Journal of Rail and Rapid Transit* [online]. 2011, **226**(1), 95–109. ISSN 09544097. doi:10.1177/0954409711408774
- [21] JAFFE, Daniel, Justin PUTZ, Greg HOF, Gordon HOF, Jonathan HEE, Dee Ann LOMMERS-JOHNSON, Francisco GABELA, Juliane L. FRY, Benjamin AYRES, Makoto KELP a Madison MINSK. Diesel particulate matter and coal dust from trains in the Columbia River Gorge, Washington State, USA. *Atmospheric Pollution Research* [online]. 2015, **6**(6), 946–952. ISSN 13091042. doi:10.1016/j.apr.2015.04.004
- [22] BRAZIL, William, Arthur WHITE, Maria NOGAL, Brian CAULFIELD, Alan O’CONNOR a Craig MORTON. Weather and rail delays: Analysis of metropolitan rail in Dublin. *Journal of Transport Geography* [online]. 2017, **59**, 69–76. ISSN 09666923. doi:10.1016/j.jtrangeo.2017.01.008
- [23] WHITE, Ben, Mike WATSON a Roger LEWIS. A year-round analysis of railway station overruns due to low adhesion conditions. *Proceedings of the Institution of Mechanical Engineers, Part F: Journal of Rail and Rapid Transit* [online]. 2022. ISSN 20413017. doi:10.1177/09544097221117314
- [24] WHITE, Ben a Roger LEWIS. Simulation and understanding the wet-rail phenomenon using twin disc testing. *Tribol. Int.* [online]. 2019, **136**, 475–486. ISSN 0301679X. doi:10.1016/j.triboint.2019.03.067

- [25] BEAGLEY, T. M. a C. PRITCHARD. Wheel/rail adhesion — the overriding influence of water. *Wear* [online]. 1975, **35**(2), 299–313. ISSN 00431648. doi:10.1016/0043-1648(75)90078-2
- [26] BEAGLEY, T. M. The Rheological Properties of Solid Rail Contaminants and their Effect on Wheel/Rail Adhesion. *Proceedings of the Institution of Mechanical Engineers* [online]. 1976, **190**(1), 419–428. ISSN 0020-3483. doi:10.1243/PIME_PROC_1976_190_044_02
- [27] GALAS, R., D. KVARDA, M. OMASTA, I. KRUPKA a M. HARTL. The role of constituents contained in water-based friction modifiers for top-of-rail application. *TRIBOLOGY INTERNATIONAL* [online]. nedatováno, **117**, 87–97. ISSN 0301-679X. doi:10.1016/j.triboint.2017.08.019
- [28] SHI, L. B., L. MA, J. GUO, Q. Y. LIU, Z. R. ZHOU a W. J. WANG. Influence of low temperature environment on the adhesion characteristics of wheel-rail contact. *Tribology International* [online]. 2018, **127**, 59–68. ISSN 0301-679X. doi:10.1016/J.TRIBOINT.2018.05.037
- [29] GUTSULYAK, Dmitry V., Louisa J. E. STANLAKE a Hao QI. Twin disc evaluation of third body materials in the wheel/rail interface. <https://doi.org/10.1080/17515831.2020.1829878> [online]. 2020, **15**(2), 115–126. ISSN 1751584X. doi:10.1080/17515831.2020.1829878
- [30] FORERO-ORTIZ, Edwar, Eduardo MARTÍNEZ-GOMARIZ, Manuel Cañas PORCUNA, Luca LOCATELLI a Beniamino RUSSO. Flood Risk Assessment in an Underground Railway System under the Impact of Climate Change—A Case Study of the Barcelona Metro. *Sustainability* [online]. 2020, **12**(13). ISSN 2071-1050. doi:10.3390/su12135291
- [31] NAGASE, K. A Study of Adhesion Between the Rails and Running Wheels on Main Lines: Results of Investigations by Slipping Adhesion Test Bogie. *Proceedings of the Institution of Mechanical Engineers, Part F: Journal of Rail and Rapid Transit* [online]. 1989, **203**(1), 33–43. ISSN 0954-4097. doi:10.1243/PIME_PROC_1989_203_206_02
- [32] HARRISON, Harold. Producing and Measuring the 3rd Body Layer. In: *2020 Joint Rail Conference* [online]. B.m.: American Society of Mechanical Engineers, 2020, s. ISBN 978-0-7918-8358-7. doi:10.1115/JRC2020-8095
- [33] KEMPKA, Reuben, Robert FALCONER, Dmitry GUTSULYAK a Roger LEWIS. Effects of oxide and water on friction of rail steel-new test method and friction mapping [online]. 2020. doi:10.1080/17515831.2020.1765611
- [34] GODET, Maurice. The third-body approach: A mechanical view of wear. *Wear* [online]. 1984, **100**(1–3), 437–452. ISSN 00431648. doi:10.1016/0043-1648(84)90025-5
- [35] DESCARTES, S., C. DESRAYAUD, E. NICCOLINI a Y. BERTHIER. Presence and role of the third body in a wheel–rail contact. *Wear* [online]. 2005, **258**(7–8), 1081–1090. ISSN 00431648. doi:10.1016/j.wear.2004.03.068
- [36] BERTHIER, Y., S. DESCARTES, M. BUSQUET, E. NICCOLINI, C. DESRAYAUD, L. BAILLET a M. C. BAIETTO-DUBOURG. The role and effects of the third body in the wheel-rail interaction. *Fatigue and Fracture of Engineering Materials and Structures* [online]. 2004, **27**(5), 423–436. ISSN 8756-758X. doi:10.1111/j.1460-2695.2004.00764.x
- [37] TRUMMER, Gerald, Zing Siang LEE, Roger LEWIS a Klaus SIX. Modelling of Frictional Conditions in the Wheel–Rail Interface Due to Application of Top-of-Rail Products. *Lubricants* [online]. 2021, **9**(10). ISSN 2075-4442. doi:10.3390/lubricants9100100
- [38] TRUMMER, G., L. E. BUCKLEY-JOHNSTONE, P. VOLTR, A. MEIERHOFER, R. LEWIS a K. SIX. Wheel-rail creep force model for predicting water induced low adhesion phenomena. *Tribology International* [online]. 2017, **109**, 409–415. ISSN 0301679X. doi:10.1016/j.triboint.2016.12.056
- [39] MARIAN, Max, Marcel BARTZ, Sandro WARTZACK a Andreas ROSENKRANZ. Non-Dimensional Groups, Film Thickness Equations and Correction Factors for Elastohydrodynamic

- Lubrication: A Review. *Lubricants* [online]. 2020, **8**(10). ISSN 2075-4442. doi:10.3390/lubricants8100095
- [40] ESFAHANIAN, M. a B. J. HAMROCK. Fluid-Film Lubrication Regimes Revisited. *Tribology Transactions* [online]. 1991, **34**(4), 628–632. ISSN 1040-2004. doi:10.1080/10402009108982081
- [41] HAMROCK, B. J. a D. DOWSON. Isothermal Elastohydrodynamic Lubrication of Point Contacts: Part III—Fully Flooded Results. *Journal of Lubrication Technology* [online]. 1977, **99**(2), 264–275. ISSN 0022-2305. doi:10.1115/1.3453074
- [42] CHEN, H, A YOSHIMURA a T OHYAMA. Numerical analysis for the influence of water film on adhesion between rail and wheel. *Proceedings of the Institution of Mechanical Engineers, Part J: Journal of Engineering Tribology* [online]. 1998, **212**(5), 359–368. ISSN 1350-6501. doi:10.1243/1350650981542173
- [43] WU, Bing, Ming CHEN, Tao WU, Zefeng WEN a Xuesong JIN. A simple 3-dimensional model to analyse wheel-rail adhesion under wet condition. *Lubrication Science* [online]. 2018, **30**(2), 45–55. ISSN 09540075. doi:10.1002/lis.1402
- [44] ISHIZAKA, Kei, Stephen R. LEWIS a Roger LEWIS. The low adhesion problem due to leaf contamination in the wheel/rail contact: Bonding and low adhesion mechanisms. *Wear* [online]. 2017, **378–379**, 183–197. ISSN 0043-1648. doi:10.1016/J.WEAR.2017.02.044
- [45] OLOFSSON, U. a K. SUNDVALL. Influence of leaf, humidity and applied lubrication on friction in the wheel-rail contact: pin-on-disc experiments. *Proceedings of the Institution of Mechanical Engineers, Part F: Journal of Rail and Rapid Transit* [online]. 2004, **218**(3), 235–242. ISSN 09544097. doi:10.1243/0954409042389364
- [46] ISHIZAKA, Kei, Stephen R. LEWIS, Deborah HAMMOND a Roger LEWIS. Chemistry of black leaf films synthesised using rail steels and their influence on the low friction mechanism. *RSC Advances* [online]. 2018, **8**(57), 32506–32521. ISSN 2046-2069. doi:10.1039/C8RA06080K
- [47] OLOFSSON, U. A multi-layer model of low adhesion between railway wheel and rail. *Proceedings of the Institution of Mechanical Engineers, Part F: Journal of Rail and Rapid Transit* [online]. 2007, **221**(3), 385–389. ISSN 0954-4097. doi:10.1243/09544097JRRT111
- [48] ALTURBEH, Hamid, Roger LEWIS, Klaus SIX, Gerald TRUMMER a Julian STOW. Improved modelling of trains braking under low adhesion conditions. *Tribology - Materials, Surfaces & Interfaces* [online]. 2020, **14**(3), 131–141. ISSN 1751-5831. doi:10.1080/17515831.2020.1720379
- [49] SKIPPER, William A., Anup CHALISEY a Roger LEWIS. A review of railway sanding system research: adhesion restoration and leaf layer removal. *Tribology - Materials, Surfaces & Interfaces* [online]. 2018, **12**(4), 237–251. ISSN 1751-5831. doi:10.1080/17515831.2018.1542791
- [50] WHITE, Ben, Jack HYLAND-KNIGHT a Roger LEWIS. Assessing the effectiveness of traction gels using full-scale and field testing. *Proceedings of the Institution of Mechanical Engineers, Part F: Journal of Rail and Rapid Transit* [online]. nedatováno. ISSN 0954-4097. doi:10.1177/0954409720953943
- [51] LANIGAN, Joseph L., Peter KRIER, Luke Buckley JOHNSTONE, Benjamin WHITE, Paul FERRIDAY a Roger LEWIS. Field trials of a methodology for locomotive brake testing to assess friction enhancement in the wheel/rail interface using a representative leaf layer. *Proceedings of the Institution of Mechanical Engineers, Part F: Journal of Rail and Rapid Transit* [online]. 2021, **235**(9), 1053–1064. ISSN 0954-4097. doi:10.1177/0954409720973135
- [52] ZHU, Yi, Ulf OLOFSSON a Rickard NILSSON. A field test study of leaf contamination on railhead surfaces. *Proceedings of the Institution of Mechanical Engineers, Part F: Journal of Rail and Rapid Transit* [online]. 2013, **228**(1), 71–84. ISSN 0954-4097. doi:10.1177/0954409712464860

- [53] ZHU, Yi. The influence of iron oxides on wheel–rail contact: a literature review. *Proc. Inst. Mech. Eng. F* [online]. 2018, **232**(3), 734–743. ISSN 20413017. doi:10.1177/0954409716689187
- [54] ZHU, Y., X. CHEN, W. WANG a H. YANG. A study on iron oxides and surface roughness in dry and wet wheel–rail contacts. *Wear* [online]. 2015, **328–329**, 241–248. ISSN 00431648. doi:10.1016/j.wear.2015.02.025
- [55] WHITE, Ben, Reuben KEMPKA, Peter LAITY, Chris HOLLAND, Klaus SIX, Gerald TRUMMER, Luke BUCKLEY-JOHNSTONE a Roger LEWIS. Iron Oxide and Water Paste Rheology and Its Effect on Low Adhesion in the Wheel/Rail Interface. *Tribology Letters* [online]. 2022, **70**(1), 1–14. ISSN 15732711. doi:10.1007/S11249-021-01549-0/FIGURES/20
- [56] SUZUMURA, Junichi, Yasutomo SONE, Atsushi ISHIZAKI, Daisuke YAMASHITA, Yoshiyuki NAKAJIMA a Makoto ISHIDA. In situ X-ray analytical study on the alteration process of iron oxide layers at the railhead surface while under railway traffic. *Wear* [online]. 2011, **271**(1–2), 47–53. ISSN 00431648. doi:10.1016/j.wear.2010.10.054
- [57] LEHEUP, E. R. a R. E. PENDLEBURY. Unlubricated reciprocating wear of stainless steel with an interfacial air flow. *Wear* [online]. 1991, **142**(2), 351–372. ISSN 00431648. doi:10.1016/0043-1648(91)90174-S
- [58] ZHU, Yi, Ulf OLOFSSON a Hua CHEN. Friction Between Wheel and Rail: A Pin-On-Disc Study of Environmental Conditions and Iron Oxides. *Tribology Letters* [online]. 2013, **52**(2), 327–339. ISSN 1023-8883. doi:10.1007/s11249-013-0220-0
- [59] FOLORUNSO, Morinoye O., Roger LEWIS a Joseph L. LANIGAN. Effects of temperature and humidity on railhead friction levels. *Proceedings of the Institution of Mechanical Engineers, Part F: Journal of Rail and Rapid Transit* [online]. 2022. ISSN 20413017. doi:10.1177/09544097221148236/ASSET/IMAGES/LARGE/10.1177_09544097221148236-FIG8.JPEG
- [60] BUCKLEY-JOHNSTONE, L. E., G. TRUMMER, P. VOLTR, A. MEIERHOFER, K. SIX, D. I. FLETCHER a R. LEWIS. Assessing the impact of small amounts of water and iron oxides on adhesion in the wheel/rail interface using High Pressure Torsion testing. *Tribol. Int.* [online]. 2019, **135**(October 2018), 55–64. ISSN 0301679X. doi:10.1016/j.triboint.2019.02.024
- [61] CHEN, H., T. BAN, M. ISHIDA a T. NAKAHARA. Adhesion between rail/wheel under water lubricated contact. *Wear* [online]. 2002, **253**(1–2), 75–81. ISSN 00431648. doi:10.1016/S0043-1648(02)00085-6
- [62] KVARDA, Daniel, Radovan GALAS, Milan OMASTA, Lu-bing SHI, Haohao DING, Wen-jian WANG, Ivan KRUPKA a Martin HARTL. Asperity-based model for prediction of traction in water-contaminated wheel-rail contact. *Tribology International* [online]. 2021, **157**. ISSN 0301679X. doi:10.1016/j.triboint.2021.106900
- [63] GALAS, Radovan, Milan OMASTA, Lu bing SHI, Haohao DING, Wen jian WANG, Ivan KRUPKA a Martin HARTL. The low adhesion problem: the effect of environmental conditions on adhesion in rolling–sliding contact. *Tribol. Int.* [online]. 2020, **151**(July), 106521. ISSN 0301679X. doi:10.1016/j.triboint.2020.106521
- [64] SKURKA, Simon, Radovan GALAS, Milan OMASTA, Bingnan WU, Haohao DING, Wen Jian WANG, Ivan KRUPKA a Martin HARTL. The performance of top-of-rail products under water contamination. *Tribology International* [online]. 2023, **188**, 108872. ISSN 0301-679X. doi:10.1016/J.TRIBOINT.2023.108872
- [65] THORNES, J. E. a B. W. DAVIS. Mitigating the impact of weather and climate on railway operations in the UK. In: *ASME/IEEE Joint Railroad Conference* [online]. B.m.: ASME, 2002, s. 29–38. ISBN 0-7803-7452-5. doi:10.1109/RRCON.2002.1000089

- [66] KOETSE, Mark J. a Piet RIETVELD. The impact of climate change and weather on transport: An overview of empirical findings. *Transportation Research Part D: Transport and Environment* [online]. 2009, **14**(3), 205–221. ISSN 13619209. doi:10.1016/j.trd.2008.12.004
- [67] STIPANOVIC, Irina, Herbert ter MAAT, Andreas HARTMANN a Geert DEWULF. *Risk Assessment Of Climate Change Impacts On Railway*. Colorado: Engineering Project Organization Conference. 2013
- [68] LEVIÄKANGAS, P., A. TUOMINEN, R. MOLARIUS a J. LUDVIGSEN. *Extreme weather impacts on transport systems*. B.m.: EU_EWENT- Extreme Weather impacts on European Networks of Transport. 2014
- [69] CHINOWSKY, Paul, Jacob HELMAN, Sahil GULATI, James NEUMANN a Jeremy MARTINICH. Impacts of climate change on operation of the US rail network. *Transport Policy* [online]. 2019, **75**, 183–191. ISSN 0967070X. doi:10.1016/j.tranpol.2017.05.007
- [70] KIMURA, Yoshitsugu a Kazumi ORADA. Lubricating Properties of Oil-In-Water Emulsions. <http://dx.doi.org/10.1080/10402008908981921> [online]. 2008, **32**(4), 524–531. ISSN 1547397X. doi:10.1080/10402008908981921
- [71] FUJITA, Noriki, Yukio KIMURA, Koji KOBAYASHI, Yosuke AMANUMA a Yasuhiro SODANI. Estimation model of plate-out oil film in high-speed tandem cold rolling. *Journal of Materials Processing Technology* [online]. 2015, **219**, 295–302. ISSN 0924-0136. doi:10.1016/J.JMATPROTEC.2015.01.002
- [72] BENNER, James J., Farshid SADEGHI, Michael R. HOEPRICH a Mark C. FRANK. Lubricating properties of water in oil emulsions. *Journal of Tribology* [online]. 2006, **128**(2), 296–311. ISSN 07424787. doi:10.1115/1.2164464
- [73] WILSON, W. R. D., Y. SAKAGUCHI a S. R. SCHMID. A dynamic concentration model for lubrication with oil-in-water emulsions. *Wear* [online]. 1993, **161**(1–2), 207–212. ISSN 0043-1648. doi:10.1016/0043-1648(93)90471-W
- [74] CHIU, Y. P. An Analysis and Prediction of Lubricant Film Starvation in Rolling Contact Systems. <http://dx.doi.org/10.1080/05698197408981435> [online]. 2008, **17**(1), 22–35. ISSN 05698197. doi:10.1080/05698197408981435
- [75] ZHANG, Chaoqun a Masahiro FUJII. Influence of Wettability and Mechanical Properties on Tribological Performance of DLC Coatings under Water Lubrication. *Journal of Surface Engineered Materials and Advanced Technology* [online]. 2015, **05**(03), 110–123. ISSN 2161-4881. doi:10.4236/jsemat.2015.53013
- [76] LIU, Xiang, Jintao WANG, Lu HUANG, Jingyue ZHANG, Changhong XU, Lin TONG a Dan GUO. Direct observation of the impact of water droplets on oil replenishment in EHD lubricated contacts. *Friction 2020 10:3* [online]. 2021, **10**(3), 388–397. ISSN 2223-7704. doi:10.1007/S40544-020-0466-0
- [77] CYRIAC, F., P. M. LUGT a R. BOSMAN. Impact of Water on the Rheology of Lubricating Greases. <http://dx.doi.org/10.1080/10402004.2015.1107929> [online]. 2016, **59**(4), 679–689. ISSN 1547397X. doi:10.1080/10402004.2015.1107929
- [78] HUDEDAGADDI, Channabasappa B., Anirudh G. RAGHAV, Angela M. TORTORA a Deepak H. VEEREGOWDA. Water molecules influence the lubricity of greases and fuel. *Wear* [online]. 2017, **376–377**, 831–835. ISSN 0043-1648. doi:10.1016/J.WEAR.2017.02.002
- [79] CYRIAC, F., P. M. LUGT, R. BOSMAN a C. H. VENNER. Impact of Water on EHL Film Thickness of Lubricating Greases in Rolling Point Contacts. *Tribology Letters* [online]. 2016, **61**(3), 1–8. ISSN 10238883. doi:10.1007/S11249-016-0642-6/TABLES/3
- [80] LI, Qun, Shu yue ZHANG, Bing nan WU, Qiang LIN, Hao hao DING, Radovan GALAS, Daniel KVARDA, Milan OMASTA, Wen jian WANG a Ze feng WEN. Analysis on the effect of

starved elastohydrodynamic lubrication on the adhesion behavior and fatigue index of wheel-rail contact. *Wear* [online]. 2022, **510–511**, 204506. ISSN 0043-1648. doi:10.1016/J.WEAR.2022.204506

[81] SKIPPER, W. A., A. CHALISEY a R. LEWIS. A review of railway sanding system research: Wheel/rail isolation, damage, and particle application. *Proceedings of the Institution of Mechanical Engineers, Part F: Journal of Rail and Rapid Transit* [online]. 2020, **234**(6), 567–583. ISSN 0954-4097. doi:10.1177/0954409719851634

[82] DESCARTES, S., A. SAULOT, C. GODEAU, S. BONDEUX, C. DAYOT a Y. BERTHIER. Wheel flange/rail gauge corner contact lubrication: Tribological investigations. *Wear* [online]. 2011, **271**(1–2), 54–61. ISSN 00431648. doi:10.1016/j.wear.2010.10.019

[83] LEWIS, R. a R. S. DWYER-JOYCE. Wear at the wheel/rail interface when sanding is used to increase adhesion. *Proceedings of the Institution of Mechanical Engineers, Part F: Journal of Rail and Rapid Transit* [online]. 2006, **220**(1), 29–41. ISSN 09544097. doi:10.1243/095440905X33260

[84] ARIAS-CUEVAS, Oscar, Zili LI a Roger LEWIS. A laboratory investigation on the influence of the particle size and slip during sanding on the adhesion and wear in the wheel–rail contact. *Wear* [online]. 2011, **271**(1–2), 14–24. ISSN 00431648. doi:10.1016/j.wear.2010.10.050

[85] ARIAS-CUEVAS, O., Z. LI a R. LEWIS. Investigating the Lubricity and Electrical Insulation Caused by Sanding in Dry Wheel–Rail Contacts. *Tribology Letters* [online]. 2010, **37**(3), 623–635. ISSN 10238883. doi:10.1007/s11249-009-9560-1

[86] LEWIS, R., R. S. DWYER-JOYCE a J. LEWIS. Disc machine study of contact isolation during railway track sanding. *Proceedings of the Institution of Mechanical Engineers, Part F: Journal of Rail and Rapid Transit* [online]. 2003, **217**(1), 11–24. ISSN 0954-4097. doi:10.1243/095440903762727311

[87] FRIDELL, Erik, Martin FERM a Anders EKBERG. Emissions of particulate matters from railways – Emission factors and condition monitoring. *Transportation Research Part D: Transport and Environment* [online]. 2010, **15**(4), 240–245. ISSN 1361-9209. doi:10.1016/J.TRD.2010.02.006

[88] LEWIS, S. R., S. RILEY, D. I. FLETCHER a R. LEWIS. Optimisation of a railway sanding system for optimal grain entrainment into the wheel–rail contact. *Proceedings of the Institution of Mechanical Engineers, Part F: Journal of Rail and Rapid Transit* [online]. 2018, **232**(1), 43–62. ISSN 0954-4097. doi:10.1177/0954409716656220

[89] SUHR, Bettina, William A. SKIPPER, Roger LEWIS a Klaus SIX. Sanded Wheel–Rail Contacts: Experiments on Sand Crushing Behaviour. *Lubricants 2023, Vol. 11, Page 38* [online]. 2023, **11**(2), 38. ISSN 2075-4442. doi:10.3390/LUBRICANTS11020038

[90] HUANG, Wanliang, Xi CAO, Zefeng WEN, Wenjian WANG, Qiyue LIU, Minhao ZHU a Xuesong JIN. A Subscale Experimental Investigation on the Influence of Sanding on Adhesion and Rolling Contact Fatigue of Wheel/Rail Under Water Condition. *Journal of Tribology* [online]. 2016, **139**(011401) [vid. 2024-04-16]. ISSN 0742-4787. doi:10.1115/1.4033100

[91] SHI, L. B., C. WANG, H. H. DING, D. KVARDA, R. GALAS, M. OMASTA, W. J. WANG, Q. Y. LIU a M. HARTL. Laboratory investigation on the particle-size effects in railway sanding: Comparisons between standard sand and its micro fragments: Comparisons between standard sand and its micro fragments. *TRIBOLOGY INTERNATIONAL* [online]. nedatováno, **146**. ISSN 0301-679X. doi:10.1016/j.triboint.2020.106259

[92] SHI, L. B., Q. LI, D. KVARDA, R. GALAS, M. OMASTA, W. J. WANG, J. GUO a Q. Y. LIU. Study on the wheel/rail adhesion restoration and damage evolution in the single application of alumina particles. *WEAR* [online]. nedatováno, **426**, 1807–1819. ISSN 0043-1648. doi:10.1016/j.wear.2019.01.021

- [93] SKIPPER, W. A., S. NADIMI, A. CHALISEY a R. LEWIS. Particle characterisation of rail sands for understanding tribological behaviour. *Wear* [online]. 2019, **432–433**. ISSN 00431648. doi:10.1016/j.wear.2019.202960
- [94] WANG, C., L. B. SHI, H. H. DING, W. J. WANG, R. GALAS, J. GUO, Q. Y. LIU, Z. R. ZHOU a M. OMASTA. Adhesion and damage characteristics of wheel/rail using different mineral particles as adhesion enhancers. *Wear* [online]. 2021, **477**, 203796. ISSN 0043-1648. doi:10.1016/J.WEAR.2021.203796
- [95] EGANA, J. I., J. VINOLAS a N. GIL-NEGRETE. Effect of liquid high positive friction (HPF) modifier on wheel-rail contact and rail corrugation. *Tribology International* [online]. 2005, **38(8)**, 769–774. ISSN 0301679x. doi:10.1016/j.triboint.2004.11.006
- [96] STOCK, Richard, Louisa STANLAKE, Chris HARDWICK, Marcia YU, Donald EADIE a Roger LEWIS. Material concepts for top of rail friction management – Classification, characterisation and application. *Wear* [online]. 2016, **366–367**, 225–232. ISSN 00431648. doi:10.1016/J.WEAR.2016.05.028
- [97] SONG, Jingdong, Lubing SHI, Haohao DING, Radovan GALAS, Milan OMASTA, Wenjian WANG, Jun GUO, Qiyue LIU a Martin HARTL. Effects of solid friction modifier on friction and rolling contact fatigue damage of wheel-rail surfaces. *Friction 2021 10:4* [online]. 2021, **10(4)**, 597–607. ISSN 2223-7704. doi:10.1007/S40544-021-0521-5
- [98] GALAS, R., M. OMASTA, I. KRUPKA a M. HARTL. Laboratory investigation of ability of oil-based friction modifiers to control adhesion at wheel-rail interface. *WEAR* [online]. nedatováno, **368**, 230–238. ISSN 0043-1648. doi:10.1016/j.wear.2016.09.015
- [99] GALAS, R., M. OMASTA, M. KLAPKA, S. KAEWUNRUEN, I. KRUPKA a M. HARTL. Case study: The influence of oil-based friction modifier quantity on tram braking distance and noise. *Tribology in Industry* [online]. 2017, **39(2)**, 198–206. ISSN 0354-8996. doi:10.24874/ti.2017.39.02.06
- [100] *Research methodology for evaluation of top-of-rail friction management in Australian heavy haul networks - Maksym Spiryagin, Mojibul Sajjad, Dwayne Nielsen, Yan Quan Sun, Dhamodharan Raman, Gopinath Chattopadhyay, 2014* [online]. [vid. 2024-04-17]. <https://journals.sagepub.com/doi/10.1177/0954409714539943>
- [101] LU, Xin, Tony W MAKOWSKY, Donald T EADIE, Kevin OLDKNOW, Jilian XUE, Jinzhong JIA, Guibao LI, Xianhong MENG, Yude XU a Yu ZHOU. Friction management on a Chinese heavy haul coal line. *Proceedings of the Institution of Mechanical Engineers, Part F: Journal of Rail and Rapid Transit* [online]. 2012, **226(6)**, 630–640. ISSN 0954-4097. doi:10.1177/0954409712447170
- [102] LUNDBERG, Jan, Matti RANTATALO, Christina WANHAINEN a Johan CASSELGREN. Measurements of friction coefficients between rails lubricated with a friction modifier and the wheels of an IORE locomotive during real working conditions. *Wear* [online]. 2015, **324–325**, 109–117. ISSN 0043-1648. doi:10.1016/j.wear.2014.12.002
- [103] EADIE, Donald T., Marco SANTORO, Kevin OLDKNOW a Yasushi OKA. Field studies of the effect of friction modifiers on short pitch corrugation generation in curves. *Wear* [online]. 2008, **265(9–10)**, 1212–1221. ISSN 00431648. doi:10.1016/j.wear.2008.02.028
- [104] EADIE, D. T. a M. SANTORO. Top-of-rail friction control for curve noise mitigation and corrugation rate reduction. *Journal of Sound and Vibration* [online]. 2006, **293(3–5)**, 747–757. ISSN 0022460X. doi:10.1016/j.jsv.2005.12.007
- [105] HARMON, M. a R. LEWIS. New laboratory methodologies to analyse the top of rail friction modifier performance across different test scales. *Proceedings of the Institution of Mechanical Engineers, Part F: Journal of Rail and Rapid Transit* [online]. 2021, **235(2)**, 191–200. ISSN 0954-4097. doi:10.1177/0954409720913759

- [106] LEWIS, S. R., R. LEWIS, G. EVANS a L. E. BUCKLEY-JOHNSTONE. Assessment of railway curve lubricant performance using a twin-disc tester. *Wear* [online]. 2014, **314**(1–2), 205–212. ISSN 0043-1648. doi:10.1016/J.WEAR.2013.11.033
- [107] LEWIS, Stephen R, Roger LEWIS, Ulf OLOFSSON, Don T EADIE, John COTTER a Xin LU. Effect of humidity, temperature and railhead contamination on the performance of friction modifiers: Pin-on-disk study. *Proceedings of the Institution of Mechanical Engineers, Part F: Journal of Rail and Rapid Transit* [online]. 2013, **227**(2), 115–127. ISSN 0954-4097. doi:10.1177/0954409712452239
- [108] WHITE, Ben, Zing Siang LEE a Roger LEWIS. Towards a Standard Approach for the Twin Disc Testing of Top-Of Rail Friction Management Products. *Lubricants 2022, Vol. 10, Page 124* [online]. 2022, **10**(6), 124. ISSN 2075-4442. doi:10.3390/LUBRICANTS10060124
- [109] BUCKLEY-JOHNSTONE, L. E., G. TRUMMER, P. VOLTR, K. SIX a R. LEWIS. Full-scale testing of low adhesion effects with small amounts of water in the wheel/rail interface. *Tribol. Int.* [online]. 2020, **141**(June 2019), 105907. ISSN 0301679X. doi:10.1016/j.triboint.2019.105907
- [110] KHAN, Saad Ahmed, Ingemar PERSSON, Jan LUNDBERG a Christer STENSTRÖM. Prediction of top-of-rail friction control effects on rail RCF suppressed by wear. *Wear* [online]. 2017, **380–381**, 106–114. ISSN 0043-1648. doi:10.1016/j.wear.2017.03.010
- [111] SEO, Jung-Won, Hyun-Kyu JUN, Seok-Jin KWON a Dong-Hyeong LEE. Effect of Friction Modifier on Rolling Contact Fatigue and Wear of Wheel and Rail Materials. *Tribology Transactions* [online]. 2017, **61**(1), 19–30. ISSN 1040-2004. doi:10.1080/10402004.2016.1271487
- [112] EVANS, M. D., Z. S. LEE, M. HARMON, K. SIX, A. MEIERHOFER, R. STOCK, D. V. GUTSULYAK a R. LEWIS. Top-of-rail friction modifier performance assessment: High pressure torsion testing; creep force modelling and field validation. *Wear* [online]. 2023, **532–533**, 205073. ISSN 0043-1648. doi:10.1016/j.wear.2023.205073
- [113] KVARDA, Daniel, Radovan GALAS, Milan OMASTA, Martin HARTL, Ivan KRUPKA a Marian DZIMKO. Shear properties of top-of-rail products in numerical modelling. *Proceedings of the Institution of Mechanical Engineers, Part F: Journal of Rail and Rapid Transit* [online]. 2023, **237**(6), 796–805. ISSN 0954-4097. doi:10.1177/09544097221138374
- [114] LEE, Zing Siang, Gerald TRUMMER, Matthew HARMON, Ben WHITE, Klaus SIX a Roger LEWIS. Studying the transfer mechanisms of water based top-of-rail products in a wheel/rail interaction. *Proceedings of the Institution of Mechanical Engineers, Part F: Journal of Rail and Rapid Transit* [online]. 2024, **238**(2), 164–174. ISSN 0954-4097. doi:10.1177/09544097231187679
- [115] *Carry distance of top-of-rail friction modifiers - Saad Ahmed Khan, Jan Lundberg, Christer Stenström,* 2018 [online]. [vid. 2024-04-17]. <https://journals.sagepub.com/doi/10.1177/0954409718772981>
- [116] MAST, Timothy, Yu PAN, Carvel HOLTON a Mehdi AHMADIAN. *Intermediate Distance Testing of Optical Top-of-Rail (TOR) Lubricity Sensors on a Remote-Controlled Rail Cart* [online]. 2021. doi:10.1115/JRC2021-58347
- [117] OMASTA, Milan, Martin MACHATKA, David SMEJKAL, Martin HARTL a Ivan KŘUPKA. Influence of sanding parameters on adhesion recovery in contaminated wheel–rail contact. *Wear* [online]. 2015, **322–323**, 218–225. ISSN 00431648. doi:10.1016/j.wear.2014.11.017
- [118] OMASTA, M., R. GALAS, J. KNAPEK, M. HARTL a I. KRUPKA. Development of an adaptive top-of-rail friction modification system. In: *Institution of Mechanical Engineers - Stephenson Conference: Research for Railways 2017*. 2017, s. 325–332. ISBN 978-1-5108-8295-9.
- [119] EVANS, M., W. A. SKIPPER, L. BUCKLEY-JOHNSTONE, A. MEIERHOFER, K. SIX a R. LEWIS. The development of a high pressure torsion test methodology for simulating wheel/rail

- contacts. *Tribology International* [online]. 2021, **156**, 106842. ISSN 0301-679X. doi:10.1016/j.triboint.2020.106842
- [120] KVARDA, Daniel, Simon SKURKA, Radovan GALAS, Milan OMASTA, Lu bing SHI, Haohao DING, Wen jian WANG, Ivan KRUPKA a Martin HARTL. The effect of top of rail lubricant composition on adhesion and rheological behaviour. *Engineering Science and Technology, an International Journal* [online]. 2022, **35**. ISSN 22150986. doi:10.1016/j.jestch.2022.101100
- [121] ABBASI, Saeed, Ulf OLOFSSON, Yi ZHU a Ulf SELLGREN. Pin-on-disc study of the effects of railway friction modifiers on airborne wear particles from wheel–rail contacts. *Tribology International* [online]. 2013, **60**, 136–139. ISSN 0301679x. doi:10.1016/j.triboint.2012.11.013
- [122] ZHU, Y., Y. LYU a U. OLOFSSON. Mapping the friction between railway wheels and rails focusing on environmental conditions. *Wear* [online]. 2015, **324–325**, 122–128. doi:10.1016/j.wear.2014.12.028
- [123] GALAS, Radovan, Simon SKURKA, Martin VALENA, Daniel KVARDA, Milan OMASTA, Haohao DING, Qiang LIN, Wen-jian WANG, Ivan KRUPKA a Martin HARTL. A benchmarking methodology for top-of-rail products. *Tribology International* [online]. 2023, **189**. ISSN 0301679X. doi:10.1016/j.triboint.2023.108910
- [124] ARIAS-CUEVAS, O., Z. LI, R. LEWIS a E. A. GALLARDO-HERNÁNDEZ. Rolling–sliding laboratory tests of friction modifiers in dry and wet wheel–rail contacts. *Wear* [online]. 2010, **268**(3–4), 543–551. ISSN 00431648. doi:10.1016/j.wear.2009.09.015
- [125] LI, Z., O. ARIAS-CUEVAS, R. LEWIS a E. A. GALLARDO-HERNÁNDEZ. Rolling–Sliding Laboratory Tests of Friction Modifiers in Leaf Contaminated Wheel–Rail Contacts. *Tribology Letters* [online]. 2009, **33**(2), 97–109. ISSN 10238883. doi:10.1007/s11249-008-9393-3
- [126] WANG, Wenjian, Shengjie LI, Haohao DING, Qiang LIN, Radovan GALAS, Milan OMASTA, Enrico MELI, Jun GUO a Qiyue LIU. Wheel/rail adhesion and damage under different contact conditions and application parameters of friction modifier. *Wear* [online]. 2023, **523**. ISSN 00431648. doi:10.1016/j.wear.2023.204870
- [127] CHEN, Hua, Akira NAMURA, Makoto ISHIDA a Tsunamitsu NAKAHARA. Influence of axle load on wheel/rail adhesion under wet conditions in consideration of running speed and surface roughness. *Wear* [online]. 2016, **366–367**, 303–309. ISSN 00431648. doi:10.1016/j.wear.2016.05.012
- [128] BOSSO, N., M. MAGELLI a N. ZAMPIERI. Investigation of adhesion recovery phenomenon using a scaled roller-rig. <https://doi.org/10.1080/00423114.2019.1677922> [online]. 2019, **59**(2), 295–312. ISSN 17445159. doi:10.1080/00423114.2019.1677922
- [129] GUIDOUM, Samy, Pierrick MERINO, Aurélien SAULOT, Yves BERTHIER a Sylvain HERVIEU. Experimental study of the influence of the relative humidity of leaves and their link to adhesion losses in the wheel-rail contact. *Mechanics & Industry* [online]. 2022, **23**, 23. ISSN 2257-7777. doi:10.1051/MECA/2022017
- [130] ZHANG, Pan a Zili LI. Experimental study on the development mechanism of short pitch corrugation using a downscale V-Track test rig. *Tribology International* [online]. 2023, **180**, 108293. ISSN 0301-679X. doi:10.1016/j.triboint.2023.108293
- [131] ZHANG, Weihua, Jianzheng CHEN, Xuejie WU a Xuesong JIN. Wheel/rail adhesion and analysis by using full scale roller rig. *Wear* [online]. 2002, **253**(1), CM2000 S.I., 82–88. ISSN 0043-1648. doi:10.1016/S0043-1648(02)00086-8
- [132] BUCKLEY-JOHNSTONE, L, M HARMON, R LEWIS, C HARDWICK a R STOCK. A comparison of friction modifier performance using two laboratory test scales. *Proceedings of the Institution of Mechanical Engineers, Part F: Journal of Rail and Rapid Transit* [online]. 2019, **233**(2), 201–210. ISSN 0954-4097. doi:10.1177/0954409718787045

- [133] LEWIS, S.R., S. RILEY, D.I. FLETCHER a R. LEWIS. Optimisation of a Railway Sanding System: Adhesion Tests. *International Journal of Railway Technology* [online]. 2017, **6**(2), 87–98. ISSN 2049-5358. doi:10.4203/ijrt.6.2.5
- [134] SHRESTHA, Sundar, Qing WU a Maksym SPIRYAGIN. Review of adhesion estimation approaches for rail vehicles. *International Journal of Rail Transportation* [online]. 2018, **7**(2), 79–102. ISSN 2324-8378. doi:10.1080/23248378.2018.1513344
- [135] LEWIS, S. R., R. LEWIS a U. OLOFSSON. An alternative method for the assessment of railhead traction. *Wear* [online]. 2011, **271**(1), Proceedings of the 8th International Conference on Contact Mechanics and Wear of Rail / Wheel Systems, Florence, 2009, 62–70. ISSN 0043-1648. doi:10.1016/j.wear.2010.10.035
- [136] LEWIS, Roger, Stephen R LEWIS, Yi ZHU, Saeed ABBASI a Ulf OLOFSSON. The modification of a slip resistance meter for measurement of railhead adhesion. *Proceedings of the Institution of Mechanical Engineers, Part F: Journal of Rail and Rapid Transit* [online]. 2013, **227**(2), 196–200. ISSN 0954-4097. doi:10.1177/0954409712455147
- [137] HARRISON, Harold. The development of a low creep regime, hand-operated tribometer. *Wear* [online]. 2008, **265**(9–10), 1526–1531. ISSN 0043-1648. doi:10.1016/J.WEAR.2008.03.028
- [138] HARMON, M., J. F. SANTA, J. A. JARAMILLO, A. TORO, A. BEAGLES a R. LEWIS. Evaluation of the coefficient of friction of rail in the field and laboratory using several devices [online]. 2020. doi:10.1080/17515831.2020.1712111
- [139] AREIZA, Y. A., S. I. GARCÉS, J. F. SANTA, G. VARGAS a A. TORO. Field measurement of coefficient of friction in rails using a hand-pushed tribometer. *Tribology International* [online]. 2015, **82**(PB), 274–279. ISSN 0301-679X. doi:10.1016/J.TRIBOINT.2014.08.009
- [140] SPIRYAGIN, Maksym, Harold HARRISON, Qing WU, Dwayne NIELSEN, Colin COLE, Peter WOLFS, Chris BOSOMWORTH a Mark HAYMAN. Locomotive Adhesion Control + Rail Friction Field Measurements = ? In: *Advances in Dynamics of Vehicles on Roads and Tracks* [online]. Cham: Springer International Publishing, 2020, s. 433–441. ISBN 978-3-030-38076-2. doi:10.1007/978-3-030-38077-9_51
- [141] SPIRYAGIN, Maksym, Ingemar PERSSON, Mark HAYMAN, Qing WU, Yan Quan SUN, Dwayne NIELSEN, Chris BOSOMWORTH a Colin COLE. Friction measurement and creep force modelling methodology for locomotive track damage studies. *Wear* [online]. 2019, **432–433**, 202932. ISSN 0043-1648. doi:10.1016/j.wear.2019.202932
- [142] PERSSON, Ingemar, Maksym SPIRYAGIN a Carlos CASANUEVA. Influence of non-dry condition creep curves in switch negotiation. *Vehicle System Dynamics* [online]. 2023, **61**(3), 892–904. ISSN 0042-3114. doi:10.1080/00423114.2022.2037668
- [143] LIU, Xiaogang a Changbin XIAO. Investigation of the generation mechanism of squeal noise under non-negative damping conditions: <https://doi.org/10.1177/0954409720966467> [online]. 2020, **235**(7), 887–897. ISSN 20413017. doi:10.1177/0954409720966467
- [144] LIU, Sheng, Uditha De SILVA, Da CHEN, Andrew C. LESLIE a Paul A. MEEHAN. Investigation of wheel squeal noise under mode coupling using two-disk testrig experiments. *Wear* [online]. 2023, **530–531**. ISSN 00431648. doi:10.1016/j.wear.2023.205035
- [145] MEEHAN, Paul A. Prediction of wheel squeal noise under mode coupling. *Journal of Sound and Vibration* [online]. 2020, **465**, 115025. ISSN 0022-460X. doi:10.1016/J.JSV.2019.115025
- [146] MEEHAN, Paul A. a Xiaogang LIU. Wheel squeal noise control under water-based friction modifiers based on instantaneous rolling contact mechanics. *Wear* [online]. 2019, **440–441**, 203052. ISSN 0043-1648. doi:10.1016/J.WEAR.2019.203052
- [147] OMASTA, Milan, Václav NAVRÁTIL, Tomáš GABRIEL, Radovan GALAS a Milan KLAPKA. Design and development of a twin disc test rig for the study of squeal noise from the

wheel – rail interface. *Applied Engineering Letters* [online]. 2022, **7**(1), 10–16. ISSN 24664847. doi:10.18485/AELETTERS.2022.7.1.2

[148] VALENA, Martin, Milan OMASTA, Daniel KVARDA, Radovan GALAS, Ivan KRUPKA a Martin HARTL. An approach for the creep-curve assessment using a new rail tribometer. *Tribology International* [online]. 2024, **191**. ISSN 0301679X. doi:10.1016/j.triboint.2023.109153

LIST OF FIGURES AND GRAPHS

Fig. 1 Issues related to the wheel-rail interface [1]	1
Fig. 2 Classification of various wheel-rail interface contaminants [1].....	3
Fig. 3 Summary of experimental reports of sudden friction drop in concentrated contacts contaminated with liquid-solid suspension [25–29].....	4
Fig. 4 Stribeck curve describing various lubricating regimes in water-contaminated contact [1]	5
Fig. 5 Water film thickness interferograms [62]	10
Fig. 6 Water film thickness measurement compared with prediction [62].....	10
Fig. 7 Preparation of leaf-contaminated condition on test sample [63].....	11
Fig. 8 Effect of RH and temperature on CoA for clean disc (a) and contaminated disc (b) [63].....	11
Fig. 9 Discussed mechanisms: a) Fluid-film regime, b) Starved fluid-film regime, c) Mixed regime. Modified from [64].....	12
Fig. 10 Wheel-rail interface and relevant friction management techniques	13
Fig. 11 Research questions in optimization of wheel-rail sanding parameters	15
Fig. 12 Main questions connected with application of TOR lubricants	15
Fig. 13 Investigation of sanding parameters in the leaf-contaminated wheel-rail contact using twin-disc approach; (a) 1 m/s; (b) 3 m/s, modified from [117]	17
Fig. 14 Evolution of CoA and disc surface after the application of TOR lubricant, modified from [118]	18
Fig. 15 CoA rate as a function of sliding speed and applied TOR lubricant quantity, modified from [118]	18
Fig. 16 Scheme of algorithms of a developed control system for TOR products application, modified from [118]	19
Fig. 17 Field tests towards the optimization of application amount to prevent extension in braking distance [99]	19
Fig. 18 Various approaches for field measurement of wheel-rail coefficient of adhesion.....	21
Fig. 19 Experimental facility for the research into wheel-rail tribology	22
Fig. 20 Implementation of the dynamic model [147].....	23
Fig. 21 Twin-disc test rig with a real tram wheel to study squealing noise	24
Fig. 22 BUT rail tribometer.....	24
Fig. 23 Typical experimental results and theoretical fits under various contact conditions, modified from [148]	25

Wheel-rail interface under extreme conditions

8

Milan Omasta^a and Hua Chen^b

^aBrno University of Technology, Brno, Czech Republic, ^bRailway Technical Research Institute, Tokyo, Japan

8.1 Introduction into the wheel-rail interface

Wheel-rail interface is essential for the safety and operational performance of rail transport. The contact between steel wheel and steel rail occurs on a small area of approximately 1–2 cm² and this contact zone is responsible for the transfer of nearly all forces between the train and the track. This is especially important when traction and braking are carried out as this contact determines how much the mechanical energy can be transferred from the train to the track.

The issues related to the wheel-rail interface are outlined in Fig. 8.1. This interface represents a complex system whose behavior is influenced by many factors. These are mainly operating conditions such as speed and vertical wheel load, dynamics of rail vehicle and track, maintenance parameters including wheel and rail head profile, surface roughness and materials. Tribological phenomena taking place in the interface determine its behavior. The most important aspect is the ability to transfer traction and braking forces in the longitudinal direction and lateral forces in the perpendicular direction. High contact pressure and shear stress is a source of various types of wear and damage. Rail head and wheel thread are vulnerable to the rolling contact fatigue, wheel flange is exposed to severe sliding wear and the wheel and rail materials undergo cyclic plastic deformation. This interface is also the source of most of the negative effects of rail transport such as rolling and squealing noise and ground-borne vibration.

Wheel-rail interface is a typical open tribological system. This means that the conditions are not stable and well-defined as in the case of the closed system, such as, e.g., a gearbox. The wheel-rail contact is subject to many kinds of environmental influences, especially weather conditions like temperature, humidity and precipitation. These conditions are constantly varying as night and day and different seasons alternate and with a change in the environment in which the train moves. On the other hand, the openness of this system also means that the substances formed in the interface or applied to the contact are dispersed into the surrounding environment. This applies in particular to products for friction management such as wheel flange lubricants, top-of-rail friction modifiers and traction enhancers. There is a growing emphasis on minimizing the negative impact of rail transport through noise and vibration mitigations, soil pollution mitigation and so on.

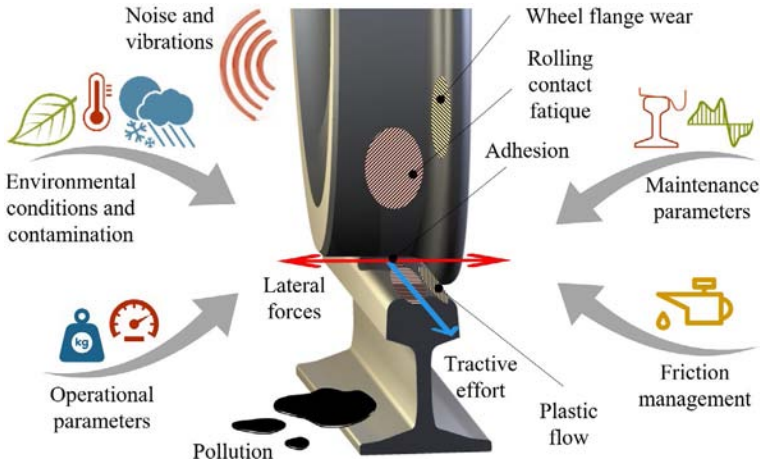


Fig. 8.1 Issues related to the wheel-rail interface.
Credit: Original artwork.

8.2 Basics of the wheel-rail contact

One of the most important aspects of the wheel-rail interface is adhesion. In the rail transport community “adhesion” is defined as the ability of the contact to transfer tangential forces. In the longitudinal direction, these forces allow traction and braking. Schematic representation of a rolling-sliding contact between the rail and the wheel under acceleration is shown in Fig. 8.2. This contact is subject to a normal force F_N representing the force of gravity acting on the wheel. The wheel moves along the rail at velocity v . The wheel rotates with angular velocity ω thanks to torque T . The result is a reaction tangential force F_T acting between the wheel and the rail. Their ratio corresponds to the coefficient of adhesion according to Eq. (8.1). This definition is similar to the coefficient of friction for pure-sliding contact, but the physical meaning is different. Under pure-rolling conditions, circumferential velocity $\omega \times r$ corresponds to the forward velocity v . However, during acceleration, circumferential velocity is higher resulting in sliding velocity in the contact v_s defined using Eq. (8.2). The ratio between the velocity difference and forward velocity is defined as creep or creepage according to Eq. (8.3). When multiplied by 100 we get it in %.

$$\mu = \frac{F_T}{F_N} \quad (8.1)$$

$$v_s = \omega \times r - v \quad (8.2)$$

$$\xi = \frac{v_s}{v} = \frac{\omega \times r - v}{\omega \times r} \quad (8.3)$$

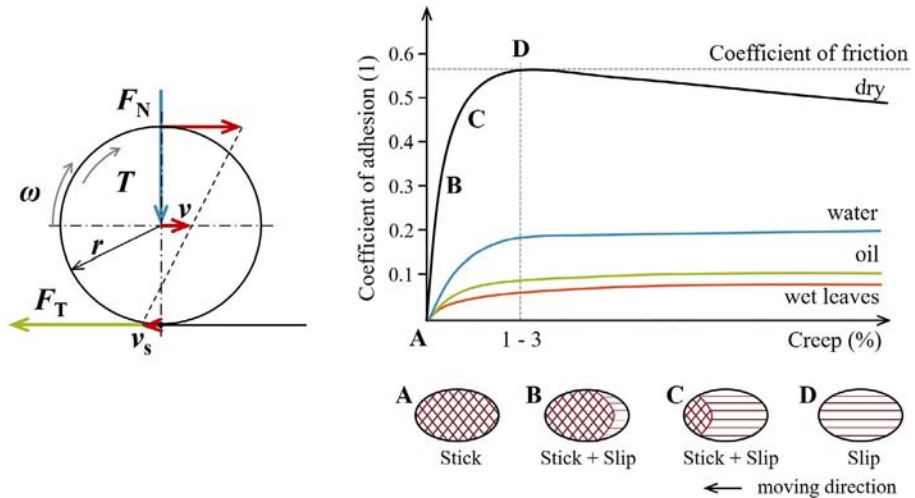


Fig. 8.2 Schematic view of rolling-sliding contact under acceleration and the relationship between the coefficient of adhesion and creep.
Credit: Original artwork.

The relationship between the coefficient of adhesion and the creep is represented by the creep curve, shown in Fig. 8.2. Point A corresponds to pure rolling, where the surfaces are sticking in the whole elastic contact area and no tangential forces are transferred, so the coefficient of friction is zero. When the tangential force appears (point B), the contact is divided into the leading part with a stick and the trailing part where slipping occurs. As the tangential force increases the slipping area extends at the expense of the sticking area (point C). When the coefficient of adhesion reaches saturation point, the stick area disappears, and the contact is fully sliding. At this point, the coefficient of adhesion corresponds to the coefficient of friction. The creep level where the coefficient of adhesion reaches its maximum usually ranges between 1% and 3%. If the applied power exceeded the adhesion limit, wheel slip would occur during acceleration. Similarly, wheel-slide may occur during braking. In both cases, undesirable deterioration of the wheels or rails occurs.

As indicated qualitatively in Fig. 8.2, the shape of the creep curve and maximum value of the coefficient of adhesion strongly depends on the conditions of the contact between the wheel and the rail. The typical value of adhesion coefficient measured using an instrumented train ranges between 0.3 and 0.4 under dry conditions. Water decreases the value to 0.25 and oil to 0.2 [1]. A wide range of field and laboratory devices for friction and adhesion coefficients measurement exists. These tribometers and test rigs are inevitable in the wheel-rail interface research [2], however, their limitations must be considered when interpreting the coefficient of adhesion.

The lowest value of the coefficient of adhesion required for braking is usually given in the range of 0.07–0.15 depending on the specific railroad. For traction, the value is around 0.2. Insufficient adhesion is a typical cause of delays, platform overruns and

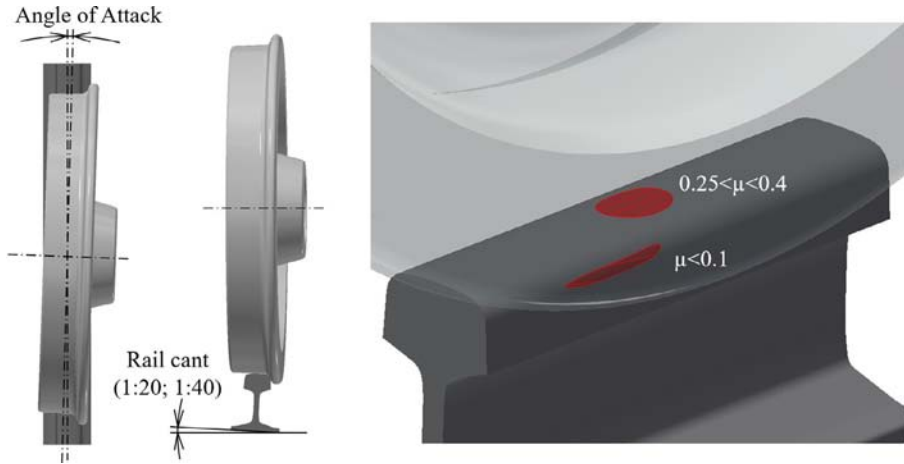


Fig. 8.3 Contact positions in the wheel-rail contact.
Credit: Original artwork.

incidents of Signals Passes at Danger (SPADs). In an extreme case, it leads to wheel burns during acceleration and the formation of wheel flats during sudden braking. On the other hand, too high adhesion/friction results in a higher wear rate and rolling contact fatigue. Higher lateral forces have a negative impact on driving comfort, noise and vibration, risk of flange climb derailment, rail corrugation, and track deterioration. The wheel-rail contact typically occurs in two distinct areas, as shown in Fig. 8.3. At the straight track, the contact appears solely between the wheel tread and the top of the rail. The optimal coefficient of adhesion in this zone is 0.25–0.4. On sharp curves, the contact extends toward the wheel flange and rail gauge. We are talking about two-point contact. A high sliding velocity acts in this contact leading to severe to catastrophic wear [3,4]. So, the lowest possible coefficient of friction is desirable. Maintaining an appropriate adhesion between the wheel and rail is very important concerning safety and efficiency.

Wheel-rail contamination and weather conditions are the most important factors influencing the behavior of the open tribological system. Various substances and materials that are found in the wheel-rail interface are categorized in Fig. 8.4. The first group is substances that naturally originate from tribological processes on the rail or in the interface, namely wear particles from the wheel and the rail and iron oxides and hydroxides that are products of chemical reaction with water and oxygen. Another group can be considered as external contaminants. The most important part covers natural contaminants from the environment like water, snow and fallen leaves. Water can be introduced to the contact through rainfall, moisture condensation, snow melting and flooding. Fallen leaves come from the vegetation along the track and are the most significant cause of low adhesion problems in autumn [5]. The contact can be further contaminated from the environment by the soil and sand, usually carried by the wind in arid and desert areas, and by rock salt or grit used to treat the roads and platforms

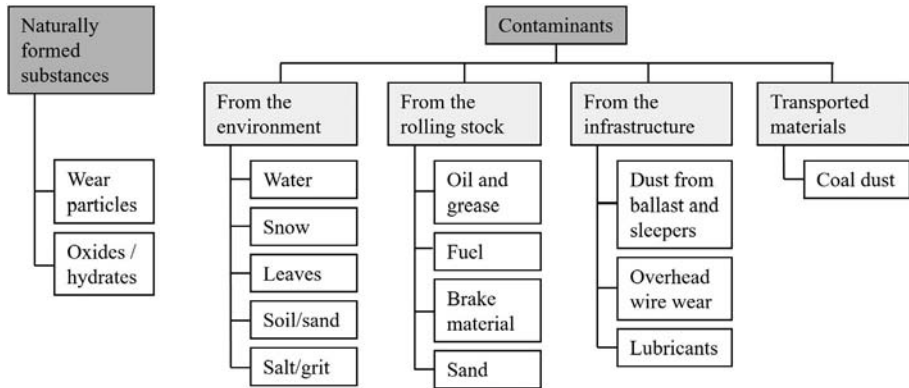


Fig. 8.4 Classification of various contact contaminants.
Credit: Original artwork.

against the winter snow and ice [6]. The source of artificial contaminants is mainly the rail vehicle itself. Operating fluids such as grease, fuel oils and transformers oils pose the greatest risk in terms of the influence on traction and braking. There is a wide range of contamination particles that originates from the other components of the train, such as wear particles from brake pads and brake discs [7]. The sand listed in this category refers to the material used by the rolling stock to restore wheel-rail adhesion. Rail infrastructure can also be a source of contamination. The rail head is exposed to dust from ballast and concrete sleepers, wear particles from overhead wires and a lubricant from way-side lubricators. An example of contamination by the transported medium could be, e.g., coal dust from the trains that carry coal in uncovered rail cars [8]. Understanding the impact and hazards resulting from the contamination is one of the main challenges in the wheel-rail interface research.

8.3 The wheel-rail interface under extreme conditions

8.3.1 *Extreme events and their consequences to the wheel-rail interface*

There is a number of studies reporting the impact of climate changes or extreme weather conditions on railway transport [9–13]. However, these studies remain on global analysis related to the whole infrastructure, rolling stock and asset management. This chapter discusses, how the predicted changes and events affect the behavior of the wheel-rail interface. Table 8.1 gives an overview of the potential impacts of extreme climate events on wheel-rail interface and consequences to the railway service and operation. The consequences are generally determined by the effect of specific contamination or climate condition on the behavior of the wheel-rail interface. So, the following sub-chapters deal in detail with these effects, especially on the adhesion in the wheel-rail interface.

Table 8.1 Overview of the potential impacts of extreme climate events on the wheel-rail interface and consequences to the railway service and operation.

Climate event	Impact	Consequence to the wheel-rail interface	Consequence to service and operation
Heavy rain	Flooding	Water contamination Increased formation of hydroxides	Risk of the low adhesion under high speed Risk of low the adhesion phenomenon
Coastal storm surges and tsunami waves	Coastal flooding	Contamination with saltwater Increased formation of hydroxides	Risk of the low adhesion under high speed Risk of low the adhesion phenomenon
Cold climate and cold waves	Extremely low temperature	Sub-zero temperature	Increased wear a rolling contact fatigue Slower adhesion recovery process
	Snow	Water contamination under sub-zero temperature	Increased wear a rolling contact fatigue
Heatwaves	High ambient and surface temperature	Thermal loading of the wheel and rail	Increased rolling contact fatigue and deterioration
Dessert storms and high winds in arid areas	Contamination by sand and soil	Formation of the third-body layer	Risk of low adhesion due to the “lubrication” action of sand layer Risk of the contact insulation and loss of track circuit function
Extreme winds	Leaf fall contamination	Formation of the third-body layer	Increased abrasive wear Risk of the low adhesion phenomenon Risk of the contact insulation and loss of track circuit function

8.3.2 Water at the wheel-rail contact

Water is one of the most common natural contaminants of the wheel-rail interface. Under normal conditions, water contamination results from rainfall or morning dew. In extreme cases, railway lines can be flooded due to heavy rain and storms, especially in low-lying land with malfunctioning drainage. The threat of flooding is also

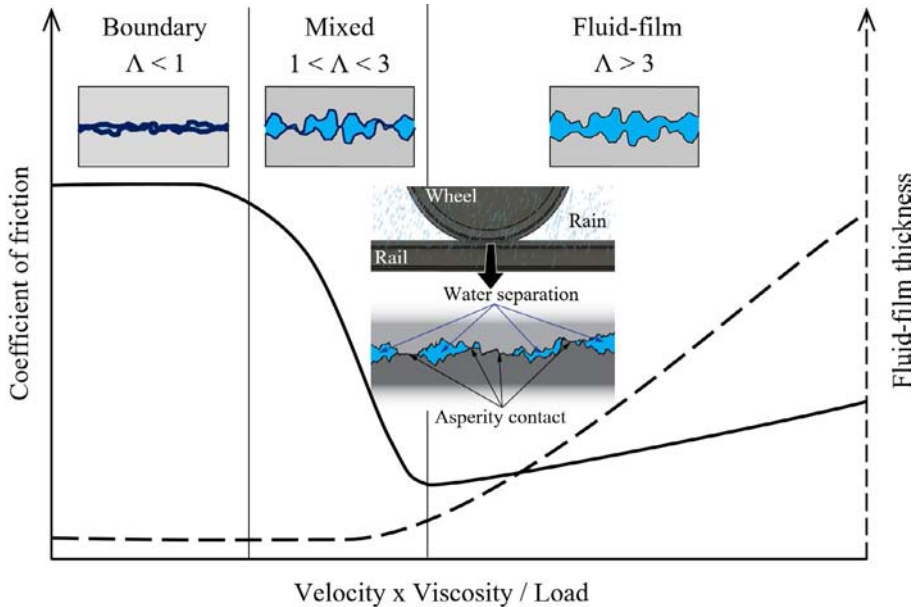


Fig. 8.5 Stribeck curve describing various lubricating regimes.

Credit: Original artwork.

relevant in the underground railway system [14]. In any case, the presence of water has a great influence on adhesion between the rails and running wheels [15].

The effect of water on adhesion in the contact is connected with different mechanisms based on the lubrication regime where the contact operates. Different lubrication regimes are described using a Stribeck's curve in Fig. 8.5. This curve shows qualitatively the coefficient of friction and lubricant-film thickness as a function of dimensionless parameters including velocity, lubricant viscosity, and load. These regimes vary according to the level of surface separation. In the boundary regime, the contact bodies are separated by a boundary friction layer that naturally occurs on the rail in an open environment. As the velocity increases and the sufficient amount of water or other fluid lubricant appears on the rail, the surfaces start to be separated because of the hydrodynamic action of the liquid. In the mixed regime, this separation is only a local while the rest of the contact carried by the surface asperities remains in the boundary regime. The hydrodynamic action increases with velocity, resulting in full separation of the bodies with a full fluid lubricating film and we are talking about fluid-film regime. The action of water in the contact depends on the regime.

8.3.2.1 Boundary lubrication

In the boundary regime, water is unlikely to act in the contact on its own but forms a mixture with other substances and contaminants. Naturally, this is mainly a combination of wear particles. The early experiments by Beagley and Pritchard [16] have

demonstrated that a small amount of water mixed with wear debris forms a lubricating paste that results in a very low friction coefficient (0.05). The decrease in adhesion is more pronounced the less water is applied. This action of water is called “Wet Rail Phenomenon” and is associated with dew on the head of the rail, misty conditions and very light rain [17]. The practical consequence of this phenomenon is that a small amount of water leads to lower adhesion than large amount that washes the contaminants away. This phenomenon usually occurs in the mornings and evenings due to dew formation.

Water is also involved in the formation of a very thin friction layer, hardly visible to the naked eye, often called “third-body layer.” The third-body concept [18] is often used in wheel-rail tribology to describe the behavior of the layer based on its rheology [19,20]. This layer is a result of mechanical, chemical and thermal interactions of the surfaces with the contaminants in the high-pressure rolling-sliding contact. In addition to water and wear particles, other natural contaminants like leaves contribute to its formation. In this case, water often acts as a trigger for the low adhesion problem in an already formed third-body layer [21–26].

8.3.2.2 *Fluid-film lubrication*

In fluid-film regime, liquid water acts as a lubricant between the contacting bodies. The wheel and the rail form a converging–diverging geometry, which together with a sufficient relative velocity creates the conditions for the development of hydrodynamic pressure. Because of the high contact pressure, elastic deformations of the contacting surfaces are of the same order of magnitude as the film thickness separating them. So, we are talking about elastohydrodynamic lubrication (EHL). Someone could look at the analogy to aquaplaning by the tires of a road vehicle when a layer of water builds between the wheels of the vehicle and the road surface, leading to the loss of control. An elastic deformation of compliant rubber tire and lower car weight leads to a low contact pressure in the order of 0.1–1 MPa. This lubrication regime is often referred to as “soft” EHL and the velocity required to develop the hydrodynamic action of water film is relatively low. However, the contact pressure between the steel wheel and rail is much higher, in order of 1 GPa. Under the “hard” EHL regime, the hydrodynamic action of water is usually too low to fully separate the wheel and the rail. The partial separation, however, becomes extremely important, especially for light-weight vehicles operated at high speed.

Water film thickness can be estimated using EHL theory. A wide range of film thickness equations and correction factors was established in last decades for various regimes and conditions [27]. These equations usually represent last-square fit of the results determined using a numerical solution for given parameters. Originally, they were intended and validated for the contacts lubricated with oil whose viscosity is highly dependent on the contact pressure. Piezo-viscosity of water is not as strong, so one option is to consider the isoviscous elastic lubrication regime. This regime is characterized as the regime where the elastic deformation of the contact bodies has a significant contribution to the fluid film, but the pressure in the contact is insufficient to cause a substantial increase in fluid viscosity. Nevertheless, it is also often interpreted as a regime where the pressure is sufficient but the pressure-viscosity

Table 8.2 Empirical equations for the lubricant-film thickness prediction.

Author	Regime and contact	Lubricant-film thickness equation
Esfahanian and Hamrock [28]	Iso-viscous elastic, elliptical	$H_{min} = 8.70U^{0.66}W^{-0.21}(1 - 0.85e^{-31k})$
Hamrock and Dowson [29]	Piezo-viscous elastic, elliptical	$H_{min} = 3.63U^{0.67}W^{-0.073}G^{0.49}(1 - e^{-68k})$
Chen et al. [30]	Piezo-viscous elastic, line	$H_{min} = 2.578U^{0.59}W^{-0.211}G^{0.002}$
Wu et al. [31]	Piezo-viscous elastic, elliptical	$H_{min} = 9.36U^{0.72}W^{-0.29}G^{0.007}(1 - e^{-68k})$

dependence of the lubricant is low. For the elliptical contact, frequently used equation by Esfahanian can be utilized (see Table 8.2), where non-dimensional parameters are given by the following: $H_{min} = \frac{h_{min}}{R_x}$; $U = \frac{\eta_0 v}{ER_x}$; $W = \frac{F}{ER_x^2}$ for point contact and $W = \frac{F_x}{ER_x}$ for elliptical contact; $G = \alpha E$; $k = 1.03 \left(\frac{R_y}{R_x}\right)^{0.64}$.

Another option is to consider water as a piezo-viscous fluid. The dependence of water viscosity on pressure and temperature in the range relevant for the wheel-rail contact was published, e.g., by Bett and Cappi [32] (see Fig. 8.6). Piesoviscosity of fluid is accounted for in film thickness prediction formulas using pressure-viscosity coefficient α . The simple value is not suitable for water because of its anomalous behavior. So, the equivalent values of pressure-viscosity coefficient depending on contact pressure and temperature were calculated [30]. Then, an equation for piezo-viscous elastic regime and elliptical contact, e.g., by Hamrock and Dowson can be used. Specific empirical equations were also developed based on the numerical simulation of the water-lubricated wheel-rail contact. Chen et al. [30] developed a

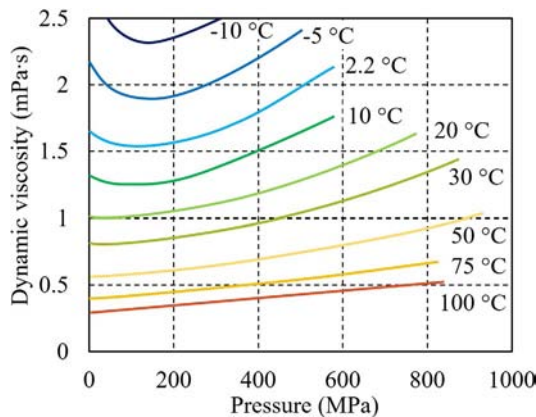


Fig. 8.6 Viscosity of water as a function of temperature and pressure, according to Bett and Cappi [32].

Credit: Adapted from Springer Nature, K. Bett, J. Cappi, Effect of pressure on the viscosity of water, Nature 207 (4997) (1965) 620–621, <https://doi.org/10.1038/207620a0>, copyright (1965).

formula for the line contact using temperature–pressure–viscosity parameters of water according to Bett and Cappi. Recently, similar solution has been extended to 3D simulation [31]. It should be noted that all the predictions are only valid for the smooth surface case and isothermal conditions. The calculated value expresses the film thickness that can be formed under the given conditions if the contact is sufficiently supplied with liquid. If there is not enough water on the rail, the contact is starving and a full liquid film does not develop.

8.3.2.3 Effect of speed

It is well known, that coefficient of adhesion is strongly affected by the train velocity even for dry contact. For the purpose of the effective application of tractive effort, equations predicting the maximum adhesion, i.e., coefficient of friction, as a function of train velocity were developed based on experimentation. These equations describe a curve that is actually the envelope of peaks of adhesion characteristics for different velocities. Well, known equation by Curtius and Kniffler adopted by Deutsche Bahn AG, equation used by the French National Railways (SNCF) and equation developed for high-speed Shinkansen vehicles are summarized in Table 8.3. The equations are available for dry and wet conditions, which usually means the best and the worst case, so the upper and lower limit of peak adhesion.

The comparison of these empirical equations is shown in graph in Fig. 8.7. The curves for wet conditions predict lower adhesion, nevertheless, the differences between the individual predictions are large. It should be noted that the classic Curtius and Kniffler equation is based on adhesion measurement using a measuring train, Ohyama’s equation was determined using a large-sized high-speed rolling contact testing machine with targeted application of water to the contact. It is evident, that the slope of the curves is the same for dry and wet contact, so the effect of velocity is not necessarily associated with a hydrodynamic action of water.

8.3.2.4 Effect of surface roughness

Lubricant-film thickness is often interpreted in relation to surface roughness using a lubrication parameter Λ [33]. This parameter is defined by Eq. (8.4) as the ratio of the corresponding minimum film thickness h_{\min} to the composite surface roughness Rq of the rail and wheel. Although the parameter does not take into account, e.g., deformation of surface asperities in the contact, it can be used for an estimation of the

Table 8.3 Empirical equations for the prediction of the coefficient of adhesion as a function of train velocity.

	Dry	Wet
Deutsche Bahn AG (Curtius–Kniffler)	$\mu = \frac{7.5}{v+44} + 0.161$	$\mu = \frac{7.5}{v+44} + 0.13$
French National Railways (SNCF)	$\mu = 0.33 \cdot \frac{8+0.1v}{8+0.2v}$	$\mu = 0.24 \cdot \frac{8+0.1v}{8+0.2v}$
Japanese Railway (Ohyama)	–	$\mu = \frac{13.6}{v+85}$

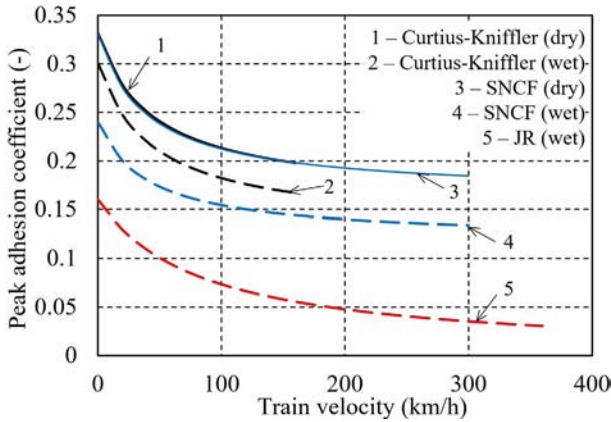


Fig. 8.7 Comparison of empirical equations for the prediction of the coefficient of adhesion as a function of train velocity.

Credit: Original artwork.

lubricating regime according to Fig. 8.5. The figure also shows that for rough surfaces in the mixed regime a part of the load is carried by the contact between surface asperities where boundary lubrication occurs, and a part by hydrodynamic action of fluid film. This is one of the most common assumptions in the theoretical solution of the problem [34].

$$\Lambda = \frac{h_{min}}{\sqrt{Rq_w^2 + Rq_r^2}} \quad (8.4)$$

It is well known that increasing surface roughness moves the lubrication regime toward a boundary lubrication. The effect of surface roughness on wheel-rail adhesion has been extensively studied at RTRI, Japan [35–39]. Experimental results confirm that in the water-lubricated contact the maximum traction coefficient increases with surfaces roughness, as described in Fig. 8.8 [35]. Fig. 8.9 shows results of the theoretical analysis with EHL model and stochastic distribution of the surface asperity heights using Greenwood–Williamson’s model [38]. It is evident and not surprising that the adhesion coefficient increases with an increase of the contact pressure, but the effect of the contact pressure (i.e., the axle load) depends on the surface roughness. For the surfaces with low roughness, the adhesion coefficient slightly increases with the pressure, but for rough surfaces, it decreases significantly. Water film thickness increases with surface roughness, but the effect nearly disappears at high contact pressure. It can be concluded that the effect of contact pressure on the adhesion of the wheel and rail depends on the surface roughness and the running speed of a vehicle [38].

8.3.2.5 Effect of water temperature

Water temperature has been identified as a parameter strongly influencing the adhesion coefficient under water-lubricated conditions, as indicated by the experimental results in Fig. 8.10. A rise in the water temperature causes an increase in the

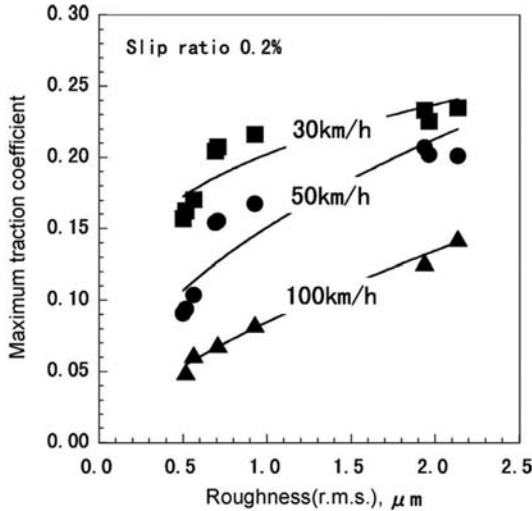


Fig. 8.8 Relationship between the maximum traction coefficient and surface roughness, from Chen et al. [35].

Credit: Reprinted from H. Chen, T. Ban, M. Ishida, T. Nakahara, Experimental investigation of influential factors on adhesion between wheel and rail under wet conditions, *Wear* 265 (9–10) (2008) 1504–1511, <https://doi.org/10.1016/j.wear.2008.02.034>, copyright (2008), with permission from Elsevier.

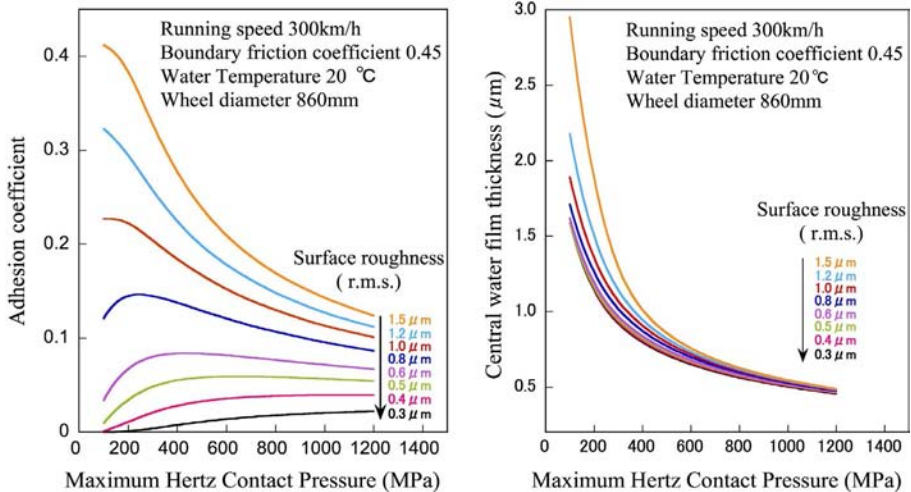


Fig. 8.9 Influences of the contact pressure and the surface roughness on the adhesion coefficient and water film thickness, from Chen et al. [38].

Credit: Reprinted from H. Chen, A. Namura, M. Ishida, T. Nakahara, Influence of axle load on wheel/rail adhesion under wet conditions in consideration of running speed and surface roughness, *Wear* 366–367 (2016) 303–309, <https://doi.org/10.1016/j.wear.2016.05.012>, copyright (2016), with permission from Elsevier.

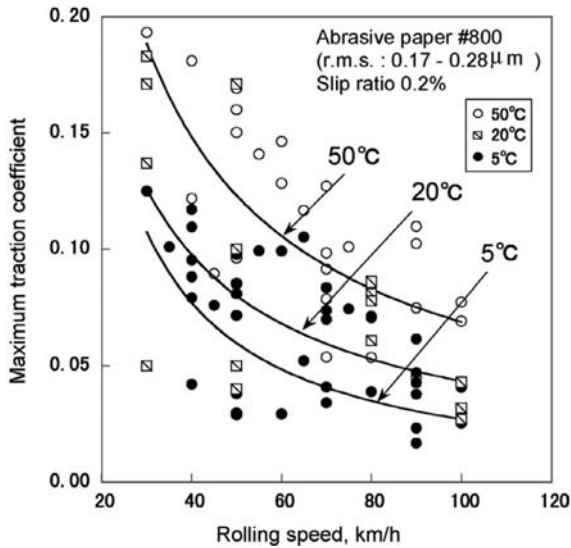


Fig. 8.10 Relationship between maximum traction coefficient and rolling speed at different water temperatures, from Chen et al. [35].

Credit: Reprinted from *Wear*, H. Chen, T. Ban, M. Ishida, T. Nakahara, Experimental investigation of influential factors on adhesion between wheel and rail under wet conditions, *Wear* 265 (9–10) (2008) 1504–1511, <https://doi.org/10.1016/j.wear.2008.02.034>, copyright (2008), with permission from Elsevier.

coefficient of adhesion [35]. Such experimental results are consistent with the theoretical analyses, where the change in water viscosity is considered as the main cause of the effect. On the other hand, recent analysis indicates that the effect is strong also in the boundary regime, where the water viscosity is of less importance. In this regime, the effect of temperature cannot simply be related to the lubrication parameter Λ [39]. The above-mentioned research suggests that under the wet conditions the coefficient of adhesion is maintainable at a relatively high level by raising water temperature or increasing the surface roughness.

8.3.3 Humidity and oxidation

The action of humid air, its temperature and surface oxidation are connected and it is not possible to clearly separate the influence of individual factors. Iron oxides are the most important contaminants occurring naturally in the wheel-rail interface [40,41]. The general designation “iron oxides” includes chemical compounds with different content in Fe cations, oxygen, hydroxyl and water. In situ measurements of rail head oxides have shown that five types of oxides are typically present on a rail head: magnetite (Fe_3O_4), hematite (Fe_2O_3), goethite ($\alpha\text{-FeOOH}$), lepidocrocite ($\gamma\text{-FeOOH}$) and akaganeite (b-FeOOHCl) [42]. Each oxide has different effect on the wheel-rail adhesion; however, usually, several oxides act together. Magnetite, known as “black oxide,” has a tendency to decrease the friction while hematite increases the friction.

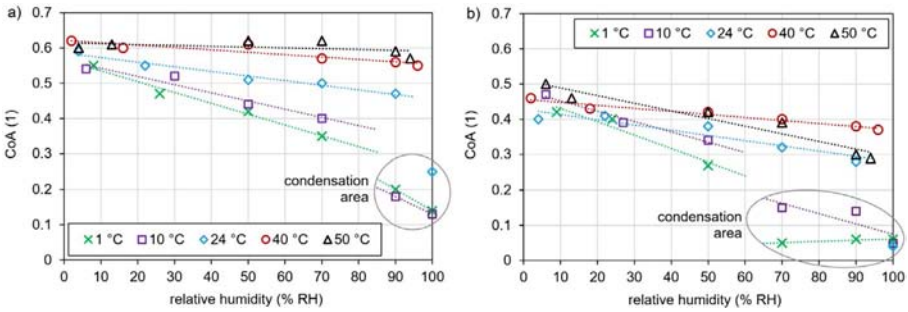


Fig. 8.11 Effect of relative humidity and temperature on coefficient of adhesion for clean disc (A) and contaminated disc (B), from Galas et al. [45].

Credit: Reprinted from Tribology International, R. Galas, M. Omasta, L. Shi, H. Ding, W. Wang, I. Krupka, M. Hartl, The low adhesion problem: the effect of environmental conditions on adhesion in rolling-sliding contact, *Tribol. Int.* 151 (2020), 106521, <https://doi.org/10.1016/j.triboint.2020.106521>, copyright (2020), with permission from Elsevier.

It is believed that under high humidity the normal atmospheric oxidation is inhibited because of the effect of water molecules in the air [43]. If the surface is covered with a thick layer of hydrates (rust), the friction becomes independent of the presence of liquid water [25,26].

Daytime evolution of relative humidity and temperature have a substantial impact on the adhesion coefficient. It has been shown that the coefficient of adhesion reduces from 0.55 to 0.22 with increasing relative humidity, while the effect of temperature is rather negligible [16]. Similar findings were reported from pin-on-disc experiments [24,25,40,44]. The effect of temperature and relative humidity on the coefficient of adhesion in the rolling-sliding contact is shown in Fig. 8.11 [45]. The first graph represents “clean” disc conditions, while the second was determined for the disc contaminated with dry leaf-based layer. In both cases, there is a clear trend in the decrease in adhesion with increasing humidity and decreasing temperature. This abrupt drop in coefficient of adhesion occurs as a result of the softening of the leaf layer due to the small amount of condensation water. Based on the results, the coefficient of adhesion can be predicted using Eqs. (8.5) and (8.6) for the clean and contaminated contact, respectively [45].

$$\mu_{\text{clean}} = 0.5461 + 0.003029 \cdot T - 0.002844 \cdot RH - 3.346 \cdot 10^{-5} \cdot T^2 + 5.401 \cdot 10^{-5} \cdot T \cdot RH \quad (8.5)$$

$$\mu_{\text{contaminated}} = 0.4153 + 0.001587 \cdot T - 0.001662 \cdot RH \quad (8.6)$$

8.3.3.1 Salt environment

Low-lying coastal areas are prone to seawater flooding. The ongoing climate changes are responsible for increasing the exposure of coastal infrastructure to coastal

flooding. Railway infrastructure may be significantly flooded as the result of extremely high tides, coastal storm surges and tsunami waves, causing seawater to spill onto land. Even without such extreme weather phenomena, the salty environment affects tribology of the wheel-rail interface. Generally, salt/water solution increases adhesion level above that for wet conditions. On the other hand, the presence of salt on rail head affects the formation of oxides. Experience from Japan Railways shows that a small amount of β -FeOOH can be found specifically in salty-environment tunnels [46]. This ferric oxyhydroxide provides a low coefficient of friction, so the roll-slip phenomenon can be expected. Increased levels of oxidation together with wet rails may cause significant low adhesion problems [6]. Deposition of saltwater is an important factor initiating corrosion and rail track degradation [47].

8.3.4 Extreme temperatures

8.3.4.1 Extremely high temperature

With changes in the global climate, severe weather events such as heatwaves are increasingly common. Temperature affects the tribological processes by influencing the properties of the contacting surfaces. It should be noted that ambient temperature is only one of the temperature-related effects. The temperature of the steel rails in direct sunlight can be more than 20 °C above ambient air temperature. On the other hand, the temperate required to soften wheel material starts at 200–250 °C. Even much important is the flash temperature acting in the contact under the high pressure and shear stress [48]. Extremely high ambient temperatures cause the critical deterioration processes on railway infrastructure like rail buckling. Heat-related deterioration processes also apply to the wheels [49,50]. However, there are no reports on the risk associated with the adhesion or deterioration specifically in the wheel-rail interface.

8.3.4.2 Sub-zero temperatures

Resilience of railway transport to extremely low temperatures is of increasing interest and importance in various parts of the world. The railway industry faces new challenges as the rail network is extended to cold alpine regions. For example, the high-speed Harbin–Dalian passenger dedicated line in Northeast China is operated at the mean air temperature in the coldest month of about -13.5 to -17.5 °C and an extreme as low as -36.5 °C [51]. The operating temperature at the high-elevation Qinghai-Tibet railway even falls to -45 °C [52]. Other challenges are related to cold waves that occur more frequently and with greater intensity. An example is the February 2021 North American cold wave that brought record-low temperatures to a significant portion of Canada and the United States.

Extremely low temperature influences the behavior of a wide range of track and train equipment depending on the type of asset. From a wheel-rail interface perspective, the effect of sub-zero temperatures on adhesion and wear is important. There are only a few studies dealing with the effects. The effect of sub-zero temperature and various contaminants on adhesion coefficient and wear was recently studied using

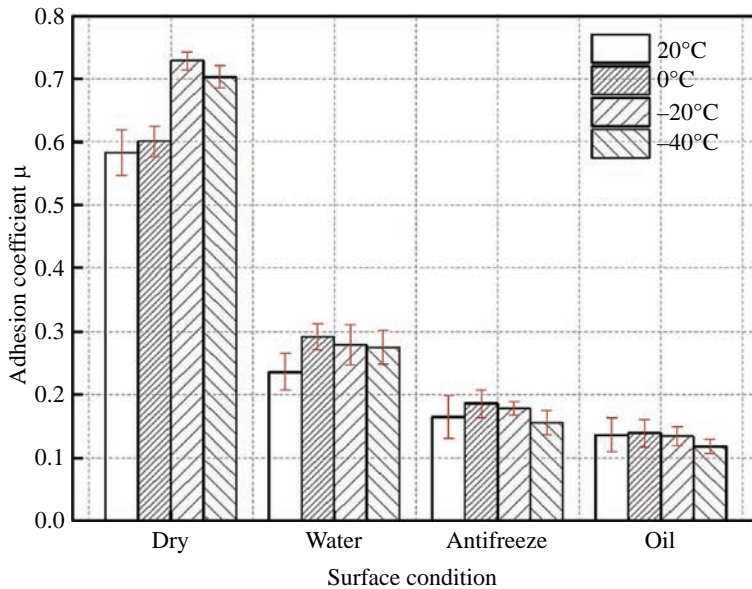


Fig. 8.12 Comparison of adhesion coefficient under different surface conditions, from Shi et al. [55].

Credit: Reprinted from L. Shi, L. Ma, J. Guo, Q. Liu, Z. Zhou, W. Wang, Influence of low temperature environment on the adhesion characteristics of wheel-rail contact, *Tribol. Int.* 127 (2018) 59–68, <https://doi.org/10.1016/j.triboint.2018.05.037>, copyright (2018), with permission from Elsevier.

a small-scale twin-disc test rig with environmental chamber and simulations at Southwest Jiaotong University, China [53–56]. The adhesion measurement shows that the adhesion coefficient at extremely low temperature is higher than that at room temperature, as shown in Fig. 8.12. The effect of contaminants is roughly the same as at room temperature, however, the adhesion recovery process is significantly slower [55]. The low temperature has a significantly negative effect on wear and rolling contact fatigue [54,56].

8.3.5 Solid particles at the wheel-rail contact

Solid particles contaminating the wheel-rail interface naturally originate from the railway superstructure such as ballast, concrete sleepers, etc. The internal source of solid particles is also sanding used by traction rail vehicles to restore adhesion during traction and braking under degraded adhesion conditions. These sources of contamination are common and usually not problematic. Extreme conditions can be caused by particles windblown from the surrounding environment. This is in the context of the spread of arid areas due to the climate change and the expansion of rail networks in the deserts of Middle and Far East and North Africa regions [57].

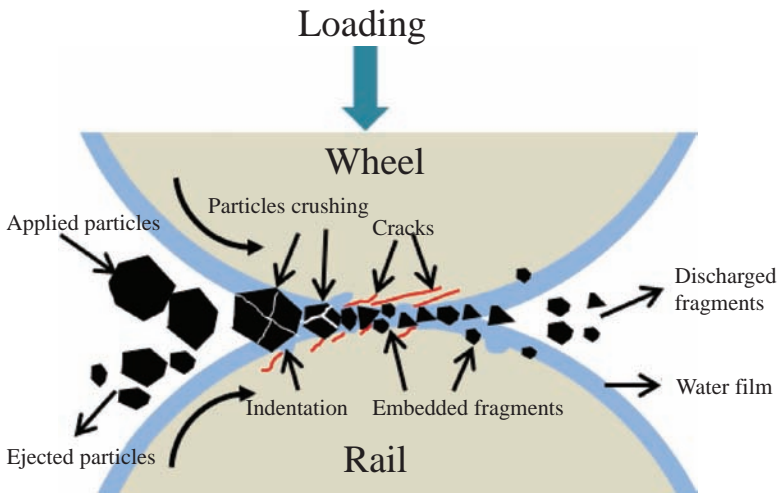


Fig. 8.13 Schematic of the behavior of solid particle in the twin-disc contact, from Wang [58]. Credit: Reprinted from C. Wang, L. Shi, H. Ding, W. Wang, R. Galas, J. Guo, Q. Liu, Z. Zhou, M. Omasta, Adhesion and damage characteristics of wheel/rail using different mineral particles as adhesion enhancers, *Wear* (2021) 203796, <https://doi.org/10.1016/j.wear.2021.203796>, copyright (2021), with permission from Elsevier.

When the sand or other mineral particles laying on the rail come into the contact, several phases occur, as illustrated for twin-disc configuration in Fig. 8.13 [58]. At first, some of the particles are ejected from the contact and the others are drawn into the converging gap between the contacting bodies. During this phase, the particles are crushed into small fragments by the normal force. An indentation of the wheel and rail appears, and some fragments can be embedded into the surfaces. As the particles enter the contact region, they are further crushed and subjected to shear stress due to the tangential force. Some particles undergo shear failure and some cause plowing of contacting bodies. If the particles are embedded in the surface, we are talking about two-body abrasion and if they are free to roll or slide, we refer to this as a three-body abrasive wear. The consequence of the particles action is increased wear. The results of the twin-disc tests simulating the effect of a desert environment show 1.4–2.2 times greater wear rate under sand conditions compared to “clean” conditions. The presence of sand also causes strong ratcheting and crack formations, whereby the particles can be pushed into existing cracks and assist their propagation [59]. Since the hard particles are usually embedded in the softer wheel material, the two-body abrasion leads to 2.5 times more wear on the harder rail material [60]. The authors of this study suggest that the initial crushing of large particles causes surface damage that is insignificant compared to the roughness of the rail surface and in-contact wear mechanism [60]. On the other hand, recent research has indicated that the sand fragments used instead of regular sand cause much milder negative effects such as wear, surface damage and plastic deformation. This is thanks to the absence of the crushing process [61].

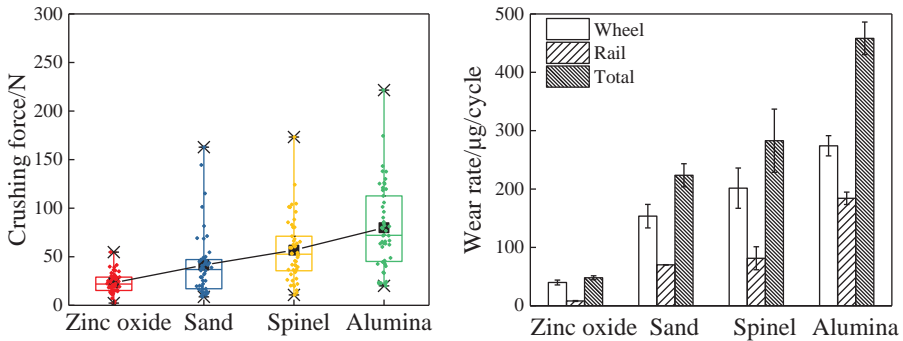


Fig. 8.14 Crushing stress and wear rate for four types of mineral particles, from Wang [58]. Credit: Reprinted from C. Wang, L. Shi, H. Ding, W. Wang, R. Galas, J. Guo, Q. Liu, Z. Zhou, M. Omasta, Adhesion and damage characteristics of wheel/rail using different mineral particles as adhesion enhancers, *Wear* (2021) 203796, <https://doi.org/10.1016/j.wear.2021.203796>, copyright (2021), with permission from Elsevier.

It is generally accepted that the wear rate caused by the contamination particles is related to their hardness. The graph in Fig. 8.14 compares crushing stress and wear rate measured at twin-disc set-up with wheel and rail steel for four types of mineral particles showing that there is an obvious correlation [58].

Although silica sand is commonly applied to the contact to restore adhesion under degraded adhesion conditions, under dry and light-wet conditions solid particles may act as a solid lubricant within the meaning of a reduction of adhesion [60,62–64]. This is clear from Fig. 8.15, where the coefficient of friction is compared for different wheel steels with and without sand application during the long-term test [59]. The effect of single application is indicated in Fig. 8.16 under wet conditions. There is a drop in the coefficient of adhesion immediately after the sand application, and this drop is more pronounced for larger applied quantity [64]. This is probably because the individual sand fragments slide over each other in the contact. A thick layer of dry sand has a relatively low shear strength.

A significant negative effect of the contact contamination is a risk of loss of the function of the track circuit used to detect the position of a train on the track. As studied by many researchers [62,63,65], too large a quantity of sand between the wheels and the rails leads to an electrical insulation of the contact. Several models have been developed to predict a critical sand density above which isolation would occur [63,65,66]. The most conservative value found is 7.5 g/m [67]. The level of insulation also depends on the size of sand particles, whereby larger particles seem to cause less electrical insulation [62]. This may be because smaller particles have a stronger tendency to stick to the surface and to build up an insulating layer that resists being pushed out of the contact. For a similar reason, a critical sand density was found to be lower when water or leaves are added into the interface [62,63,65].

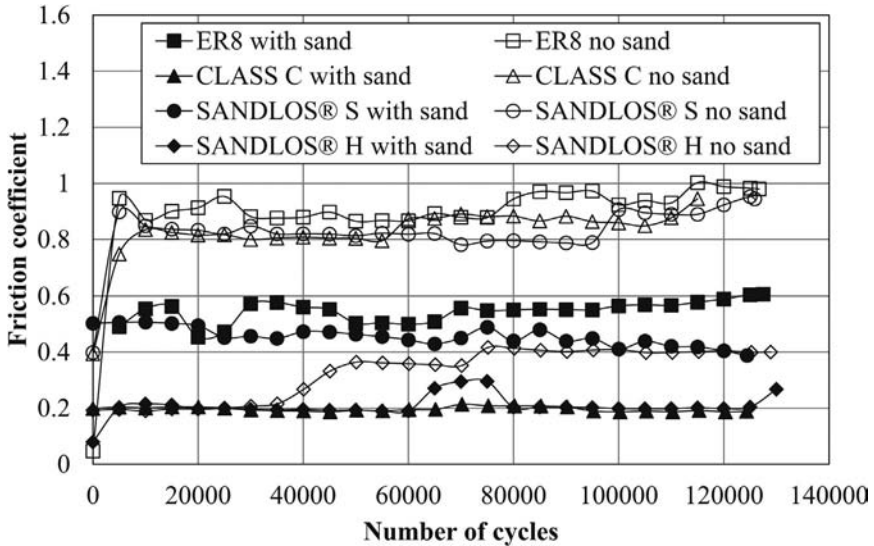


Fig. 8.15 Friction coefficients of the tests with and without sand., from Faccoli et al. [59]. Credit: Reprinted from M. Faccoli, C. Petrogalli, M. Lancini, A. Ghidini, A. Mazzù, Effect of desert sand on wear and rolling contact fatigue behaviour of various railway wheel steels, *Wear* 396-397 (2018) 146–161, <https://doi.org/10.1016/j.wear.2017.05.012>, copyright (2018), with permission from Elsevier.

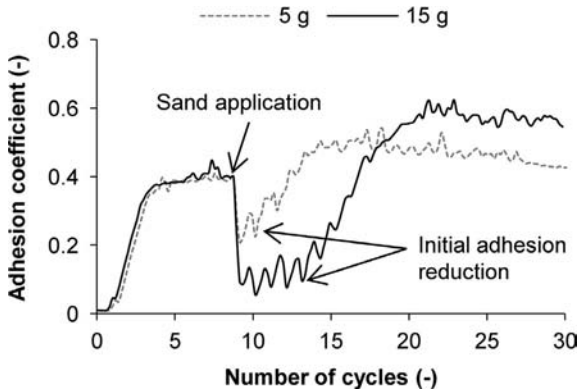


Fig. 8.16 The effect of adhesion coefficient after the single application of sand particles under light-wet conditions, from Omasta [64]. Credit: Reprinted from M. Omasta, M. Machatka, D. Smejkal, M. Hartl, I. Krúpka, Influence of sanding parameters on adhesion recovery in contaminated wheel–rail contact, *Wear* 322-323 (2015) 218–225, <https://doi.org/10.1016/j.wear.2014.11.017>, copyright (2015), with permission from Elsevier.

References

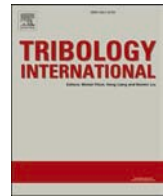
- [1] C. Logston, G. Itami, Locomotive friction-creep studies, *J. Eng. Ind.* 102 (3) (1980) 275–281, <https://doi.org/10.1115/1.3183865>.
- [2] M. Harmon, J. Santa, J. Jaramillo, A. Toro, A. Beagles, R. Lewis, Evaluation of the coefficient of friction of rail in the field and laboratory using several devices, *Tribol. Mater. Surf. Interfaces* 14 (2) (2020) 119–129, <https://doi.org/10.1080/17515831.2020.1712111>.
- [3] R. Lewis, U. Olofsson, Mapping rail wear regimes and transitions, *Wear* 257 (7–8) (2004) 721–729, <https://doi.org/10.1016/j.wear.2004.03.019>.
- [4] R. Lewis, R. Dwyer-Joyce, U. Olofsson, J. Pombo, J. Ambrósio, M. Pereira, C. Ariaudo, N. Kuka, Mapping railway wheel material wear mechanisms and transitions, *Proc. Inst. Mech. Eng. F J. Rail Rapid Transit* 224 (3) (2010) 125–137, <https://doi.org/10.1243/09544097JRRRT328>.
- [5] A. Meierhofer, G. Trummer, C. Bernsteiner, K. Six, Vehicle tests showing how the weather in autumn influences the wheel–rail traction characteristics, *Proc. Inst. Mech. Eng. F J. Rail Rapid Transit* 234 (4) (2020) 426–435, <https://doi.org/10.1177/0954409719863643>.
- [6] C. Hardwick, R. Lewis, U. Olofsson, Low adhesion due to oxide formation in the presence of salt, *Proc. Inst. Mech. Eng. F J. Rail Rapid Transit* 228 (8) (2013) 887–897, <https://doi.org/10.1177/0954409713495666>.
- [7] S. Abbasi, L. Olander, C. Larsson, U. Olofsson, A. Jansson, U. Sellgren, A field test study of airborne wear particles from a running regional train, *Proc. Inst. Mech. Eng. F J. Rail Rapid Transit* 226 (1) (2011) 95–109, <https://doi.org/10.1177/0954409711408774>.
- [8] D. Jaffe, J. Putz, G. Hof, G. Hof, J. Hee, D. Lommers-Johnson, F. Gabela, J. Fry, B. Ayres, M. Kelp, M. Minsk, Diesel particulate matter and coal dust from trains in the Columbia River Gorge, Washington State, USA, *Atmos. Pollut. Res.* 6 (6) (2015) 946–952, <https://doi.org/10.1016/j.apr.2015.04.004>.
- [9] P. Chinowsky, J. Helman, S. Gulati, J. Neumann, J. Martinich, Impacts of climate change on operation of the US rail network, *Transp. Policy* 75 (2019) 183–191, <https://doi.org/10.1016/j.tranpol.2017.05.007>.
- [10] M. Koetse, P. Rietveld, The impact of climate change and weather on transport: an overview of empirical findings, *Transp. Res. Part D: Transp. Environ.* 14 (3) (2009) 205–221, <https://doi.org/10.1016/j.trd.2008.12.004>.
- [11] P. Leviäkangas, A. Tuominen, R. Molarius, J. Ludvigsen, et al., Extreme weather impacts on transport systems, in: *EU_EWENT—Extreme Weather impacts on European Networks of Transport*, 2014.
- [12] I. Stipanovic, H. ter Maat, A. Hartmann, G. Dewulf, Risk assessment of climate change impacts on railway, in: *Engineering Project Organization Conference*, 2013.
- [13] J. Thornes, B. Davis, Mitigating the impact of weather and climate on railway operations in the UK, in: *ASME/IEEE Joint Railroad Conference*, ASME, 2002, pp. 29–38, <https://doi.org/10.1109/RRCON.2002.1000089>.
- [14] E. Forero-Ortiz, E. Martínez-Gomariz, M. Cañas Porcuna, L. Locatelli, B. Russo, Flood risk assessment in an underground railway system under the impact of climate change—a case study of the Barcelona metro, *Sustainability* 12 (13) (2020), <https://doi.org/10.3390/su12135291>.
- [15] K. Nagase, A study of adhesion between the rails and running wheels on main lines: results of investigations by slipping adhesion test bogie, *Proc. Inst. Mech. Eng. F J. Rail Rapid Transit* 203 (1) (1989) 33–43, https://doi.org/10.1243/PIME_PROC_1989_203_206_02.

- [16] T. Beagley, C. Pritchard, Wheel/rail adhesion—the overriding influence of water, *Wear* 35 (2) (1975) 299–313, [https://doi.org/10.1016/0043-1648\(75\)90078-2](https://doi.org/10.1016/0043-1648(75)90078-2).
- [17] Adhesion Research Group, Investigation Into the Effect of Moisture on Rail Adhesion (T1042), RSSB, 2014. <https://www.sparkrail.org/Lists/Records/DispForm.aspx?ID=11364>.
- [18] M. Godet, The third-body approach: a mechanical view of wear, *Wear* 100 (1–3) (1984) 437–452, [https://doi.org/10.1016/0043-1648\(84\)90025-5](https://doi.org/10.1016/0043-1648(84)90025-5).
- [19] S. Descartes, C. Desrayaud, E. Niccolini, Y. Berthier, Presence and role of the third body in a wheel–rail contact, *Wear* 258 (7–8) (2005) 1081–1090, <https://doi.org/10.1016/j.wear.2004.03.068>.
- [20] G. Trummer, L. Buckley-Johnstone, P. Voltr, A. Meierhofer, R. Lewis, K. Six, Wheel-rail creep force model for predicting water induced low adhesion phenomena, *Tribol. Int.* 109 (2017) 409–415, <https://doi.org/10.1016/j.triboint.2016.12.056>.
- [21] P. Cann, The “leaves on the line” problem—a study of leaf residue film formation and lubricity under laboratory test conditions, *Tribol. Lett.* 24 (2) (2006) 151–158, <https://doi.org/10.1007/s11249-006-9152-2>.
- [22] H. Chen, T. Furuya, S. Fukagai, S. Saga, J. Ikoma, K. Kimura, J. Suzumura, Wheel slip/slide and low adhesion caused by fallen leaves, *Wear* 446–447 (2020), <https://doi.org/10.1016/j.wear.2020.203187>.
- [23] K. Ishizaka, S. Lewis, D. Hammond, R. Lewis, Chemistry of black leaf films synthesised using rail steels and their influence on the low friction mechanism, *RSC Adv.* 8 (57) (2018) 32506–32521, <https://doi.org/10.1039/C8RA06080K>.
- [24] U. Olofsson, K. Sundvall, Influence of leaf, humidity and applied lubrication on friction in the wheel-rail contact: pin-on-disc experiments, *Proc. Inst. Mech. Eng. F J. Rail Rapid Transit* 218 (3) (2004) 235–242, <https://doi.org/10.1243/0954409042389364>.
- [25] Y. Zhu, U. Olofsson, H. Chen, Friction between wheel and rail: a pin-on-disc study of environmental conditions and iron oxides, *Tribol. Lett.* 52 (2) (2013) 327–339, <https://doi.org/10.1007/s11249-013-0220-0>.
- [26] Y. Zhu, U. Olofsson, R. Nilsson, A field test study of leaf contamination on railhead surfaces, *Proc. Inst. Mech. Eng. F J. Rail Rapid Transit* 228 (1) (2013) 71–84, <https://doi.org/10.1177/0954409712464860>.
- [27] M. Marian, M. Bartz, S. Wartzack, A. Rosenkranz, Non-dimensional groups, film thickness equations and correction factors for elastohydrodynamic lubrication: a review, *Lubricants* 8 (10) (2020), <https://doi.org/10.3390/lubricants8100095>.
- [28] M. Esfahanian, B. Hamrock, Fluid-film lubrication regimes revisited, *Tribol. Trans.* 34 (4) (1991) 628–632, <https://doi.org/10.1080/10402009108982081>.
- [29] B. Hamrock, D. Dowson, Isothermal elastohydrodynamic lubrication of point contacts: part III—fully flooded results, *J. Lubr. Technol.* 99 (2) (1977) 264–275, <https://doi.org/10.1115/1.3453074>.
- [30] H. Chen, A. Yoshimura, T. Ohyama, Numerical analysis for the influence of water film on adhesion between rail and wheel, *Proc. Inst. Mech. Eng. J. J. Eng. Tribol.* 212 (5) (1998) 359–368, <https://doi.org/10.1243/1350650981542173>.
- [31] B. Wu, M. Chen, T. Wu, Z. Wen, X. Jin, A simple 3-dimensional model to analyse wheel-rail adhesion under wet condition, *Lubr. Sci.* 30 (2) (2018) 45–55, <https://doi.org/10.1002/lc.1402>.
- [32] K. Bett, J. Cappi, Effect of pressure on the viscosity of water, *Nature* 207 (4997) (1965) 620–621, <https://doi.org/10.1038/207620a0>.
- [33] T. Tallian, On competing failure modes in rolling contact, *ASLE Trans.* 10 (4) (1967) 418–439, <https://doi.org/10.1080/05698196708972201>.

- [34] D. Kvarda, R. Galas, M. Omasta, L. Shi, H. Ding, W. Wang, I. Krupka, M. Hartl, Asperity-based model for prediction of traction in water-contaminated wheel-rail contact, *Tribol. Int.* 157 (2021), <https://doi.org/10.1016/j.triboint.2021.106900>.
- [35] H. Chen, T. Ban, M. Ishida, T. Nakahara, Experimental investigation of influential factors on adhesion between wheel and rail under wet conditions, *Wear* 265 (9–10) (2008) 1504–1511, <https://doi.org/10.1016/j.wear.2008.02.034>.
- [36] H. Chen, M. Ishida, T. Nakahara, Analysis of adhesion under wet conditions for three-dimensional contact considering surface roughness, *Wear* 258 (7–8) (2005) 1209–1216, <https://doi.org/10.1016/j.wear.2004.03.031>.
- [37] H. Chen, T. Ban, M. Ishida, T. Nakahara, Effect of water temperature on the adhesion between rail and wheel, *Proc. Inst. Mech. Eng. J. J. Eng. Tribol.* 220 (7) (2006) 571–579, <https://doi.org/10.1243/13506501JET75>.
- [38] H. Chen, A. Namura, M. Ishida, T. Nakahara, Influence of axle load on wheel/rail adhesion under wet conditions in consideration of running speed and surface roughness, *Wear* 366–367 (2016) 303–309, <https://doi.org/10.1016/j.wear.2016.05.012>.
- [39] H. Chen, H. Tanimoto, Experimental observation of temperature and surface roughness effects on wheel/rail adhesion in wet conditions, *Int. J. Rail Transp.* 6 (2) (2017) 101–112, <https://doi.org/10.1080/23248378.2017.1415772>.
- [40] Y. Zhu, X. Chen, W. Wang, H. Yang, A study on iron oxides and surface roughness in dry and wet wheel–rail contacts, *Wear* 328–329 (2015) 241–248, <https://doi.org/10.1016/j.wear.2015.02.025>.
- [41] Y. Zhu, The influence of iron oxides on wheel–rail contact: a literature review, *Proc. Inst. Mech. Eng. F J. Rail Rapid Transit* 232 (3) (2017) 734–743, <https://doi.org/10.1177/0954409716689187>.
- [42] J. Suzumura, Y. Sone, A. Ishizaki, D. Yamashita, Y. Nakajima, M. Ishida, In situ X-ray analytical study on the alteration process of iron oxide layers at the railhead surface while under railway traffic, *Wear* 271 (1–2) (2011) 47–53, <https://doi.org/10.1016/j.wear.2010.10.054>.
- [43] E. Leheup, R. Pendlebury, Unlubricated reciprocating wear of stainless steel with an interfacial air flow, *Wear* 142 (2) (1991) 351–372, [https://doi.org/10.1016/0043-1648\(91\)90174-S](https://doi.org/10.1016/0043-1648(91)90174-S).
- [44] Y. Zhu, Y. Lyu, U. Olofsson, Mapping the friction between railway wheels and rails focusing on environmental conditions, *Wear* 324–325 (2015) 122–128, <https://doi.org/10.1016/j.wear.2014.12.028>.
- [45] R. Galas, M. Omasta, L. Shi, H. Ding, W. Wang, I. Krupka, M. Hartl, The low adhesion problem: the effect of environmental conditions on adhesion in rolling-sliding contact, *Tribol. Int.* 151 (2020), <https://doi.org/10.1016/j.triboint.2020.106521>.
- [46] M. Ishida, Managing the wheel–rail interface: the Japanese experience, in: *Wheel–Rail Interface Handbook*, Elsevier, 2009, pp. 701–758, <https://doi.org/10.1533/9781845696788.2.701>.
- [47] W. Xu, B. Zhang, Y. Deng, Z. Wang, Q. Jiang, L. Yang, J. Zhang, Corrosion of rail tracks and their protection, *Corros. Rev.* 39 (1) (2021) 1–13, <https://doi.org/10.1515/corrrev-2020-0069>.
- [48] C. Tomberger, P. Dietmaier, W. Sextro, K. Six, Friction in wheel–rail contact: a model comprising interfacial fluids, surface roughness and temperature, *Wear* 271 (1–2) (2011) 2–12, <https://doi.org/10.1016/j.wear.2010.10.025>.
- [49] S. Dedmon, Effect of temperature on the performance of railroad wheels, *Proc. Inst. Mech. Eng. F J. Rail Rapid Transit* 231 (7) (2017) 786–793, <https://doi.org/10.1177/0954409717712072>.

- [50] T. Kato, H. Kato, T. Makino, Effect of elevated temperature on shelling property of railway wheel steel, *Wear* 366–367 (2016) 359–367, <https://doi.org/10.1016/j.wear.2016.04.015>.
- [51] H. Liu, F. Niu, Y. Niu, J. Xu, T. Wang, Effect of structures and sunny–shady slopes on thermal characteristics of subgrade along the Harbin–Dalian passenger dedicated line in Northeast China, *Cold Reg. Sci. Technol.* 123 (2016) 14–21, <https://doi.org/10.1016/j.coldregions.2015.11.007>.
- [52] Y. Wang, H. Zhou, Y. Shi, B. Feng, Mechanical properties and fracture toughness of rail steels and thermite welds at low temperature, *Int. J. Miner. Metall. Mater.* 19 (5) (2012) 409–420, <https://doi.org/10.1007/s12613-012-0572-8>.
- [53] R. Luo, W. Teng, X. Wu, H. Shi, J. Zeng, Dynamics simulation of a high-speed railway car operating in low-temperature environments with stochastic parameters, *Veh. Syst. Dyn.* 58 (12) (2020) 1914–1934, <https://doi.org/10.1080/00423114.2019.1662922>.
- [54] L. Ma, L. Shi, J. Guo, Q. Liu, W. Wang, On the wear and damage characteristics of rail material under low temperature environment condition, *Wear* 394–395 (2018) 149–158, <https://doi.org/10.1016/j.wear.2017.10.011>.
- [55] L. Shi, L. Ma, J. Guo, Q. Liu, Z. Zhou, W. Wang, Influence of low temperature environment on the adhesion characteristics of wheel-rail contact, *Tribol. Int.* 127 (2018) 59–68, <https://doi.org/10.1016/j.triboint.2018.05.037>.
- [56] L. Zhou, Y. Hu, H. Ding, Q. Liu, J. Guo, W. Wang, Experimental study on the wear and damage of wheel-rail steels under alternating temperature conditions, *Wear* (2021), <https://doi.org/10.1016/j.wear.2021.203829>.
- [57] L. Bruno, M. Horvat, L. Raffaele, Windblown sand along railway infrastructures: a review of challenges and mitigation measures, *J. Wind Eng. Ind. Aerodyn.* 177 (2018) 340–365, <https://doi.org/10.1016/j.jweia.2018.04.021>.
- [58] C. Wang, L. Shi, H. Ding, W. Wang, R. Galas, J. Guo, Q. Liu, Z. Zhou, M. Omasta, Adhesion and damage characteristics of wheel/rail using different mineral particles as adhesion enhancers, *Wear* (2021), <https://doi.org/10.1016/j.wear.2021.203796>.
- [59] M. Faccoli, C. Petrogalli, M. Lancini, A. Ghidini, A. Mazzù, Effect of desert sand on wear and rolling contact fatigue behaviour of various railway wheel steels, *Wear* 396–397 (2018) 146–161, <https://doi.org/10.1016/j.wear.2017.05.012>.
- [60] D. Grieve, R. Dwyer-Joyce, J. Beynon, Abrasive wear of railway track by solid contaminants, *Proc. Inst. Mech. Eng. F J. Rail Rapid Transit* 215 (3) (2005) 193–205, <https://doi.org/10.1243/0954409011531512>.
- [61] L. Shi, C. Wang, D. Ding, D. Kvarda, R. Galas, M. Omasta, W. Wang, Q. Liu, M. Hartl, Laboratory investigation on the particle-size effects in railway sanding: comparisons between standard sand and its micro fragments, *Tribol. Int.* 146 (2020) 106259, <https://doi.org/10.1016/j.triboint.2020.106259>.
- [62] O. Arias-Cuevas, Z. Li, R. Lewis, Investigating the lubricity and electrical insulation caused by sanding in dry wheel–rail contacts, *Tribol. Lett.* 37 (3) (2010) 623–635, <https://doi.org/10.1007/s11249-009-9560-1>.
- [63] R. Lewis, R. Dwyer-Joyce, J. Lewis, Disc machine study of contact isolation during railway track sanding, *Proc. Inst. Mech. Eng. F J. Rail Rapid Transit* 217 (1) (2003) 11–24, <https://doi.org/10.1243/095440903762727311>.
- [64] M. Omasta, M. Machatka, D. Smejkal, M. Hartl, I. Křupka, Influence of sanding parameters on adhesion recovery in contaminated wheel–rail contact, *Wear* 322–323 (2015) 218–225, <https://doi.org/10.1016/j.wear.2014.11.017>.
- [65] R. Lewis, J. Masing, Static wheel/rail contact isolation due to track contamination, *Proc. Inst. Mech. Eng. F J. Rail Rapid Transit* 220 (1) (2006) 43–53, <https://doi.org/10.1243/095440906X77919>.

-
- [66] S. Descartes, M. Renouf, N. Fillot, B. Gautier, A. Descamps, Y. Berthier, P. Demanche, A new mechanical–electrical approach to the wheel–rail contact, *Wear* 265 (9–10) (2008) 1408–1416, <https://doi.org/10.1016/j.wear.2008.02.040>.
- [67] W. Skipper, A. Chalisey, R. Lewis, A review of railway sanding system research: wheel/rail isolation, damage, and particle application, *Proc. Inst. Mech. Eng. F J. Rail Rapid Transit* 234 (6) (2020) 567–583, <https://doi.org/10.1177/0954409719851634>.



Asperity-based model for prediction of traction in water-contaminated wheel-rail contact

Daniel Kvarda^{a,*}, Radovan Galas^a, Milan Omasta^a, Lu-bing Shi^{b,c}, Haohao Ding^b, Wen-jian Wang^b, Ivan Krupka^a, Martin Hartl^a

^a Faculty of Mechanical Engineering, Brno University of Technology, Technická 2896/2, 616 69, Brno, Czech Republic

^b Tribology Research Institute, State Key Laboratory of Traction Power, Southwest Jiaotong University, Chengdu, 610031, China

^c Zhengzhou Research Institute of Mechanical Engineering Co., Ltd., Zhengzhou, 450001, China

ARTICLE INFO

Keywords:

Adhesion coefficient
Water
Low adhesion
Rail-wheel tribology

ABSTRACT

The wheel-rail contact is subjected to various environmental contaminations, while one of the most common is water. A numerical model has been used to evaluate friction in water-contaminated contact. The Greenwood and Tripp theory is used to calculate the load carried by asperities and liquid film. This model uses Kalker's simplified theory with an implemented third body layer to determine the frictional values of asperity contact and elasto-hydrodynamic theory for friction generated by liquid. The results are compared with experiments on two types of surface roughness. The results show the difference between elastic and plastic asperity deformation model, where the plastic model predicts more accurate transition in mixed lubrication regime. The plastic deformation model was used to predict traction curves.

1. Introduction

As an open tribological system, the wheel-rail contact is subject to many kinds of environmental influences. It is crucial to ensure safe and reliable operation of railway vehicles under those conditions. Contaminants such as water, oil and products used to manage wheel-rail friction (top-of-rail lubricants, flange lubricants) change the frictional behaviour of the contact interface. These substances influence the friction in both boundary and elasto-hydrodynamic (EHL) regimes where solid shear strength and viscosity define the frictional behaviour, respectively.

Water is the most common contaminant and contamination can happen on a rainy day or as a dew condensate from humid air. As a dew condensate, low amounts of water mixed with wear debris on contact surfaces create a film with low shear strength [1,2] and high viscosity [2] that can cause low adhesion [2,3]. On a rainy day, the water floods the contact and at very high speeds, a surface separation can lead to low adhesion [4]. The degree of adhesion in wheel-rail contact is commonly expressed by the adhesion coefficient, which is defined as the ratio between tangential frictional force and normal load. Depending on the slip value, this coefficient takes value from 0 to the value representing the coefficient of friction. Under dry conditions, the typical coefficient of friction is between 0.5 and 0.8 [5]. A low adhesion means that the

tangential frictional force is not sufficient to provide the required force for traction or braking. In terms of coefficient of adhesion, the low adhesion is generally considered with values lower than 0.1 [6]. Studies report that with increasing speed the coefficient of adhesion is decreasing [7–11]. The rate of decrease depends on the change in film thickness and roughness profile. Increasing the roughness causes the contact to shift closer to the boundary regime and thus increasing the coefficient of adhesion [8,9,12,13].

The friction generated in liquid separating two surfaces can be predicted by means of hydrodynamic theory. One key variable is a surface separation, which can be calculated from the Reynolds equation or analytical formulas [14]. The resulting shear stress is then solved using Newton's law of viscosity. The friction generated by solid asperity contact is mostly simplified by using a fixed value of the coefficient of friction [4,9,13,15] or by varying based on defined parameters such as slip and rolling speed [16,17]. Studies set this value based on experimental data of dry contact conditions. To determine this value numerically, Kalker's simplified theory can also be used [18]. This approach and its modifications are widely used [16,17,19] since it provides good accuracy and fast computational time compared to more accurate and demanding exact theory implemented in CONTACT [20]. The coefficient of friction in real contact depends on conditions such as material

* Corresponding author.

E-mail address: Daniel.Kvarda@vut.cz (D. Kvarda).

<https://doi.org/10.1016/j.triboint.2021.106900>

Received 11 November 2020; Received in revised form 15 January 2021; Accepted 25 January 2021

Available online 27 January 2021

0301-679X/© 2021 Elsevier Ltd. All rights reserved.

properties, contamination and roughness. This is taken into account by Kalker [21] as another layer that adds displacement and changes the flexibility coefficient.

A lot of numerical work has been done showing ways to address the problem of predicting coefficient of adhesion in mixed lubrication regime. The main problem is determining the magnitude of asperity contact. One of the first analytical solutions to model asperity contact was done by Greenwood and Tripp [22], which was applied by the following publications [4,9,15,19,23]. This approach uses the statistical distribution of asperity heights and defined geometry of asperity peaks. Using such a stochastic method allows for fast solution of asperity contact status. Once it is known what portion of the contact area is realized through asperity contact and interfacial fluid, the resulting coefficient of friction can be determined. New approaches to prediction of asperity contact were published [24–28] with different ways to tackle the effect of elasto-plastic asperity behaviour. These models are mathematically and computationally more complex than the approach of Greenwood and Tripp [22]. The main differences are in the way plasticity is considered by the model.

Many recent studies deal with the problem of water contamination and model prediction [1,12,29–33]. Publication [1] uses a high pressure torsion device and friction model, which is similar to previous publication by Beagley [2]. This model is used to assess the boundary shear properties of water and iron oxide particles mixture. However, this does not consider the EHL effect and transition in mixed lubrication regime. Studies [30,31] use a parametrised model based on laboratory experiments to estimate the coefficient of adhesion. Such models are good for fast evaluation based on the contact conditions but are not built on physical processes and material properties of the contact interface. Lastly, the work of Chen [4,13,23] uses EHL model to predict the surface separation and fluid friction. To evaluate the change in coefficient of adhesion, this model uses a fixed value of coefficient of adhesion for boundary friction based on experimental data.

The presented approach aims to use the fundamental solid shear and viscosity properties of the interfacial layer. The bulk liquid responds to the rate of displacement in EHL regime which is accounted for by the EHL solver. The solid shear responds to surface displacement alone in boundary regime and that is implemented using Kalker's simplified theory with contamination accounted for. This frees the solution from knowing the boundary coefficient of adhesion, but rather uses the fundamental properties of solid interface shearing. Both procedures are connected in mixed lubrication regime by asperity contact calculation. This approach allows the prediction of Stribeck and traction curves simultaneously across all lubrication regimes. With this, we can identify the train running conditions that can lead to severe loss of adhesion based on the physical properties of the contact interface, making such model very versatile. It also allows for the prediction of coefficient of adhesion in many conditions with materials of different properties. Such an advantage is valuable in wheel-rail contact, where many different materials and conditions may occur.

Further use of this model is beneficial in problems such as design and testing of products applied into the wheel-rail contact and the use in dynamic simulations to prevent the generation of wheel squeal noise. Using a numerical approach makes it easy to implement any shear dependency such as pressure, temperature, shear-thinning and others. The presented study is limited to pure water contamination to assess the feasibility of this modelling approach. This is due to the experimental methods used which are not suited for non-transparent substances such as water and oxide mixture. Transparent water allows us to control the main parameters of the model simultaneously – film thickness and coefficient of adhesion.

2. Material and methods

Contact area of two bodies with interfacial fluid can be separated into partly contact of asperities and partly into areas where the fluid is

separating both surfaces as shown in Fig. 1. When there is a relative motion of contacting surfaces, shear stresses arise creating a reaction opposite to the direction of relative motion. Considering the concept of fluid entrapped between contact asperities, the shear stress can either result from asperity interaction or hydrodynamic processes in areas separated by fluid. Solids react to deformation, while fluids react to the rate of deformation. Combining the fundamentally different shear stress mechanism is a problem of finding the portion of shear taken up by asperities and a portion taken up by fluid. For that, an asperity contact model based on the previous work of Greenwood and Tripp [22] can be deployed. This model presents both elastic and plastic predictions. It is simpler and might not be as accurate for some conditions as more recent models for elasto-plastic asperity contact. However, for the current study we found that the Greenwood and Tripp model was accurate enough and allowed us to compare elastic and plastic asperity contact. It also allowed for faster calculation of each iteration algorithm, which is convenient since calculating Stribeck and traction curves requires varying both slip and speed parameters.

2.1. Asperity contact model

For the calculation of load carried by asperities and fluid a theory developed by Greenwood and Tripp is used [22]. A similar algorithm to the one published by Chen [4] is applied in this study as described in Fig. 2. Calculation of load carried by the lubricating film and asperity contact is compared to the total load applied to get the error of calculation. The solution is acquired by minimizing this error value by Newton-Raphson method.

The defining parameter for calculating resulting mean asperity pressure is separation of surface reference planes. In lubricated rolling-sliding contact, this is represented as the thickness of lubricant film. In this work, water is used as lubricant and thus Newtonian behaviour with respect to shear rate is assumed and there is no change in viscosity with change of pressure. For the separation of surfaces, a film thickness formula assuming iso-viscous behaviour is used [14]:

$$h_c = 5.08 U^{0.66} W_{EHL}^{-0.21} r \quad (1)$$

where the non-dimensional parameters are defined as:

$$U = \frac{\eta_0 v}{Er} \quad (2)$$

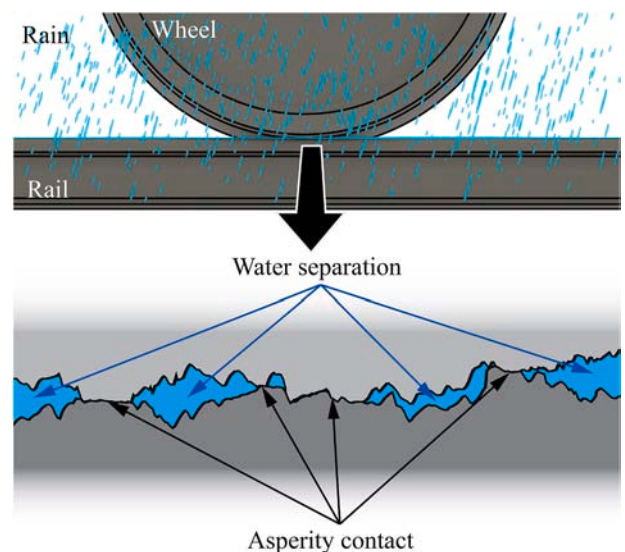


Fig. 1. Wheel-rail asperity contact illustration.

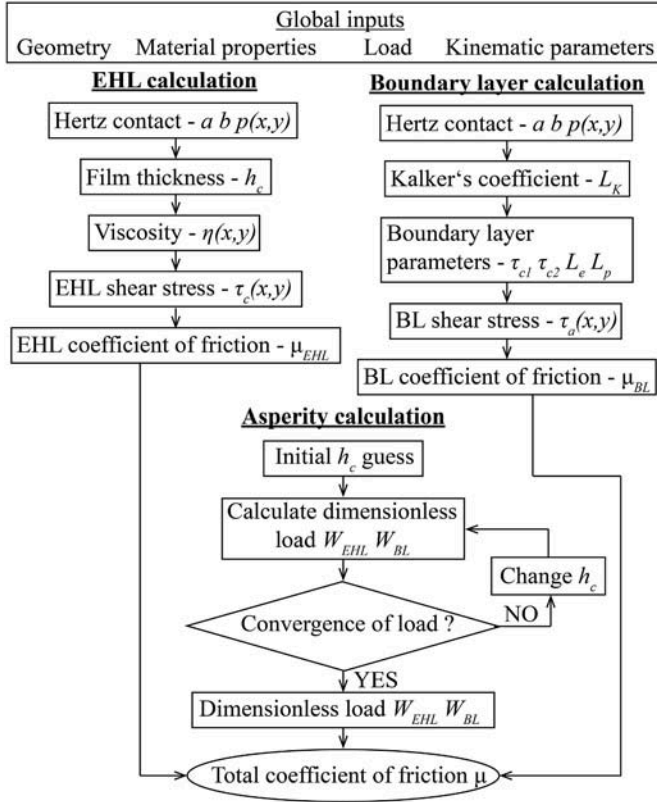


Fig. 2. Solution algorithm.

$$W_{EHL} = \frac{F_{EHL}}{Er^2} \quad (3)$$

The value of load carried by lubrication film F_{EHL} in the first iteration of calculation is equal to the total load applied to the contact F . Each other subsequent iteration uses Eq. (1) to evaluate the nondimensional load parameter of fluid film.

Calculation of central film thickness is used as surface separation in the mean asperity pressure p_a evaluation. In the current study, two approaches from Greenwood and Tripp theory [22] are used for comparison. The first approach described by Eq. (4) assumes paraboloidal asperity and elastic deformations. The asperities follow Gaussian distribution and are defined by three parameters: standard deviation σ , curvature of asperity peak β and density of asperity peaks ρ . Here we define $K = \sigma\beta\rho$ to compare different cases of surface topography. The function $F_{3/2}$ for Gaussian distribution is calculated from Eq. (5) given by Greenwood and Williamson [34]. For good accuracy of the numerical integration, the integral's upper limit is set to 30 with 1000 steps between integral bounds.

$$p_a = \frac{4}{3} \frac{K}{2} EF_{3/2} \left(\frac{h_c}{\sigma} \right) \sqrt{\frac{\sigma}{\rho}} \quad (4)$$

$$F_n(h) = \frac{1}{\sqrt{2\pi}} \int_h^\infty (u-h)^n e^{-u^2/2} du \quad (5)$$

The second approach to mean asperity pressure differs by assuming conical asperities and plastic deformation. The parameters of paraboloidal asperities are used by inscribing the cone into equivalent paraboloid. Greenwood and Tripp then give:

$$p_a = \frac{2}{3} \pi^2 HK^2 F_4 \left(\frac{h_c}{\sigma} \right) \quad (6)$$

Where H is mean pressure related to the hardness. A good estimation can

be made that the value of H equals to approximately 6x yield stress in shear [35].

For the case of numerical calculation, the asperity load from mean asperity pressure is given by non-dimensional parameter:

$$W_{BL} = \frac{p_a \pi a^2}{Er^2} \quad (7)$$

The non-dimensional loads of hydrodynamic film and asperity contact are then compared to give the error of calculation:

$$\varepsilon = \left| \frac{W^2 - (W_{EHL} + W_{BL})^2}{W^2} \right| \quad (8)$$

$$W = \frac{F}{Er^2} \quad (9)$$

The terminating condition is that the error should be lower than 0.1%. In the first iteration, when this condition is not met, the surface separation h_c is changed by step of $h_c/1000$. Subsequent steps and changes in separation are controlled by the numerical method. Each new step recalculates the hydrodynamic load W_{EHL} , mean asperity contact pressure p_a and asperity load W_{BL} with new surface separation h_c until the condition of maximum error is satisfied.

Dividing by the non-dimensional total load, the numbers W_{EHL}/W and W_{BL}/W represent a portion of load carried by lubricant film and asperity contact respectively. If we assume that the frictional forces are governed by Coulomb's law, then based on the coefficients of friction for hydrodynamic film μ_{EHL} and asperity contact μ_{BL} we get Eq. (10). The resulting coefficient of friction μ is:

$$\mu = \frac{\mu_{EHL} W_{EHL} + \mu_{BL} W_{BL}}{W_{EHL} + W_{BL}} \quad (10)$$

The parameters μ_{EHL} and μ_{BL} are defined in the following sections based on EHL theory and Kalker's simplified theory.

2.2. Friction in fluid film lubrication

To calculate the traction force and coefficient of friction in EHL, a basic simplification used in most analyses is made. For the purpose of calculating both EHL and asperity contact traction, the contact area is discretized into n by m areas as shown in Fig. 3. This discretization is not necessary for iso-viscous EHL calculation, because all variables for

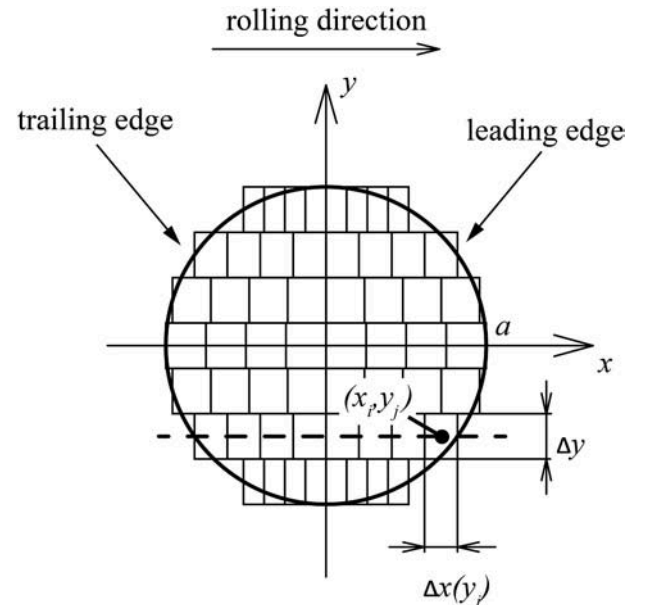


Fig. 3. Contact area discretization.

calculating traction force are constant across the contact patch. However other regimes as well as asperity contact require discrete mesh for calculation and thus for the convenience of changing regimes it is used here. Moreover, the discretization along the axis of rolling is variable, depending on the length of the contact at specific y coordinate. The model was set up in such a way, that each strip is divided into same number of discrete points. This increases the resolution at the side edges of the contact area.

The contact pressure of circular contact at each coordinate is described by semi-ellipsoid distribution given by Hertz:

$$p(x_i, y_j) = \frac{3F}{2\pi a^2} \left(1 - \left(\frac{x_i}{a}\right)^2 - \left(\frac{y_j}{a}\right)^2 \right) \quad (11)$$

Since iso-viscous lubricant is assumed, there is no change in viscosity due to the Hertzian distribution of pressure in contact. Thus we assume viscosity distribution $\eta(x, y) = \eta_0$. Using Newtonian fluid with viscosity η between sliding surfaces separated by h_c with sliding speed equal to entrainment velocity v times slip ratio s . The shear stress is given by the equation:

$$\tau_{EHL}(x_i, y_j) = \eta(x_i, y_j) \frac{vc}{h_c} \quad (12)$$

The resulting coefficient of friction is calculated assuming Coulomb's law by the following equation:

$$\mu_{EHL} = \frac{\tau_{EHL}}{p} \quad (13)$$

2.3. Friction in asperity contact

Calculation of friction in asperity contact is based on Kalker's simplified theory implemented into FASTSIM algorithm [18]. We assume the influence of asperity and contamination as a change in the flexibility parameter as suggested by previous studies [16]. Instead of using a limiting coefficient of friction, the interface is modelled as a material following Voce's hardening law as mentioned in the study by Six. et al. [36]. The influence of pressure and temperature is neglected in the current study.

Imagining a particle on the surface entering contact at the leading edge, this is represented in Fig. 3 on the right side of the ellipse. At the leading edge the particle is undeformed, and no shear or normal stress is acting upon it from contact interaction. As the time progresses, the particle moves along the axis of rolling direction into the contact from the leading edge towards the trailing edge. As it passes through the contact area, stresses and relative motion are applied to it. The normal stress is defined by Eq. (11). To work towards the shear stress, we first define the slip velocity w . For the steady-state case, the interfacial slip velocity is given by kinematic equations:

$$w = c - (\partial u / \partial x)v \quad (14)$$

where c is rigid creep velocity and u is surface displacement. The simplified theory presumes that the displacement of each point on the surface is only affected by the shear stress at this point. The slip velocity w is equal to zero at the leading edge and only gains non-zero values in points where the surface displacements exceed the elastic capability of contact. Given this presumption, the simplified theory introduces load-displacement law where surface displacements and shear stresses are connected by a flexibility parameter L .

$$u = L\tau \quad (15)$$

Combining Eq. (14) and Eq. (15) and applying them to the previously described discretization of the contact area, as shown in Fig. 3, gives the shear stress in each elastically deformed point of contact.

$$\tau_{BL}(x_i, y_j) = \tau_{BL}(x_{i-1}, y_j) - \frac{2a(y_j)c}{vm} \frac{c}{L} \quad (16)$$

The flexibility L is originally defined for clean contact and ideal geometry of contact bodies. In reality, the contact is influenced by surface condition and third body materials in the interface. To represent real surfaces closer to reality, the elasto-plastic behaviour of contact is introduced. During the elastic deformations, the shear stress is calculated by Eq. (16) where the flexibility L is calculated from Kalker's flexibility coefficient L_K and flexibility coefficient representing real contact conditions L_e (Eq. (17)).

$$L = L_K + L_e \quad (17)$$

When the surface deformations exceed the elastic limit, the shear stress is calculated from the plastic part of Voce's hardening material model [37] described by Eq. (18). The surface deformation u in this equation is calculated by discretizing Eq. (14).

$$\tau_{BL} = \tau_{c1} + (\tau_{c2} - \tau_{c1}) \left(1 - e^{(-u + \tau_{c1}L_e)/L_p} \right) \quad (18)$$

The parameters τ_{c1} and τ_{c2} separate the regions where shear stress behaves elastically and plastically as shown in Fig. 4. Parameter L_e defines the slope of initial elastic region. The shape of plastic region is defined by parameter L_p .

Since pressure distribution in contact area changes at each point as represented by Eq. (11), also the shear stress needs to follow pressure changes. Assuming a simplification with linear relationship between shear stress and pressure, the parameters of Eq. (18) can be obtained by introducing new parameters μ_{c1} , μ_{c2} , $L_{\mu e}$ and $L_{\mu p}$ in such a way that:

$$\tau_{c1} = \mu_{c1}P \quad (19)$$

$$\tau_{c2} = \mu_{c2}P \quad (20)$$

$$L_e = L_{\mu e}/P \quad (21)$$

$$L_p = L_{\mu p} \quad (22)$$

The asperity contact coefficient of friction μ_{BL} is calculated using the same relationship for μ_{EHL} as shown in Eq. (23):

$$\mu_{BL} = \frac{\tau_{BL}}{p} \quad (23)$$

2.4. Experimental validation

The verification experiments were conducted using ball-on-disc tribometer with the capability of using optical interferometry to measure lubricant film thickness. Measured values of film thickness were acquired from thin-film interferometry evaluation software [38]. The ball specimen with 25.4 mm diameter resulting in circular contact. The ball was made from bearing steel AISI 52100 and had measured

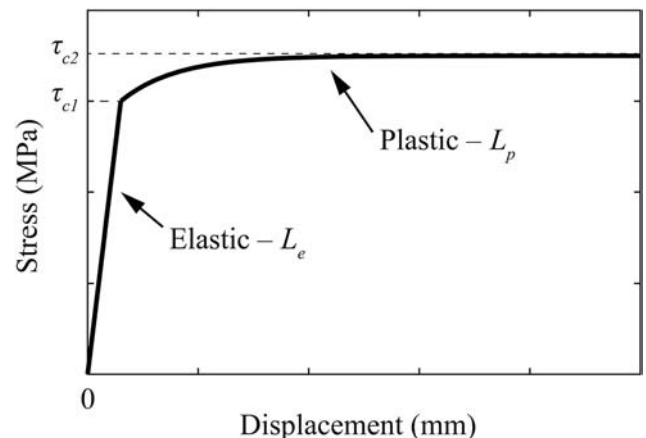


Fig. 4. Parameters of Voce's hardening material model.

hardness 53HRC (standard deviation 0.3HRC) which corresponds to a mean pressure related to the hardness of approximately 6 GPa. A smooth surface of the ball specimen was prepared by polishing with diamond paste. A rough surface was prepared by 5-minute dry run-in test with maximum Hertzian pressure of 0.75 GPa, 5% slip and 500 mm/s entrainment speed. Surface parameters were measured by optical profilometer Bruker Contour GTX and are stated in Table 1. The steel ball was loaded against the glass disc with a thin chromium coating that allows the partial reflection of light, creating an interferometric image together with reflection from the ball surface. The glass disc had roughness lower than 1 nm and because of this low roughness, the calculation neglects the effect of glass disc surface topography. A schematic of the test rig is shown in Fig. 5.

The ball-on-disc tribometer uses servo motors to separately drive the ball and disc to achieve set speed and slip. However, to ensure precise values the slip and speed were calculated from measured true rotations of both ball and disc drive shafts. Shaft with an attached ball is connected through a torque transducer that records at sampling frequency 1 kHz. Based on the measured radius of the ball and its position with regards to the disc's rotational axis, the true speeds of both surfaces in contact and the resulting slip is calculated. Coefficient of adhesion (marked as CoA in figures) is calculated from the loading force, torque and radius of the ball specimen.

The applied water used in this study was previously distilled to guarantee its pureness and stable properties during tests. The viscosity of distilled water is taken from the following study [39] based on ambient temperature during measurement. Application of water was done directly into contact through a syringe with a needle.

Film thickness measurements were done at 0% slip with a speed range from 0 to 2 m/s. Stribeck curves were measured at 5% slip with a sequence of increasing speed from 0 m/s up to 2 m/s and then decreasing back to 0 m/s. Dry traction and traction curve measurements were done by increasing the slip values from negative to positive slip (see Table 2). Assuming a symmetrical behaviour of slip, the negative values were transformed into the first quadrant to make sure there is no shift of the traction curve with regards to 0% slip. Each point of coefficient of adhesion was measured by averaging a 4 s long reading from torque transducer at the set speed and slip.

The roughness of the ball specimen was measured after each test to guarantee minimal deviation from the parameters stated in Table 1. However, higher deviations of roughness parameters (more than 15%) were seen after traction tests with smooth surface at lower speeds. This might have been because of longer time spent at saturated values of traction curves in the mixed lubrication regime. Such behaviour was not observed with Stribeck tests due to only a few measured points being in the mixed lubrication regime. Because of this, only rough surface traction measurements were evaluated.

3. Results and discussion

3.1. Determining the parameters for model

Prior to the main experiments comparing rough and smooth surfaces contaminated with water, the unknown parameters of the Voce's hardening model had to be determined. The relationship between surface deformation and resulting shear stresses can be acquired by slow relative movement of two surfaces while measuring the relative

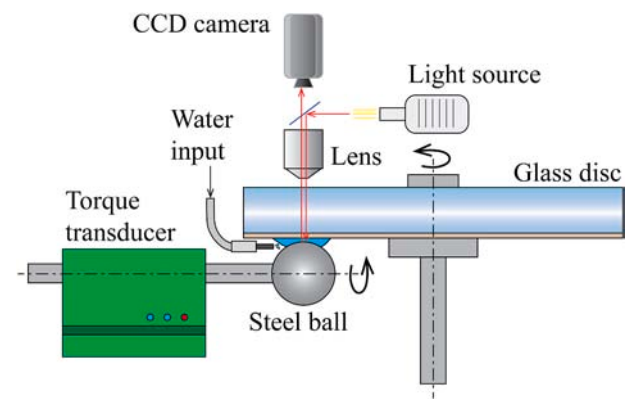


Fig. 5. Scheme of ball-on-disc tribometer.

displacement and resulting frictional force. This type of experiment has been previously used to identify the influence of small amounts of water and iron oxide mixture on adhesion in wheel-rail contact [1]. However, in this study it was not feasible to conduct such experiment with the specimens used. Because of this, the stress-displacement relationship had to be determined based on the traction measurements. Subsequently, a model fit and identification of main parameters was done.

Results of traction curve measurement under dry conditions are shown in Fig. 6. The measured values of the coefficient of adhesion show an initial increase up to 0.01 slip. To determine the exact shape of traction curve around saturation point, more measurements were done around this slip value. In terms of wheel-rail contact, the saturation at 0.01 slip is a good representation as suggested by other experimental [7, 8] and numerical [16,19] studies. Even though some studies with similar geometry show much later onset of saturation [12]. At the coefficient of adhesion value 0.16 saturation is reached and only a slight positive change with a further increase of slip is achieved. The saturated values converge around the coefficient of adhesion 0.18. Such low values are the result of glass contact specimen used with different material properties of glass and chromium layer compared to steel. Moreover, the glass disc with negligible roughness and the steel ball with polished surface do not provide strong enough surface interaction to overcome the coefficient of adhesion values higher than 0.2, which is quite low compared to steel-steel contact. Conducting experiments under dry conditions also causes excessive wear of the chromium layer, which can change surface properties and makes the wear path unusable for further study of film thickness. The fitted traction curve and corresponding parameters for model prediction are also noted in Fig. 6. These parameters were used throughout this whole study.

3.2. Film thickness

For a correct prediction of load carried by asperities, the film separation predicted by the model needs to correspond to experimental measurement. The measured values of average central film thickness and standard deviation are shown in Fig. 7. The prediction in this figure corresponds to iso-viscous regime defined by Eq. (1). At speeds lower than 100 mm/s the measured film thickness values run into the resolution limit of coloric interferometry method. At film thickness of 1.25 nm at 50 mm/s the error due to a resolution limit (0.5 nm) is 40% of the measured value. These values at low speed should thus be interpreted with caution. However, with increasing speed the film thickness follows the same trend as predicted values. At speeds higher than 1 m/s the standard deviation almost always crosses the predicted value.

These results show that using iso-viscous elastic film prediction formula yields accurate values compared with experimental measurement for the measured conditions. Interferograms for selected speeds can be seen in Fig. 8. Visible contact areas show the different hue for specified film thickness. Due to the monochromatic nature of

Table 1

Surface parameters.

Surface condition	Roughness standard deviation σ (nm)	Asperity peak curvature β (mm)	Asperity peak density ρ (1/mm ²)	K (-)
Smooth	8.3	0.301	24200	0.0605
Rough	9.56	0.373	21500	0.0767

Table 2
Experimental conditions and type of experiment.

Test type	Roughness type	Speed (m/s)	Slip (%)	Max. Hertz. pressure (MPa)	Fig. No
Dry traction	Rough	0.5	-10 - 10	750	6
Film thickness	Smooth	0-2	0	750	7,8
Stribeck	Smooth	0.1-2	5	750	9
Stribeck	Rough	0.1-2	5	750	10
Traction	Rough	0.25, 0.5, 1, 1.5, 2	-5-5	750	13

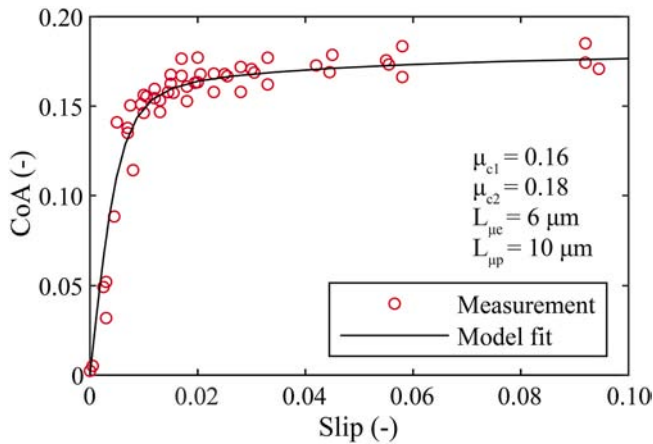


Fig. 6. Traction curve under dry conditions.

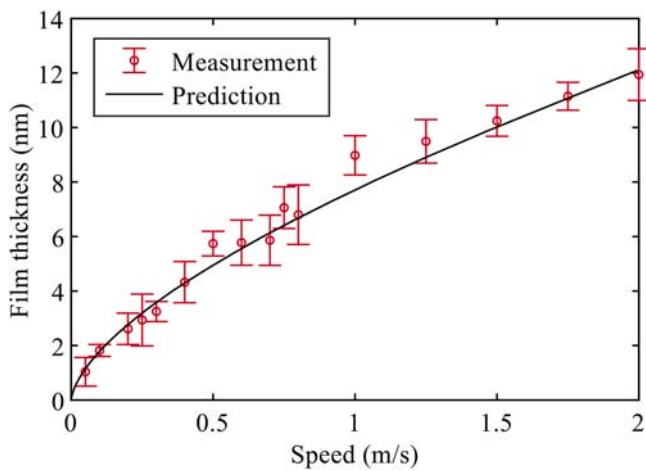


Fig. 7. Water film thickness measurement compared with prediction.

interferograms, the precise calibration before and after each set of speed sequence had to be done. This ensured that the calibration scale was stable throughout the whole experiment. The chromatic layer was not uniform as can be seen from the interferograms. This can be as a result of prior damage from contact interaction since the direction of non-

uniformity is the same as the direction of rolling. However, this has negligible influence on the average film thickness. The film was mostly uniform across the whole contact area. No visible side lobes or minimum film thickness regions occur making it easier for evaluation.

3.3. Friction and model prediction

The Stribeck experiment with smooth surface indicates some discrepancy compared with the presented model, see Fig. 9. *Measurement 1* represents sequence with increasing speed, while *Measurement 2* was done by decreasing speed. Minimal changes between the direction of speed change are present. The initial slope of the coefficient of adhesion with increased speed is low, which suggests that the contact is at the mixed lubrication regime and the roughness parameters do not allow the transition to boundary regime. This is also validated by low values of the coefficient of adhesion in comparison with values for dry contact. The lowest measured value of coefficient of adhesion was 0.007 with a standard deviation of 0.004. With the speed increasing from 1 m/s to 2 m/s the coefficient of adhesion changed only about 30%.

Looking at the prediction models, the elastic formula for asperity contact predicts extremely low values at lower speeds. With a range of speed 1 mm/s to 2 m/s the coefficient of adhesion changes from 0.0033 to 0.0004. Such low values would indicate that almost no load is carried by asperity peaks and the regime of lubrication fluid dominated. This does not represent well the experimental data at lower speeds, even

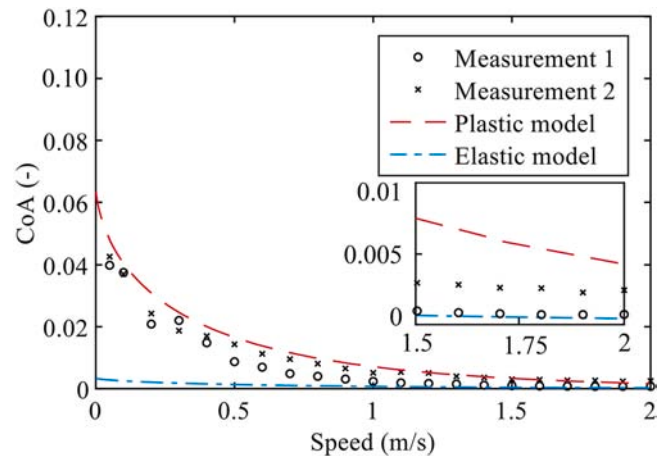


Fig. 9. Stribeck curve for smooth surface.

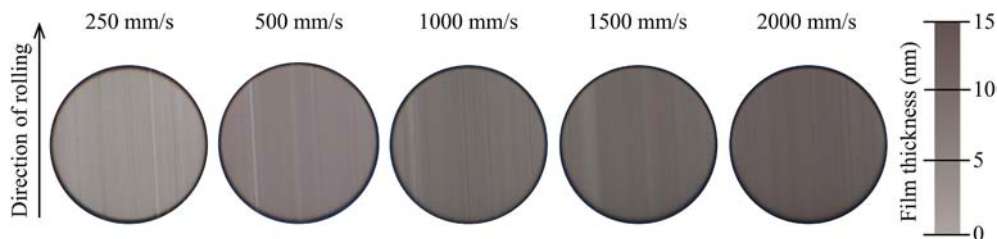


Fig. 8. Water film thickness interferograms.

though a big part of past research published on the topic of using Greenwood and Tripp theory [22] works with the elastic formula [4,9,15,23]. However, new approaches to elasto-plastic behaviour of contact asperities have been studied [10,19,40]. The simple plastic asperity model used in this study suggests much clearly the change in coefficient of adhesion with increasing speed compared to the elastic model. It can be seen that the experimental data show similar trend to the predicted values. This implies that the roughness is close to the one measured by the optical profilometer.

From the interference images obtained during the experiment it was obvious that the increase of wear on the chromatic layer has happened during the test sequence. Because of this the film thickness measurement was impossible to perform. The wear of the chromatic layer caused inhomogeneous reflection intensity across the contact area. This meant that it would be much more complicated to evaluate the true film thickness due to changes in calibration across the taken interference image. However, a qualitative assessment could be made to make sure that the film thickness is within expected values and no contamination of water happened during the experiment.

The effect of increased roughness parameters is depicted in Fig. 10. As in the test with a smooth surface, the direction of speed change has a negligible effect on the coefficient of adhesion. The initial slope at lower speed is much steeper in comparison with the smooth surface experiment and reaches higher values. This corresponds well with the plasticity based predictive model used, where higher roughness causes higher mean asperity pressure for the same separation h_c/σ as reported by other studies [4,13,19,41,42]. Thus, the contact is located closer to the boundary lubrication regime. For the lowest measured speeds, there was no saturation of measured values, which would suggest boundary lubrication regime. Moreover, the highest measured value of coefficient of adhesion was 0.085 with a standard deviation of 0.009. This value is closer to dry contact conditions than the smooth surface experiment. The lowest value at 2 m/s was 0.015 with a standard deviation of 0.0003. A similar order of values were measured using Mini Traction Machine [12] with a polished steel specimen at speed 1.5 m/s with roughness almost equivalent to the specimens used in this study. Other numerical studies also suggest such a low coefficient of adhesion for either an extremely smooth surface or high enough speed to separate contact bodies [10,23,42].

The predictive formula for elastic deformation of asperities gives extremely low values of the coefficient of adhesion similarly to smooth surface conditions. Increasing the roughness parameters had no significant influence on the elastic model prediction. Higher predicted coefficient of adhesion was acquired with increased roughness of the rough surface. At lower speed, the increased roughness caused 60% higher values of coefficient of adhesion compared with the smooth surface. This

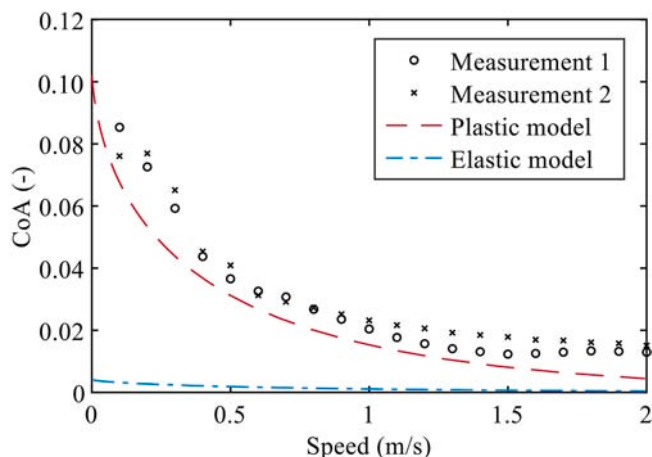


Fig. 10. Stribeck curve for rough surface.

happened even though the parameter K had only a small change going from smooth to rough surface. This can be explained by the sensitivity of predictive model to the change in roughness on a scale where film thickness and roughness are of the same order. The fact that small changes in surface roughness parameter can cause significant changes in the coefficient of adhesion was previously studied numerically [4,19], however it is important to distinguish the scale of roughness and speed on which this is studied. The roughness studied in this paper are not representative of real wheel-rail contact. For the case of rough surface, it is clearly visible that the plastic model predicts a slightly lower coefficient of adhesion than experimental data throughout the whole range of speeds. Around 1.2 m/s, it is clear that the measurement slowly saturates at the lowest measured value while the plastic model prediction continues a decreasing trend.

The changes in lubrication regime are controlled by the surface asperity distribution function in Eq. (5). A more accurate representation of the Stribeck curve might be achieved with a specific surface function to the measured surface topography. Previous studies [43] show that the functions F_n with Gaussian distribution might not have satisfiable precision and it is recommended to use surface-specific functions which better represent the true geometrical asperity distribution. It should also be noted that because of the method used to prepare a smooth surface of the ball specimen, there might be some dominant direction of asperities. Some research [10,13] shows that the coefficient of adhesion can change depending on the angle between the direction of rolling and the roughness orientation. However, this effect should become predominant at higher speeds rather than the lower speeds that reach the mixed lubrication regime in this study.

The film thickness defines surface separation which is key to determining the asperity load and coefficient of adhesion. Since the presented model uses iterative algorithm of changing the film thickness to obtain a solution, it is of interest to compare the iterative solution to analytical iso-viscous elastic formula, see Fig. 11. These results show the change difference in calculated film thickness compared to the analytical prediction by Esfahanian and Hamrock [14]. For both simulated surface conditions with the plastic model, the error is decreasing with the increase of speed. The smooth surface shows smaller changes in film thickness difference, which was also reported by Chen et al. [44]. However, the highest difference values mean only an order of a tenth of a nanometre, which is insignificant compared to the overall roughness. Higher speed makes the difference drop slightly under 0% and the iterative prediction slowly converges to around -4% in the observed range of speeds. This says that the lower the speed, the higher the surface separation needs to be. And thus, the asperity load is smaller than if the analytical film thickness was used.

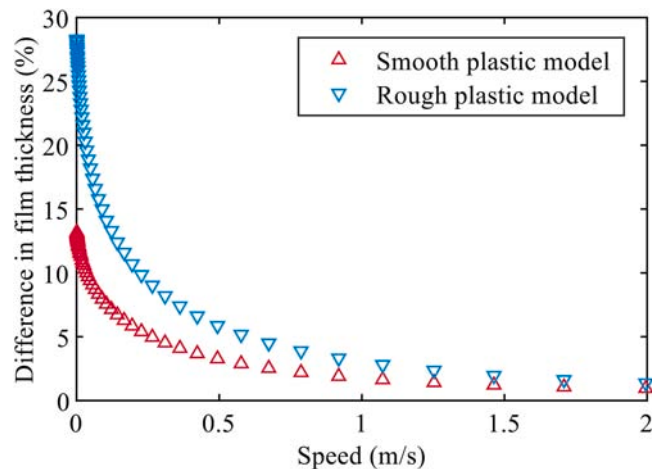


Fig. 11. Difference in film thickness acquired in comparison with analytical prediction.

Looking at the predicted values of load carried by asperities as shown in Fig. 12, the boundary regime can be clearly seen. The transition point from the boundary to mixed lubrication regime is located around $10e^{-2}$ to $10e^{-1}$ m/s. Asperity load proportion for the boundary regime increases with increased roughness of the contact surface. Using the data from dry experiment we can assume that the coefficient of adhesion for boundary regime of rough surface should be around 0.126 while for smooth surface 0.08. Further increasing the roughness should allow the contact to carry the full load by asperities in boundary regime. This would result in achieving a maximal coefficient of adhesion limited by dry contact. For the roughness cases used in this study, it would be optimal to accurately study the speed from 1 mm/s to 10 m/s to represent all three lubrication regimes: boundary, mixed and elastohydrodynamic. It is evident that such range of speed is not reachable with the used tribometer. For a future study on a larger scale experimental device, the operating conditions should be adequately chosen to allow the experiment to represent the whole range of Stribeck curve where the regime changes. For the real wheel-rail contact, the mixed lubrication regime should be between 50 and 200 m/s depending on the specific roughness based on previously conducted studies [4,7,8,23].

3.4. Traction measurements

Traction curves for the selected speeds are shown in Fig. 13. The initial part of traction curve before reaching the saturation point conveys the same trend for both measured and predicted values. The saturation point should be reached around 0.01 slip as suggested by the model, which is well correlated with the measured data. After reaching the saturation point there is only a small increase in the coefficient of adhesion with increasing slip as represented by both the model and experiment. The only exception is the lowest measured speed in Fig. 13a. At this speed, the trend of traction curve after saturation is decreasing. Other speeds measured do not exhibit this behaviour. This difference compared with other measurements might be because of higher values of the coefficient of adhesion influencing the asperity interaction and temperature changes. For real wheel-rail materials, it is expected that the coefficient of adhesion should drop with large slip values as reported by Refs. [7,11,45]. The largest discrepancy between model and experiment is present at a higher speed. For 1 m/s (Fig. 13c) the experiment shows higher values than the model prediction with still increasing values of the coefficient of adhesion. Similarly, the highest speed of 2 m/s (Fig. 13e) also shows higher measured values at higher slips. As seen from the Stribeck curves (Fig. 10), the model seems to predict decreasing values of adhesion coefficient even after 2 m/s. While the experiments show that around 1.5 m/s the lowest values are reached, and no further decrease is happening with increased speed. The measured values in

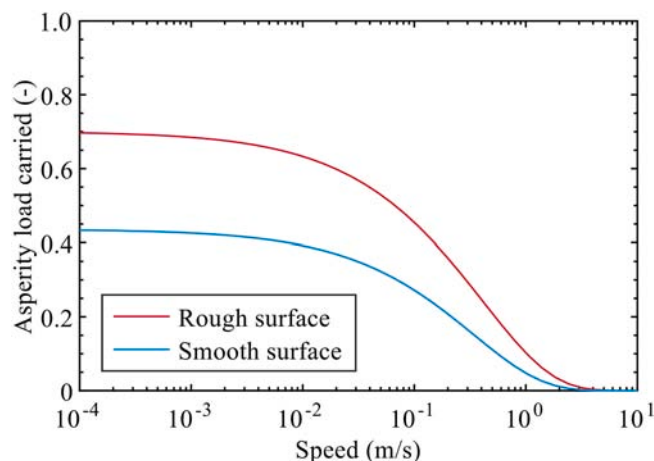


Fig. 12. Asperity load portion carried for different surface conditions.

Fig. 10 for speed 2 m/s and the corresponding values at 0.005 slip in Fig. 13e show a small discrepancy. The Stribeck curve measurement showed higher values of coefficient of adhesion in comparison with traction measurement. However, the difference is not too significant and most importantly, the trend with regards to the prediction model is the same.

3.5. Limitations and further development

Due to this study being conducted on a scaled apparatus with different materials of contact specimen, there are some aspects of the model that should be considered for future work. The material and roughness are far from the wheel-rail interface. However, for model validation the harder bearing steel and low roughness allow us to maintain stable surface conditions and work in the mixed lubrication regime. Also, these specimens prevent excessive wear to chrome layer which is important to determine film thickness which is a key parameter of the model. The generation of heat and its influence on lowering the coefficient of adhesion with an increase of slip [7,10,11,45] should be taken into consideration. A solution to this is using a temperature calculation across the contact area. A simple temperature calculation model using slip-velocity generated heat [46] can be used to give enough accuracy of temperature rise. The temperature influences not only the solid contact of materials [47,48] but also the behaviour of interfacial liquid [4,41]. For oil-based contaminants, a non-Newtonian property might also be expected at higher shear rates. Such a study [49] was previously conducted for shear-thinning properties of oil on a similar scale as this paper.

Another phenomenon that the presented model neglects is the dependence on pressure. Assuming iso-viscous water in the model means that viscosity does not change with pressure. However, liquids in general will increase viscosity with such pressure as in wheel-rail contact and this should be implemented accordingly as studied before [10,15,42]. For solid to solid contact, the pressure also influences the coefficient of adhesion. For dry contact, the increase in pressure causes a decrease in the coefficient of adhesion [1,7,16,19]. The calculated mean pressure from asperity contact defines the region of lubrication for set parameters. A more precise calculation can be done by using a more sophisticated modelling approach to plasticity [24–28,35,40]. These models could more accurately represent wheel-rail material and different types of contact conditions where the plasticity effect might be negligible or more dominant than what was observed in the current study. Moreover, the surface specific functions (Eq. (5)) can be defined more precisely [43], due to modern methods for roughness measurement.

4. Conclusions

The interfacial shear-based model together with ball-on-disc apparatus has been used to study the applicability of this model on rolling-sliding frictional contact contaminated with water. The asperity contact models studied are based on a simple formula for elastic or plastic deformation of asperities. The friction from asperity contact is based on Kalker's simplified theory, while the friction from liquid uses general EHL theory. For experimental validation, a tribometer with the capability to measure film thickness and coefficient of adhesion is used.

- For the studied conditions, the elastic model predicts a significantly lower coefficient of adhesion than the plastic model. The experimental data are in line with the plastic model. However, a difference in the trend at higher speed was found in an experiment with a rough surface. A deeper consideration should be taken when determining which asperity model to use for specific cases.
- The minimum coefficient of adhesion reached with water-contaminated smooth surface was equal to 0.4% of dry contact. Using a rough surface, the value increased to 7.2% of dry contact.

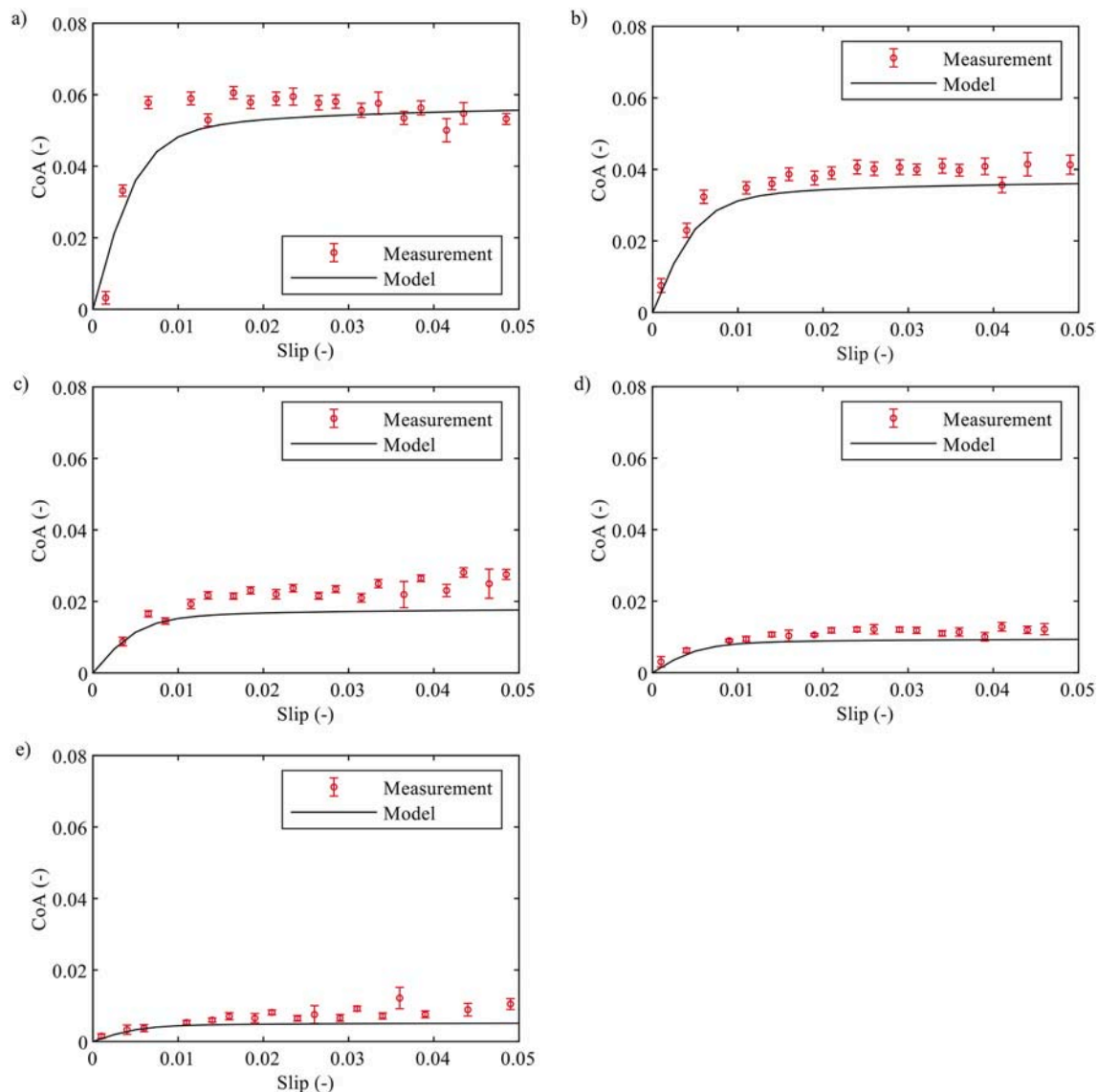


Fig. 13. Traction curves for speed: a) 0.25 m/s, b) 0.5 m/s, c) 1 m/s, d) 1.5 m/s, e) 2 m/s.

Such a difference was achieved with only 15% of change in roughness standard deviation σ .

- The shape of predicted Stribeck curves does not seem to fully correspond with measurement, especially at higher speed for the rough surface. The presented model predicts a more gradual decrease of coefficient of adhesion with an increase of speed. More accurate prediction of asperity load might be achieved with a surface specific function instead of Gaussian surface distribution. In addition, a more refined elasto-plastic asperity contact model can improve the estimation of mean asperity pressure.
- The presented model shows a good accuracy in predicting traction curves. Small differences between the experiment and model were observed. However, the trend of change with increasing speed and values of coefficient of adhesion is well within satisfiable accuracy.

The presented model gives a different approach for predicting friction in rolling–sliding contact. Using Kalker’s FASTSIM algorithm frees the solution from using a set value for asperity friction. This comes into more of importance in the real wheel–rail contact where the real friction in contact is not easy to precisely determine. However, further development is necessary to increase the accuracy of the model and to experimentally determine the properties of the contact interface.

CRediT authorship contribution statement

Daniel Kvarda: Conceptualization, Methodology, Investigation, Data curation, Writing - original draft. **Radovan Galas:** Conceptualization, Methodology, Investigation, Writing - review & editing. **Milan Omasta:** Conceptualization, Investigation, Methodology, Writing - review & editing, Project administration. **Lu-bing Shi:** Data curation, Writing - review & editing, Visualization. **Haohao Ding:** Writing - review & editing, Visualization. **Wen-jian Wang:** Conceptualization, Data curation, Writing - review & editing, Project administration. **Ivan Krupka:** Data curation, Writing - review & editing. **Martin Hartl:** Supervision, Funding acquisition.

Declaration of competing interest

The authors declare that they have no known competing financial interests or personal relationships that could have appeared to influence the work reported in this paper.

Acknowledgments

This research was supported by the Czech Science Foundation

(Project No. 20-23482S). The authors also thank the support by National Key R&D Program Intergovernmental Key Items for International Scientific and Technological Innovation Cooperation (No.2018YFE0109400) and Sichuan Science and Technology Program (No.2020YFH0057).

Appendix A. Nomenclature

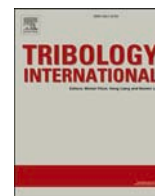
Nomenclature

a	Radius of contact area (m)
c	Rigid slip (m/s)
E	Effective elastic modulus ($1/E = 1/2((1-\nu_1^2)/E_1 + (1-\nu_2^2)/E_2)$, Pa)
E_1, E_2	Elastic modulus of body 1 and body 2 (Pa)
F	Total load applied to the contact (N)
F_{EHL}	Load carried by EHL film (N)
F_n	Surface function (–)
H	Mean pressure related to the hardness (Pa)
h_c	Central film thickness (m)
K	Surface roughness parameter (–)
L	Kalker's contact flexibility (mm^3/N)
L_e	Elastic flexibility of asperity contact (mm^3/N)
L_K	Kalker's contact flexibility (mm^3/N)
L_p	Plasticity parameter (m)
p	Contact pressure (Pa)
p_a	Average pressure carried by asperity (Pa)
r	Rolling radius (m)
U	Dimensionless speed parameter (–)
u	Surface displacement (m)
v	Rolling velocity (m/s)
W	Dimensionless load (–)
w	Slip velocity (m/s)
W_{BL}	Dimensionless load carried by asperity (–)
W_{EHL}	Dimensionless load carried by EHL film (–)
x	x coordinate in rolling direction (m)
y	y coordinate in lateral direction (m)
β	Asperity peak radius of curvature (m)
ϵ	Error tolerance for calculation convergence (–)
η	Viscosity of water at operating conditions (Pa s)
η_0	Viscosity of water at room temperature and ambient pressure (Pa s)
μ	Total coefficient of friction (–)
μ_{BL}	Coefficient of friction related to the asperity contact (–)
μ_{EHL}	Coefficient of friction related to the lubrication film (–)
ν_1, ν_2	Poisson ratio of body 1 and body 2 (–)
ρ	Density of asperity peaks ($1/\text{m}^2$)
σ	Standard deviation of roughness (m)
τ	Shear stress (Pa)
τ_{BL}	Shear stress in asperity contact (Pa)
τ_{c1}	Elasticity limiting shear stress (Pa)
τ_{c2}	Plasticity limiting shear stress (Pa)
τ_{EHL}	Shear stress in lubricant film (Pa)

References

- [1] Buckley-Johnstone LE, Trummer G, Voltr P, Meierhofer A, Six K, Fletcher DI, et al. Assessing the impact of small amounts of water and iron oxides on adhesion in the wheel/rail interface using High Pressure Torsion testing. *Tribol Int* 2019;135: 55–64.
- [2] Beagley TM. The rheological properties of solid rail contaminants and their effect on wheel/rail adhesion. *Proc Inst Mech Eng - Part F J Rail Rapid Transit* 1976;190: 419–28.
- [3] White B, Lewis R. Simulation and understanding the wet-rail phenomenon using twin disc testing. *Tribol Int* 2019;136:475–86.
- [4] Chen H, Ban T, Ishida M, Nakahara T. Adhesion between rail/wheel under water lubricated contact. *Wear* 2002;253:75–81.
- [5] Stock R, Stanlake L, Hardwick C, Eadie DT, Lewis R. Material concepts for top of rail friction management – classification, characterization and application. In: *Proceedings of 10th International Conference on Contact Mechanics and Wear of Rail/Wheel Systems*; 2015. p. 1–8.
- [6] Harmon M, Lewis R. Review of top of rail friction modifier tribology. *Tribol Mater Surface Interfac* 2016;5831:1–13.
- [7] Wang WJ, Shen P, Song JH, Guo J, Liu QY, Jin XS. Experimental study on adhesion behavior of wheel/rail under dry and water conditions. *Wear* 2011;271: 2699–705.
- [8] Chen H, Ban T, Ishida M, Nakahara T. Experimental investigation of influential factors on adhesion between wheel and rail under wet conditions. *Wear* 2008;265: 1504–11.
- [9] Wang H, Wang W, Liu Q. Numerical and experimental investigation on adhesion characteristic of wheel/rail under the third body condition. *Proc IME J J Eng Tribol* 2016;230:111–8.
- [10] Wu B, Wen Z, Wu T, Jin X. Analysis on thermal effect on high-speed wheel/rail adhesion under interfacial contamination using a three-dimensional model with surface roughness. *Wear* 2016;366–367:95–104.
- [11] Zhang W, Chen J, Wu X, Jin X. Wheel/rail adhesion and analysis by using full scale roller rig. *Wear* 2002;253:82–8.
- [12] Zhu Y, Olofsson U, Persson K. Investigation of factors influencing wheel-rail adhesion using a mini-traction machine. *Wear* 2012;292–293:218–31.
- [13] Chen H, Ban T, Ishida M, Nakahara T. Influential factors on adhesion between wheel and rail under wet conditions. *Q Rep RTRI* 2012;53:223–30.
- [14] Esfahanian M, Hamrock BJ. Fluid-film lubrication regimes revisited. *Tribol Trans* 1991;34:628–32.
- [15] Wu B, Wen Z, Wang H, Jin X. Numerical analysis on wheel/rail adhesion under mixed contamination of oil and water with surface roughness. *Wear* 2014;314: 140–7.
- [16] Rovira A, Roda A, Lewis R, Marshall MB. Application of Fastsim with variable coefficient of friction using twin disc experimental measurements. *Wear* 2012; 274–275:109–26.
- [17] Jin XS, Zhang WH, Zeng J, Zhou ZR, Liu QY, Wen ZF. Adhesion experiment on a wheel/rail system and its numerical analysis. *Proc IME J J Eng Tribol* 2004;218: 293–303.
- [18] Kalker JJ, Johnson KL. Three-dimensional elastic bodies in rolling contact, vol. 60. *Eisenbahntechnische Rundschau*; 1993.
- [19] Tomberger C, Dietmaier P, Sextro W, Six K. Friction in wheel-rail contact: a model comprising interfacial fluids, surface roughness and temperature. *Wear* 2011;271: 2–12.
- [20] Kalker JJ. On the rolling contact of two elastic bodies in the presence of dry friction. *Delft University of Technology*; 1967.
- [21] Kalker JJ. Survey of Wheel–Rail rolling contact theory. *Vehicle system dynamics. Int J Veh Mech Mobil* 1979;8:317–58.
- [22] Greenwood JA, Tripp JH. The contact of two nominally flat rough surfaces. *Proc Inst Mech Engrs* 1970;185:625–33.
- [23] Chen H, Yoshimura A, Ohyama T. Numerical analysis for the influence of water film on adhesion between rail and wheel. *Proc IME J J Eng Tribol* 1998;212: 359–68.
- [24] Kogut L, Etsion I. Elastic-plastic contact analysis of a sphere and a rigid flat. *J Appl Mech Trans ASME* 2002;69:657–62.
- [25] Jackson RL, Green I. A statistical model of elasto-plastic asperity contact between rough surfaces. *Tribol Int* 2006;39:906–14.
- [26] Li L, Etsion I, Talke FE. Contact area and static friction of rough surfaces with high plasticity index. *J Tribol* 2010;132:1–10.
- [27] Jackson RL, Green I. A finite element study of elasto-plastic hemispherical contact against a rigid flat. *J Tribol* 2005;127:343–54.
- [28] Cohen O, Kligerman Y, Etsion I. A model for contact and static friction of nominally flat rough surfaces under full stick contact condition. *J Tribol* 2008;130:1–9.
- [29] Buckley-Johnstone LE, Trummer G, Voltr P, Six K, Lewis R. Full-scale testing of low adhesion effects with small amounts of water in the wheel/rail interface. *Tribol Int* 2020;141:105907.
- [30] Galas R, Omasta M, Shi LB, Ding H, Wang WJ, Krupka I, et al. The low adhesion problem: the effect of environmental conditions on adhesion in rolling-sliding contact. *Tribol Int* 2020;151:106521.
- [31] Trummer G, Buckley-Johnstone LE, Voltr P, Meierhofer A, Lewis R, Six K. Wheel-rail creep force model for predicting water induced low adhesion phenomena. *Tribol Int* 2017;109:409–15.
- [32] Shi LB, Wang C, Ding HH, Kvarda D, Galas R, Omasta M, et al. Laboratory investigation on the particle-size effects in railway sanding: comparisons between standard sand and its micro fragments. *Tribol Int* 2020;146:106259.
- [33] Galas R, Kvarda D, Omasta M, Krupka I, Hartl M. The role of constituents contained in water-based friction modifiers for top-of-rail application. *Tribol Int* 2018;117: 87–97.
- [34] McCool JI. Comparison of models for the contact of rough surfaces. *Wear* 1986; 107:37–60.
- [35] Bhusan B. Contact mechanics of rough surfaces in tribology: multiple asperity contact. *Tribol Lett* 1998;4:1–35.
- [36] Six K, Meierhofer A, Mueller G, Dietmaier P. Physical processes in wheel-rail contact and its implications on vehicle-track interaction. *Veh Syst Dyn* 2015;53: 635–50.
- [37] Voce E. The relationship between stress and strain for homogeneous deformation. *J Inst Met* 1948;74:537–62.
- [38] Hartl M, Krupka I, Poliscuk R, Liska M. An automatic system for real-time evaluation of EHD film thickness and shape based on the colorimetric interferometry. *Tribol Trans* 1999;42:303–9.
- [39] Eisenberg D, Kauzmann W. The structure and properties of water. *Oxford University Press*; 2007.

- [40] Zhao Y, Marietta DM, Chang L. An asperity microcontact model incorporating the transition from elastic deformation to fully plastic flow. *J Tribol* 2000;122:479–80.
- [41] Tanimoto H, Chen H. Influence of surface roughness and temperature on wheel/rail adhesion in wet conditions. *Q Rep* 2015;56:206–11.
- [42] Wu B, Wu T, An B. Numerical investigation on the high-speed wheel/rail adhesion under the starved interfacial contaminations with surface roughness. *Lubric Sci* 2020;32:93–107.
- [43] Morris N. Asperity contact modelling for measured surfaces. 11th Int. Tribol. Conf. SAIT Tribol. 2015 0–7.
- [44] Chen H, Namura A, Ishida M, Nakahara T. Influence of axle load on wheel/rail adhesion under wet conditions in consideration of running speed and surface roughness. *Wear* 2016;366–367:303–9.
- [45] Gallardo-Hernandez EA, Lewis R. Twin disc assessment of wheel/rail adhesion. *Wear* 2008;265:1309–16.
- [46] Ertz M, Knothe K. A comparison of analytical and numerical methods for the calculation of temperatures in wheel/rail contact. *Wear* 2002;253:498–508.
- [47] Baek KS, Kyogoku K, Nakahara T. An experimental study of transient traction characteristics between rail and wheel under low slip and low speed conditions. *Wear* 2008;265:1417–24.
- [48] Ertz M, Bucher F. Improved creep force model for wheel/rail contact considering roughness and temperature. *Veh Syst Dyn* 2002;37:314–25.
- [49] Morgado PL, Otero JE, Lejarraga JBSP, Sanz JLM, Lantada AD, Munoz-Guijosa JM, et al. Models for predicting friction coefficient and parameters with influence in elastohydrodynamic lubrication. *Proc IME J J Eng Tribol* 2009;223:949–58.



The low adhesion problem: The effect of environmental conditions on adhesion in rolling-sliding contact

Radovan Galas^{a,*}, Milan Omasta^a, Lu-bing Shi^b, Haohao Ding^b, Wen-jian Wang^b, Ivan Krupka^a, Martin Hartl^a

^a Faculty of Mechanical Engineering, Brno University of Technology, Technická 2896/2, 616 69, Brno, Czech Republic

^b Tribology Research Institute, State Key Laboratory of Traction Power, Southwest Jiaotong University, Chengdu, 610031, China

ARTICLE INFO

Keywords:

Low adhesion
Wheel-rail tribology
Environmental conditions
Contaminated contact

ABSTRACT

Low adhesion problem is one of the major problems for railways all over the world because this phenomenon can occur anytime and anywhere. To investigate when poor adhesion conditions can be expected in real operation, a ball-on-disc tribometer with a climate chamber was employed to simulate rolling-sliding contact under various environmental conditions. Clean and contaminated discs with leaf extract were used to simulate different surface conditions. Results indicate that contact operating under rolling-sliding conditions is more prone to the occurrence of low adhesion than found by others for pure sliding contact. Very low adhesion (≤ 0.05) were identified for contaminated and oxidized specimens operating under humid and wet conditions. For clean surfaces, low adhesion (≤ 0.15) were found under dew conditions.

1. Introduction

Low adhesion between rail head and wheel tread is one of the major problems for railways in many countries all over the world. This phenomenon has a negative impact on cost, performance, and safety. The term “low adhesion” or “poor adhesion” is usually associated with the autumn season when a slippery layer from crushed fallen leaves is formed on the track. Both laboratory [1–3] and field research [4,5] revealed that this layer can result in the coefficient of adhesion (CoA) lower than 0.15, in some critical cases even lower than 0.05 [6]. Although it is a well-known fact that leaf contamination causes serious problems in railways all over the world; it must be emphasized that fallen leaves are not the only cause of low adhesion incidents. Besides fallen leaves, there are other causes of low adhesion which are mainly related to environmental conditions.

Water can be considered as one of the most common contaminants influencing adhesion in the wheel-rail contact. Water in the field can be found in various forms such as morning dew, fog, and light or heavy rain. These different forms may lead to different adhesion levels. In the case of bulk water, CoA can take values between 0.05 and 0.5 [7–12] depending on speed, roughness, and other parameters. More significant adhesion drop can be expected for slightly wet conditions, which usually occurs due to dew or light rain. Beagley et al. [13] observed that a small

amount of water from condensation decreased CoA to 0.22. Even more critical case was found when the rail was not free of solid particles. This combination of a small amount of water and solid particles (such e.g. wear debris) led to the formation of a viscous paste, which provided low (< 0.15) [14] or even very low CoA (< 0.05) [15].

In the case of weather conditions, daytime evolution of relative humidity (RH) and temperature can have a substantial impact on CoA. Beagley et al. [13] showed that CoA was reduced from 0.55 to 0.22 with increasing RH, while the effect of temperature was rather negligible during these tests. Similar findings were reported by Olofsson et al. [16] where the effect of RH on CoA was studied for dry and leaf contaminated contact using the pin-on-disc apparatus. It was found that the coefficient of friction (CoF) was reduced to 0.37 (dry) and 0.27 (leaf) when RH reached 95%. A pin-on-disc device was used also by Zhu et al. [17,18] who investigated the effect of RH and temperature on CoF for clean and rusted specimens. These complex studies showed that rusted discs generally led to lower CoF than found for clean discs; however, the lowest observed adhesion was still 0.4 or higher for both disc types. The lowest values of CoF was observed when RH reached 70%. A subsequent increase in RH did not lead to a further decrease in CoF.

Previous research works have shown that adhesion/friction is very variable depending on contaminants and current weather conditions. It means that low adhesion problem can happen anytime and anywhere.

* Corresponding author.

E-mail address: Radovan.Galas@vut.cz (R. Galas).

<https://doi.org/10.1016/j.triboint.2020.106521>

Received 12 May 2020; Received in revised form 15 June 2020; Accepted 19 June 2020

Available online 5 July 2020

0301-679X/© 2020 Elsevier Ltd. All rights reserved.

Although a decrease of CoA/CoF was observed in all above-mentioned studies, low CoA or CoF (<0.15) was found predominantly when contact was contaminated with leaves. However, White et al. [19] reported that many of low adhesion incidents in a real operation were not associated only with leaf contamination but there were other factors leading to low adhesion incidents. These authors suggested several reasons why these low adhesion incidents happened, such as due to the presence of water, moisture or not detectable leaf layer. The conditions and mechanisms leading to low adhesion phenomenon are not fully understood.

The main objective of this study is to reveal conditions when low adhesion ($\mu \leq 0.15$) and very low adhesion conditions ($\mu \leq 0.05$) can be expected in the wheel-rail contact. Special attention is paid to the effect of RH, temperature and leaf contamination. For this purpose, a ball-on-disc tribometer with a climate chamber is employed. This contact configuration is chosen because it enables to set typical rolling-sliding conditions occurring in the wheel-rail interface. Based on the previous studies, it is assumed that pure sliding configuration, where a pin is in permanent contact with the counterpart, is not sufficiently representative in terms of the formation and action of the third-body layer. The presence of this layer is important to study low adhesion problem.

2. Material and methods

2.1. Test setup and specimens

Adhesion measurements were conducted on the ball-on-disc tribometer (Mini-traction-Machine, PCS Instruments) where a 19.05 mm steel ball and 46 mm diameter flat steel disc was loaded against each other as is depicted in Fig. 1. Both these specimens were independently driven, thus a rolling-sliding contact (where the slip was accurately controlled) can be achieved. The slip is defined in Eq. (1), where w_{ball} and w_{disc} are the angular speeds of the ball and the disc respectively and r_{ball} and r_{disc} represent the radii of specimens. CoA was calculated as a ratio between traction and normal forces which were directly measured using embedded sensors.

$$\text{slip} = \frac{w_{ball} \cdot r_{ball} - w_{disc} \cdot r_{disc}}{w_{ball} \cdot r_{ball} + w_{disc} \cdot r_{disc}} \cdot 200\% \quad (1)$$

The material of both the ball and the disk was bearing steel AISI 52 100 with the hardness of 800–920 HV (ball) and 720–780 HV (disc). The initial roughness of the ball and the disc was Ra 0.01 μm and Ra 0.02 μm respectively. These specimens were enclosed in a climate chamber where temperature and air humidity were controlled. Heating was ensured by heaters installed in the tribometer body while cooling was

provided by an external cooling unit with cooling oil circulating through the tribometer body. Air with controlled RH and ambient temperature was fed to the chamber from external humidity unit. Thanks to the method of cooling, this equipment enables to reach dew point conditions resulting in water condensation on the surface of the disc. Detail parameters of employed sensors are listed in Appendix A.

2.2. Experimental conditions and procedure

Several sets of adhesion measurements were conducted under various operating and environmental conditions, see Table 1a. For all sets, a contact pressure of 750 MPa (a normal force of 17 N) was used to achieve representative light rail system contact conditions. In the beginning, tests under dry and wet (fully-flooded) conditions were run to obtain reference CoA values for dry and wet (heavy rain) conditions. Based on these tests, adhesion characteristics for dry and wet (fully-flooded) conditions were drawn for a speed range of 0.5–3 m/s. Each point on adhesion characteristics was evaluated as the average value from a 30-s test. After the completion of these reference tests, other tests were always conducted with a fixed slip value of 5% and a speed of 1 m/s. Test sets No. 3 and 4 were focused on the effect of water (light precipitation) and leaf extract amounts on CoA. Last two test sets (No. 5 and 6) were performed under various temperature (1–50 $^{\circ}\text{C}$) and RH values (6–100%) to investigate conditions occurring throughout the day. Moreover, the last test set was conducted with the contaminated disc (described below) to combine the effects of leaf contamination, RH, and temperature on CoA.

Leaf contamination was represented in two ways: as a liquid leaf extract and as a dry friction layer (from the extract) on the disc. The leaf extract was prepared from leaves which were gathered from fallen maple, beech, birch and oak leaves near the railway network in autumn. Subsequently, leaves were chopped into small pieces (approx. 5 μm) and soaked in water for 5 days. After that, excess water was separated and the leaf extract was obtained as shown in Fig. 1b. A dry layer from leaf extract was prepared one day before testing. The preparation of the layer proceeded in several steps. At first, 20 μl of leaf extract was applied on the disc and then, several cycles under pure rolling conditions were carried out to create a uniform friction layer around the circumference of the disc. Finally, the disc was left for several hours to ensure that all liquid contained in the friction layer was evaporated. This preparation process of dry leaf layer was needed before each particular measurement. The disc with the layer is further referred to as “contaminated disc”.

Each test in Table 1, except tests with the contaminated disc, was started by a running-in to remove oxides and any other residual layers adhered on contact surfaces. This running-in was stopped when a stable and dry level of adhesion was reached. Experimental conditions of running-in (speed, slip, etc.) were the same as the conditions of the “main” test performed immediately after this running-in. As is evident from Table 1, some tests were carried out with oxidized disc. In this case, the clean disc was run under wet (fully-flooded) conditions to form the oxide layer. This wet running-in was stopped when CoA was dropped (due to the presence of oxides) and stabilized. All liquids were applied to the contact using a micropipette with a dosing accuracy of $\pm 0.04 \mu\text{l}$. In the case of fully-flooded conditions, the disc was immersed in water. At the end of each test, both specimens were removed from tribometer and ultrasonically cleaned with acetone. The statistics data of all tests are listed in Appendix B.

To judge the effects of tested contaminants and environmental conditions listed in Table 1, the following intervals of CoA were considered in this study: *high adhesion* $\mu > 0.4$, *intermediate adhesion* $0.4 \geq \mu > 0.15$, *low adhesion* $0.15 \geq \mu > 0.05$, and *very low adhesion* $0.05 \geq \mu$.

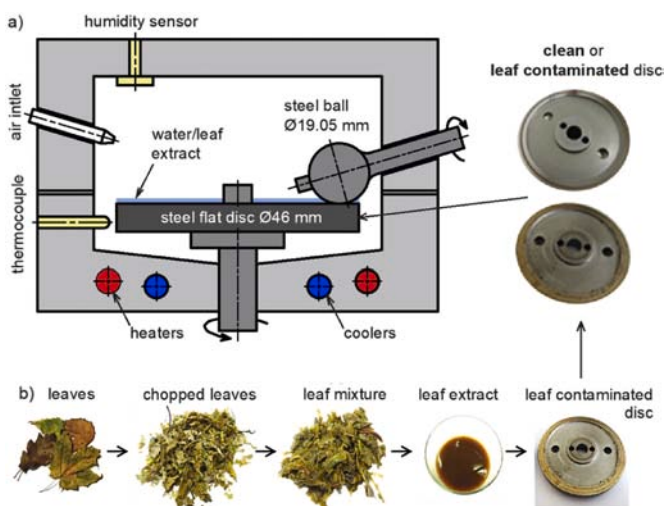


Fig. 1. (a) Scheme of the ball-on-disc apparatus with a climate chamber, (b) preparation of leaf extract and contaminated disc.

Table 1
Experimental conditions of the tests.

set of tests	contaminant	disc	amount (µl)	running-in	mean speed (m/s)	temp. (°C)	RH (%)	Hertz pressure (MPa)	slip	correspond Fig. No.
1r ^a	none	clean	–	dry	0.5–3	ambient	ambient	750 ± 3	0–8	2
2r ^a	water	clean	fully-flooded	wet						3a
3	water	oxidized	1–10	dry	1				5	3a, 3b
4	leaf extract	clean	1–20							4, 5, 8
5	none					1–50	8–100			6, 7, 8
6	none	contam.	–	none			6–100			9, 10a, 11a, 12a, 13a
overview of selected results										10b, 11b, 12b, 13b
										16

^a Reference tests.

3. Results and discussion

3.1. Reference tests under dry and wet conditions

To obtain reference values of CoA, adhesion characteristics under dry and wet (fully-flooded) conditions were measured for four different mean speeds (Fig. 2 and Fig. 3).

Fig. 2 shows data from the tests ran in dry conditions where CoA reached the typical values for non-lubricated rolling-sliding contact operating in laboratory conditions [9,20]. The results also indicate that there was almost no significant change in CoA as the speed increased; however, the tested speed range used in this study was rather limited. As was shown in Table 1, most of the tests were carried out at 5% slip. For this particular slip value, CoA reached approximately 0.6 for all tested speeds. The value of 0.6 is considered as a reference value of CoA for dry conditions in later parts of this study.

Besides the value of CoA, the shape of the adhesion characteristic is another important factor influencing a maximum available adhesion in the contact and wear (corrugation formation especially). From the results in Fig. 2, it is obvious that a positive slope of the adhesion characteristic was found in all cases even though the negative adhesion characteristic is generally expected for non-lubricated wheel-rail contact as was found in Ref. [21]. The reason for this discrepancy may be the fact that the slip in laboratory research is usually set as a fixed value, while the slip in a real wheel-rail contact can immediately change depending on current operating conditions. This hypothesis is consistent with the findings from previous laboratory research, where the positive adhesion characteristic was also observed under dry conditions [22,23].

When tests under dry conditions were completed, the same set of experiment was conducted again with pure water under fully-flooded conditions, which ensured that the contact did not starve during the test, see the set of tests in Fig. 3a marked as “no oxide”. The results give evidence that no significant drop of CoA occurred under these conditions. Even at the maximum speed, CoA reached a relatively high value

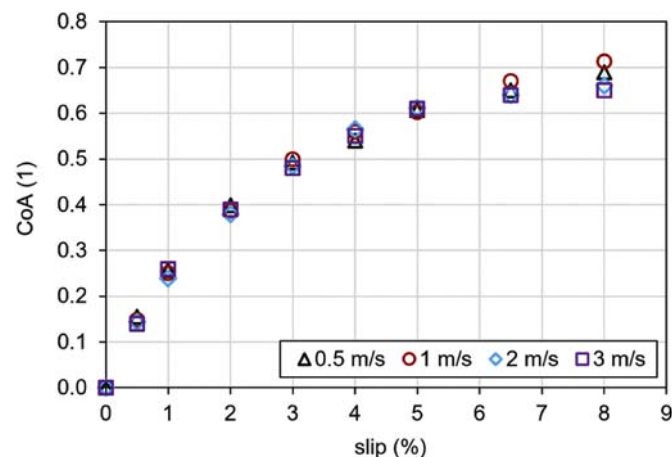


Fig. 2. Adhesion characteristics for different speeds in dry conditions.

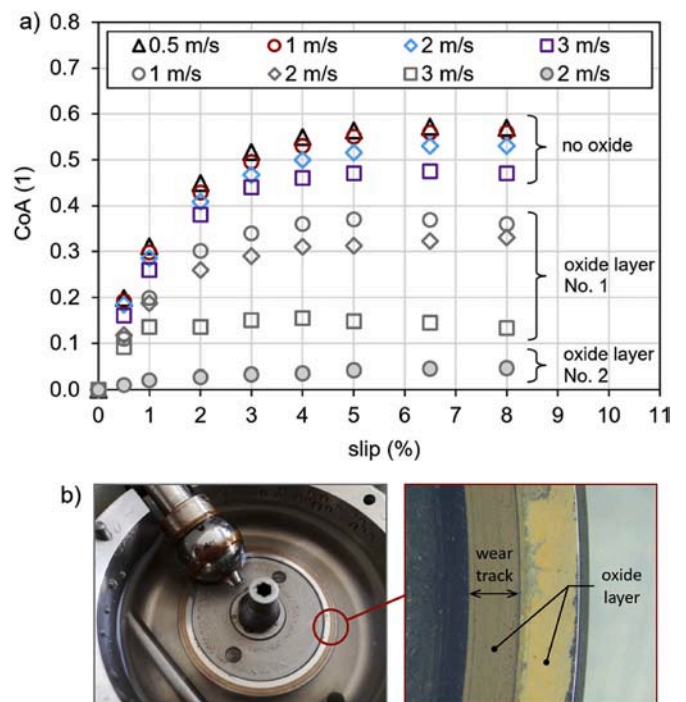


Fig. 3. (a) Adhesion characteristics in wet (fully-flooded) conditions for clean (colour points) and oxidized disc (grey points), (b) the oxide layer No. 1. (For interpretation of the references to colour in this figure legend, the reader is referred to the Web version of this article.)

of 0.47 at 5% slip which means that CoA was reduced by 28% compared to dry conditions. The fact that wet conditions did not lead to low adhesion is well correlated with lambda prediction for isoviscous-elastic lubrication regime. For the tested range of speeds (from 0.5 to 3 m/s), the lambda parameter ranged between 0.02 and 0.07 which means that the contact was operating in the boundary lubrication regime. This regime can be supposed for trams and non-high speed trains when rain is heavy and other contaminants are washed away from the rail surface. The similar findings were reported by Chen et al. [10] where CoA under wet conditions was measured by the twin-disc machine. Chen’s results showed that CoA at low speed ($v < 2$ m/s) reached high values ($\mu > 0.4$). Moreover, these authors conducted the tests with a lower slip ($s = 0.7\%$) and also the roughness of specimens was approx. half in comparison with the roughness in the present study.

However, there are some publications [1,3,9] where the application of water resulted in substantially lower CoA (between 0.17 and 0.28) than found in the present study. There are two things which can explain this important difference. Firstly, other authors used lower slip values leading to lower values of CoA. Note that the slip value of 5% in this study was chosen based on the actual shape of adhesion characteristics in Fig. 2. This slip value should ensure that the contact was operating near to the saturation point as is apparent from curves in Fig. 3a. The

second thing is that in this study the material of specimens was the bearing steel AISI 52 100 which differs from common wheel and rail materials in chemical composition as well as in the hardness. Note that the bearing steel contains Cr (1.3–1.6%) which can affect an oxidation rate. These different properties of specimens could slow down the formation of the oxide body layer between contact surfaces.

Consequently, the second set of tests under wet conditions were conducted. In that case, each test was started by running-in under wet (fully-flooded) conditions to oxidize the disc. This wet run-in period of the test took approx. 30 min until a visible oxide layer has been formed on both contact surfaces, see Fig. 3b. After that, CoA was evaluated for the same experimental conditions as before, see the set of tests in Fig. 3a marked as “oxide layer No. 1”. Subsequently, the same test with wet run-in period was conducted again for the speed of 2 m/s, but the duration of wet running-in was doubled compared to the previous test. This longer wet run-in period ensured that a different level of surface oxidation was reached, see the test in Fig. 3a marked as “oxide layer No. 2”. By comparing the results in Fig. 3a, it can be concluded that the presence of an oxide layer under wet conditions can cause a significant adhesion decrease. At 2 m/s and 5% slip, CoA was reduced to 0.37 and 0.041 depending on the level of surface oxidation. These results imply that heavy rain does not generally cause poor adhesion conditions itself but CoA can be significantly impacted by heavy rain when contact surfaces are covered by an oxide layer. These findings are consistent with the findings in Ref. [24] where the presence of an oxide layer under wet conditions caused that CoA was reduced by up to 75% compared to a reference wet test without oxide layer.

3.2. Effect of a small amount of water on CoA

To imitate light rain, the effect of small amounts of water on CoA over time was investigated, see Fig. 4a. These friction curves show that a drop of CoA occurred immediately after water application; however, poor adhesion conditions were not observed in any of the tests. On the other hand, small amounts of water reduced CoA significantly more than found under fully-flooded conditions, see Fig. 4b. Comparing to dry (0.6) and wet fully-flooded conditions (0.55), CoA was reduced up to by 35 and 20% respectively when small amounts of water were applied into the contact. The results show that the larger the amount of water, the less significant decrease in CoA (the average value in the middle part of friction curve) and the longer drop time of CoA “ t ” (from 5 to 39 s).

Friction curves in Fig. 4a are compared to each other in detail in Fig. 4b. This figure shows that friction curves can be described by three followings points: μ_0 , μ_m , μ_{min} . The first point μ_0 represents the drop of CoA occurring immediately after the application of water; so this point describes the transition between dry and wet conditions. After that, CoA usually slightly increases and CoA is more or less stable because a friction boundary layer is formed. This “middle” part of the friction curve

can be described by the second point μ_m . The last point μ_{min} describes the transition between wet and dry conditions. This phenomenon is usually accompanied by a significant decrease in adhesion as can be seen in Fig. 4b for 10 μl . This is in line with Ref. [25] where a similar trend of friction curve was found for the case when water was applied continuously and then water was stopped and hot air drier was started. Note that in that study the second adhesion drop μ_{min} was observed after several cycles since stopping the water.

The data from this and the following subchapter are summarized in Fig. 6. As was mentioned above, no poor adhesion conditions were found for contact contaminated with a small amount of water. The lowest observed CoA during all tests was 0.36. Nevertheless, considering the results in the previous chapter, it can be reasonably expected that the combination of a small amount of water and oxides or other solid contaminants can lead to very low CoA. In that case, a small amount of water and solid particles can form non-Newtonian viscous mixture/paste [13] resulting in low or even very low CoA, e.g. $\mu = 0.14$ in Refs. [23], and 0.05 in Ref. [26].

3.3. Effect of leaf contamination on CoA

To investigate the conditions typical for autumn months, friction tests with different amounts of leaf extract were carried out, see Fig. 5a. It was found that all tested amounts of leaf extract caused a rapid drop in CoA leading to low adhesion conditions ($\mu \leq 0.15$), see Fig. 5b. These results are in good agreement with previous laboratory studies where CoA was lower than 0.1 for both leaves [2] and leaf extract contamination [27].

As can be seen from the comparison of Figs. 4b and 5b, there are similarities between friction curves for a small amount of water and leaf extract. For both of these tests, the same following stages of friction curves can be identified: (1) a rapid decrease of CoA occurring after the application (μ_0 , μ_{0L}), (2) relatively stable middle part of CoA (μ_m , μ_{mL}), (3) the second drop in CoA related to the transition between wet and dry conditions (μ_{min} , μ_{minL}), and (4) the final rapid increase of CoA. The only exceptions are the tests with the smallest applied amount of water/leaf extract because these amounts seem to be insufficient for forming of a lubrication film around the circumference of the ball and the disc; thus, the contact quickly starved and CoA increased rapidly. Besides this, it should be emphasized that in case of tests with leaf extract, CoA was stabilized at values less than the reference value for dry adhesion, see ΔCoA in Fig. 5b. This difference in CoA may be due to the changes in surface conditions of specimens that occurred during the test. Furthermore, CoA may be also affected by the presence of residual components from leaf extract, which remained in the wear track.

As mentioned in Chapter 2, a leaf extract is a mixture of water and a liquid lubricant released from the chopped leaf pieces. This composition may explain the similarity of a shape of friction curves under wet and

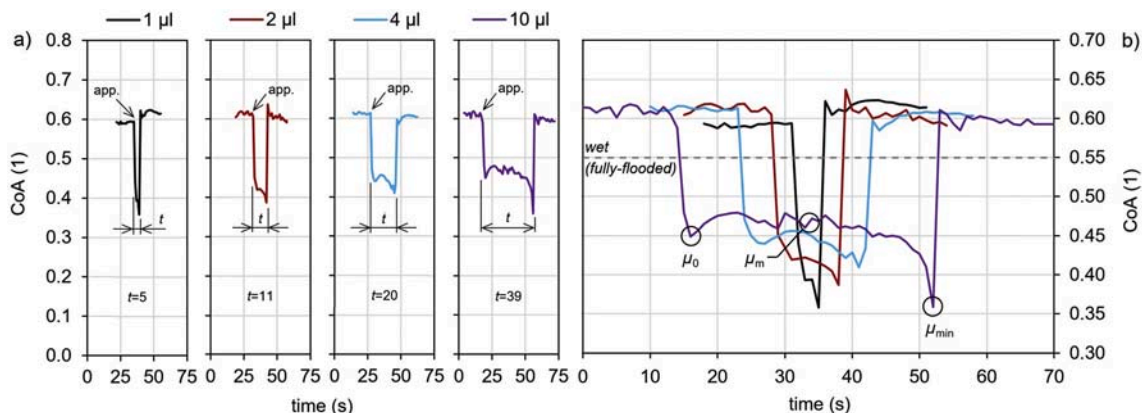


Fig. 4. (a) Friction curves for contact contaminated with a small amount of water, (b) detailed comparison of these curves.

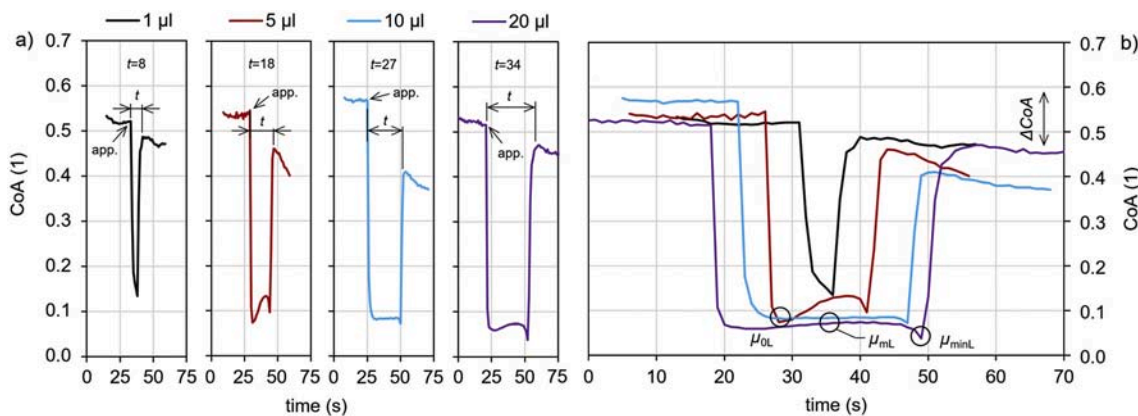


Fig. 5. (a) Friction curves for contact contaminated with different amount of leaf extract, (b) detailed comparison of these curves.

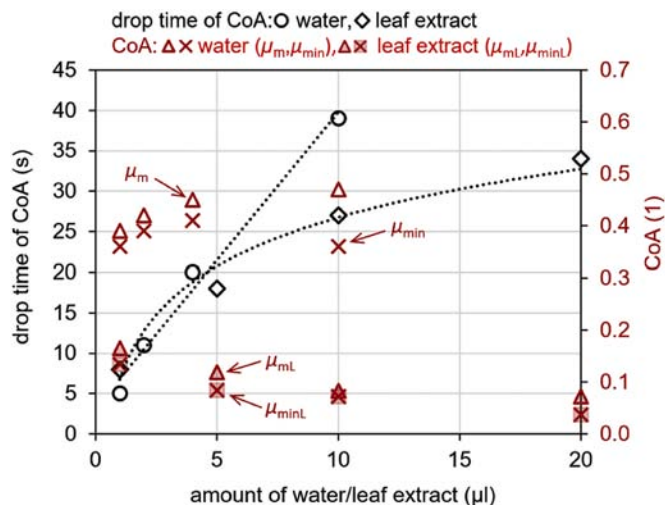


Fig. 6. The effect of the amount of water/leaf extract on drop time of CoA and on the level of “CoA”.

leaf extract conditions. Moreover, this composition explains why CoA was even lower than 0.05, see Fig. 6. It is a well-known fact that a mixture of water and oil leads to very low CoA, even lower than for pure oil [28]. Fig. 6 also shows that there is an opposite dependence between the applied amount of leaf extract and CoA than was observed for different (small) amounts of water.

3.4. Effect of humidity and temperature on CoA

The influence of humidity and temperature on CoA was studied for the clean and contaminated disc, see Fig. 1. Fig. 7 shows an example of friction tests with a clean disc where the effect of various RH on CoA was investigated at a constant air temperature of 1 °C. The same set of tests were carried out, for both clean and contaminated disc, for various temperatures according to Table 1. Based on the data from the last 30 s of each measurement, the average CoA was calculated and Fig. 8 and Fig. 10, which describe the relationship between CoA and RH for various air temperatures, was plotted.

The results in Fig. 8 show that an increasing RH reduces CoA for all tested conditions and the trend is nearly linear. For the clean disc (Fig. 8a), it was investigated that CoA is almost insensitive to changes in RH for temperature higher than approximately 30 °C. In contrast, the effect of RH on CoA becomes substantial when the temperature drops to or below 24 °C. The combination of low temperature and high RH led to the condensation resulting in a rapid decrease of CoA, see the

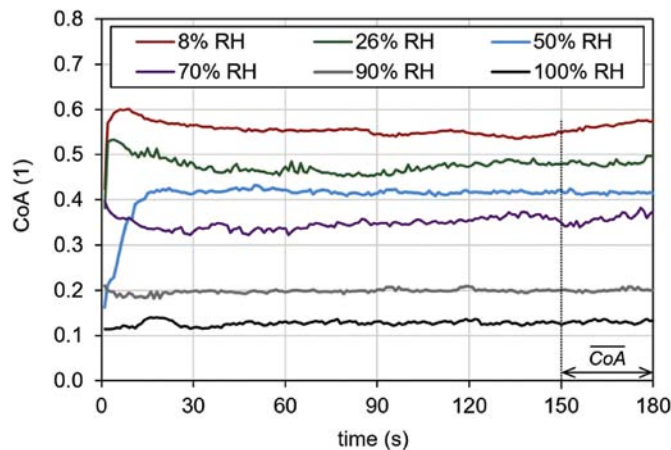


Fig. 7. Effect of RH on CoA for the clean disc at air temperature 1 °C.

condensation area in Figs. 8a and 9a. Under these undesirable conditions, low adhesion conditions occurred ($\mu \leq 0.15$) when the air was fully-saturated with water (RH = 100%).

An even more significant decrease in CoA was found for the tests with the contaminated disc. The results in Fig. 8b revealed that for RH values below 10% the presence of the leaf layer on the disc decreases CoA by only 0.1 (compared to the tests with the clean disc). Once RH starts to rise, CoA falls more dramatically than for the clean disc. Unlike tests with the clean disk, a significant decrease of CoA was observed even for high temperatures. A substantial decrease of CoA was found for lower temperatures (1 and 10 °C) when RH value was higher than 60%. As expected, the lowest CoA was found when a dew point occurred, see the condensation area in Figs. 8b and 9b. Under these conditions, CoA was lower than 0.1 and at some points even lower than 0.05; so very low adhesion conditions were found. This abrupt fall of CoA could occur as a result of the softening of the leaf layer with a small amount of condensation water. This softening could lead to a decrease in the shear strength of the leaf layer; thus, the maximum achievable CoA in the contact was reduced.

The results above revealed that CoA decreases with increasing value of RH. The most considerable adhesion drop was observed for the temperature to be 24 °C and lower, once the condensation occurred. Under these conditions, CoA was reduced to 0.13 and 0.04 for clean and contaminated disc respectively. These results are well correlated with Ref. [14,16–18] where a gradual decrease of CoA with increasing RH was also observed. However, it must be noted that the lowest observed CoA in these studies was 0.22 [14], 0.28 [16], 0.41 [17], and 0.40 [18], even though the tests were performed with leaves [16], with the rusted

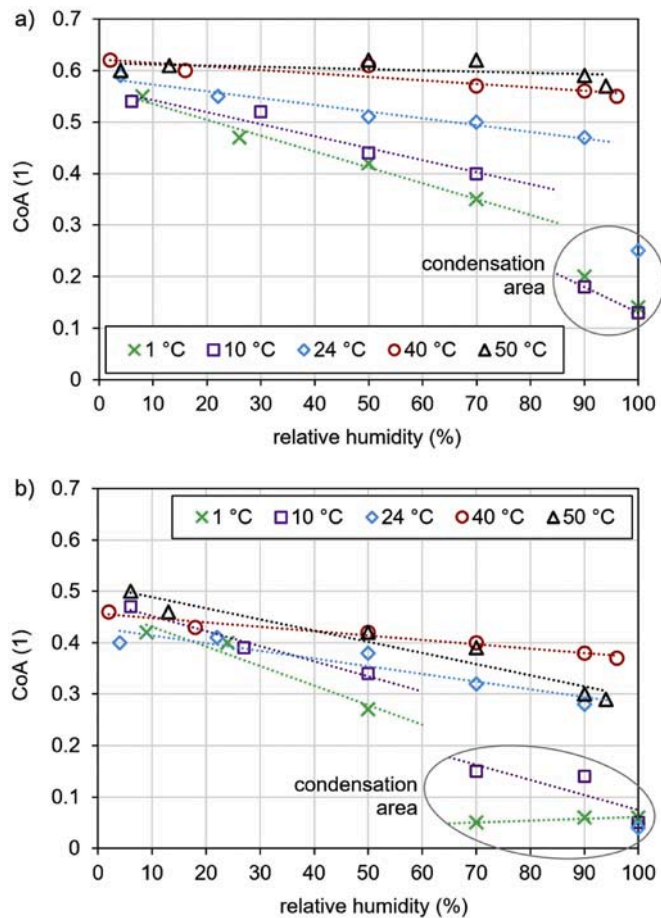


Fig. 8. Effect of RH and temperature on CoA for clean disc (a) and contaminated disc (b).

disc [17,18], and with the heavily rusted disc [17]. In the case of Ref. [14], a twin-disc Amsler machine was employed and the temperature range during tests was from 20 to 40 °C. Results in Ref. [14] showed the friction coefficient was almost independent of temperature; however, the tested temperature range was very limited. As was shown in the present study, the greatest decrease in CoA was found for the temperatures lower than 20 °C. In the case of Ref. [16–18], tests were conducted using a pin-on-disc tribometer operating under pure sliding conditions. Generally, these conditions can lead to a higher contact temperature and can cause severe removal of oxide layers formed on surfaces, whereby the occurrence of low adhesion associated with high RH value, or even with condensation, can be suppressed.

Finally, the data from Fig. 8 were recalculated to the absolute humidity (AH) in g/m³ with the following equation using Bolton's approximation for the saturation vapour pressure of water [29]:

$$AH = \frac{6.112 \cdot e^{\left[\frac{17.67 \cdot T}{T + 243.5} \right]} \cdot RH \cdot 2.1674}{273.15 + T} \quad (2)$$

where T is a temperature in °C and RH is the relative humidity in %RH. The results in Fig. 10 show that the trend is nearly linear for each temperature; however, the data in the condensation area do not follow the trend for the specific temperature without condensation.

3.5. Analytical model for prediction of CoA

The results of CoA measurements for various temperatures and various RH values are summarized for both clean and contaminated

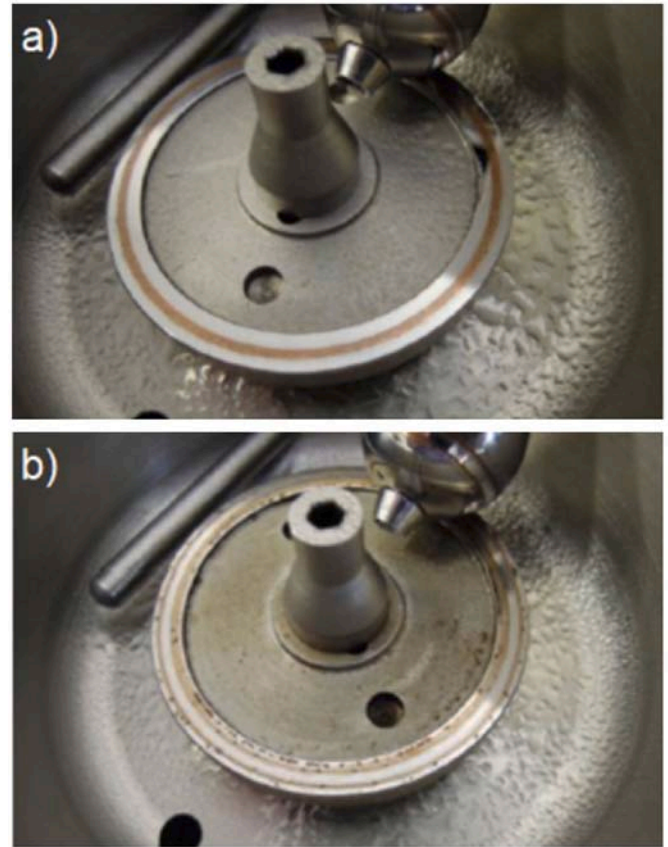


Fig. 9. Condensation during tests with the clean disc (a) and contaminated disc (b).

conditions in the contour plot in Fig. 11. It should be noted that the data when condensation occurred are not included in these graphs. The experimental data were fitted to the following regression equations:

$$\mu_{clean} = 0,5461 + 0,003029 \cdot T - 0,002844 \cdot RH - 3,346 \cdot 10^{-5} \cdot T^2 + 5,401 \cdot 10^{-5} \cdot T \cdot RH \quad (3)$$

$$\mu_{contaminated} = 0,4153 + 0,001587 \cdot T - 0,001662 \cdot RH \quad (4)$$

where T is a temperature in °C and RH is the relative humidity in %RH. In the model, the dependence of CoA on temperature is a quadratic polynomial for clean conditions while for leaf-contaminated conditions is linear. The dependency on RH is linear in for both cases. This regression model leads to a very good determination coefficient of 0.962 for clean conditions and fairly good value of 0.725 for contaminated conditions. Generally, CoA for contaminated conditions is in average 25% lower than that under clean conditions. The difference is very low for the lowest adhesion that starts at app. 0.25 because the contaminated data are not included. The area of occurrence of relatively low or intermediate adhesion is larger for contaminated conditions. Larger differences can be observed for higher adhesion values where the maximum CoA 0.65 and 0.45 for clean and contaminated conditions respectively.

The analytical model for the clean disc, created as an approximation of measured data, predicts the effect of RH on CoA as a linear function with a very good determination coefficient. However, previously published studies [17,18,30–34] have reported an uneven trend. Some of them [30–32] point to a more significant drop in friction accompanied by an abrupt change in wear mechanism, although the transition level of RH varies across the studies between 15% [30], 45–55% [31] and 50 a 60% RH [33]. Other studies predict the trend as bilinear, wherein the

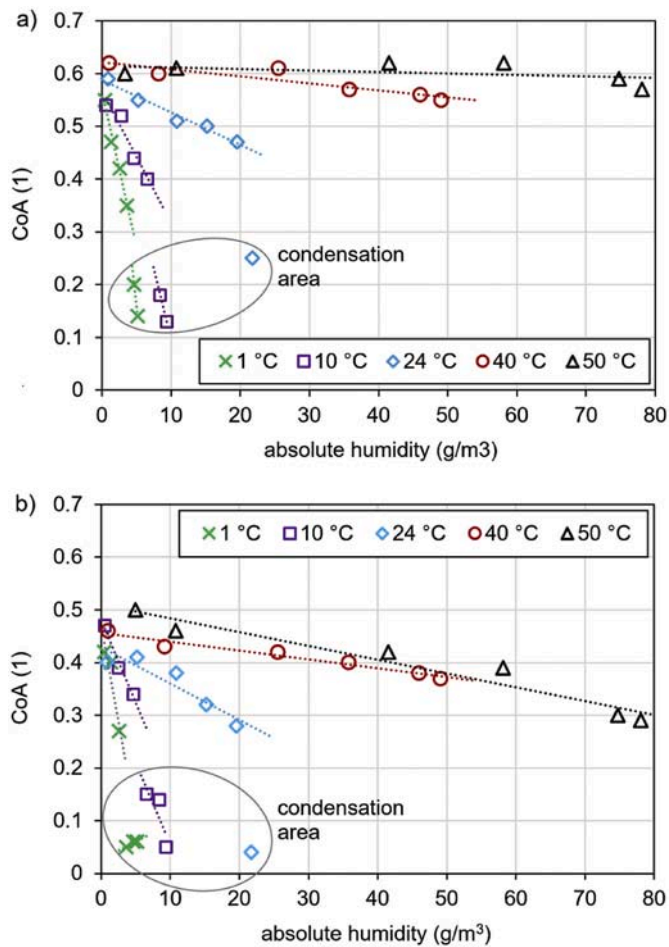


Fig. 10. Effect of AH and temperature on CoA for the clean disc (a) and contaminated disc (b).

change in behaviour occurring at 65% RH is explained by counterbalancing the effect of the boundary layer formed by the water molecules and hematite film formation at higher RH [17,18,33]. This difference in the trend can be explained by two following facts.

Firstly, the data in the present work represents CoA determined in rolling-sliding contact at a slip of 5%, whereas most of the previous studies utilized a pure sliding friction approach to measure CoF. As apparent in Figs. 2 and 3a, this slip was still before the saturation point in the ball-on-disc configuration, so the difference between CoA and CoF was substantial. The second difference is associated with the formation and retention of oxide layers between pure sliding and rolling-sliding tests. In real wheel-rail contact (rolling-sliding contact), the oxide layer usually consists of two types of oxides, magnetite (Fe₃O₄) and hematite (α-Fe₂O₃) [33,35,36]. Magnetite, known as “black oxide”, decreases friction while hematite has generally a tendency to increase friction [35]. Some hypotheses consider that under higher humidity normal atmospheric oxidation is inhibited because of the effect of water molecules in the surrounding air [37]. This could explain decreasing friction with RH when considering slowed down the formation of hematite. However, the process of oxide layer formation under pure sliding conditions can vary greatly. A pin operating under pure sliding conditions is in permanent contact with a counterpart that generally leads to higher flash temperature and heat dissipation can cause higher pin bulk temperature. Moreover, the formation of oxide layers on the pin/disc surface is prevented, as well as the access of water molecules to the wear track [38]. This is in contrast to rolling-sliding contact which provides a time for the environment to act on both surfaces during each cycle and it does not cause such an intensive removal of the formed layer.

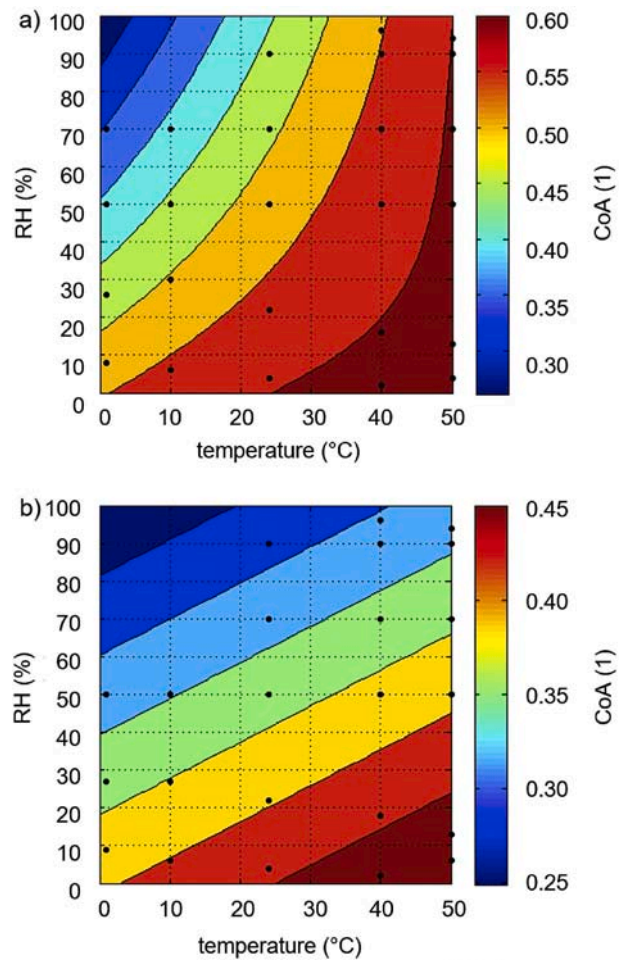


Fig. 11. Contour plot of the regression model of the effect of RH and temperature on CoA for clean conditions (a) and contaminated conditions (b).

Note that there is also a question about the effect of sample material. From this perspective, the most representative studies are those using a real rail and wheel steels [17,18,32,36,38]. Nevertheless, a fundamental discussion on the effect of relative humidity on friction and wear comes from studies using more general materials such as carbon steels [31], austenitic stainless steel [33,39] and bearing steel [30,40] and the trends are qualitatively similar. It is believed that the effect of the material is not as significant as the effect of the testing configuration.

3.6. General discussion: possible occurrence of low adhesion

The summary of the selected results is depicted in Fig. 12 where the results are categorized into different adhesion intervals. This figure gives evidence that neither heavy nor light rain does not lead to low adhesion conditions when contact surfaces are clean (free of debris). However, clean surfaces in operation can be expected very rarely such as after heavy rain when contaminants are washed away. Otherwise, rail and wheel surfaces are contaminated with dust, wear debris, their oxides, etc. These solid contaminants affect adhesion even under dry conditions; however, their impact on CoA can be much more substantial under wet conditions as was observed for oxidized surfaces operating under fully-flooded conditions, see Fig. 12. Under these conditions, even very low adhesion conditions were found when the contact was run-in under wet conditions before the test; thus, the thick and uniform oxide layer has been formed on the surfaces. With respect to these findings, it can be reasonably expected that more significant adhesion drops may occur even for light precipitation when contact surfaces are covered by the

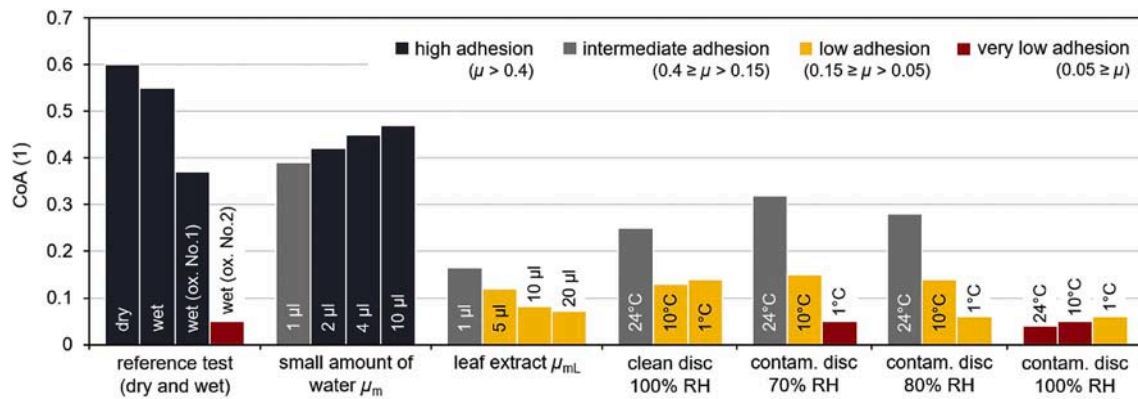


Fig. 12. Overview of selected results.

oxide layer or contaminated with free solid particles, as was observed in Ref. [13,15,23,26].

Besides water, leaves are common natural contaminants causing an annual problem for rail transportation. To study the effect of leaves on adhesion, two approaches were used in this study. In the former case, a liquid leaf extract was used as a lubricant which was applied directly into the contact, while in the latter case, a solid friction layer was prepared from the leaf extract on the disc surface. For a liquid leaf extract, low adhesion was found for all tested amounts. These results indicate that not only thick black leaf film can lead to poor adhesion conditions, as was observed before [4], but poor adhesion conditions can also occur due to the release of natural lubricant from the crushed leaves, such as pectin gel [41]. These results are in a line with Ref. [19] where a large number of low adhesion incidents have been reported for “non-contaminated” surfaces. Authors in Ref. [19] proposed these incidents can be caused by not detectable leaf layer. As was shown in the present study, the leaf extract can cause traction/braking difficulties and it can be difficult to detect this almost invisible layer on the rail surfaces.

In the last part of this study, the influence of RH and temperature on CoA was studied for the clean and contaminated disc. These results show that low adhesion can be expected especially during cold mornings and evenings when low temperature and very high RH usually occur [19, 41], see Fig. 12.

An even more critical case may occur in the autumn months when a leaf layer is formed on rail heads, see tests with the contaminated disc in Fig. 12. Under these conditions, low adhesion incidents can be anticipated more often for two reasons. First, CoA reaches critically low values when a leaf layer on the rail is wetted by a small amount of water from condensation. In such a situation, CoA can be even lower than 0.05. Second, the presence of leaf layer on the rail causes that very high RH is not needed for a rapid adhesion decrease because an adhesion drop may even occur at RH of 70% when the temperature is low ($<10^{\circ}\text{C}$). It means that adhesion problems can be observed even the dew point has not been reached yet.

This study showed that the most substantial adhesion drop occurs when contact is contaminated with water from condensation. This adhesion drop is much more serious than in tests with small amounts of water, see Fig. 12. Although it is difficult to quantify the amount of condensed water in the wear track, it can be assumed that the amount was similar to amounts applied during the set of tests No. 3 (1–10 μl). It means that this difference in adhesion drops is likely not attributed only to different amounts of water in the wear track, but can be the result of another phenomenon. The specimens used in sets of test No. 5 and 6 were exposed to high RH before starting the test because it was necessary to wait for RH and temperature to stabilize. It is hypothesised that the contact surfaces exposed to high RH for longer time are covered with a thin oxide layer. If RH is subsequently high enough for condensation, then a small amount of condensed water between oxidized surfaces results in low adhesion conditions. This hypothesis is contradictory to

several studies that have noted that the pre-created oxides have a little effect since they are easily removed due to the contact conditions in pin-on-disc [17,18] as well as twin-disc [36] tests. So the hypothesis will be tested in the future study in detail.

4. Conclusions

In this work, the ball-on-disc tribometer with the climate chamber was used to identify conditions when low adhesion incidents can be expected in operation due to weather and season changes. The performed tests investigated the effect of several factors influencing adhesion. Unlike previously published articles dealing with the effect of environmental conditions on adhesion, the low and even very low adhesion conditions have been found for several contact conditions. These low and very low adhesion conditions were mostly associated with a high value of RH leading to the formation of oxide layer between surfaces. Based on this, the authors recommend studying “low adhesion phenomenon” under rolling-sliding conditions. This experimental approach seems to be more suitable than tests under pure sliding conditions where an oxide layer is quickly removed; thus CoA is almost unaffected by this layer. With regard to a possible occurrence of low adhesion incidents, the main conclusions of this study are as follows:

- The lowest value of CoA was found when the contaminated disc (by leaf extract) was run at RH of 70% or higher. Under these conditions, CoA fell even below 0.05. In real operation, this undesirable situation can occur especially during autumn mornings even though no visible leaf layer may be detectable on the rails.
- For leaf extract contamination, low adhesion conditions were observed for all tested amounts of extract but very low adhesion conditions did not occur.
- If contact surfaces are clean, very low adhesion conditions were not found for any tests; however, low adhesion incidents may occur under dew conditions.
- In the case of water as the most common natural contaminant, no important adhesion drops were observed for clean surfaces but very low adhesion was found when an oxide layer was formed on the surfaces.

Future work should be focused on the effect of condensate water on adhesion for various surface conditions of specimens occurring due to surface oxidation. Besides this, an interaction of condensed water and leaf residuals should be investigated to explore if these conditions may be responsible for unexpected low adhesion incidents during the autumn season.

Declaration of competing interest

The authors declare that they have no known competing financial

interests or personal relationships that could have appeared to influence the work reported in this paper.

CRedit authorship contribution statement

Radovan Galas: Conceptualization, Methodology, Investigation, Data curation, Writing - original draft. **Milan Omasta:** Conceptualization, Investigation, Methodology, Writing - review & editing, Project administration. **Lu-bing Shi:** Data curation, Writing - review & editing, Visualization. **Haohao Ding:** Writing - review & editing, Visualization. **Wen-jian Wang:** Conceptualization, Data curation, Writing - review & editing, Project administration. **Ivan Krupka:** Data curation, Writing -

review & editing. **Martin Hartl:** Supervision, Funding acquisition.

Acknowledgements

The authors are sincerely grateful to European Commission for the financial sponsorship of the H2020-MSCA-RISE Project No. 691135 “RISEN: Rail Infrastructure Systems Engineering Network,” which enables a global research network that tackles the grand challenge in railway infrastructure resilience and advanced sensing under extreme environments. The authors also thank the support of National Key R&D Program Intergovernmental Key Items for International Scientific and Technological Innovation Cooperation (No.2018YFE0109400).

Appendix A. Parameters of employed sensors

sensor	range	accuracy	nonlinearity
load cell for normal force	2–75 N	±0.3 N	±1% of full scale
load cell for friction force	–20 to +20 N	±0.3 N	±2% of full scale
servodrives	–4 to +4 m/s	±1 mm/s or 0.1% of speed, whichever is larger	not applicable
temperature sensor	0–150 °C	±0.5 °C	±1% of full scale
relative humidity sensor	0–100% RH (for temperature between –20 and + 60 °C)	2% RH	<1% RH

Appendix B. Mean standard deviations for sets of tests listed in Table 1

set No. 1	adhesion characteristics under dry conditions										
	stats	surface	0.5%	1%	2%	3%	4%	5%	6.5%	8%	n*
0.5 m/s	mean	clean	0.14	0.26	0.39	0.48	0.55	0.61	0.64	0.65	20
	Std Dev		0.005	0.002	0.003	0.004	0.004	0.005	0.006	0.005	20
1 m/s	mean		0.15	0.25	0.39	0.50	0.56	0.60	0.67	0.71	20
	Std Dev		0.002	0.003	0.003	0.006	0.005	0.004	0.004	0.005	20
2 m/s	mean		0.14	0.23	0.38	0.48	0.57	0.61	0.64	0.66	20
	Std Dev		0.001	0.003	0.002	0.001	0.002	0.001	0.003	0.003	20
3 m/s	mean		0.14	0.26	0.39	0.48	0.55	0.61	0.64	0.65	20
	Std Dev		0.002	0.002	0.006	0.004	0.004	0.003	0.002	0.003	20
set No. 2	adhesion characteristics in wet conditions for different speeds and surface conditions										
	stats	surface	0.5%	1%	2%	3%	4%	5%	6.5%	8%	n*
0.5 m/s	mean	clean	0.20	0.31	0.45	0.52	0.55	0.56	0.57	0.57	20
	Std Dev		0.006	0.005	0.002	0.002	0.001	0.001	0.001	0.003	20
1 m/s	mean		0.19	0.30	0.43	0.50	0.53	0.55	0.56	0.56	20
	Std Dev		0.003	0.003	0.003	0.001	0.001	0.004	0.002	0.001	20
2 m/s	mean		0.18	0.29	0.41	0.47	0.50	0.52	0.53	0.53	20
	Std Dev		0.003	0.002	0.003	0.002	0.001	0.002	0.003	0.002	20
3 m/s	mean		0.16	0.26	0.38	0.44	0.46	0.47	0.47	0.47	20
	Std Dev		0.005	0.006	0.003	0.002	0.002	0.004	0.008	0.002	20
1 m/s	mean	ox. layer No. 1	0.11	0.20	0.30	0.34	0.36	0.37	0.37	0.36	20
	Std Dev		0.003	0.002	0.004	0.02	0.02	0.003	0.004	0.002	20
2 m/s	mean		0.12	0.19	0.26	0.29	0.31	0.31	0.32	0.33	20
	Std Dev		0.004	0.02	0.001	0.003	0.002	0.002	0.005	0.002	20
3 m/s	mean		0.09	0.14	0.14	0.15	0.16	0.15	0.14	0.13	20
	Std Dev		0.002	0.004	0.003	0.002	0.005	0.001	0.003	0.003	20
2 m/s	mean	ox. layer No. 2	0.01	0.02	0.03	0.03	0.04	0.04	0.05	0.05	20
	Std Dev		0.003	0.001	0.003	0.001	0.003	0.004	0.002	0.003	20
set No. 3	small amount of water					set No. 4	leaf extract				
	stats	1 µl	2 µl	4 µl	10 µl		1 µl	5 µl	10 µl	20 µl	
µ _m	mean	0.39	0.42	0.45	0.47	µ _{mL}	0.17	0.12	0.08	0.07	
	Std Dev	0.029	0.012	0.006	0.006		0.012	0.012	0.001	0.002	
	n*	4	6	10	10		3	7	10	10	
set No. 5	clean disc										
	stats	8% RH	26% RH	50% RH	70% RH	90% RH	100% RH				
1 °C	mean	0.56	0.48	0.43	0.36	0.23	0.15				
	Std Dev	0.008	0.006	0.015	0.011	0.025	0.002				
	n*	30	30	30	30	30	30				
RH	mean	6%	27%	50%	70%	90%	100%				
	Std Dev	0.57	0.52	0.46	0.40	0.18	0.14				
	n*	0.006	0.007	0.011	0.016	0.012	0.005				
10 °C	mean	0.57	0.52	0.46	0.40	0.18	0.14				
	Std Dev	0.006	0.007	0.011	0.016	0.012	0.005				
	n*	30	30	30	30	30	30				

(continued on next page)

(continued)

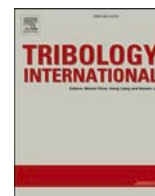
set No. 5		clean disc					
	stats	8% RH	26% RH	50% RH	70% RH	90% RH	100% RH
RH		4%	22%	50%	70%	90%	100%
24 °C	mean	0.60	0.55	0.52	0.51	0.48	0.27
	Std Dev	0.001	0.002	0.003	0.002	0.011	0.005
	n*	30	30	30	30	30	30
RH		2%	16%	50%	70%	90%	96%
40 °C	mean	0.62	0.60	0.60	0.57	0.56	0.55
	Std Dev	0.002	0.008	0.003	0.003	0.004	0.005
	n*	30	30	30	30	30	30
RH		6%	13%	50%	70%	90%	94%
50 °C	mean	0.60	0.61	0.61	0.61	0.58	0.57
	Std Dev	0.005	0.004	0.002	0.003	0.004	0.003
	n*	30	30	30	30	30	30
set No. 6		contaminated disc					
	stats	9% RH	24% RH	50% RH	70% RH	90% RH	100% RH
1 °C	mean	0.42	0.38	0.28	0.06	0.06	0.06
	Std Dev	0.003	0.038	0.013	0.004	0.003	0.001
	n*	30	30	30	30	30	30
RH		6%	27%	50%	70%	90%	100%
10 °C	mean	0.48	0.38	0.35	0.14	0.17	0.06
	Std Dev	0.007	0.003	0.005	0.006	0.005	0.001
	n*	30	30	30	30	30	30
RH		4%	22%	50%	70%	90%	100%
24 °C	mean	0.41	0.38	0.38	0.33	0.28	0.04
	Std Dev	0.004	0.004	0.004	0.007	0.009	0.004
	n*	30	30	30	30	30	30
RH		2%	18%	50%	70%	90%	100%
40 °C	mean	0.45	0.43	0.43	0.40	0.38	0.35
	Std Dev	0.004	0.004	0.003	0.002	0.004	0.009
	n*	30	30	30	30	30	30
RH		6%	13%	50%	70%	90%	94%
50 °C	mean	0.50	0.46	0.42	0.39	0.32	0.29
	Std Dev	0.002	0.002	0.003	0.002	0.009	0.037
	n*	30	30	30	30	30	30

*n – sample size.

References

- Wang WJ, Liu TF, Wang HY, Liu QY, Zhu MH, Jin XS. Influence of friction modifiers on improving adhesion and surface damage of wheel/rail under low adhesion conditions. *Tribol Int* 2014;75:16–23. <https://doi.org/10.1016/j.triboint.2014.03.008>.
- Shi LB, Wang C, Ding HH, Kvarda D, Galas R, Omasta M, et al. Laboratory investigation on the particle-size effects in railway sanding: comparisons between standard sand and its micro fragments. *Tribol Int* 2020;146:62–70. <https://doi.org/10.1016/j.triboint.2020.106259>.
- Cann PM, Olofsson U, Persson K. The “leaves on the line” problem—a study of leaf residue film formation and lubricity under laboratory test conditions. *Tribol Lett* 2006;24:151–8. <https://doi.org/10.1007/s11249-006-9152-2>.
- Chen H, Furuya T, Fukagai S, Saga S, Ikoma J, Kimura K, et al. Wheel slip/Slide and low adhesion caused by fallen leaves. *Wear* 2020;446–7. <https://doi.org/10.1016/j.wear.2020.203187>.
- Zhu Y, Olofsson U, Nilsson R. A field test study of leaf contamination on railhead surfaces. *Proc Inst Mech Eng - Part F J Rail Rapid Transit* 2013;228:71–84. <https://doi.org/10.1177/0954409712464860>.
- Arias-Cuevas O, Li Z. Field investigations into the adhesion recovery in leaf-contaminated wheel–rail contacts with locomotive sanders. *Proc Inst Mech Eng - Part F J Rail Rapid Transit* 2011;225:443–56. <https://doi.org/10.1177/2041301710394921>.
- Broster M, Pritchard C, Smith DA. Wheel/rail adhesion: its relation to rail contamination on british railways. *Wear* 1974;29:309–21. [https://doi.org/10.1016/0043-1648\(74\)90017-9](https://doi.org/10.1016/0043-1648(74)90017-9).
- Nagase K, Pritchard C, Smith DA. A study of adhesion between the rails and running wheels on main lines: results of investigations by slipping adhesion test bogie. *Proc Inst Mech Eng - Part F J Rail Rapid Transit* 2016;203:33–43. https://doi.org/10.1243/PIME_PROC_1989_203_206_02.
- Gallardo-Hernandez EA, Lewis R. Twin disc assessment of wheel/rail adhesion. *Wear* 2008;265:1309–16. <https://doi.org/10.1016/j.wear.2008.03.020>.
- Chen H, Ishida M, Namura A, Baek K-S, Nakahara T, Leban B, et al. Estimation of wheel/rail adhesion coefficient under wet condition with measured boundary friction coefficient and real contact area. *Wear* 2011;271:32–9. <https://doi.org/10.1016/j.wear.2010.10.022>.
- Lewis SR, Lewis R, Olofsson U. An alternative method for the assessment of railhead traction. *Wear* 2011;271:62–70. <https://doi.org/10.1016/j.wear.2010.10.035>.
- Shi LB, Li Q, Kvarda D, Galas R, Omasta M, Wang WJ, et al. Study on the wheel/rail adhesion restoration and damage evolution in the single application of alumina particles. *Wear* 2019;426–427:1807–19. <https://doi.org/10.1016/j.wear.2019.01.021>.
- Beagley TM, Pritchard C. Wheel/rail adhesion — the overriding influence of water. *Wear* 1975;35:299–313. [https://doi.org/10.1016/0043-1648\(75\)90078-2](https://doi.org/10.1016/0043-1648(75)90078-2).
- Beagley TM, McEwen IJ, Pritchard C. Wheel/rail adhesion — the influence of railhead debris. *Wear* 1975;33:141–52. [https://doi.org/10.1016/0043-1648\(75\)90230-6](https://doi.org/10.1016/0043-1648(75)90230-6).
- White B, Lewis R. Simulation and understanding the wet-rail phenomenon using twin disc testing. *Tribol Int* 2019;136:475–86. <https://doi.org/10.1016/j.triboint.2019.03.067>.
- Olofsson U, Sundvall K. Influence of leaf, humidity and applied lubrication on friction in the wheel-rail contact: pin-on-disc experiments. *Proc Inst Mech Eng - Part F J Rail Rapid Transit* 2005;218:235–42. <https://doi.org/10.1243/0954409042389364>.
- Zhu Y, Olofsson U, Chen H. Friction between wheel and rail: a pin-on-disc study of environmental conditions and iron oxides. *Tribol Lett* 2013;52:327–39. <https://doi.org/10.1007/s11249-013-0220-0>.
- Zhu Y, Lyu Y, Olofsson U. Mapping the friction between railway wheels and rails focusing on environmental conditions. *Wear* 2015;324–325:122–8. <https://doi.org/10.1016/j.wear.2014.12.028>.
- White BT, Nilsson R, Olofsson U, Arnall AD, Evans MD, Armitage T, et al. Effect of the presence of moisture at the wheel–rail interface during dew and damp conditions. *Proc Inst Mech Eng - Part F J Rail Rapid Transit* 2017;232:979–89. <https://doi.org/10.1177/0954409717706251>.
- Arias-Cuevas O, Li Z, Lewis R, Gallardo-Hernández EA. Rolling–sliding laboratory tests of friction modifiers in dry and wet wheel–rail contacts. *Wear* 2010;268:543–51. <https://doi.org/10.1016/j.wear.2009.09.015>.
- Voltr P, Lata M. Transient wheel–rail adhesion characteristics under the cleaning effect of sliding. *Veh Syst Dyn* 2015;53:605–18. <https://doi.org/10.1080/00423114.2014.961488>.
- Galas R, Omasta M, Krupka I, Hartl M. Laboratory investigation of ability of oil-based friction modifiers to control adhesion at wheel-rail interface. *Wear* 2016;368–369:230–8.
- Shi LB, Ma L, Guo J, Liu QY, Zhou ZR, Wang WJ. Influence of low temperature environment on the adhesion characteristics of wheel-rail contact. *Tribol Int* 2018;127:59–68. <https://doi.org/10.1016/j.triboint.2018.05.037>.

- [24] Hardwick C, Lewis R, Olofsson U. Low adhesion due to oxide formation in the presence of salt. *Proc Inst Mech Eng - Part F J Rail Rapid Transit* 2013;228:887–97. <https://doi.org/10.1177/0954409713495666>.
- [25] Lewis R, Gallardo-Hernandez EA, Hilton T, Armitage T. Effect of oil and water mixtures on adhesion in the wheel/rail contact. *Proc Inst Mech Eng - Part F J Rail Rapid Transit* 2009;223:275–83. <https://doi.org/10.1243/09544097JRR248>.
- [26] Galas R, Kvarda D, Omasta M, Krupka I, Hartl M. The role of constituents contained in water-based friction modifiers for top-of-rail application. *Tribol Int* 2018;117:87–97. <https://doi.org/10.1016/j.triboint.2017.08.019>.
- [27] Omasta M, Machatka M, Smejkal D, Hartl M, Krupka I. Influence of sanding parameters on adhesion recovery in contaminated wheel–rail contact. *Wear* 2015;322–323:218–25. <https://doi.org/10.1016/j.wear.2014.11.017>.
- [28] Wang WJ, Shen P, Song JH, Guo J, Liu QY, Jin XS. Experimental study on adhesion behavior of wheel/rail under dry and water conditions. *Wear* 2011;271:2699–705. <https://doi.org/10.1016/j.wear.2011.01.070>.
- [29] Bolton D. The computation of equivalent potential temperature. *Mon Weather Rev* 1980;108(7):1046–53. [https://doi.org/10.1175/1520-0493\(1980\)108<1046:TCOEPT>2.0.CO;2](https://doi.org/10.1175/1520-0493(1980)108<1046:TCOEPT>2.0.CO;2).
- [30] Klaffke D. On the repeatability of friction and wear results and on the influence of humidity in oscillating sliding tests of steel-steel pairings. *Wear* 1995;189:117–21. [https://doi.org/10.1016/0043-1648\(95\)06672-1](https://doi.org/10.1016/0043-1648(95)06672-1).
- [31] Oh H-K, Yeon K-H, Yun Kim H. The influence of atmospheric humidity on the friction and wear of carbon steels. *J Mater Process Technol* 1999;95:10–6. [https://doi.org/10.1016/S0924-0136\(99\)00259-9](https://doi.org/10.1016/S0924-0136(99)00259-9).
- [32] Liew WYH. Effect of relative humidity on the unlubricated wear of metals. *Wear* 2006;260:720–7. <https://doi.org/10.1016/j.wear.2005.04.011>.
- [33] Zhu Y. The influence of iron oxides on wheel–rail contact: a literature review. *Proc Inst Mech Eng - Part F J Rail Rapid Transit* 2017;232:734–43. <https://doi.org/10.1177/0954409716689187>.
- [34] Chen Z, He X, Xiao C, Kim S. Effect of humidity on friction and wear—a critical review. *Lubricants* 2018;6. <https://doi.org/10.3390/lubricants6030074>.
- [35] Godfrey D. Iron oxides and rust (hydrated iron oxides) in tribology. *Tribol Lubric Technol* 1999;55(2):33–7.
- [36] Zhu Y, Chen X, Wang W, Yang H. A study on iron oxides and surface roughness in dry and wet wheel–rail contacts: a literature review. *Wear* 2015;328–329:241–8. <https://doi.org/10.1016/j.wear.2015.02.025>.
- [37] Leheup ER, Pendlebury RE. Unlubricated reciprocating wear of stainless steel with an interfacial air flow. *Wear* 1991;142:351–72. [https://doi.org/10.1016/0043-1648\(91\)90174-S](https://doi.org/10.1016/0043-1648(91)90174-S).
- [38] Zhu Y, Yang H, Wang W. Twin-disc tests of iron oxides in dry and wet wheel–rail contacts. *Proc Inst Mech Eng - Part F J Rail Rapid Transit* 2015;230:1066–76. <https://doi.org/10.1177/0954409715575093>.
- [39] Bregliozzi G, Di Schino A, Kenny JM, Haefke H. The influence of atmospheric humidity and grain size on the friction and wear of AISI 304 austenitic stainless steel. *Mater Lett* 2003;57:4505–8. [https://doi.org/10.1016/S0167-577X\(03\)00351-3](https://doi.org/10.1016/S0167-577X(03)00351-3).
- [40] de Baets P, Kalacska G, Strijckmans K, Van de Velde F, Van Peteghem AP. Experimental study by means of thin layer activation of the humidity influence on the fretting wear of steel surfaces. *Wear* 1998;216:131–7. [https://doi.org/10.1016/S0043-1648\(97\)00189-0](https://doi.org/10.1016/S0043-1648(97)00189-0).
- [41] Ishizaka K, Lewis SR, Lewis R. The low adhesion problem due to leaf contamination in the wheel/rail contact: bonding and low adhesion mechanisms. *Wear* 2017;378–379:183–97. <https://doi.org/10.1016/j.wear.2017.02.044>.



The performance of top-of-rail products under water contamination

Simon Skurka^{a,*}, Radovan Galas^a, Milan Omasta^a, Bingnan Wu^b, Haohao Ding^b, Wen-Jian Wang^b, Ivan Krupka^a, Martin Hartl^a

^a Faculty of Mechanical Engineering, Brno University of Technology, Technická 2896/2, 616 69 Brno, Czech Republic

^b Tribology Research Institute, State Key Laboratory of Traction Power, Southwest Jiaotong University, Chengdu 610031, China

ARTICLE INFO

Keywords:

Wheel-rail tribology
Friction modification
Low adhesion
Water contamination

ABSTRACT

Top-of-rail products are commonly used for friction modification in wheel-rail contact. However, the effect of environmental conditions and contaminants on their performance remains unclear. In this study, three commercial top-of-rail products were contaminated by different amounts of water. The laboratory tribometer in ball-on-disc configuration was used to measure the coefficient of adhesion in contaminated contact. The results show that water influenced tested top-of-rail products significantly. A very low coefficient of adhesion occurred in tests with oil-based top-of-rail products suggesting that water could cause traction problems on the actual railway where friction modification is being used. Water-based top-of-rail products showed more resistance to water contamination.

1. Introduction

Friction modification presents a practical approach to dealing with high friction in railway transportation. Nowadays, top-of-rail (TOR) products are applied on railheads via trackside applicators or systems mounted on a train [1]. Initially, these products were used as solid sticks containing solid lubricants like graphite or molybdenum disulfide [2]. However, liquid-based products containing water [3] or oil with thickeners [4] as a base medium are often used. Dealing with friction is an important task to improve the energy efficiency of rail transportation and decrease maintenance costs. High friction causes rail corrugation [5] and is also the leading cause of excessive wear on both wheels and rail [6–9]. Also, friction in the wheel-rail contact and the shape of the traction curve contribute to noise pollution. According to WHO, the noise limit of 55 dB is harmful in case of long-term exposure. It is estimated that up to 113 million people in Europe (of which rail transport contributes approximately 20%) are exposed to traffic noise above this limit [10]. Various field and laboratory tests confirmed the ability of TOR products to reduce friction [11] and influence corresponding effects like wear [12–14], noise [15,16] and energy consumption [17].

On the other hand, maintaining a sufficient level of friction is required to transmit traction forces from wheel to rail to accelerate or stop the vehicle. The coefficient of adhesion (CoA) describes the effectivity of this transmission. Generally, CoA lower than 0.2 and 0.09 is considered insufficient for traction and braking, respectively [18]. Thus,

TOR products often contain mineral or metal particles to secure sufficient CoA. A liquid base (water, oil or less often a combination of both) is included to carry these particles along the rail [4]. The performance of some TOR products, especially oil-based ones, strongly depends on the applied amount [19]. As shown in [20], excessive amounts of product could cause low CoA problems resulting in an extension of the braking distance. TOR products are developed and tested to reduce friction while maintaining a required level of CoA for traction/braking. This can be achieved only with a suitable composition of the product and its optimal dosing.

Both water and oil-based TOR products are commonly referred to as friction modifiers (FMs) in literature. However, the mechanism of friction modification differs significantly for both types. In the case of water-based TOR products, the base medium quickly evaporates after application, and solid particles mix with the third body layer on the rail surface, providing a shear displacement compensation mechanism [21]. On the other hand, oil-based TOR products do not dry up and rely on a mixed/boundary lubrication regime. Because the base medium stays liquid, these TOR products can be redistributed for longer distances than water-based ones. However, it also carries the risk of low CoA occurrence close to the application unit due to overdosing [20]. Following [19], this paper will refer to water-based TOR products as "friction modifiers" and oil-based TOR products as "TOR lubricants" for clarity.

As stated above, the performance of friction modifiers and TOR lubricants in dry and clean contact has been well examined. However,

* Corresponding author.

E-mail address: Simon.Skurka@vut.cz (S. Skurka).

<https://doi.org/10.1016/j.triboint.2023.108872>

Received 27 April 2023; Received in revised form 8 August 2023; Accepted 12 August 2023

Available online 21 August 2023

0301-679X/© 2023 Elsevier Ltd. All rights reserved.

while the coefficient of friction in dry wheel-rail contact is usually between 0.5 and 0.6 [22], in contaminated contact, the friction decreases significantly, causing also drop in CoA. It is caused by third body layers naturally occurring on the rail surface and environmental contaminants [23]. Water is one of the most common environmental contaminants. It can be found on the track from rain, morning dew, or even leakage from passing vehicles. Several laboratory studies show that water can reduce the CoA under 0.2 [23–25] and even lower depending on quantity and temperature. Also, water forms a highly viscous mixture if combined with iron oxides, leading to a CoA of 0.05 or lower [24].

Although contamination of wheel-rail contact is practically inevitable in reality, very little is known about the interaction between contaminants and TOR products. In most studies, TOR products were tested only in laboratory-clean conditions without contamination, or the effect of contamination was not considered. Chen et al. compared the lubrication performance of several lubricants on dry and wet rails [25]. They showed that the reduction of lateral forces was greater on the wet rail for all tested lubricants. Lewis et al. tested the influence of air humidity on friction modifiers. They discovered that when exposed to air with a higher % of relative humidity, CoF reaches lower values than in less humid air [26]. This phenomenon could be explained by water condensation and contamination of friction modifiers. The case study [27] shows that the combined effect of water and oil can cause traction problems on the top of the railhead. As oil is the main component in TOR lubricants, a question arises as to if a similar phenomenon can happen when a TOR product is contaminated by water. TOR products usually maintain CoA sufficient for traction/braking thanks to the balance between base medium and solid particles. However, there is a possibility that if TOR products are contaminated with water, the balance will be disturbed, product performance will decrease, and the minimum required CoA will not be kept.

This study uses three commercial TOR products. Two of them are TOR lubricants, and one is a friction modifier. All CoA tests were conducted on a laboratory tribometer in a ball-on-disc configuration. On an actual railway, contamination by water can occur, resulting in an insufficient CoA level. The degree of the contamination can differ depending on the water source (dew, rain, leakage from passing trains). Therefore, all TOR products were tested in dry and wet conditions. Small and large amounts of water were applied. Also, single and continuous water application was tested to simulate different ways of contamination. This study aims to describe the influence of water and its amount on the TOR product performance in terms of CoA.

2. Material and methods

2.1. Test setup and specimens

A laboratory tribometer MTM (Mini-Traction Machine, PCS Instruments) in a ball-on-disc configuration was used for all tests, see Fig. 1. Technical norms specify the measuring procedure on this device. However, these norms are mainly focused on traction curve evaluation. Therefore, they are unsuitable for observation of CoA drop caused by

contamination. Thus, a different approach previously used in papers [3, 4] will be used in this study. The contact bodies were discs and balls of 46 mm and 19.05 mm in diameter, so the contact has a circular shape. Both specimens were made of AISI 52100 bearing steel with a Vickers macro-hardness of 800–920 HV and 720–780 HV for ball and disc. The bearing steel is not a typical rail material. However, higher hardness ensures stable conditions during experiments and better repeatability due to reduced wear compared to standard wheel/rail steel. The initial roughness of the surface of both specimens was Ra 0.01 µm; however, it grew to Ra 0.15 µm (ball) and Ra 0.3 µm (disc) after the initial wear-in and the following run-in.

Both specimens were loaded against each other and driven by independent servo motors so the required slide-roll ratio (SRR) could be achieved according to the given equation:

$$SRR = \frac{w_{ball} \cdot r_{ball} - w_{disc} \cdot r_{disc}}{w_{ball} \cdot r_{ball} + w_{disc} \cdot r_{disc}} \cdot 200\% \quad (1)$$

where w_{ball} and w_{disc} are angular speeds of specimens and r_{ball} and r_{disc} stands for its radii. The embedded sensor measures the normal force (N) with ± 0.3 N accuracy. Traction force (T) is calculated from the torque measured by the transducer attached to the disc shaft, so the adhesion coefficient (CoA) could be determined as follows:

$$CoA = \frac{N}{T} \quad (2)$$

Data from force sensors are acquired with a 1 Hz sampling frequency. However, this signal results from averaging a non-specified higher frequency input signal.

2.2. Tested TOR products and contaminants

Two commercial TOR lubricants (referred to as "TORL-A" and "TORL-B"; oil-based TOR products) and one friction modifier ("FM-A"; water-based TOR product) were used in this study. Essential information about the composition of both TOR lubricants can be read from data-sheets, see Table 1.

Although water-based TOR products are meant to form a dry film after base medium evaporation, wet film lubrication occurs immediately after application. Thus FM-A was tested both before and after the evaporation of the base medium. Distilled water was used as a contaminant in all tests.

2.3. Wear-in, run-in and cleaning of specimens

Before any experiments, an initial 60-minute dry wear-in of specimens was conducted. This is because severe wear of contact surfaces occurs with a new pair of specimens. After 60 min of wear-in, the wear rate decreases significantly, and stable test conditions could be secured. According to Hertz's Theory, the diameter of the contact is calculated to be 0.2 mm for a new pair of specimens. However, due to wear and topography changes caused by the wear-in, the actual contact will differ from the theory, and the diameter will be higher. Please note that described 60-minute wear-in is performed only once at the beginning of

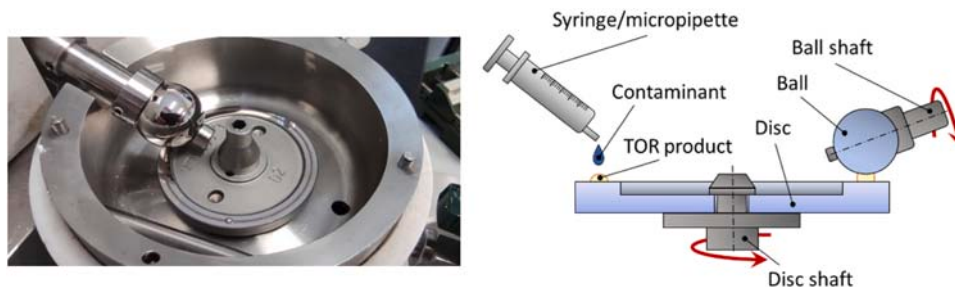


Fig. 1. Photo (left) and scheme (right) of the apparatus.

Table 1
Composition and characteristics of tested TOR lubricants.

TOR product	Structure	NLGI grade	Base oil	Thickener	Particles	Base oil viscosity at 40 °C (mm ² /s)
TORL-A	Paste	0	Biodegradable ester	Organic	Soft metal	41–53
TORL-B	Gel paste	00	Synthetic ester	Inorganic (silicate)	Soft metal	46

each new pair of specimens. The wear-in parameters (speed, load and SRR) are the same as for adhesion tests and run-ins and will be described later.

A 15-minute run-in was performed before every adhesion test to remove the oxide layer and TOR product residual from the track and to stabilize surface roughness. During this process, the CoA stabilized around 0.39 (a reference value for dry contact), ensuring that every test started from the same initial conditions. Unlike a wear-in, a run-in was performed before every adhesion test, not only at the beginning for a new pair of specimens. Specimens were cleaned manually with a paper towel and ultrasonically in an acetone bath for 10 min after each test.

The wear-in/run-in and cleaning parameters are based on a preliminary study conducted before this work in the experiment design process. The base value of 0.39 for the dry contact CoA and the duration of 60 min and 15 min for wear-in and run-in were selected based on the results of 20 tests focusing on adhesion and wear development. After the end of every test, the surface topography was checked on an optical profilometer. Also, the contact path surface was checked under a microscope to visually confirm that the cleaning process removed any remaining lubricant residue or particles.

2.4. Adhesion test: performance of water/TOR product under dry conditions

Firstly, different amounts of water and TOR products were tested in dry conditions to investigate their separate influence on CoA, see Table 2. The following parameters were set for all tests: a fixed value of 2% SRR, a mean speed of 1 m/s, and a load of 18 ± 0.01 N normal force (corresponding to 0.8 GPa Hertzian contact pressure). The same parameters were used in wear-ins and run-ins. The set SRR represents a value from the effective linear part of the traction curve near the saturation point commonly found in actual railway operations. Moreover, higher values of SRR could cause excessive wear. According to [28], the chosen value of the mean speed represents the velocity of approx. 60 km/h in actual wheel-rail contact corresponding to the light-rail system.

The performance of oil-based TOR products strongly depends on applied quantity [19]. Thus, choosing the optimal amount for tests in the main part of this work was necessary. Different amounts of each TOR

product were tested to determine the optimal amount (regarding retentivity, low/intermediate CoA). The 15-minute run-in was performed before each test.

2.5. Stribeck test: water, oil and water-oil mixture under fully flooded conditions

A Stribeck test of water, oil, and a 1:1 water-oil (W/O) mixture under fully flooded conditions was conducted. TORL-A bleed oil with a viscosity of 64 mPa.s was used in this test. The set parameters for this test were 18 N of load and 2% SRR. The mean speed of specimens was 100–2500 mm/s for water and 50–2500 mm/s for oil and W/O mixture. For each tested speed, one mean value of CoA was calculated from the 6-second test. This test revealed the lubrication regime and thickness of the lubrication film and will be further discussed in the Sections Results and Discussion.

2.6. Adhesion test: performance of TOR product under wet conditions

In the main part of this work, TOR products were tested under wet conditions. Please note that water was applied to the contact only after the TOR product. The moment of application varied and is specified in Table 2. The parameters of these tests were the same as in adhesion tests under dry contact conditions (see Section 2.4). The tested amount of each product was determined regarding optimal performance in dry conditions. TOR products were applied to the disc surface using an electronic micropipette (error ± 0.04 μ l). There were two types of tests: (1) single water application using a syringe/electronic micropipette and (2) continuous water application via a peristaltic pump. The procedure of all adhesion tests is summarised in Table 2.

In addition, water-based FM-A was tested both before ("wet film") and after ("dry film") base medium evaporation. To prepare a dry film, a short 30-second test immediately followed the application of FM-A to spread it on contact bodies. The parameters of this test were: 0% SRR, 300 mm/s mean speed, and 18 N load. A 10-minute pause follows to provide enough time for water evaporation. These two steps ensure the formation of an evenly distributed dry film. This procedure only applies to FM-A (dry film) tests.

In the case of single application tests, the TORL-A and FM-A (wet/dry

Table 2
Procedure of adhesion tests: dry and wet conditions (see 2.4 and 2.6).

Type of test	Water/TOR product	Run-in duration (min)	Amount of TOR product (μ l)	T1–T3 ^a (CoA)	Amount of water (μ l)	Test duration (s)	Fig. # in Results
Dry conditions, a single water/TOR product application	TORL-A	15	1; 2; 3; 4	-	-	600	3 a)
	TORL-B	15	1; 2; 3; 4	-	-	900	3 b)
	FMA-(wet film)	15	2; 4; 6; 8	-	-	600	3c)
	FM-A (dry film)	15	4	-	-	600	3c)
	Water	15	-	-	2; 8; 32; 2000	150	3 d)
Wet conditions, a single water application	TORL-A	15	2	0.13; 0.2; 0.3	2; 8; 32; 2000	600	5
	TORL-B	15	1	0.13; 0.2; 0.3	2; 8; 32; 2000	900	6
	FM-A (wet film)	15	4	0.13; 0.2; 0.3	2; 8; 32; 2000	600	7
	FM-A (dry film)	15	4	0.3	2; 8; 32; 2000	600	8
Wet conditions, continuous water application	TORL-A	15	2	0.18	2150	2000	9
	TORL-B	15	1	0.18	2150	2000	9
	FM-A (wet film)	15	4	0.23	2150	1000	10
	FM-A (dry film)	15	4	0.32	2150	1000	10

^a T1–T3 are defined values of CoA. When reached during the test, water was applied to the TOR product.

film) test duration was 600 s. For TORL-B, the test duration was extended to 900 s due to its longer retentivity. For the continuous application of water, the duration was 2 000 s for TOR lubricants and 1 000 s for friction modifiers.

In various tests, water was applied at different times after the start of the test. The reason for this was to observe the effect of water on TOR products at different phases of its performance. The exact moment of application was determined by the value of CoA defined in Table 2. Water was applied only once per adhesion test when CoA reached the specified value. In the Section Results, points where water was applied, are marked as T1–T3 in the graphs. These values vary for TOR lubricants and friction modifiers because both types of TOR products led to different CoA.

A typical adhesion test of TOR product with a single and continuous water application can be seen in Fig. 2a) and b). First, a 15-minute run-in was conducted before every test. Only the final parts of the run-in are shown in Fig. 2. Second, a TOR product was applied. In the FM-A (dry film) tests, the spreading and drying procedure followed (not shown in Fig. 2). After that, the adhesion test with described parameters started. The CoA development during the typical test was as follows: after a TOR product application, an initial drop caused by a large amount of TOR product occurred. However, part of the TOR product dosage was quickly pushed away from the track, and the CoA slowly rose to 0.15–0.25. When the trigger value of CoA was reached (T1–T3), water was applied either by a) a micropipette/syringe or b) a peristaltic pump. The magnitude and duration of the drop of CoA caused by the water application on the disc with the tested TOR product depended on the amount of applied water. During test b), 430 $\mu\text{l}/\text{min}$ of water was continuously applied for 5 min (2 150 μl in total). Both small and large amounts of water were used to determine the influence on product performance (2–2 000 μl for a single application and 430 $\mu\text{l}/\text{min}$ for a continuous application).

3. Results

3.1. Results: performance of water/TOR product under dry conditions

First, TOR products and distilled water were tested separately in a series of adhesion tests. Each TOR product was tested in different amounts to determine the best-performing amount, which was later used for the adhesion tests of TOR products in wet conditions in the main part of this work. The term "best-performing amount" means the amount of TOR product, which ensures a good ratio between the duration of the initial drop of CoA under 0.1 (which is undesired but inevitable in most cases for TOR lubricants) and the duration of a period of intermediate CoA (desired effect of TOR products). Also, the three phases after application can be distinguished: the initial rise in CoA, stabilization at the desired adhesion level, and starvation and dry contact restoration.

In the case of TORL-A (Fig. 3a), the amount of 4 μl was unsuitable for further testing as it caused over-lubrication, and the CoA restoration did not occur during the standard test duration. On the contrary, both 1 μl

and 2 μl led to desired adhesion development. Finally, the amount of 2 μl was chosen because, for this amount, the product stays in effect slightly longer than for 1 μl . Also, the repeatability of the measurement was tested. Two dashed lines in Fig. 3a) represent additional measurements of 2 μl of TORL-A. After comparing all three curves, it can be said that in all three tests, very similar values of CoA were measured. The curves slightly differ only at the end when the starvation occurs, which should not be a problem as contamination will not be tested at this part of the curve.

In the case of TORL-B (Fig. 3b), 4 μl of the product led to over-lubrication of the contact. Although 2 μl did not cause the over-lubrication, the tests would be inefficiently long for this amount. As the 1 μl showed desired adhesion development in the standard test duration, this amount was chosen for the rest of the experiments.

Contrary to TOR lubricants, the over-lubrication did not occur for any tested amount of FM-A. Although it shows some adhesion-amount dependency, generally, it is much less significant than in the case of TOR lubricants. The 4 μl was chosen from all tested amounts as it led to a similar test duration compared to TORL-A and TORL-B. Afterward, this amount was also tested as dry film (red dashed line in Fig. 3c).

Four different amounts of water (2, 8, 32 μl , and 2 ml) were tested). These exact amounts were later used for adhesion tests under wet conditions. Fig. 3d) shows that with the increase of water amount, the duration of CoA drop also increases. However, there is no significant difference between 32 μl and 2 ml. The effect of the amount on the CoA level is relatively negligible. For tested amounts, the CoA ranged from 0.32 to 0.35.

3.2. Results: Stribeck test of water, oil and W/O mixture

The results of the Stribeck test are displayed in Fig. 4. Please note that each line represents the mean value calculated from three measurements. The lubrication parameter λ was calculated for water and oil to determine the lubrication regime. Value $\lambda = 1$, often used in literature as a transition between boundary and mixed lubrication regime [29], is marked for oil conditions in the figure.

For water, the boundary regime occurs for all tested speeds. For oil, the boundary regime occurs up to 280 mm/s. Above this speed, the contact operates mainly in the mixed lubrication regime. For the W/O mixture, parameter λ was not calculated. In addition, Fig. 4 shows that with the increase in speed, the CoA decreased. The highest CoA of 0.56 was measured for water. With increasing speed, the decrease of CoA was somewhat limited, and the lowest value of 0.43 was measured for a mean speed of 2 500 mm/s. On the other hand, a W/O mixture led to significantly lower CoA. The measured value for a speed of 1000 mm/s was 0.04 and 0.02 for the oil and W/O mixture, respectively. Meanwhile, the CoA of water was 0.45 at this speed.

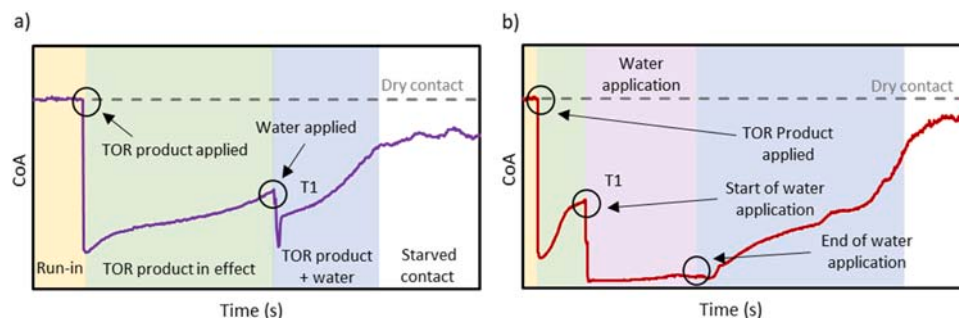


Fig. 2. (a) Adhesion test – a single application of water, (b) adhesion test – continuous application of water.

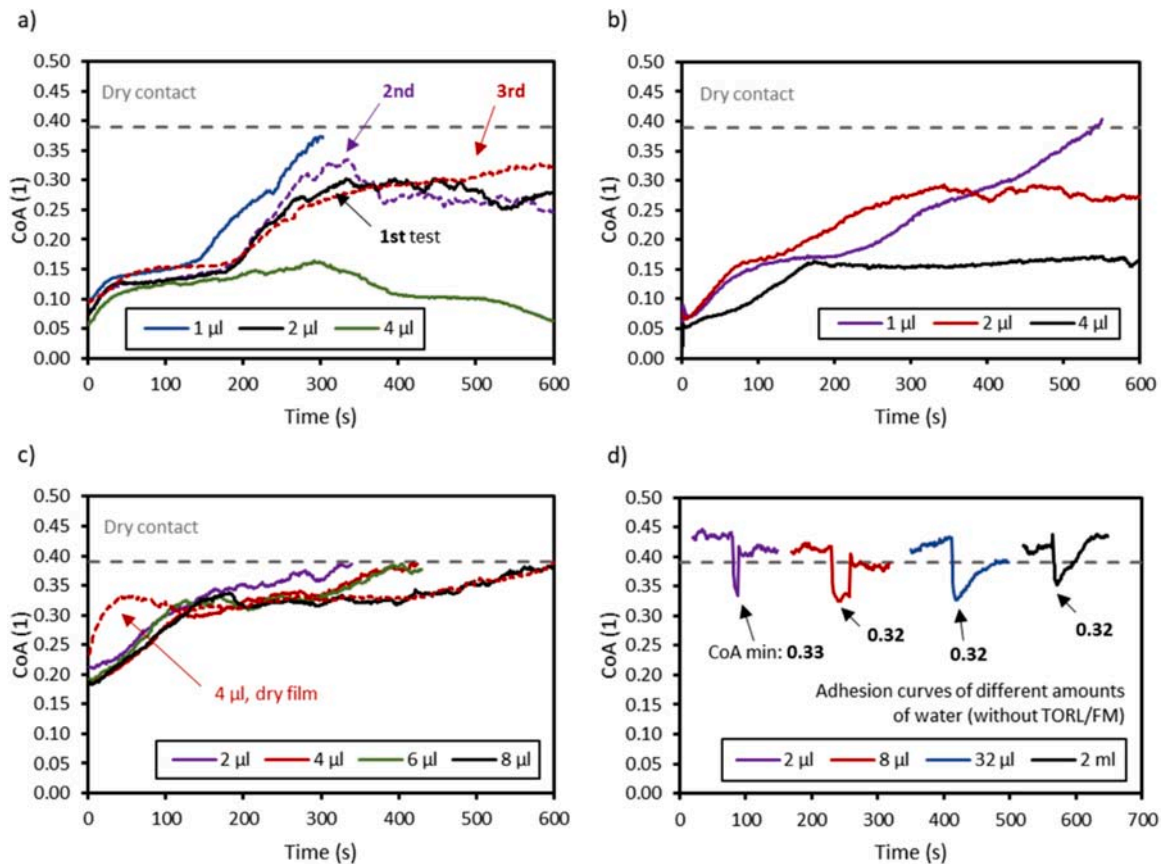


Fig. 3. Adhesion tests: different amounts of (a) TORL-A, (b) TORL-B, (c) FM-A, and (d) distilled water.

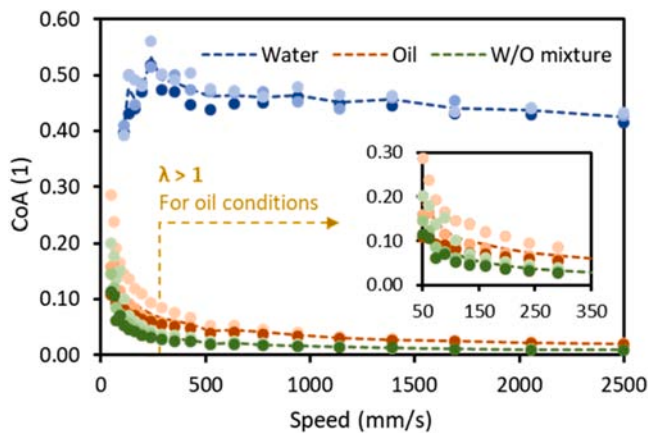


Fig. 4. Stribeck test of water, oil, and W/O mixture.

3.3. Results: performance of TOR products under a single water application

Figs. 5 and 6 represent TORL-A and TORL-B adhesion tests after a single water application. Both figures consist of four independent graphs marked as a–d). In each graph, a different amount of water was applied, see the upper left corner. There are two types of curves in these graphs. Dashed lines represent the dry contact CoA level (grey) and adhesion tests of TOR products measured under dry conditions (black). These curves are already depicted in Fig. 3a) and b). The purpose of showing them again in these graphs is to enable a quick comparison between adhesion tests with and without water application. Solid lines represent adhesion tests where water was applied into contact with TORL-A and

TORL-B. Each graph includes three curves because three measurements were conducted for the same amount of water. Although each has a different color, this is only for clarity, and the test parameters for the triplet of tests were the same. The only difference was the time when water was applied to the contact. Water was applied when a specific value of CoA was reached. These values are for each TOR product listed in

Table 2 and are marked as T1–T3 in all graphs. In addition, the minimum values of CoA reached during the initial adhesion drop are displayed. There are slight differences between curves of the same TOR product measured at different tests. These could be caused by different contact temperatures, surface topography changes as wear progresses during the experiment, or slightly different amounts of TOR product in the contact path. However, these differences are not statistically significant.

Fig. 5 shows results for TORL-A. For 2 μl of water, a drop to the lowest CoA value of 0.084 was observed when water was applied in T3. Similar drops were also observed in T1 and T2 applications. Compared to b–d), the CoA drop caused by 2 μl of water had the shortest duration. The CoA was restored to the level before water application in all three measurements. For the rest of the tests, the lowest CoA measured were: 0.037 in T3 for b); 0.035 in T3 for c) and 0.026 in T1 for d). As can be seen, with an increase in water amount, the CoA decreases to lower levels. Moreover, larger amounts of water also slow the CoA restoration after the initial drop. In c) and d), the CoA was not restored during the standard test duration (except for T3; 2 ml). The CoA stayed in the 0.05–0.1 interval until the end of the test.

The curves for TORL-B measured in dry conditions are more flattened than those of TORL-A. However, under wet conditions, they show similar behavior, see Fig. 6. With the increasing amount of water, CoA decrease, and it takes more time for CoA to reach dry contact levels. The lowest CoA measured: 0.069 in T3 for a); 0.028 in T2 for b); 0.017 in T1

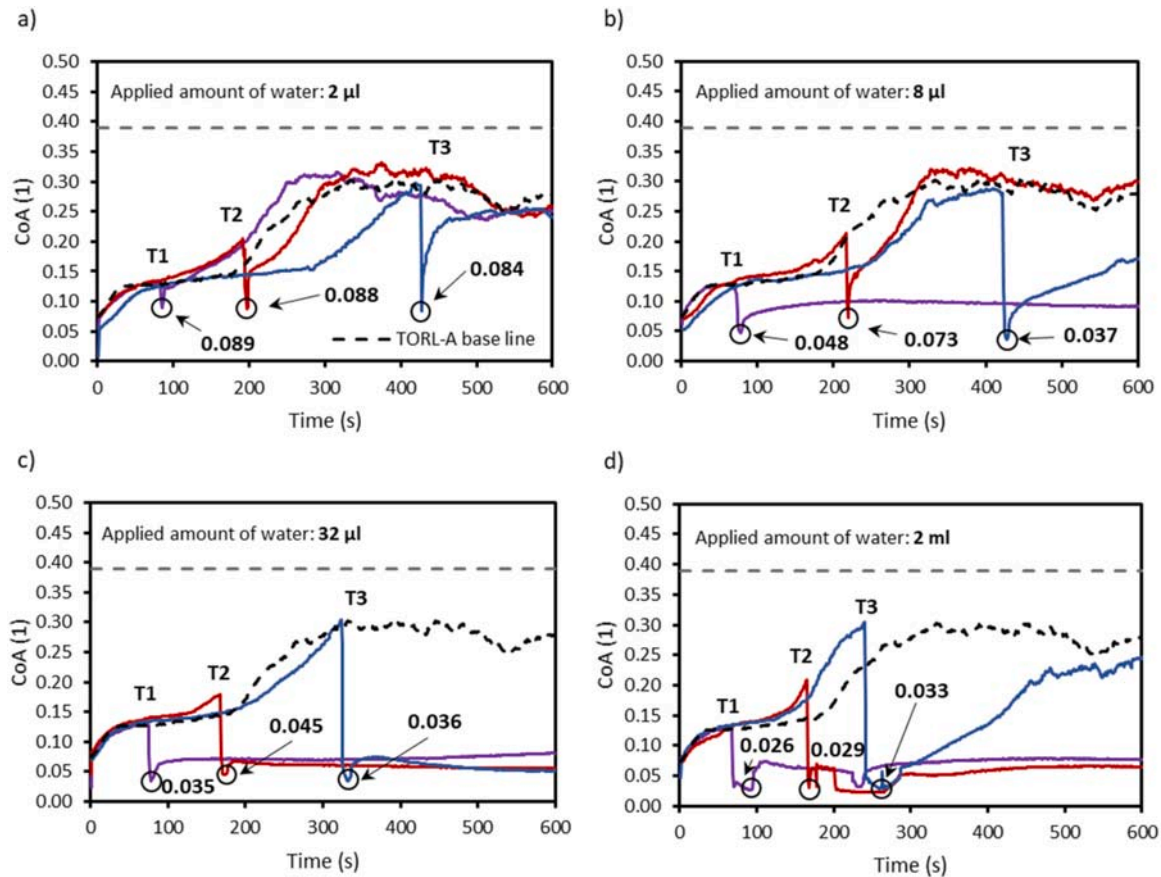


Fig. 5. Adhesion tests of TORL-A under wet conditions. Amounts of water: a) 2 µl; b) 8 µl; c) 32 µl; and d) 2 ml.

for c) and 0.026 in T1 for d). Compared to TORL-A, lower values of minimum CoA than in the case of TORL-B. In addition, except for experiments with 2 µl of water a), the dry adhesion level restoration did not occur during the standard test duration.

Fig. 7 shows the results of tests with FM-A (wet film). Please note that points T1–T3, where water was applied, now have different values of CoA than in the case of TOR lubricants (see Table 2). This is because FM-A generally led to the different development of CoA than tested TOR lubricants. From a–c), a clear relationship between the increase in the amount of water and the magnitude of the initial drop of CoA after water was applied can be seen. The lowest reached CoA was 0.086 in T1 for a); 0.042 in T2 for b), and 0.021 in T1 for c). Moreover, the CoA restoration slows down with the increase in the amount of water. For the lowest amount, the CoA drop lasts only a couple of seconds after water application. On the contrary, CoA recovery in case c) took more than 100 s. Still, the duration of the drop is relatively short compared to tests with TOR lubricants. Case d) does not fit this trend. From all tested amounts of water, in tests where 2 ml was applied, the initial adhesion drop was the shortest, and the CoA was quickly restored to a dry level and even higher. This behavior will be further discussed in the Section Discussion.

Fig. 8 shows the results of experiments with dry friction film. Contrary to wet film experiments, water was only applied at one value of CoA marked as T1 for all tested amounts. Thus different line colors in the graph represent different amounts of water; please see the legend. Similarly to the wet film tests, the higher the amount of water applied, the lower the CoA and the longer the adhesion recovery. The only exception is the test with 2 ml of water, where CoA first rises after contamination but then decreases to 0.061. This value is higher than 0.047 in the case of 32 µl of water but lower compared to tests with 2 µl and 8 µl, with measured values of 0.151 and 0.077, respectively. The

CoA drop is slow and divided into two parts – after the first initial drop, second to lower values follow. Water significantly reduces CoA compared to non-contaminated dry friction modifier film in all cases.

3.4. Results: performance of TOR products under continuous water application

Figs. 9 and 10 show the results for continuous water application, and in terms of visualization, they follow the same rules as the figures in the previous section. In Fig. 9, it can be seen that TORL-A shows a similar behavior under continuous water application as in tests with a single application of large amounts of water. The lowest reached CoA for TORL-A was 0.025. TORL-B reached an even lower value of 0.015, the same value as in the test with a single application of 2 ml of water, see Fig. 6d). In terms of CoA restoration, even though TORL-B led to lower CoA than TORL-A, approx. 100 s from the end of the water application, the CoA starts to rise, reaching dry-level CoA significantly quicker. The CoA restoration is also faster than in the tests with a single application of larger amounts of water (8 µl, 32 µl, and 2 ml). The gradient of the CoA increase in tests with TORL-A is comparable to tests with a single application of water.

Regarding water-based product FM-A, wet and dry film behaves differently compared to tests with a single application, see Fig. 10. In the case of the wet film, the lowest measured CoA was 0.073, which is lower than in tests with a single application (2 ml). Also, the CoA restoration to dry level takes longer (183 s). On the other hand, the CoA drops only to 0.168 in the case of dry film, and it takes approximately 180 s to restore CoA to dry levels. In both cases (dry/wet film), CoA was restored before the end of the water application.

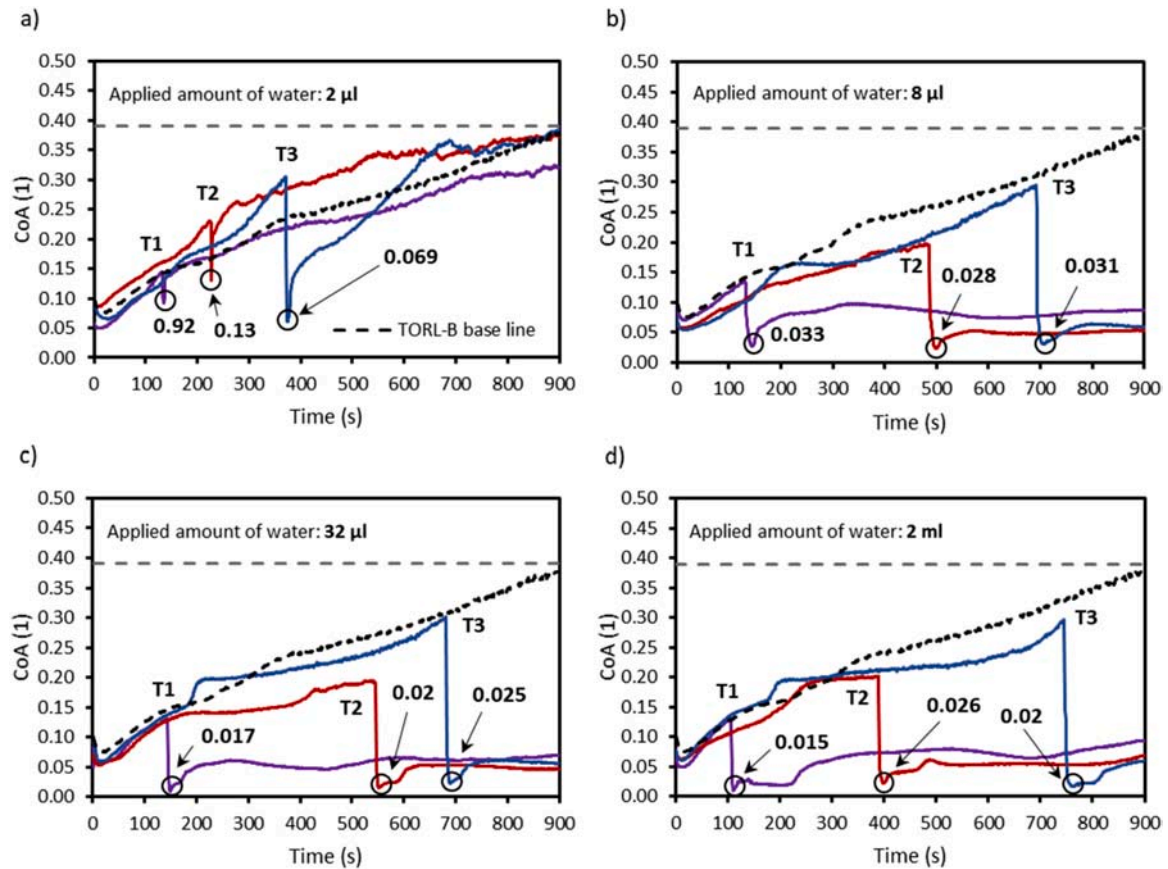


Fig. 6. Adhesion tests of TORL-B under wet conditions. Amounts of water: a) 2 µl; b) 8 µl; c) 32 µl; and d) 2 ml.

4. Discussion

4.1. The influence of the water amount on CoA

The Section Results show that water affects oil-based and water-based TOR products differently. In data evaluation, two main parameters were examined: (1) the lowest CoA reached after water was applied to the TOR product and (2) the duration of the interval of CoA < 0.1 (low adhesion). The overall results of experiments are summarised in the bar graphs in Fig. 11a) and b). Bars of different colors represent mean values evaluated from three measurements (applications in T1–T3), except FM-A (dry film), where water was applied only once at T1. Each color refers to a specific TOR product. Different shades of the same color indicate the amount of water applied, see the label of each bar. For Fig. 11a), the height of each bar represents the lowest CoA reached after water was applied to the TOR product. In Fig. 11b), the height of each bar represents the time duration in seconds for which the CoA was lower than 0.1. Note that a CoA did not drop under 0.1 in some tests. On the other hand, in some tests, the CoA restoration did not occur after water was applied, and the CoA did not reach 0.1 again during the test duration. These tests are marked with the "*" symbol in Fig. 11b). Please note that only tests with single water application were included in this evaluation. During tests with continuous water application, the CoA stays under 0.1 during the whole water application process. So, the CoA remained under the limit value for five extra minutes compared to tests with a single water application. Thus, time durations of CoA lower than 0.1 in those two types of tests cannot be compared.

For TORL-A, Fig. 11a) shows that as the amount of water increases, the CoA decreases to lower minimal values. For comparison, the mean CoA of 0.029 reached after 2 ml of water was applied is nearly three times lower than CoA of 0.086 in the case of 2 µl. TORL-B follows the same trend with an exception between 32 µl and 2 ml, where CoA

decreases to a slightly lower value of 0.017 for 32 µl compared to CoA of 0.02 for 2 ml of water. For both oil-based TOR products, it can be said that the higher the amount of water, the longer the CoA stays under 0.1. In the case of a larger amount of water, the CoA restoration did not occur at all. Under continuous water application, both oil-based TOR products behaved similarly to a single application of 2 ml.

In the case of the FM-A (wet film), with an increasing amount of water, CoA reaches lower minimal values. The only exception was between 32 µl and 2 ml, which was caused due to a large amount of water flushing TOR product away from the track, causing quick CoA recovery. When water was applied to dried FM-A film, the drop of CoA was less significant compared to wet FM-A film, and the time of CoA lower than 0.1 was also shorter. Higher values of minimal CoA and shorter duration of the low adhesion period are probably caused by the absence of the evaporated base medium. An exception was the tests with 2 ml of water, where the combined effect of water and dried particles led to better lubrication than in the case of FM-A (wet film). Under continuous water application, the CoA restoration was quicker for dried FM-A film than for wet film.

In most tests, the CoA drop was not as high for water-based TOR products as for oil-based TOR products. Although the oil does not easily mix with water, contamination of oil-based TOR products poses a more significant risk in terms of low CoA. This is mainly supported by the fact that CoA stayed below 0.1 for no or very little time for water-based TOR products.

From a practical point of view, the amount of water on an actual rail can be either small (morning dew, leakage from passing train) or large (mostly rain). By comparing the approximate contact area of tested samples under set conditions to the expected size of the actual wheel-rail contact, the amounts of water tested in this paper correspond to the following amounts in the field conditions: 2 µl ≈ 3 ml; 8 µl ≈ 12 ml; 32 µl ≈ 46 ml; 2 ml and 2.15 ml ≈ 3 l. Single contamination of the

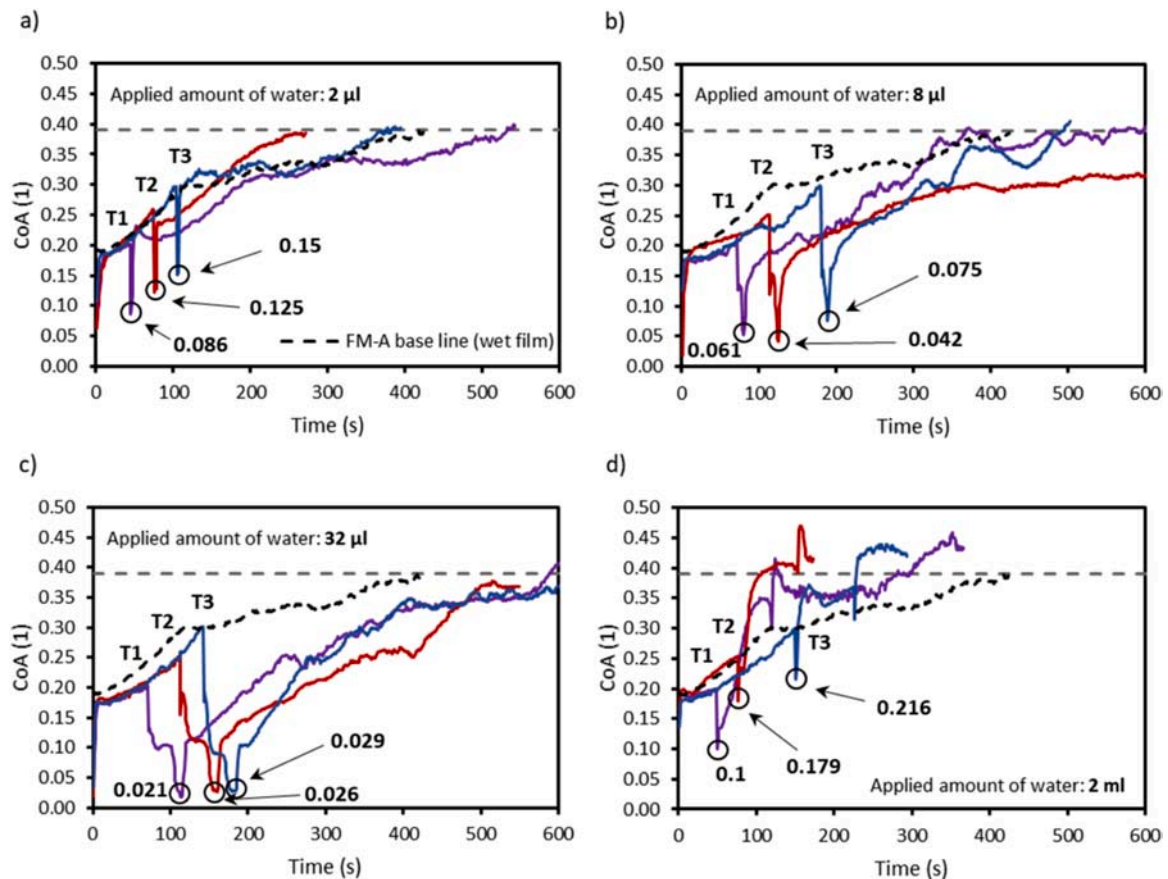


Fig. 7. Adhesion tests of FM-A (wet film) under wet conditions. Amounts of water: a) 2 µl; b) 8 µl; c) 32 µl; and d) 2 ml.

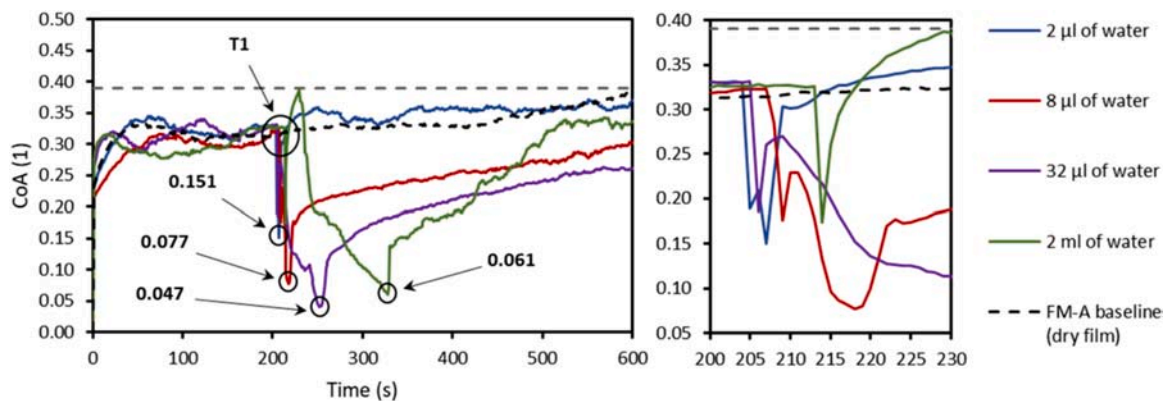


Fig. 8. Adhesion tests of FM-A (dry film) under wet conditions. Each line represents a different amount of water, see the legend.

contact by liters of water in actual railway operation seems to be unlikely. However, knowing the worst-case scenario is still necessary when dealing with passenger safety. On the other hand, it is possible for the smaller amounts in the order of milliliters to be accumulated over a short period from the rain or the overnight condensation from the humid air. Thus, tested amounts of water (especially 2 µl and 8 µl) are relevant to actual field conditions.

Results indicate that the risk of low CoA rises with the amount of water. However, this is contrary to field measurements, which suggest that it is rather a small amount of water leading to low CoA. The analysis in [5] shows that low CoA-related incidents are most probable when morning dew is on a rail. Similarly, findings in [24] show that when a small amount of water is mixed with particles of iron oxides, CoA lower

than 0.05 can occur. On the other hand, several papers showed that although the exact value of CoA depends on water temperature [30], larger amounts generally lead to much higher CoA [31,32]. The effect of water also depends on the presence of the third-body layer, consisting of iron oxides, wear particles, environmental contaminants, or even TOR product residua. Thus, possible mechanisms of water contamination of TOR products will be discussed next.

4.2. Fluid-film regime / Mechanisms relevant to oil-water system

First, the question arises as to why the CoA of the W/O mixture is lower than that of bleed oil, as revealed by the Stribeck test under fully flooded conditions in Chapter 3.2. Similar observations were made in

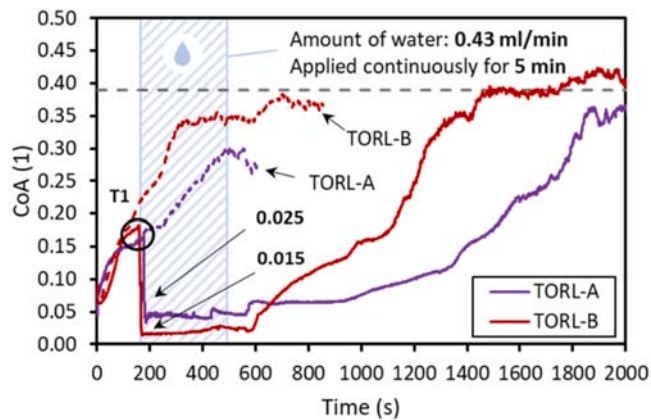


Fig. 9. Adhesion tests of TORL-A and TORL-B under wet conditions. Water was applied continuously for 5 min.

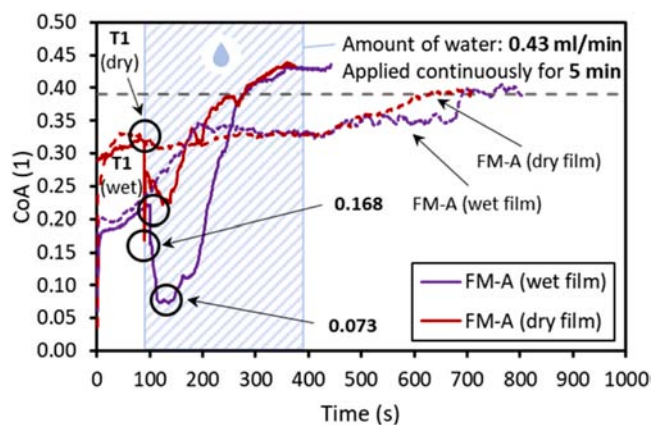


Fig. 10. Adhesion tests of FM-A (dry film) and FM-A (wet film) under wet conditions. Water was applied continuously for 5 min.

simulated wheel-rail contact [31]. Over the last decades, several theories have been proposed on the lubrication mechanism of water-in-oil (W/O) or oil-in-water (O/W) emulsions. Those theories can help to explain the behavior of water-contaminated EHL contacts.

At low speeds, the behavior can be explained by the well-accepted plate-out theory [33,34]. This theory assumes that water is excluded from the contact due to the stronger wetting ability of oil, creating an oil pool around EHL contact, see Fig. 12a). This mechanism is in accordance with the theory of energy displacement [33]. Ideally, a lubricant film in the contact is fully composed of the oil phase, and there is no negative effect on lubricant film thickness [35,36]. For larger droplets, dynamic concentration theory describing the increasing concentration of oil in the inlet zone as water is gradually excluded from the gap is more appropriate [37].

According to a starvation theory [38], the first critical speed exists, after which the oil pool becomes unstable, and lubricant film thickness in the contact decreases [39–41]. While remaining in full-film lubrication, lower film thickness means lower shear stress in lubricating film and, therefore, lower traction [40]. After the second critical speed, lubricant film thickness starts to increase. However, due to starvation, water can no longer be excluded from the contact inlet, and a certain amount of water phase, given by the dynamic concentration theory [37], passes through the contact resulting in a much lower coefficient of traction. This behavior strongly depends on the size of water droplets [42]. A single application of a water droplet may differ from the behavior of emulsified water. A large water droplet is more easily expelled from the oil. If it occurs under contact starvation, water can

easily enter the contact [43]. Those theories can explain low CoA in the water-contaminated oil-lubricated contact.

4.3. Starved fluid-film regime / Mechanisms relevant to grease-water system

Oil-based TOR products are usually based on grease, i.e., they contain thickener and base oil. In this case, water influences the oil pool in the contact and structure and the rheology of bulk grease [44]. Evaluation of its water resistance is covered by industry standards [45]. Unlike lubricating oil, grease can absorb a larger amount of water due to the polar nature of its thickener and additives. This ability strongly depends on a thickener type, while some greases become stiffer and others soften [44].

Grease-lubricated contact is much more susceptible to starvation since a relatively thick grease is being pushed out of the contact track. Lubricant replenishment from the reservoirs on track sides is very slow, and the replenishment flow is inversely proportional to viscosity [46, 47]. Absorbed water influences stiffness and oil-bleeding, i.e., the ability to replenish the contacts. The effects can be positive or negative depending on the type of thickener [48,49]. If the water absorption leads to an enhanced contact replenishment, higher oil film thickness under starved conditions and lower friction in the mixed regime may occur, which is consistent with our observations. For visualization of this mechanism, please see Fig. 12b). On the other hand, oil-based TOR products intended for the open tribology system are designed as water-repellent with low water adsorption, so the "free water" should rather occur in the contact.

4.4. Mixed regime / Mechanisms relevant to TOR-water system

When severe starvation occurs, lubricant film thickness further decreases, resulting in a mixed regime, where a part of the load is transmitted by the contacts of surface asperities and CoA increases [50]. Under these conditions, boundary friction is given by the composition of the created tribological layer. TOR products contain solid lubricants like graphite or molybdenum disulfide. The frictional properties of those particles are affected by water in different ways. The coefficient of friction of graphite usually decreases in the presence of water because of the dissociative chemisorption of water. On the contrary, the lubricity of MoS₂ decreases due to oxidation and physisorption of water molecules. However, the effect may be reduced by interaction with metal particles, which are also a common component of TOR products [51].

More significant is probably the interaction of water with other components of TOR products as particles for friction modification or wear particles. When mixed with a small amount of water, solid particles create a paste that causes a transient decrease in friction. This mechanism is known as a "wet-rail" phenomenon [52] and is depicted in Fig. 12c). Since the decrease in CoA appears to be independent of the water application time during friction development, it can be assumed to be due to particles contained in the TOR products rather than wear particles.

4.5. Mechanisms relevant to water-based TOR product contamination

Regarding the water-based TOR product, a similar dependence of magnitude and duration of CoA drop on the applied amount of water exists up to 32 μ l. However, large amounts (2 ml) flush the product out of the surface, quickly restoring CoA to dry contact levels. This happened for both single and continuous applications, although in dry film test single application, the results are not entirely clear. Even if a CoA lower than 0.1 occurs immediately after the contamination, it remains below this limit only for a short period and then rises.

The drop of CoA can be divided into two parts. After the first drop, the second more significant follows, see Fig. 7a-c). This behavior was already seen in the study [53], in which the authors performed various

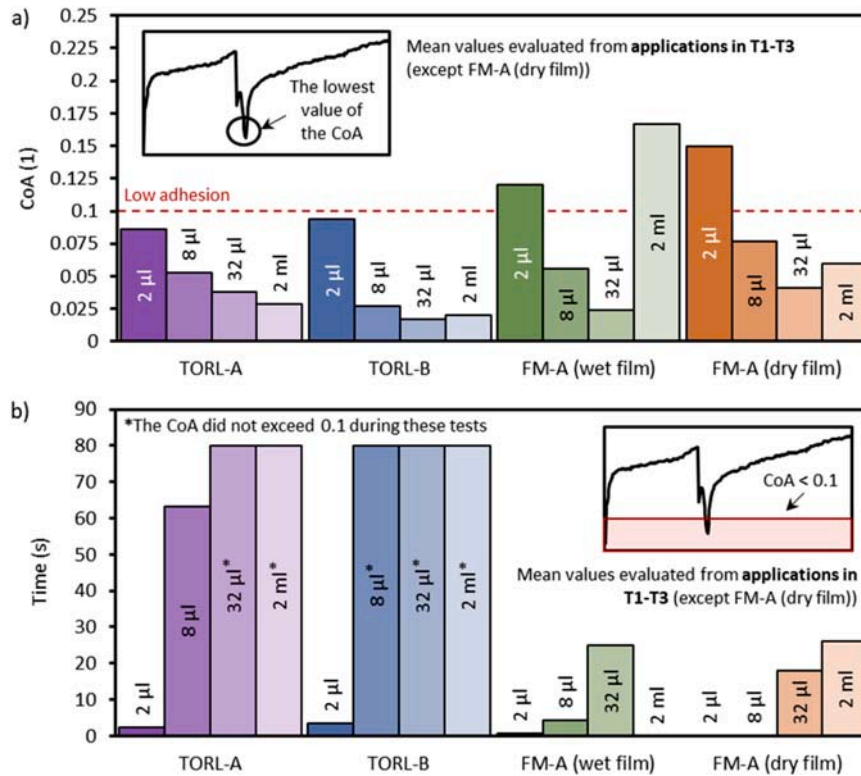


Fig. 11. Mean (a) adhesion drop after water application and (b) duration of a period when CoA was lower than 0.1.

tests with water alone. Similar behavior was also observed in a paper [3] focused on water-based TOR products. It can be assumed that this behavior relates to the water contained in the product and thus did not occur in tests with oil-based TOR products.

Results presented in this study are comparable with findings in [54], where two water-based TOR products were tested under various slips and water contamination. Although both products differ from those tested in this study in the type of particles contained, the trends in CoA development seem similar. In an extreme case, the CoA after water contamination drops to approx. 0.05, which is comparable to tests with FM-A (8 µl). In other cases, the magnitude of the drop was not as high, probably caused by different product particles. As was shown in [2], product performance strongly depends on the type of contained particles. Tested products in [54] had particles of metals with a diameter as large as 100 µm. Particles in [3] were mainly minerals like bentonite or talc, and their diameter did not exceed 10 µm. Substances with mineral particles of smaller diameters reach lower CoA comparable to one of the products used in this study. Thus, the type and scale of the particles play an essential role in achieving sufficient CoA. In both studies, it seems that water slows CoA development rather than interrupts it, contrary to the case of oil-based TOR products. As shown in Fig. 7a-c), the CoA develops similarly to the situation before contamination, only starting again from lower values.

Authors propose that the contamination mechanism of water-based TOR products lay in the refill of the evaporated base medium. After contamination, water mixes with dried particles and the mixture act as a freshly applied product. This is supported by Fig. 8, which summarises the results of dry FM-A film tests. The dry film leads to higher CoA (higher than 0.3) than the wet film. However, after contamination, water mixes with dried particles, and the CoA drops to values comparable to values of the original TOR product before base medium evaporation, see Fig. 7. After that, the mixture behaves similarly to tests with FM-A (wet film).

4.6. Limitations of the Study

The CoA values and performance of tested oil-based TOR products measured in this study follow results published in [13], which were also measured on a ball-on-disc tribometer. As was shown in [11], measured adhesion strongly depends on the measuring device. The point contact between the ball and the disc simplifies actual rail conditions. However, many previous studies on wheel-rail tribology already used universal tribometers in the ball-on-disc configuration, obtaining useful results [3, 4, 28]. Although conclusions from laboratory tests can be limited due to simplifications, they are suitable for preliminary studies as these tests are more controllable than field tests. Regarding used specimens, there are three main differences compared to actual wheel-rail contact: the contact shape, the surface roughness, and the material hardness.

As for the point contact, Chen et al. [30] measured the adhesion of water-contaminated contact on a twin disc machine. The use of discs as contact bodies led to line contact, and still, values obtained for given conditions correspond to values represented in Fig. 3d) or published in [53].

Pieringer et al. [55] measured the surface roughness of wheel and rail to be tens of micrometers which is significantly higher compared to Ra 0.15–0.3 µm of specimens in this study. Conversely, Chen et al. assumed that surface roughness depends on the current state of the wheel and rail (new/worn/after grinding) and can be expected in the range of 0.3–1.5 µm [56]. Previously, Galas et al. [13] used specimens with surface roughness varying from 0.05 to 0.45 µm to conduct similar experiments and achieved representative results. Furthermore, Zhu et al. [57] used discs with Ra as low as 0.2 µm to measure CoA in contaminated contact on a twin disc machine. Since surface roughness influences the lubrication regime, Stribeck tests were conducted in this study. Fig. 4 shows that the tested configuration operated in similar conditions to the actual wheel-rail contact. So, in theory, measured CoA should be representative.

Regarding hardness, sets of standard material grades were established around the world. In Europe, rail steels are typically pearlitic and

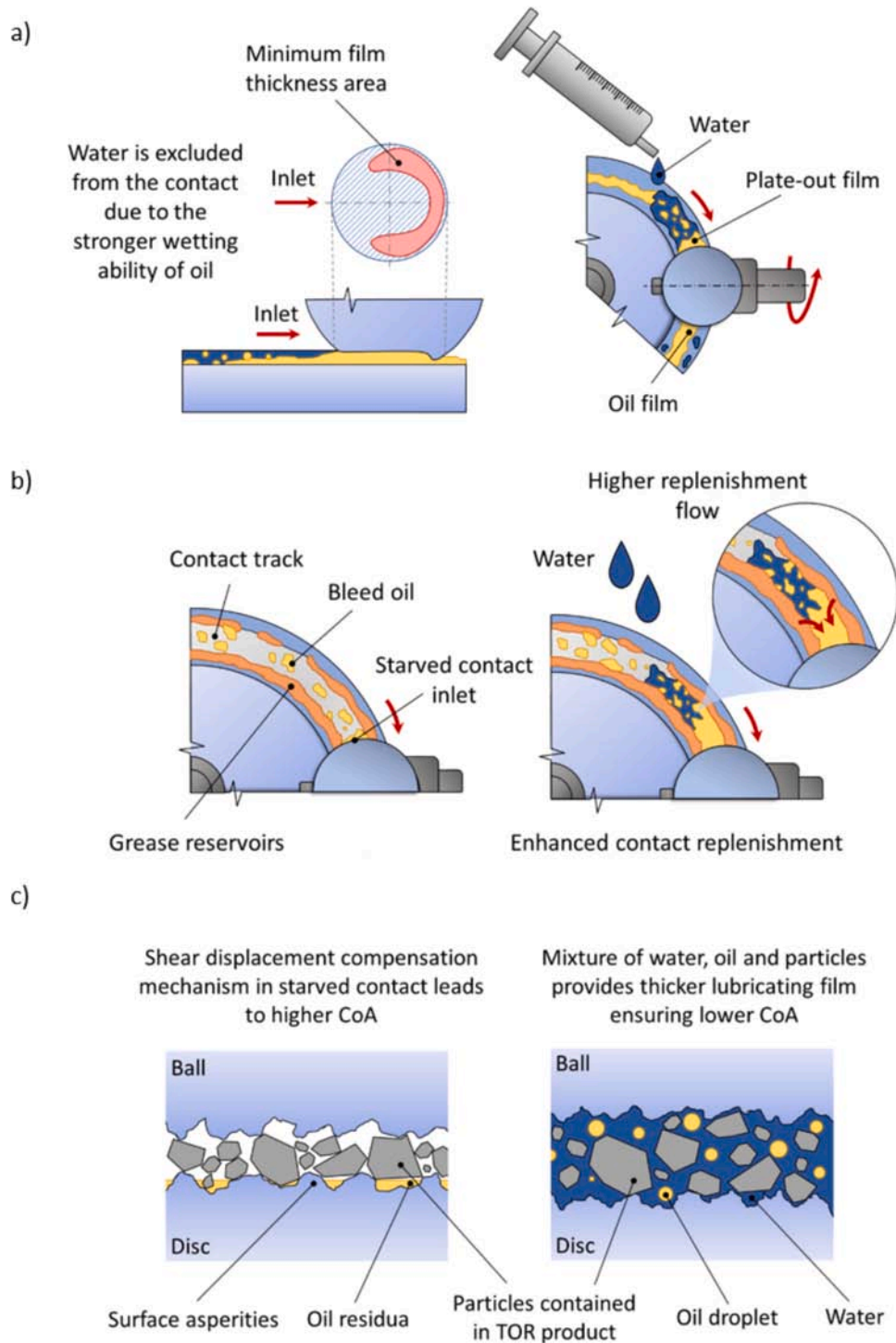


Fig. 12. Discussed mechanisms: a) Fluid-film regime, b) Starved fluid-film regime, c) Mixed regime.

could be heat-treated. Lewis et al., in their paper, compared the hardness of several materials [7]. They showed that the bulk hardness of conventional R260 steel was approx. 275 HV, and for heat-treated R350HT steel was 350 HV. It should also be noted that due to the work-hardening effect, the hardness close to the surface can be 2.5 times higher than the hardness of the bulk [58]. On the other hand, the hardness of specimens in this study was 800–920 HV and 720–780 HV for ball and disc, which is significantly higher, meaning their behavior can differ from actual rail materials. Harmon et al. showed that with a higher hardness of specimens, the slightly lower values of CoA will be measured compared to

specimens made of softer materials [59].

The main purpose of choosing harder material was to reduce wear. The surface topography changes as the wear progresses during the test, causing a decrease in contact pressure. It was observed that the most severe wear occurred during the first 60 min of the test with new pair of specimens. But after this period, the wear becomes stable, and the width and depth of the contact path increased only a little. Thus, contact pressure remains relatively constant. The wear-in period was conducted on all new specimens to overcome the initial rapid wear and ensure stable test conditions. Although the actual contact pressure during tests

was probably lower than the initial 800 MPa, it remains relatively the same for all tests, so the results should be comparable.

A similar approach was used before in [3,4,13] and enabled focusing primarily on the effect of tested substances without bias from other factors that were not in the scope of the study. Measured results show a clear influence of water on TOR products. However, their transferability into railway operation could be limited and should be validated on specimens made from authentic rail material with more realistic geometry.

There is one more significant difference compared to the actual rail track. While in the laboratory tribometer, the contact between bodies occurs on the same spots as both bodies rotate, in reality, the wheel passes an exact location on the rail only once per ride. In laboratory conditions, this means that enough amount of lubricant is always present because it has nowhere to go. However, as shown in [15], the product is carried by wheels on an actual track for several hundred meters. Thus, larger amounts of lubricant are present only for a limited distance from an application unit. It is unclear if this increases or decreases the probability of low CoA. On one side, the probability of overdosing decreases with distance from the application unit. On the other, it was shown that water is most likely to cause low CoA when only a small amount is mixed with the third body layer [18,24]. From this point of view, the effect of water will be more significant if only a thin layer of TOR product is present, which could be expected farther away from the application unit. Either way, water will always influence the performance of TOR product, and the extent of this influence should be known for the safety of passengers and the efficiency of rail transport.

5. Conclusion

The ball-on-disc tribometer MTM was used in this study to investigate the influence of water contamination on TOR product performance. One commercial water-based and two oil-based TOR products were tested. The water-based TOR product was tested both before and after the base medium evaporation. Four different amounts of water were applied by syringe/electronic micropipette to TOR products. Also, continuous water application by a peristaltic pump was tested. The results could be summarized in the following points:

- 1) A low amount of water (2 μ l) had a limited effect on tested TOR products and did not cause low CoA. However, it is important to mention that the contact surfaces of specimens were cleaned before every test. In actual railway, water could mix with third body layer particles and form a highly-viscous paste known for lowering CoA to insufficient levels.
- 2) Contamination of oil-based TOR products by a large amount of water resulted in a long-lasting period of low CoA (the lowest measured value was 0.015). A suggested explanation for this derives from W/O emulsion lubrication theories. Due to its low viscosity, water helped the oil to move into contact. Thus, lower values of CoA could be achieved for a prolonged time.
- 3) Low CoA rarely occurred in tests with water-based TOR products. Although CoA dropped after water was applied, after several dozen seconds, it was restored to the level before contamination. The water and dried solid particles formed a mixture similar to the original TOR product before the base medium evaporation. From this point of view, adding water to the dried water-based TOR product extended its lasting effect rather than causing low CoA problems. However, excessive amounts of water (2 ml) flushed the TOR product out of the contacting surfaces and significantly shortened its performance.
- 4) No significant difference existed between a single or continuous application of the same amount of water that contaminated oil-based TOR products. In the case of a water-based TOR product, CoA was restored slightly slower under continuous application.

The wheel-rail interface is an open system, meaning water and other

contaminants can enter the contact. The presented results showed the strong influence of water contamination on the performance of TOR products. A long-lasting period of CoA lower than 0.1 occurred in several tests, suggesting that traction problems could also happen in actual railway conditions. This potential risk should be taken into account in the TOR conditioning deployment. Also, the interaction of TOR products with water should be considered in product development and testing. Although several hypotheses were proposed, the exact mechanism of the described phenomenon was not revealed and thus will be the object of the following research work.

Statement of Originality

As a corresponding author, I, Simon Skurka, hereby confirm on behalf of all authors that:

- 1) The authors have obtained the necessary authority for publication.
- 2) The paper has not been published previously, that it is not under consideration for publication elsewhere, and that if accepted it will not be published elsewhere in the same form, in English or in any other language, without the written consent of the publisher.
- 3) The paper does not contain material which has been published previously, by the current authors or by others, of which the source is not explicitly cited in the paper.

Upon acceptance of an article by the journal, the author(s) will be asked to transfer the copyright of the article to the publisher. This transfer will ensure the widest possible dissemination of information.

CRediT authorship contribution statement

Simon Skurka: Conceptualization, Methodology, Investigation, Data curation, Writing – original draft. **Radovan Galas:** Conceptualization, Investigation, Methodology, Writing – review & editing. **Milan Omasta:** Conceptualization, Investigation, Methodology, Writing – review & editing, Project administration. **Bingnan Wu:** Data curation, Writing – review & editing, Visualization. **Haohao Ding:** Writing – review & editing, Visualization. **Wen-Jian Wang:** Conceptualization, Data curation, Writing – review & editing, Project administration. **Ivan Krupka:** Data curation, Writing – review & editing. **Martin Hartl:** Supervision, Funding acquisition.

Declaration of Competing Interest

The authors declare that they have no known competing financial interests or personal relationships that could have appeared to influence the work reported in this paper.

Data Availability

Data will be made available on request.

Acknowledgments

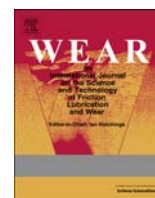
This research was carried out under project EG20_321/0025198 with financial support from the Ministry of Industry and Trade of the Czech Republic and under project GA20-23482S with financial support from the Czech Science Foundation. Also, the authors thank the support of the National Natural Science Foundation of China (No. 52272443).

References

- [1] Suda Y, Iwasa T, Komine H, Tomeoka M, Nakazawa H, Matsumoto K, et al. Development of onboard friction control. *Wear* 2005;258:1109–14. <https://doi.org/10.1016/j.wear.2004.03.059>.

- [2] Kalousek J, Johnson KL. An investigation of short pitch wheel and rail corrugations on the vancouver mass transit system. *Proc Inst Mech Eng F J Rail Rapid Transit* 1992;206:127–35. https://doi.org/10.1243/PIME_PROC.1992.206.226.02.
- [3] Galas R, Kvarda D, Omasta M, Krupka I, Hartl M. The role of constituents contained in water-based friction modifiers for top-of-rail application. *Tribol Int* 2018;117:87–97. <https://doi.org/10.1016/j.triboint.2017.08.019>.
- [4] Kvarda D, Skurka S, Galas R, Omasta M, Shi L, Ding H, et al. The effect of top of rail lubricant composition on adhesion and rheological behaviour. *Eng Sci Technol, Int J* 2022;35:101100. <https://doi.org/10.1016/j.jestech.2022.101100>.
- [5] Valehrach J, Guziur P, Riha T, Plasek O. Assessment of rail long-pitch corrugation. *IOP Conf Ser Mater Sci Eng* 2017;236:012048. <https://doi.org/10.1088/1757-899X/236/1/012048>.
- [6] Stock R, Pippan R. RCF and wear in theory and practice—The influence of rail grade on wear and RCF. *Wear* 2011;271:125–33. <https://doi.org/10.1016/j.wear.2010.10.015>.
- [7] Lewis R, Christoforou P, Wang WJ, Beagles A, Burstow M, Lewis SR. Investigation of the influence of rail hardness on the wear of rail and wheel materials under dry conditions (ICRI wear mapping project). *Wear* 2019;430–431:383–92. <https://doi.org/10.1016/j.wear.2019.05.030>.
- [8] Braghin F, Lewis R, Dwyer-Joyce RS, Bruni S. A mathematical model to predict railway wheel profile evolution due to wear. *Wear* 2006;261:1253–64. <https://doi.org/10.1016/j.wear.2006.03.025>.
- [9] Olofsson U, Telliskivi T. Wear, plastic deformation and friction of two rail steels—a full-scale test and a laboratory study. *Wear* 2003;254:80–93. [https://doi.org/10.1016/S0043-1648\(02\)0291-0](https://doi.org/10.1016/S0043-1648(02)0291-0).
- [10] Number of Europeans exposed to harmful noise pollution expected to increase — European Environment Agency n.d. (<https://www.eea.europa.eu/highlights/number-of-europeans-exposed-to>) (accessed August 12, 2022).
- [11] Lundberg J, Rantatalo M, Wanhaien C, Casselgren J. Measurements of friction coefficients between rails lubricated with a friction modifier and the wheels of an IORE locomotive during real working conditions. *Wear* 2015;324–325:109–17. <https://doi.org/10.1016/j.wear.2014.12.002>.
- [12] Eadie DT, Elvidge D, Oldknow K, Stock R, Pointner P, Kalousek J, et al. The effects of top of rail friction modifier on wear and rolling contact fatigue: Full-scale rail-wheel test rig evaluation, analysis and modelling. *Wear* 2008;265:1222–30. <https://doi.org/10.1016/j.wear.2008.02.029>.
- [13] Galas R, Omasta M, Krupka I, Hartl M. Laboratory investigation of ability of oil-based friction modifiers to control adhesion at wheel-rail interface. *Wear* 2016;368–369:230–8. <https://doi.org/10.1016/j.wear.2016.09.015>.
- [14] Abbasi S, Olofsson U, Zhu Y, Sellgren U. Pin-on-disc study of the effects of railway friction modifiers on airborne wear particles from wheel-rail contacts. *Tribol Int* 2013;60:136–9. <https://doi.org/10.1016/j.triboint.2012.11.013>.
- [15] Han J, He Y, Xiao X, Sheng X, Zhao G, Jin X. Effect of Control Measures on Wheel/Rail Noise When the Vehicle Curves. *Appl Sci* 2017;7:1144. <https://doi.org/10.3390/app7111144>.
- [16] Meehan PA, Liu X. Wheel squeal noise control under water-based friction modifiers based on instantaneous rolling contact mechanics. *Wear* 2019;440–441:203052. <https://doi.org/10.1016/j.wear.2019.203052>.
- [17] Szablewski D, LoPresti J, Sultana T. Testing of latest top-of-rail friction modification materials at FAST. *Railw Track Struct* 2015;111:13–6.
- [18] Ishizaka K, Lewis SR, Lewis R. The low adhesion problem due to leaf contamination in the wheel/rail contact: Bonding and low adhesion mechanisms. *Wear* 2017;378–379:183–97. <https://doi.org/10.1016/j.wear.2017.02.044>.
- [19] Stock R, Stanlake L, Hardwick C, Yu M, Eadie D, Lewis R. Material concepts for top of rail friction management – Classification, characterisation and application. *Wear* 2016;366–367:225–32. <https://doi.org/10.1016/j.wear.2016.05.028>.
- [20] Galas R, Omasta M, Klapka M, Kaewunruen S, Krupka I, Hartl M. Case study: the influence of oil-based friction modifier quantity on tram braking distance and noise. *Tribol Ind* 2017;39:198–206. <https://doi.org/10.24874/ti.2017.39.02.06>.
- [21] Harmon M, Lewis R. Review of top of rail friction modifier tribology. *Tribology - Mater, Surf Interfaces* 2016;10:150–62. <https://doi.org/10.1080/17515831.2016.1216265>.
- [22] Areiza YA, Garcés SI, Santa JF, Vargas G, Toro A. Field measurement of coefficient of friction in rails using a hand-pushed tribometer. *Tribol Int* 2015;82:274–9. <https://doi.org/10.1016/j.triboint.2014.08.009>.
- [23] Olofsson U, Lyu Y. Open system tribology in the wheel-rail contact—a literature review. *Appl Mech Rev* 2017;69. <https://doi.org/10.1115/1.4038229>.
- [24] White B, Lewis R. Simulation and understanding the wet-rail phenomenon using twin disc testing. *Tribol Int* 2019;136:475–86. <https://doi.org/10.1016/j.triboint.2019.03.067>.
- [25] Chen H, Fukagai S, Sone Y, Ban T, Namura A. Assessment of lubricant applied to wheel/rail interface in curves. *Wear* 2014;314:228–35. <https://doi.org/10.1016/j.wear.2013.12.006>.
- [26] Lewis SR, Lewis R, Olofsson U, Eadie DT, Cotter J, Lu X. Effect of humidity, temperature and railhead contamination on the performance of friction modifiers: pin-on-disk study. *Proc Inst Mech Eng F J Rail Rapid Transit* 2013;227:115–27. <https://doi.org/10.1177/0954409712452239>.
- [27] Moreno-Ríos M, Gallardo-Hernández EA, Vite-Torres M, Peña-Bautista A. Field and laboratory assessments of the friction coefficient at a railhead. *Proc Inst Mech Eng F J Rail Rapid Transit* 2016;230:313–20. <https://doi.org/10.1177/0954409714536383>.
- [28] Zhu Y, Olofsson U, Persson K. Investigation of factors influencing wheel-rail adhesion using a mini-traction machine. *Wear* 2012;292–293:218–31. <https://doi.org/10.1016/j.wear.2012.05.006>.
- [29] Kalin M, Velkavrh I, Vizintin J. The Stribeck curve and lubrication design for non-fully wetted surfaces. *Wear* 2009;267:1232–40. <https://doi.org/10.1016/j.wear.2008.12.072>.
- [30] Chen H, Ishida M, Namura A, Baek KS, Nakahara T, Leban B, et al. Estimation of wheel/rail adhesion coefficient under wet condition with measured boundary friction coefficient and real contact area. *Wear* 2011;271:32–9. <https://doi.org/10.1016/j.wear.2010.10.022>.
- [31] Wang WJ, Zhang HF, Wang HY, Liu QY, Zhu MH. Study on the adhesion behavior of wheel/rail under oil, water and sanding conditions. *Wear* 2011;271:2693–8. <https://doi.org/10.1016/j.wear.2010.12.019>.
- [32] Wang WJ, Shen P, Song JH, Guo J, Liu QY, Jin XS. Experimental study on adhesion behavior of wheel/rail under dry and water conditions. *Wear* 2011;271:2699–705. <https://doi.org/10.1016/j.wear.2011.01.070>.
- [33] Kimura Y, Okada K. Lubricating properties of oil-in-water emulsions. *Tribology Trans* 1989;32:524–32. <https://doi.org/10.1080/10402008908981921>.
- [34] Fujita N, Kimura Y, Kobayashi K, Amanuma Y, Sodani Y. Estimation model of plate-out oil film in high-speed tandem cold rolling. *J Mater Process Technol* 2015;219:295–302. <https://doi.org/10.1016/j.jmatprotec.2015.01.002>.
- [35] Nakahara T, Makino T, Kyogoku K. Observations of liquid droplet behavior and oil film formation in O/W type emulsion lubrication. *J Tribol* 1988;110:348–53. <https://doi.org/10.1115/1.3261630>.
- [36] Benner JJ, Sadeghi F, Hoepflich MR, Frank MC. Lubricating properties of water in oil emulsions. *J Tribol* 2006;128:296–311. <https://doi.org/10.1115/1.2164464>.
- [37] Wilson WRD, Sakaguchi Y, Schmid SR. A dynamic concentration model for lubrication with oil-in-water emulsions. *Wear* 1993;161:207–12. [https://doi.org/10.1016/0043-1648\(93\)90471-W](https://doi.org/10.1016/0043-1648(93)90471-W).
- [38] Chiu YP. An analysis and prediction of lubricant film starvation in rolling contact systems. *A S L E Trans* 1974;17:22–35. <https://doi.org/10.1080/05698197408981435>.
- [39] Zhu D, Biresaw G, Clark SJ, Kasun TJ. Elastohydrodynamic lubrication with O/W emulsions. *J Tribol* 1994;116:310–9. <https://doi.org/10.1115/1.2927216>.
- [40] Yang H, Schmid SR, Kasun TJ, Reich RA. Elastohydrodynamic film thickness and tractions for oil-in-water emulsions. *Tribol Trans* 2004;47:123–9. <https://doi.org/10.1080/05698190490278976>.
- [41] Liang H, Guo D, Ma L, Luo J. Investigation of film formation mechanism of oil-in-water (O/W) emulsions at high speeds. *Tribol Int* 2017;109:428–34. <https://doi.org/10.1016/j.triboint.2017.01.006>.
- [42] Zhang F, Fillot N, Bouscharain N, Devaux N, Philippon D, Matta C, et al. Water droplets in oil at the inlet of an EHD contact: A dual experimental and numerical investigation. *Tribol Int* 2023;177:108015. <https://doi.org/10.1016/j.triboint.2022.108015>.
- [43] Liu X, Wang J, Huang L, Zhang J, Xu C, Tong L, et al. Direct observation of the impact of water droplets on oil replenishment in EHD lubricated contacts. *Friction* 2022;10:388–97. <https://doi.org/10.1007/s40544-020-0466-0>.
- [44] Cyriac F, Lugt PM, Bosman R. Impact of water on the rheology of lubricating greases. *Tribol Trans* 2016;59:679–89. <https://doi.org/10.1080/10402004.2015.1107929>.
- [45] Gurt A, Khonsari M. An overview of grease water resistance. *Lubricants* 2020;8:86. <https://doi.org/10.3390/lubricants8090086>.
- [46] Cann PME, Damiens B, Lubrecht AA. The transition between fully flooded and starved regimes in EHL. *Tribol Int* 2004;37:859–64. <https://doi.org/10.1016/j.triboint.2004.05.005>.
- [47] Jacob B., Pubilier F, E. Cann P.M., Lubrecht A.A. An Analysis of Track Replenishment Mechanisms in the Starved Regime, 1999, p. 483–492. ([https://doi.org/10.1016/S0167-8922\(99\)80069-8](https://doi.org/10.1016/S0167-8922(99)80069-8)).
- [48] Cyriac F, Lugt PM, Bosman R, Venner CH. Impact of water on EHL film thickness of lubricating greases in rolling point contacts. *Tribol Lett* 2016;61:23. <https://doi.org/10.1007/s11249-016-0642-6>.
- [49] Hudedagaddi CB, Raghav AG, Tortora AM, Veeregowda DH. Water molecules influence the lubricity of greases and fuel. *Wear* 2017;376–377:831–5. <https://doi.org/10.1016/j.wear.2017.02.002>.
- [50] Li Q, Zhang S, Wu B, Lin Q, Ding H, Galas R, et al. Analysis on the effect of starved elastohydrodynamic lubrication on the adhesion behavior and fatigue index of wheel-rail contact. *Wear* 2022;510–511:204506. <https://doi.org/10.1016/j.wear.2022.204506>.
- [51] Chen Z, He X, Xiao C, Kim S. Effect of humidity on friction and wear—a critical review. *Lubricants* 2018;6:74. <https://doi.org/10.3390/lubricants6030074>.
- [52] White B, Kempka R, Laity P, Holland C, Six K, Trummer G, et al. Iron oxide and water paste rheology and its effect on low adhesion in the wheel/rail interface. *Tribol Lett* 2022;70:8. <https://doi.org/10.1007/s11249-021-01549-0>.
- [53] Galas R, Omasta M, Shi L, Ding H, Wang W, jian, Krupka I, et al. The low adhesion problem: The effect of environmental conditions on adhesion in rolling-sliding contact. *Tribol Int* 2020;151:106521. <https://doi.org/10.1016/j.triboint.2020.106521>.
- [54] Arias-Cuevas O, Li Z, Lewis R, Gallardo-Hernández EA. Rolling-sliding laboratory tests of friction modifiers in dry and wet wheel-rail contacts. *Wear* 2010;268:543–51. <https://doi.org/10.1016/j.wear.2009.09.015>.
- [55] Pieringer A, Kropp W. Model-based estimation of rail roughness from axle box acceleration. *Appl Acoust* 2022;193:108760. <https://doi.org/10.1016/j.apacoust.2022.108760>.
- [56] Chen H, Namura A, Ishida M, Nakahara T. Influence of axle load on wheel/rail adhesion under wet conditions in consideration of running speed and surface roughness. *Wear* 2016;366–367:303–9. <https://doi.org/10.1016/j.wear.2016.05.012>.

- [57] Zhu Y, Chen X, Wang W, Yang H. A study on iron oxides and surface roughness in dry and wet wheel-rail contacts. *Wear* 2015;328–329:241–8. <https://doi.org/10.1016/j.wear.2015.02.025>.
- [58] Tyfour W.R., Beynon J.H., Kapoor A. The steady state wear behaviour of pearlitic rail steel under dry rolling-sliding contact conditions. vol. 180. 1995.
- [59] Harmon M, Santa JF, Jaramillo JA, Toro A, Beagles A, Lewis R. Evaluation of the coefficient of friction of rail in the field and laboratory using several devices. *Tribol Mater Surf Interfaces* 2020;14:119–29. <https://doi.org/10.1080/17515831.2020.1712111>.



Influence of sanding parameters on adhesion recovery in contaminated wheel–rail contact



Milan Omasta*, Martin Machatka, David Smejkal, Martin Hartl, Ivan Křupka

Faculty of Mechanical Engineering, Brno University of Technology, Czech Republic

ARTICLE INFO

Article history:

Received 11 June 2014

Received in revised form

18 November 2014

Accepted 19 November 2014

Available online 27 November 2014

Keywords:

Wheel/rail

Adhesion coefficient

Sand

Leaves

Rolling–sliding

Twin-disc

ABSTRACT

Adhesion in wheel/rail contact influences performance and safety of railway traffic. Low adhesion brings problems during braking and traction. Sanding is the most common way how to increase adhesion when the poor contact conditions due to a contamination occur. On the other hand, excessive sanding leads to higher wear of wheel and rail. To optimize the sanding process, description of the influence of sanding parameters on the adhesion in the contaminated contact is highly required.

In this work a new twin-disc machine in scale 1:3 was developed and addressed to the study of wheel/rail adhesion under different contact conditions. An influence of sanding parameters such as sand quantity, wheel slip and rolling speed was investigated using a real sanding system in the contact contaminated with water, leaves and wheel flange grease.

It has been shown that under wet, leaf or grease contamination, quantity of the sand applied during fixed time period has significant effect on adhesion recovery only for low wheel slip and low rolling speed. In the contaminated contact the effect of sanding on adhesion recovery increases with wheel slip and rolling speed.

© 2014 Elsevier B.V. All rights reserved.

1. Introduction

In comparison with other modes of transport particularly road and air, rail transport is among the most energy efficient and environment and social-friendly. To further improve the efficiency and performance a wheel–rail interface is the subject of interdisciplinary research efforts. The interaction between wheel and rail depends on vehicle–track dynamics, contact mechanics and tribology. These phenomena are related to cost, safety, maintenance, reliability, environment and energy consumption.

Tribology of the wheel and rail contact substantially determines performance and safety of railway traffic. The amount of energy transferred through the contact depends on adhesion level. When traction effort exceeds an adhesion limit a wheel slipping occurs, while a sliding arises when the adhesion is low during a braking. In the first case the low adhesion is responsible for delays in railway traffic and increased wear of wheel and rail when wheel is slipping. The low adhesion during braking causes extension in the braking distance which may result in crossing of platforms and which may bring safety risks in emergency cases.

Low adhesion is mainly caused by poor contact conditions due to the contact contamination. The most significant natural contaminants are humidity [1,2] and water [3–9]. Serious adhesion problems mainly during autumn months create leaves on the track [1,10–12]. Another common contaminant is oil or wheel flange grease [1,8] and natural layer called third body [13] made up of a mixture of dust, wear particles and other contaminant. Investigation of the behavior of such contaminants in the wheel–rail contact is essential for an understanding of low adhesion problems.

Various experimental methods and models have been used during last decades. Next to field measurements [14] laboratory experiments are of great importance in the research in tribology of the wheel–rail contact. The most accurate experimental model uses a full-scale wheel–rail test rig [15] with real geometry and kinematics. The wheel on rail model has been also applied in a reduced scale [13,16]. A rail is often replaced by a disc in full-scale test rigs [15,18]. The most widely used is a twin-disc approach at different scales. A small scale allows cutting specimens from real rail and wheel [2,4,5,7,8,11,19]. To incorporate a real dynamic of contact, testing with scaled boogie and wheel set has also been carried out [6,20–22]. Recently a new twin-disc test method with continuously variable creep was developed which allows measuring a creep curve in a single run [23]. In this way the creep curve parameters can be determined from large amount of data. This work has been focused on low levels of creep. For simulation of a

* Corresponding author. Tel.: +420 541143238.

E-mail address: omasta@fme.vutbr.cz (M. Omasta).

wheel–rail contact a Mini-Traction-Machine in ball-on-disc configuration has also been used [10,24]. Another approach assumes a pure sliding condition in pin-on-disc [1,25,26] and ball-on-disc [27] configuration.

Sanding is a classic and the most important method how to increase adhesion in contaminated wheel–rail contact. On the other hand, sanding is connected with higher wear of wheel and rail. An effect of sanding on adhesion recovery has been studied by several authors [11,19,28–31]. The effect of sanding is influenced by various sanding parameters which are mainly particle size of sand [28–30], sanding rate [28,29] and wheel slip [28–30].

It has been also stated that sand may act as a solid lubricant within the meaning of a reduction of adhesion under dry conditions [28,31]. Moreover, excessive sanding may cause an electric insulation between train and rails [28,31,32] which may negatively affect functionality of a railway track circuits that are used for detection of trains. Using electric voltage measurements partial and full lubrication regimes during sanding under dry conditions were identified [28]. Above the certain sanding rate no direct metal to metal contact occur which indicates formation of a coating of crushed and compacted sand in the contact. As the feed rate increases the adhesion coefficient during sanding decreases; nevertheless the coefficient is recovered to the same level at some time after the sanding. Sanding causes severe wear of wheel and rail. It was shown that sanding increases wear by factors between 2 and 10 [19]. The wear was higher under wet conditions because of higher entraining capacity of wet discs [19].

Besides sanding, friction modifiers or solid particles are used to increase adhesion in contaminated contact [7,12,33] and to control lateral forces and specific wear regimes such as short pitch corrugation [34–36]. Moreover, hydrophobic products as a combatant for low adhesion were tested [37].

Low adhesion is a serious problem in railway traffic and sanding is still the most important method how to overcome the issues connected with poor contact conditions. On the other hand,

sanding is connected with higher wear and may bring other problems when an excessive amount of sand is used. So the information about proper sanding parameters for various contact conditions is highly required for optimization of the sanding process.

Sanding rate is one of the most important parameter. Although a number of studies that deals with the effect of sanding have been published, only several of them are focused on the effect of sanding parameters. Especially an effect of sanding rate under different contact conditions has been insufficiently described yet.

The present paper is focused on the experimental study of the sanding process in simulated wheel–rail contact. The main aim of this paper is to investigate the effect of sanding rate on adhesion recovery in contaminated wheel/rail contact under various contact conditions. Common contaminants like water, grease and leaves have been used. For the purposes of this study a new twin-disc machine has been developed.

2. Material and methods

2.1. Test apparatus

A scheme of the new twin-disc machine is shown in Fig. 1 and its photographs are shown in Fig. 2. The experimental machine consists of main frame and secondary frame for the drive system. Major components include two discs of the same diameter situated in a contamination chamber, which enables application of contaminants and provides protection from pollution. Each of these discs is independently driven by 15 kW AC motor with gearbox. Torque from drive in secondary frame is transmitted using a drive shaft. Frequency converters together with control software are used to set up various rolling speed and slip. The slip in the contact is achieved by different rotational speed of the discs and is calculated

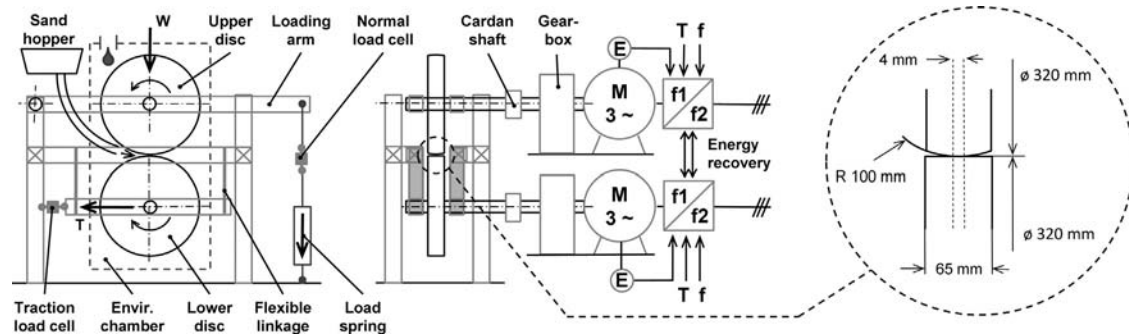


Fig. 1. Schematic representation of twin-disc machine.



Fig. 2. Photographs of twin-disc machine with detailed views on sanding application.

using the following equation:

$$s = \frac{W_{wheel} \cdot r_{wheel} - W_{rail} \cdot r_{rail}}{W_{wheel} \cdot r_{wheel} + W_{rail} \cdot r_{rail}} \cdot 200 \quad (1)$$

where w_{wheel} and w_{rail} are rotational speeds of discs and r_{wheel} and r_{rail} are radii of the discs.

Normal load is applied to upper disc using a spring–screw loading system and a loading arm. Quick loading and unloading of the contact are allowed by an AC motor-driven screw jack. Lower disc is mounted on a separate frame which is fixed to the main frame using a flexible linkage which allows horizontal displacement. Load cells are used to measure normal force W produced by the loading arm and traction force T generated by friction in the contact. The data are collected and adhesion coefficient is calculated according to the following equation:

$$\mu = \frac{T}{W} \quad (2)$$

The measuring system was calibrated so that positive and negative slip provides the same magnitude of the adhesion coefficient.

2.2. Specimens

The wheel and rail disc specimens have a diameter of 320 mm which corresponds to scale 1:3 with respect to real wheel diameter. The wheel disc is cylindrical whereas the rail disc is rounded with radius of 100 mm which corresponds to UIC 60 rail profile according to the same scale, as shown in Fig. 1. So, initial contact patch is elliptical. Width of the discs is 50 mm. Both discs were made from C45 steel that have similar chemical composition as UIC 900A and R7T rail and wheel steels. Because of the large scale it was impossible to cut-off specimens directly from wheel and rail. Different hardness of the discs was achieved according to real wheel and rail, as stated in Table 1. Before each experiment the discs were grounded to initial roughness Ra 0.8 μm ; however, it should be noted that wear processes influenced roughness of the surfaces very early after the beginning of experiments.

Table 1
Material specifications of the specimens.

	Chemical composition (wt%)					Hardness (HB)
	C	Si	Mn	Ni	Cr	
Rail disc	0.46	0.25	0.65	0.30	0.25	290
Wheel disc	0.46	0.25	0.65	0.30	0.25	245
UIC 900A	0.70	0.35	1.10	–	–	280–300
R7T	0.52	0.40	0.80	0.30	0.30	245

2.3. Experimental conditions

Most experiments were performed under normal load of 3.2 kN which corresponds to the theoretical Hertzian pressure of 1 GPa which is the current limit of the test rig. Rolling speed was in range from 0.8 to 3 m/s and wheel slip was in range from 1% to 10% which represents typical values occurring during traction. All tests were carried out under ambient temperature of 23 °C and humidity of 35–40%.

During the experiments the contact was contaminated with water, grease and leaves. Water was applied on the upper rail disc using nozzle with adjustable flow rate. Application of the water was in the form of drops (approximately 10 ml/min) or weak stream (68 and 90 ml/min) representing wet and rainy conditions respectively. In case of lubricated conditions, wheel flange grease with rapeseed oil and graphite was used. Application was carried out by pipette around the rail disc in total quantity of 90 μl to simulate reasonable degree of contamination which could occur in the real wheel/rail contact.

Other contaminant was leaves that occur on a track during a leaf fall. Mix of the fallen leaves including maple, beech, oak and birch was collected near railway network in autumn. Partly dead leaves had typical brown–yellow color with some green spots. Collected dry leaves were then chopped into small pieces (approximately 5 mm) and soaked in water for 5 days. In the next step, excess water was separated so both the leaf extract and the leaf mixture with tiny pieces of leaves were obtained (see Fig. 3). Finally, both the components were frozen to avoid spoilage. Before each testing the sample was defrosted. In most experiments leaf mixture was applied manually to circumference of both discs (approximately 25 g) prior to testing. The mixture was not completely dry, so it easily kept on a disk surface.

For better understanding of poor adhesion caused by leaves, tests with leaf extract were carried out too, with advantage of more stable testing conditions. The extract was applied by syringe on upper disc in rate of about 15 ml/min during testing.

For sanding a commercial railway sand with silica content above 95% was used. Particle size distribution of this sand is in range 0.3–1.6 mm with mean value of 0.8 mm and moisture content up to 8%. For the sand application a real on-board sanding system was used. Sand was applied to the contact by hose using a compressed air (see Fig. 2). The system was adjusted so that the amount of sand which goes through the contact corresponds to real situation with respect to scaled contact area. In tests various sand quantities in range 3–15 g was used with fixed application period of 1.5 s to simulate different sanding rates. This time was found to be sufficient for evaluation of adhesion recovery. The sand quantity is defined as that which goes through the contact area defined by discs width. The amount applied by hose was approximately 25% higher due to the partial reflection of sand particles from the surfaces.



Fig. 3. Leaves and leaf extract preparation.

2.4. Experimental procedure

Two different types of tests were conducted in this study. In the first one, the adhesion curves for different contact conditions and contaminants were determined. New set of disc was used for each type of contamination. At the beginning of the test the discs were run in with contaminant under given slip until the stabilization of the adhesion coefficient was achieved. After that, the slip was varied automatically and the adhesion coefficient was recorded during a short period of time, as shown in Fig. 4. Some noise in adhesion is caused by wear processes in the point contact. The highest adhesion peaks are connected with step change in the slip. From the data the adhesion curve was then evaluated.

The second type tests were addressed to determination of the effect of sanding rate on adhesion recovery under contaminated conditions. At the beginning, adhesion coefficient had been stabilized like in the first case. Then an amount of sand was applied and coefficient of adhesion was recorded. Similar time-test procedure has been used by several authors [7,11,12,28,29]. From the values of adhesion coefficient before and after the sand application an adhesion recovery capacity was evaluated. This procedure is illustrated in Fig. 5 for the contact contaminated with leaf extract.

3. Results and discussion

3.1. Adhesion curves

3.1.1. Dry conditions

In order to assess the validity of twin-disc results, adhesion curves under basic conditions were determined and compared with other studies. Graph in Fig. 6 shows adhesion curves for different speed under dry conditions. Maximum adhesion varies from 0.45 to 0.6 which corresponds to commonly reported values obtained using twin-disc machine in laboratory conditions [6,11,17]. Data also show a reduction of adhesion with speed even under the dry conditions. However, there is no significant local

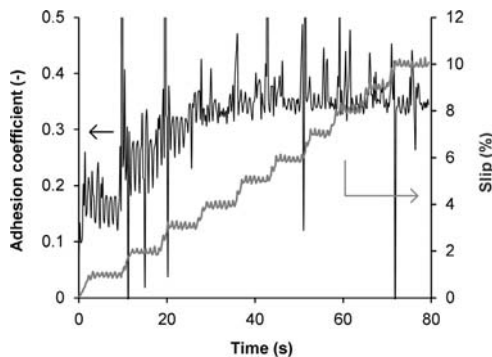


Fig. 4. Adhesion curve assessment using variable slip.

maximum in adhesion in the slip range. It is believed that a reduced adhesion after the saturation is due to a temperature rise in the contact. So the missing adhesion maximum can be attributed to the low speed and slip range and low normal load for point contact in the experiments. It was also found that the contact pressure has only a very low effect on adhesion in pressure range of 0.8 to 1.2 GPa. Weak effect of pressure on adhesion was reported in Refs. [6,17].

3.1.2. Wet conditions

When water is present in the contact a lower adhesion arises, as shown in Fig. 7. In this case a local maximum can be identified between 1% and 3% slip. Well-known effect of speed on adhesion due to hydrodynamic action is also evident even for the small range of speed.

3.2. Effect of contact contamination

3.2.1. Wet conditions

The effect of water contamination was partially described using the adhesion curves in previous section. Water leads to reduction in adhesion; however this reduction is not as high as reported by other authors [3,4,6,9]. For higher flow rate of 68 ml/min adhesion coefficient is around value of 0.3 and for low flow rate of 10 ml/min adhesion coefficient is reduced to 0.4. This weak effect of water contamination can be attributed to low amount of water, low speed and surface preparation procedure avoiding the presence of other contaminants. The latter reason is important mainly when comparing the data with field tests results. In real railway traffic no contaminant acts separately and rather a mixture of various contaminants influences tribology of wheel/rail contact. The effect of water on adhesion reduction is much more significant in combination with leaves, dust etc.

3.2.2. Leaf contamination

Effect of leaf contamination on adhesion is illustrated in Fig. 8. When a small amount of leaf mixture was applied to the contact an immediate drop of adhesion occurred. After the application the

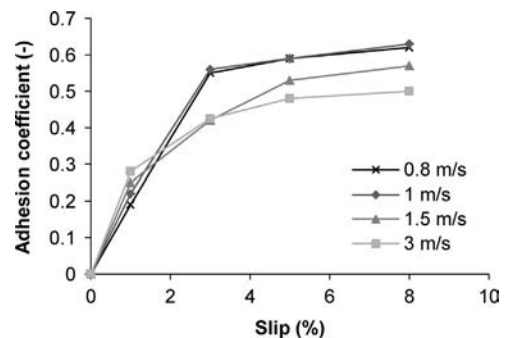


Fig. 6. Adhesion curves under dry conditions.

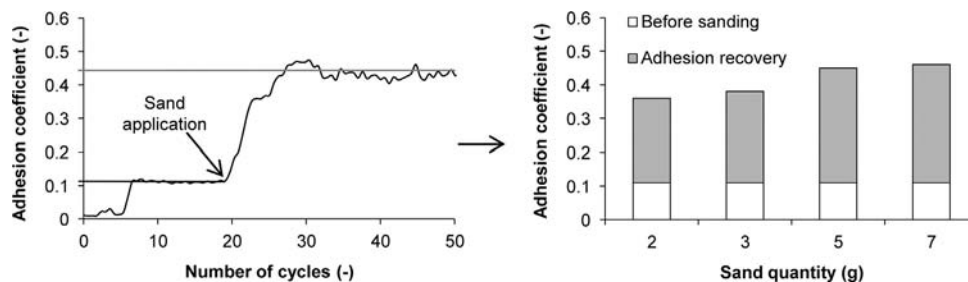


Fig. 5. Determination of adhesion recovery capacity – leaf extract (3% slip; 3 m/s).

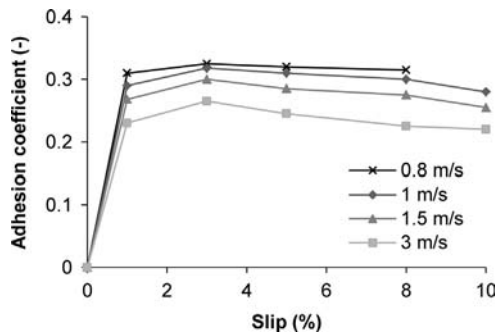


Fig. 7. Adhesion curves under wet conditions (water flow rate 90 ml/min).

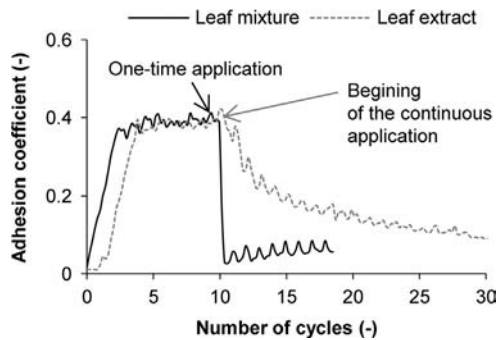


Fig. 8. Time-test with application of leaf mixture and leaf extract (1 m/s; 3% slip).

adhesion shows a slight increase accompanied by some fluctuations due to the irregular formation of leaf layer around the circumference of the discs. On the other hand, the application of leaf extract does not cause immediate drop of adhesion. The difference in adhesion reduction in Fig. 8 is due to the different application methods. The leaf mixture was applied one time; however the leaf extract was sprayed over a longer time with low rate. Nevertheless the lowest adhesion level is similar. It is believed that the component responsible for low friction is the same in the two cases: water-soluble leaf components, mainly pectin [10].

In this study no tests with dry leaves are presented because dry leaves cause large pressure fluctuations when passing through the contact which leads to severe wear of discs.

3.2.3. Grease contamination

Single application of small amount of grease causes immediate drop of adhesion to value of approximately 0.1. After some time the adhesion coefficient increases and the adhesion is finally almost completely restored. We can conclude that the lubricant layer which is created on discs can be quite easily removed even without sanding. From this point of view lubricating oil or grease does not present a serious problem when its amount is low. Moreover, in real contact oil and grease can absorb wear debris, dust and other contaminants which may also increase or decrease adhesion coefficient.

3.3. Effect of sanding

3.3.1. Wet conditions

Influence of sanding on adhesion under wet conditions is illustrated in Fig. 9. It can be seen that sand causes initial reduction in adhesion. This effect was apparent particularly for low water flow rate. Similar reduction caused by solid lubrication was observed earlier during sanding of dry contact [28]. In this case, crushed sand creates low-shear-strength solid layer which prevent

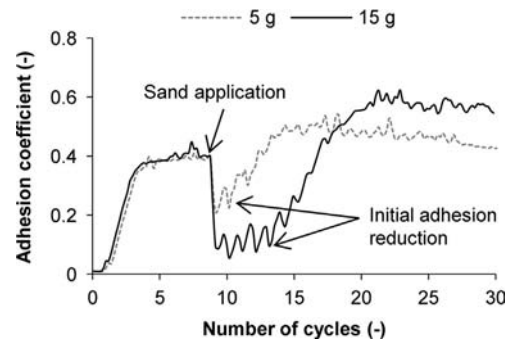


Fig. 9. Time-test with sanding at different sand quantity under wet conditions (1 m/s; 3% slip; water flow rate 11 ml/min).

direct steel-to-steel contact. After this reduction when the layer is broken, adhesion coefficient increases rapidly. Higher sanding rate brings greater and longer initial adhesion reduction but also higher adhesion coefficient after adhesion recovery.

Influence of sanding parameters on adhesion recovery under water contamination was investigated in more detail for higher water flow rate, as shown in graphs in Fig. 10. The results indicate that larger sand quantity brings higher level of adhesion; however, this tendency is not too strong particularly over quantity of 7 g. Much significant is the effect of wheel slip. The slip improves efficiency of sanding significantly mainly between 1% and 5% slip. Two graphs in Fig. 10 differ by rolling speed. Although initial adhesion is lower at higher speed, adhesion coefficient after sanding increases with increasing speed. As can be seen for speed of 3 m/s sanding under wet conditions is able to increase adhesion above the level which appears under dry conditions. This effect was observed mainly at higher speeds when the adhesion under dry conditions is relatively low. This is consistent with findings in Refs. [19,31], although the results were achieved under different conditions.

The effect of sanding on surface damage of wheel disc after approximately 300 cycles is shown in Fig. 11. Surface pits because of the sand indentations are visible on the surface around the contact path. Also abrasive score marks are evident indicating that three-body abrasive wear occurred. In the contact path defined by the Hertzian contact width the wear is much severe. Surface cracks and voids and severe plastic flow of material can be identified. This type of wear can be described by various mechanisms. Subsurface cracks and associated delamination are typical for the fatigue wear process; however, it is unlikely because of the low number of cycles. Likewise, ratcheting wear caused by plastic strain accumulation is not likely. Much more probably the fracture process is related to adhesion that is produced by the formation and shearing of welded junctions between the surfaces due to high flash temperature and pressure. It should be noted that the similar wear occurs also in dry contact without sanding. Moreover, a presence of third body between contacting surfaces should reduce the tendency for adhesion to occur. So that the severe wear in contact path may not be directly connected with sanding. No significant difference between the wear of rail and wheel disc was observed.

3.3.2. Leaf contamination

Fig. 12 shows the typical time-test results with sanding in the contact contaminated with leaf mixture. Corresponding disc surface before the test, after running-in and after sanding, is shown in Fig. 13. It can be seen that during run in a very thin layer is formed on the discs. Sanding causes immediate increase in adhesion; however, after few disc revolutions adhesion decreases gradually

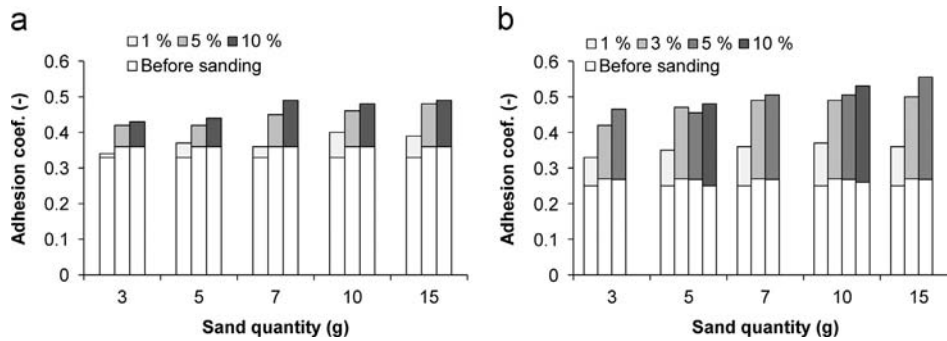


Fig. 10. Adhesion recovery under various slip and sand quantity under wet conditions (water flow rate 68 ml/min; (a) 1 m/s; (b) 3 m/s).



Fig. 11. Photographs of wheel disc surface after 300 cycles when sanding under wet conditions.

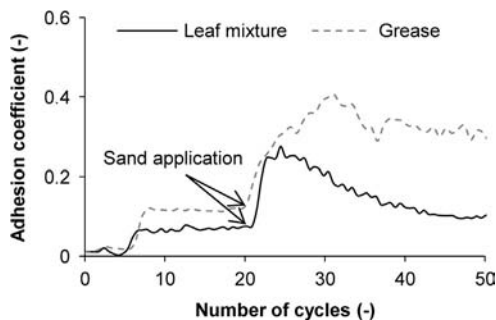


Fig. 12. Time-test with sanding in the contact contaminated with leaf mixture and grease (1 m/s; 3% slip).

to adhesion level close to initial adhesion under leaf contamination. So the quantity of sand is able to increase adhesion when the sand goes through the contact; however, it is insufficient to remove leaf layer from discs.

On the other hand, if the leaf extract is used as a contaminant, adhesion recovery is much stable, as shown in Fig. 5. The difference should be in a mechanism of adhesion recovery. In the case of the leaf extract, sand particles break lubrication layer easily and provide interaction with metal surfaces. However, the leaf mixture creates thick hardly-removal layer. Sand particles can break the layer only locally and the adhesion coefficient starts to fall soon after the sanding as shown in Fig. 12. For complete adhesion recovery the sand has to remove the layer by abrasion.

Bar graphs in Fig. 14 show dependence of adhesion on sanding parameters under leaf contamination. Compared to wet conditions, sanding rate has only a limited effect on adhesion. Much important seems to be wheel slip and rolling speed. In fact, both the parameters influence sliding speed that is responsible for the removal of leaf layer on discs. When the slip and the speed are large enough, sufficient adhesion coefficient of 0.2 can be achieved. Nevertheless, in this case a sanding time period seems to be much important sanding parameter. These results confirm serious problems associated with the occurrence of leaves on the track.

3.3.3. Grease contamination

Dashed line in graph in Fig. 12 describes effect of sanding in contact contaminated with grease. Compared to leaf contamination, initial adhesion coefficient is higher and increase in adhesion after sand application is much more gradual. Much more important is fact that the adhesion coefficient does not decrease significantly afterwards. Bar graphs for a specific wheel slip are shown in Fig. 15. It is evident that effect of sand quantity is significant under low rolling speed. When the speed is sufficient coefficient of adhesion of approximately 0.35 is achieved and higher sand quantity has only a limited effect on adhesion.

4. Conclusions

In this work a new twin disc machine was developed and addressed to study of wheel/rail adhesion under different contact conditions. Particularly an influence of sanding parameters such as wheel slip, rolling speed and sand quantity was investigated using a real sanding system. Effect of sand quantity in contaminated contact has not been described yet. The main conclusions of this study are as follows:

1. Under dry and slightly wet conditions sanding causes immediate drop in adhesion. The adhesion reduction and its duration increase with sanding rate.
2. Despite the fact that adhesion coefficient decreases with rolling speed under wet conditions, adhesion recovery increases with speed during sanding under the conditions. Moreover, a higher adhesion coefficient compared to dry conditions can be achieved.
3. Under wet, leaf or grease contamination, quantity of sand applied during fixed time period has significant effect on adhesion recovery only for low wheel slip and low rolling speed. In contaminated contact the effect of sanding on adhesion recovery increases with wheel slip and rolling speed.
4. Wet leaves in contact cause the lowest adhesion coefficient of approximately 0.05. Adhesion can be temporarily improved when sand passes through the contact; however, then the adhesion decreases again due to hard-to-remove layer formed by leaves on discs surfaces.



Fig. 13. Photographs of disc surface during test with leaf mixture (a) before the test; (b) after run in; (c) after sanding.

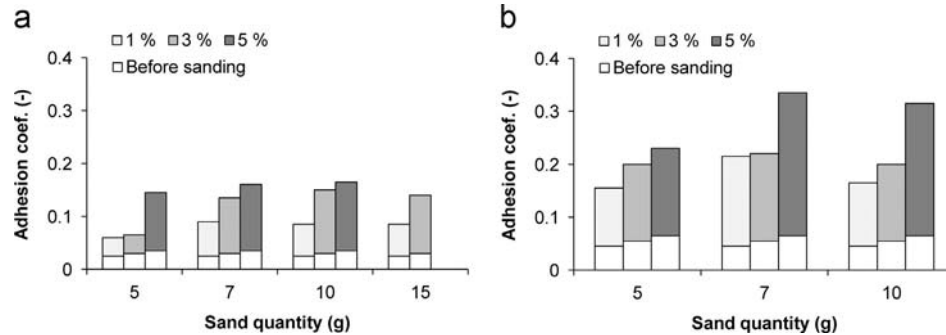


Fig. 14. Adhesion recovery under various slip and sand quantity in the contact contaminated with leaves (a) 1 m/s; (b) 3 m/s.

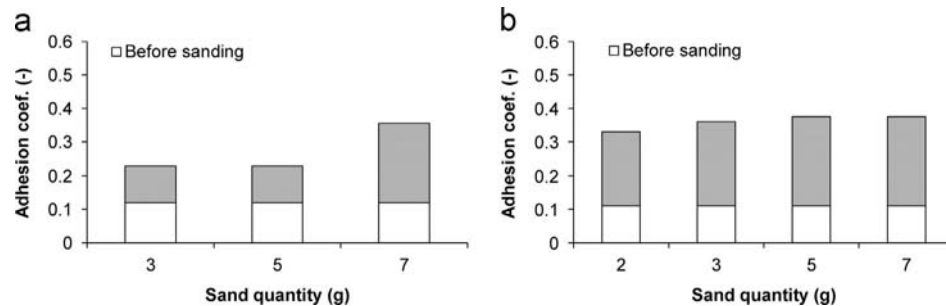


Fig. 15. Adhesion recovery in the contact contaminated with grease (a) 1 m/s; (b) 3 m/s (3% slip).

Acknowledgments

This research was carried out under the project NETME CENTRE PLUS (LO1202) with financial support from the Ministry of Education, Youth and Sports under the National Sustainability Programme I.

References

- [1] U. Olofsson, K. Sundvall, Influence of leaf, humidity and applied lubrication on friction in the wheel–rail contact: pin-on-disc experiments, *Proc. Inst. Mech. Eng., Part F: J. Rail Rapid Transit* 218 (2004) 235–242.
- [2] K.-S. Baek, K. Kyogoku, T. Nakahara, An experimental study of transient traction characteristics between rail and wheel under low slip and low speed conditions, *Wear* 265 (2008) 1417–1424.
- [3] H. Chen, T. Ban, M. Ishida, T. Nakahara, Adhesion between rail/wheel under water lubricated contact, *Wear* 253 (2002) 75–81.
- [4] H. Chen, T. Ban, M. Ishida, T. Nakahara, Experimental investigation of influential factors on adhesion between wheel and rail under wet conditions, *Wear* 265 (2008) 1504–1511.
- [5] H. Chen, M. Ishida, A. Namura, K.-S. Baek, T. Nakahara, B. Leban, M. Pau, Estimation of wheel/rail adhesion coefficient under wet condition with measured boundary friction coefficient and real contact area, *Wear* 271 (2011) 32–39.
- [6] W.J. Wang, P. Shen, J.H. Song, J. Guo, Q.Y. Liu, X.S. Jin, Experimental study on adhesion behavior of wheel/rail under dry and water conditions, *Wear* 271 (2011) 2699–2705.
- [7] O. Arias-Cuevas, Z. Li, R. Lewis, E.A. Gallardo-Hernández, Rolling–sliding laboratory tests of friction modifiers in dry and wet wheel–rail contacts, *Wear* 268 (2010) 543–551.
- [8] C. Hardwick, R. Lewis, D.T. Eadie, Wheel and rail wear—understanding the effects of water and grease, *Wear* 314 (2014) 198–204.
- [9] B. Wu, Z. Wen, H. Wang, X. Jin, Numerical analysis on wheel/rail adhesion under mixed contamination of oil and water with surface roughness, *Wear* 314 (2014) 140–147.
- [10] P.M. Cann, The “leaves on the line” problem—a study of leaf residue film formation and lubricity under laboratory test conditions, *Tribol. Lett.* 24 (2006) 151–158.
- [11] E.A. Gallardo-Hernandez, R. Lewis, Twin disc assessment of wheel/rail adhesion, *Wear* 265 (2008) 1309–1316.
- [12] Z. Li, O. Arias-Cuevas, R. Lewis, E.A. Gallardo-Hernández, Rolling–sliding laboratory tests of friction modifiers in leaf contaminated wheel–rail contacts, *Tribol. Lett.* 33 (2009) 97–109.
- [13] E. Niccolini, Y. Berthier, Wheel–rail adhesion: laboratory study of “natural” third body role on locomotives wheels and rails, *Wear* 258 (2005) 1172–1178.
- [14] B.R. Meyer, High-Adhesion Locomotives With Controlled Creep, *ImechE* (1987) 209–218.
- [15] D.T. Eadie, D. Elvidge, K. Oldknow, R. Stock, P. Pointner, J. Kalousek, P. Klauser, The effects of top of rail friction modifier on wear and rolling contact fatigue: full-scale rail–wheel test rig evaluation, analysis and modelling, *Wear* 265 (2008) 1222–1230.
- [16] S. Descartes, A. Saulot, C. Godeau, et al., Wheel flange/rail gauge corner contact lubrication: tribological investigations, *Wear* 271 (2011) 54–61.
- [17] W. Zhang, J. Chen, X. Wu, X. Jin, Wheel/rail adhesion and analysis by using full scale roller rig, *Wear* 253 (2002) 82–88.

- [18] A. Saulot, S. Descartes, Y. Berthier, Sharp curved track corrugation: from corrugation observed on-site, to corrugation reproduced on simulators, *Tribol. Int.* 42 (2009) 1691–1705.
- [19] R. Lewis, R.S. Dwyer-Joyce, Wear at the wheel/rail interface when sanding is used to increase adhesion, *Proc. Inst. Mech. Eng., Part F: J. Rail Rapid Transit* 220 (2006) 29–41.
- [20] A. Matsumoto, Y. Sato, H. Ono, M. Tanimoto, Y. Oka, E. Miyauchi, Formation mechanism and countermeasures of rail corrugation on curved track, *Wear* 253 (2002) 178–184.
- [21] W.J. Wang, H.F. Zhang, H.Y. Wang, Q.Y. Liu, M.H. Zhu, Study on the adhesion behavior of wheel/rail under oil, water and sanding conditions, *Wear* 271 (2011) 2693–2698.
- [22] W.J. Wang, H. Wang, H.Y. Wang, J. Guo, Q.Y. Liu, M.H. Zhu, X.S. Jin, Sub-scale simulation and measurement of railroad wheel/rail adhesion under dry and wet conditions, *Wear* 302 (2013) 1461–1467.
- [23] D.I. Fletcher, S. Lewis, Creep curve measurement to support wear and adhesion modelling, using a continuously variable creep twin disc machine, *Wear* 298–299 (2013) 57–65.
- [24] Y. Zhu, U. Olofsson, K. Persson, Investigation of factors influencing wheel–rail adhesion using a mini-traction machine, *Wear* 292–293 (2012) 218–231.
- [25] J. Sundh, U. Olofsson, K. Sundvall, Seizure and wear rate testing of wheel–rail contacts under lubricated conditions using pin-on-disc methodology, *Wear* 265 (2008) 1425–1430.
- [26] S. Abbasi, U. Olofsson, Y. Zhu, U. Sellgren, Pin-on-disc study of the effects of railway friction modifiers on airborne wear particles from wheel–rail contacts, *Tribol. Int.* 60 (2013) 136–139.
- [27] J. Sundh, U. Olofsson, Seizure mechanisms of wheel–rail contacts under lubricated conditions using a transient ball-on-disc test method, *Tribol. Int.* 41 (2008) 867–874.
- [28] O. Arias-Cuevas, Z. Li, R. Lewis, Investigating the lubricity and electrical insulation caused by sanding in dry wheel–rail contacts, *Tribol. Lett.* 37 (2010) 623–635.
- [29] O. Arias-Cuevas, Z. Li, R. Lewis, E.A. Gallardo-Hernández, Laboratory investigation of some sanding parameters to improve the adhesion in leaf-contaminated wheel–rail contacts, *Proc. Inst. Mech. Eng., Part F: J. Rail Rapid Transit* 224 (2010) 139–157.
- [30] O. Arias-Cuevas, Z. Li, R. Lewis, A laboratory investigation on the influence of the particle size and slip during sanding on the adhesion and wear in the wheel–rail contact, *Wear* 271 (2011) 14–24.
- [31] R. Lewis, R.S. Dwyer-Joyce, J. Lewis, Disc machine study of contact isolation during railway track sanding, *Proc. Inst. Mech. Eng., Part F: J. Rail Rapid Transit* 217 (2003) 11–24.
- [32] R. Lewis, J. Masing, Static wheel/rail contact isolation due to track contamination, *Proc. Inst. Mech. Eng., Part F: J. Rail Rapid Transit* 220 (2006) 43–53.
- [33] W.J. Wang, T.F. Liu, H.Y. Wang, Q.Y. Liu, M.H. Zhu, X.S. Jin, Influence of friction modifiers on improving adhesion and surface damage of wheel/rail under low adhesion conditions, *Tribol. Int.* 75 (2014) 16–23.
- [34] D.T. Eadie, J. Kalousek, K.C. Chiddick, The role of high positive friction (HPF) modifier in the control of short pitch corrugations and related phenomena, *Wear* 253 (2002) 185–192.
- [35] M. Tomeoka, N. Kabe, M. Tanimoto, E. Miyauchi, M. Nakata, Friction control between wheel and rail by means of on-board lubrication, *Wear* 253 (2002) 124–129.
- [36] Y. Suda, T. Iwasa, H. Komine, M. Tomeoka, H. Nakazawa, K. Matsumoto, T. Nakai, M. Tanimoto, Y. Kishimoto, Development of onboard friction control, *Wear* 258 (2005) 1109–1114.
- [37] S.R. Lewis, R. Lewis, P. Richards, L.E. Buckley-Johnstone, Investigation of the isolation and frictional properties of hydrophobic products on the rail head, when used to combat low adhesion, *Wear* 314 (2014) 213–219.

Development of an adaptive top-of-rail friction modification system

M. Omasta, R. Galas, J. Knappek, M. Hartl and I. Krupka
Faculty of Mechanical Engineering, Brno University of Technology, Czech Republic

ABSTRACT

This work describes a development of a control system for top-of-rail friction modification based on on-board application. This adaptive system is used to evaluate an appropriate application amount and interval according to a position on the track using a GPS data. The parameters take into account actual operating and weather conditions.

The main part of the work presents an experimental approach to determine an appropriate TOR FM amount and application intervals depending on operating conditions. Laboratory scale test rigs are used in this study.

1 INTRODUCTION

Friction modifiers (FM) began to be utilized to managing friction in contact between wheel tread and top of rail (TOR). Generally the TOR FMs are used to optimize forces in wheel/rail interface and reduce noise and rail head corrugation. Wide range of friction modifiers and application strategies are available to provide corresponding benefits.

During last decade significant development of TOR-FM technology has been done. Several field studies have supported merits resulting from TOR FM application. Most of them dealt with way side application of water-based FM in critical curves of track. In North America and Australia these studies are aimed at improving fuel efficiency in heavy haul networks (1), (2), (3). TOR FM application was tested in metro and tram systems in Europe (4), (5) and in other systems (6). On-board systems with water-based FM were applied in subway lines (7), (8).

Nowadays, the TOR concept begins to gain sufficient support from rail network owners and train operators. On-board applications are still more frequent, mainly in mainland Europe and in connection with oil-based FMs. This type of application provides some benefits mainly related to cost and safety aspects associated with maintenance and refilling.

The aim of this paper is to propose a methodology for a development of on-board TOR-FM system with an adaptive control of FM application. The system is designed primarily for tram networks and for the use of standard oil-based FMs. The question of how much and when to apply the modifier are crucial for an adequate system function.

2 APPLICATION SYSTEM

On-board TOR-FM application offers three possibilities: FM is totally consumed by the vehicle carrying an application system (eg. (1)), FM is applied for the following vehicle(s) (mainly with water-based FM; eg. (7), (8)) or both, carrying and following vehicles take merit of applied FM. The two last mentioned are usually preferred by operators as it requires lower investments. On the other hand this system cannot be fully adaptive as it can hardly predict actual operating conditions of the following vehicles, especially when different types of vehicles are operated on the same track. So the proposed system assumes that applied FM is consumed just by a carrying vehicle.

In the intended tram network the primary purpose of TOR FM application is to mitigate annoying wheel squeal and to improve steering forces in curves. An appropriate amount of FM is essential. Insufficient application does not lead to the desired noise reduction; on the other hand, excess application may increase braking distance and cause other safety issues especially when tram track runs directly along public streets with automobile traffic.

The system is based on use of GNSS and map data which together provide information on position of the car on the track and track parameters (eg. curvature, direction and length of curve). Fluid oil-based FM is sprayed at individual doses on the TOR with nozzle by compressed air. Key questions for a control system are When, How much and How often to apply FM? The first question is covered by track sections for FM application defined in map data. These sections can be determined automatically by a threshold of track curvature or manually based on specific application requirements. Also some restrictions for application in braking sections and those with high demand on traction are possible.

The other two questions relate to the behavior of FM in wheel-rail contact. Laboratory investigations indicate that after application of a small amount of FM, coefficient of adhesion (CoA) immediately drops to a certain level and then increases during a time. The low level depends mainly on applied amount of FM; the following increase is given by behavior of created friction layer. Water-based FMs usually provide a stabilization of CoA for some time; while oil-based FMs rather lead to a continuous rise back to dry conditions (9), (10) as shown in Fig. 1 (9).

Reapplication interval corresponds to time period during which CoA will reach a specific value. If we assume a linear increase in adhesion over time for oil-based FMs, then the period can be estimated considering the rate of increase of CoA. This rate strongly depends on FM amount and operating conditions. In order to determine these influences laboratory experimental investigation was made.

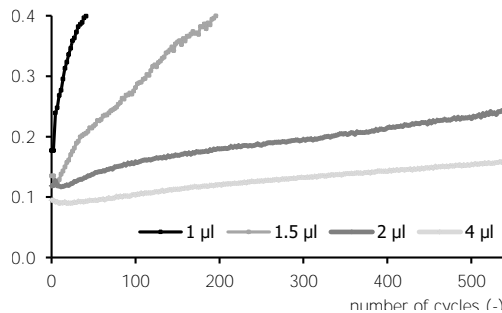


Fig. 1 Effect of oil-based FM amount (Slip 8 %; Speed 1 m/s; Pressure 0.8 GPa).

3 MATERIAL AND METHODS

3.1 Experimental test rig

The twin-disc machine was used to simulate wheel-rail contact, see Fig. 2. The major parts of device are the main frame and the frame for drive system. The main frame includes a pair of discs with the same diameter. The upper disc is mounted on the loading arm. The required contact force is achieved by the spring-screw loading system.

This loading system, as well as a load cell for normal force, is placed at the end of the loading arm. The lower disc is mounted on the separate frame which is hinged on the main frame using flexible linkages allowing horizontal displacement. This enables to transfer a traction force from the contact to a load cell for friction force. Data from these two load cells are used to evaluation of the coefficient of adhesion (CoA) according to the following equation:

$$CoA = \frac{T}{W} \quad (1)$$

where T is friction force and W is a normal load in the contact. Both discs are cylindrical with radius of 80 mm and width of 8 mm, which results in line contact. This configuration was chosen because compared to point-contact the wear process does not influence real contact pressure for a given load. Discs are placed in chamber which enables to carry out experiments under various environmental conditions (contaminants, temperature, etc.). Both discs are independently driven with variable-speed and thus the slip ratio between the discs can be accurately controlled according to Eq. (2) where W_{wheel} and W_{rail} are rotational speeds of discs and r_{wheel} and r_{rail} are diameters of discs.

$$Slip = \frac{W_{wheel} \cdot r_{wheel} - W_{rail} \cdot r_{rail}}{W_{wheel} \cdot r_{wheel} + W_{rail} \cdot r_{rail}} \cdot 200 \quad (2)$$

All tests presented in this study were made under the conditions listed in Tab. 1.

3.2 Materials

Both discs were made from the C45 steel whose chemical composition is similar to commonly used rail steel UIC 900A and wheel steel R7T. In addition, hardness of both discs was chosen according to the real wheel and rail hardness. In the case of rail disc hardness was 280-300 HB while hardness of wheel disc was 245 HB. The initial average roughness of both discs was **Ra 0.45 μm**.

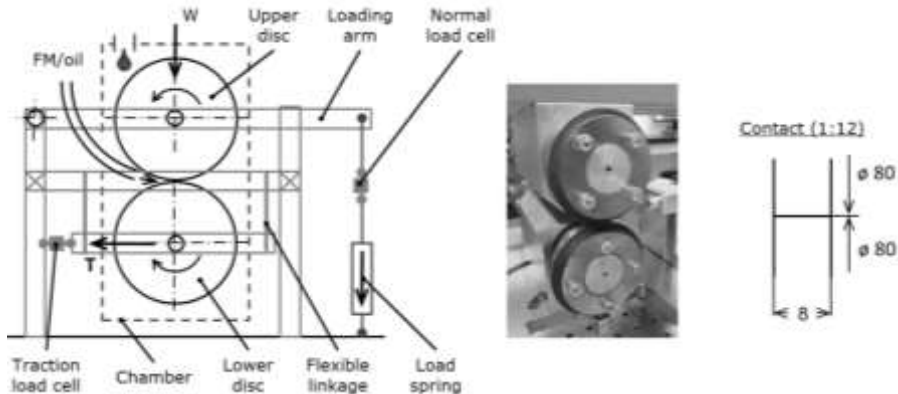


Fig. 2 Scheme of twin-disc machine and contact configuration.

Table 1 Test conditions

Rolling speed	(m/s)	{ 0.5, 1, 1.5 }
Slip ratio (longitudinal)	(%)	{ 1, 3, 5, 8 }
Hertzian pressure	(GPa)	0.8
FM amount	(μl)	{ 0.5, 1, 2, 3, 4, 5, 6, 7, 10, 15 }

In this study, three types of commercial oil-based FMs with solid metal particles identified as FMA, FMB and FMC were used. These FMs especially contain flakes of Al, Cu and Zn where the length of flakes is in the range of 4-10 μm . The detail description and information about size distribution of metal particles is reported in (9).

4 RESULTS

4.1 CoA after FM application

Fig. 3 shows typical evolution of CoA after application of oil-based FM and corresponding photographs of disc surface. Before the application run-in is done which leads to a dry level of adhesion of app. 0.62. This level corresponds well with those measured in laboratory conditions but is higher than field results (11). After the application, coherent friction layer appearing as a dark is formed on the disc circumference. This layer is then gradually worn out, which can be seen as expanding light colored area in contact path. This behavior is accompanied by nearly linear increase in CoA. When the visible friction layer is completely removed CoA saturates at app. 0.43. Further in time wear process continues but is not associated with increase in CoA. After some time this behavior becomes unstable and roll-slip oscillation is evident in friction data, which suggests that the system reached its adhesion limit. After this period disc exhibits significant worn areas periodically distributed over the circumference of the disc.

The final adhesion is lower than that for laboratory dry conditions, which indicates that some friction layer still exist on discs. The adhesion level is however high for a given application, so the period with linear increase of CoA is considered as an effective regime of FM. This regime can be described by CoA rate defined as a ratio between CoA difference and time difference, as indicated in Fig. 3.

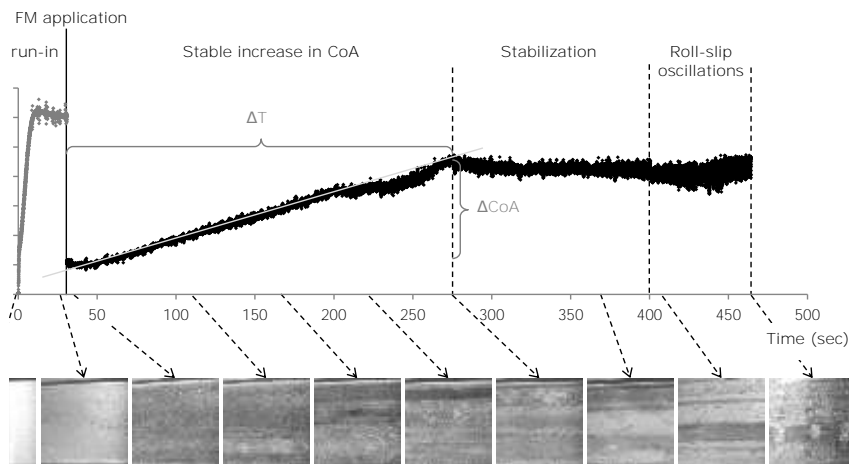


Fig. 3 Evolution of CoA and disc surface after application of FM (Speed 1 m/s; Slip 8 %; FM amount 5 μl).

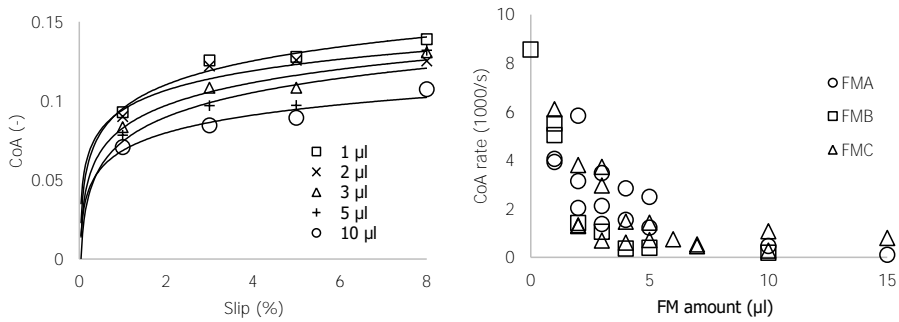


Fig. 4a Adh. curves immediately after FM application for different amount;
 Fig. 4b Effect of FM amount on CoA rate for different FMs
 (Speed 1 m/s; Slip 8 %)

The amount of FM also influences low adhesion occurring immediately after the application. This effect is shown in Fig. 4a, where adhesion curves are reconstructed from initial sections of time tests for each amount and slip. The results are considered in the design of dosing amount of FM since this lowest level is essential from a safety perspective.

4.2 Effect of operation conditions on CoA rate

The most influencing parameters of increase rate of CoA are applied amount of FM, rolling speed and slip, so the effect of these parameters is described in this study. Fig. 4b compares the effect of FM amount for three different oil-based FMs. It is evident that with increasing amount the CoA rate decreases. This effect is exponential-like and is consistent for different FMs, although the parameters should be determined independently for specific FM.

Increase in adhesion is caused by shear degradation and wear of friction layer. It is supposed that these processes depend on shear stress that is proportional to slip velocity. This velocity is given by rolling speed and slip rate. 55 tests were made with different combination of FM amount, rolling speed and slip rate and the results of CoA rate were plotted against resulting slip velocity a FM amount, as shown in Fig. 5. Data were approximated with exponential function for both the slip velocity and FM amount. The correlation coefficient is calculated to be 0.96.

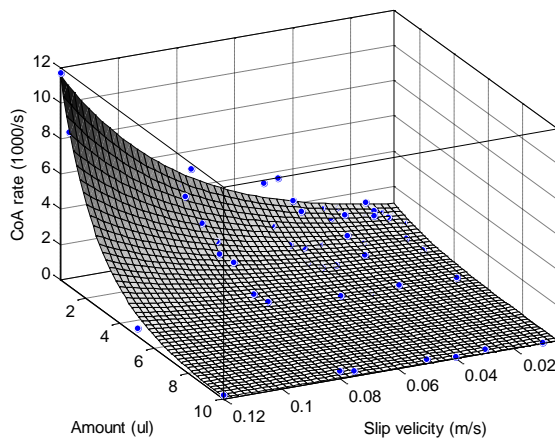


Fig. 5 Effect of slip velocity and FM amount on CoA rate and approximation.

5 DISCUSSION AND FUTURE WORK

5.1 Control system

The proposed control system is outlined in Fig. 6. Considering the experimental findings, slip velocity is the main parameter used for real-time determination of FM consumption time. An essential prerequisite is an ability to estimate the actual slip rate between wheel and rail. This rate is comprised of the contributions from rigid-body motion and elastic deformation and is given by longitudinal and lateral creepage and spin. This parameter depends on geometry and kinematics of the wheelset and track. It can be found from the solution of the dynamic model of vehicle movement using MBS-based software. With a certain level of simplification an analytical dependence of slip ratio on track curvature for high and low rail can be determined for a specific track **and vehicle that are considered as a "constant" in the on-board system.** This issue is not further discussed in this work.

In real time, system evaluates actual slip velocity and predicts a consumption time. The resulting parameter should be further corrected by considering the model of FM redistribution between wheels and rail and by climate conditions. This evaluation is carried out independently for both rails.

5.2 Other effects and transferability

The above mentioned approach simplifies the effect of rolling speed and slip rate only to a kinematic point of view, so that the effect of rolling speed and slip ratio on slip velocity is interchangeable. Experimental results justify this assumption only at a given range of speed and FM amount. Rolling speed influences heat transfer and temperature distribution in the contact. Resulting flash temperature can significantly affect strength of materials and so friction and wear (12), (13). For higher amount of FM, high rolling speed may decrease friction in the mixed lubrication regime (14). Higher speed range should be further investigated.

This paper does not consider other operating conditions such as load, temperature and contact contamination. Load is more or less constant for a given vehicle, but contact pressure varies as contact position changes in curved track. In this work, this effect is neglected. Nevertheless, the experimental data should be determined for a specific range of contact pressure since it strongly influences wear rate and wear regime.

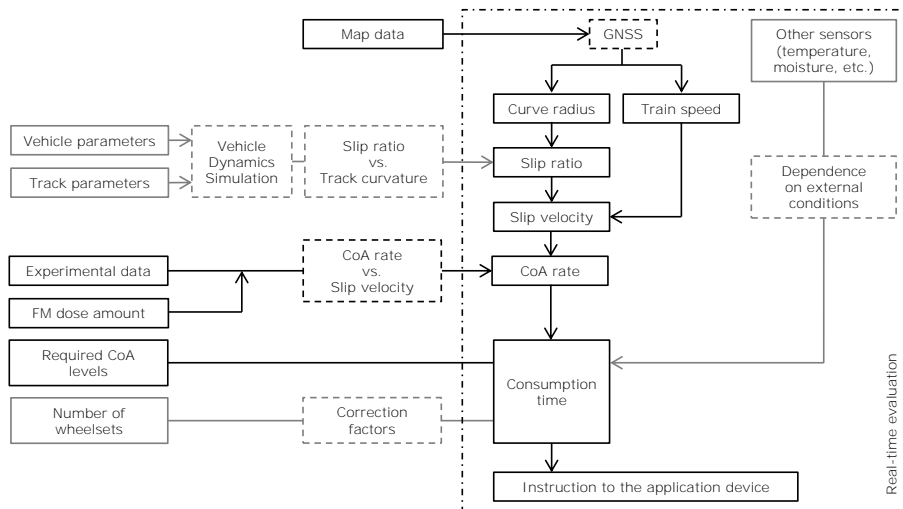


Fig. 6 Functional block diagram of control system

Environmental conditions also influences friction a wear and are of great importance when considering transferability from lab to field. Detailed description of the effect of real contaminants (water, dust, oxides, sand, grease and leaves) and their combination should allow the transferability. The effect of ambient temperature and contact contaminants will be considered using the proposed experimental approach in future studies.

One of the most important aspects concerning the transferability is a geometrical scale and redistribution of FM layer between surfaces. The scale consists in the relationship between size of Hertzian contact and applied amount. In the control system, the amount is expressed as relative to contact width or application width. This point also relates to the fact that not all the applied amount is effectively utilized in real contact. After application FM is subjected to initial push-out from the contact. Nevertheless, the push-out effect is important especially in way-side application, but nearly negligible in on-board system, where the application takes several seconds while moving a vehicle.

Redistribution aspect relates to formation and migration of FM layer in longitudinal direction. Laboratory experiments with discs having larger diameter (320 mm) have confirmed that in the twin-disc system applied amount of FM should be proportional to the circumference of discs for equivalent behavior. Twin-disc situation, however, is far away from the real, where the FM layer is formed primarily on wheel and rail surface along application length and then these surfaces come to contact with unaffected wheels or rail sections. This fact certainly reduces real consumption time. To a certain degree, this effect can be investigated by using one disc with formed FM layer and other unaffected in twin-disc test rig. The determination of correction factors taking into account redistribution of FM between rail and wheels will be made in future study.

6 CONCLUSIONS

This work proposed experimental approach for assessment of consumption time for oil-based FMs based on rate of increase of CoA. This rate strongly depends on applied amount of FM and slip velocity. With increasing slip velocity and decreasing amount the rate increases and this effect can be modeled as an exponential. Based on this dependency an adaptive control system was designed. Future work is needed to address other effects and to ensure transferability of experimental results to real application.

ACKNOWLEDGEMENT

This work was supported by the Technology Agency of the Czech Republic (Project No. TA04030528).

REFERENCE LIST

1. R. Stock, K. Oldknow, D. Mitchell, J. VanderMarel, Top of rail friction control for heavy haul: status and opportunities, Proceedings of the AusRail Plus 2015 Conference, (2015), Melbourne, Australia.
2. K. Davis, W. Stickland, Evaluation of a top-of-rail lubrication system, Applied Technology And Engineering Division. (1999) 1-59.
3. M. Spiryagin, M. Sajjad, D. Nielsen, Y.Q. Sun, D. Raman, D. Chattopadhyay, Research methodology for evaluation of top-of-rail friction management in Australian heavy haul networks, Proceedings of the Institution of Mechanical

- Engineers, Part F: Journal of Rail and Rapid Transit (2014) 228: 631-641, doi: 10.1177/0954409714539943.
4. D.T. Eadie, K. Oldknow, L. Maglalang, T. Makowsky, R. Reiff, P. Sroba, W. Powell, Implementation of wayside top of rail friction control on North American heavy haul railways, in: Proceedings, 7thWorld Congress on Railway Research, Montreal, 2006.
 5. D. Eadie, M. Santoro, K. Oldknow, Y. Oka, Field studies of the effect of friction modifiers on short pitch corrugation generation in curves, *Wear* 265 (2008) 1212–1221, <http://dx.doi.org/10.1016/j.wear.2008.02.028>.
 6. J.I. Egana, J. Vinolas, N. Gil-Negrete, Effect of liquid high positive friction (HPF) modifier on wheel-rail contact and rail corrugation, *Tribol. Int.* 38 (8) (2005) 769–774, <http://dx.doi.org/10.1016/j.triboint.2004.11.006>.
 7. D. Eadie, M. Santoro, J. Kalousek, Railway noise and the effect of top of rail liquid friction modifiers: changes in sound and vibration spectral distributions in curves, *Wear* 258(7–8) (2005) 1148–1155, <http://dx.doi.org/10.1016/j.wear.2004.03.061>.
 8. M. Tomeoka, N. Kabe, M. Tanimoto, E. Miyauchi, M. Nakata, Friction control between wheel and rail by means of on-board lubrication, *Wear* 253 (2002) 124–129, [http://dx.doi.org/10.1016/S0043-1648\(02\)00091-1](http://dx.doi.org/10.1016/S0043-1648(02)00091-1).
 9. Y. Suda, T. Iwasa, H. Komine, M. Tomeoka, H. Nakazawa, K. Matsumoto, et al., Development of onboard friction control, *Wear* 258 (2005) 1109–1114, <http://dx.doi.org/10.1016/j.wear.2004.03.059>.
 10. R. Galas, M. Omasta, I. Krupka, M. Hartl, Laboratory investigation of ability of oil-based friction modifiers to control adhesion at wheel-rail interface, *Wear*, <http://dx.doi.org/10.1016/j.wear.2016.09.015>.
 11. L. Buckley-Johnstone, R. Lewis, S. Lewis, Ch. Hardwick, Friction modification of the wheel/rail contact - A comparison between full-scale and twin disc experimentation, Proceedings of the 33rd Leeds-Lyon symposium on tribology (2013), <http://tribo-lyon2013.sciencesconf.org/17910>.
 12. **Y.A. Areiza, S.I. Garcés**, J.F. Santa, G. Vargas, A. Toro, Field measurement of coefficient of friction in rails using a hand-pushed tribometer, *Tribol Int* 82, 274–279 (2015), <http://dx.doi.org/10.1016/j.triboint.2014.08.009>.
 13. **K. Six, A. Meierhofer, G. Müller, P. Dietmaier**, Physical processes in wheel-rail contact and its implications on vehicle-track interaction, *Vehicle System Dynamics* (2015) 53:5, 635-650, doi: 10.1080/00423114.2014.983675.
 14. M. Spiryagin, K.S. Lee, H.H. Yoo, O. Kashura, O. Kostyuchevich, Modeling of Adhesion for Railway Vehicles, *Journal of Adhesion Science and Technology* 22 (2008), 1017–1034, doi:10.1163/156856108X335757.
 15. R. Stock, L. Stanlake, C. Hardwick, M. Yu, D. Eadie, R. Lewis, Material concepts for top of rail friction management – Classification, characterisation and application, doi: 10.1016/j.wear.2016.05.028.

See discussions, stats, and author profiles for this publication at: <https://www.researchgate.net/publication/317779774>

Case Study: the Influence of Oil-based Friction Modifier Quantity on Tram Braking Distance and Noise

Article in Tribology in Industry · June 2017

DOI: 10.24874/ti.2017.39.02.06

CITATIONS

0

READS

41

6 authors, including:



Radovan Galas

Brno University of Technology

8 PUBLICATIONS 2 CITATIONS

SEE PROFILE



Milan Klapka

Brno University of Technology

15 PUBLICATIONS 22 CITATIONS

SEE PROFILE



Ivan Krupka

Brno University of Technology

168 PUBLICATIONS 1,153 CITATIONS

SEE PROFILE



Martin Hartl

Brno University of Technology

154 PUBLICATIONS 1,217 CITATIONS

SEE PROFILE

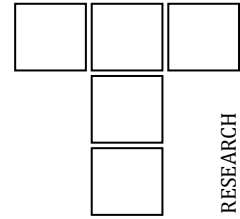
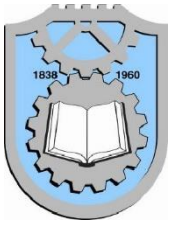
Some of the authors of this publication are also working on these related projects:



Development of an adaptive top-of-rail friction modification system [View project](#)

All content following this page was uploaded by [Radovan Galas](#) on 23 June 2017.

The user has requested enhancement of the downloaded file.



Case Study: the Influence of Oil-based Friction Modifier Quantity on Tram Braking Distance and Noise

R. Galas^a, M. Omasta^a, M. Klapka^a, S. Kaewunruen^b, I. Krupka^a, M. Hartl^a

^aBrno University of Technology, Technická 2896/2 Brno, Czech Republic,

^bUniversity of Birmingham, Edgbaston Birmingham B15 2TT, United Kingdom.

Keywords:

Adhesion
Braking distance
Friction modifier
Noise
Wheel-rail contact

ABSTRACT

In the present study, the twin disc machine and the light rail system was employed in order to investigate the ability of oil-based friction modifier (FM) to optimize adhesion and to reduce noise. The risks associated with poor adhesion conditions after the application of FM were evaluated. Both laboratory and field experiments showed that if the contact is overdosed by FM, the poor adhesion, which results in the extension of braking distance, can occur. In contrast, the smaller quantities do not cause critical adhesion but the effect of FM on the noise reduction is negligible. This study indicates that it can be quite difficult to achieve a reasonable noise reduction without a significant impact on braking distance of tram when the oil-based FM is applied. The field experiments also showed that the carry distance of FM is rather limited, approximately 100 m.

Corresponding author:

Galas Radovan
Brno University of Technology,
Technická 2896/2 Brno,
Czech Republic.
E-mail: galas@fme.vutbr.cz

© 2017 Published by Faculty of Engineering

1. INTRODUCTION

In the last decade, friction modifiers (FMs) have been used in order to control friction in wheel-rail contact. The solid FM was already employed in Vancouver, Canada by the end of the eighties because the new track was corrugated a few months after its opening [1]. This investigation showed that the application of solid FMs can suppressed roll-slip oscillation which is a one of the initiation mechanisms of corrugation [1]. Subsequently, the liquid version of FM (water-based FM) was developed in 1996. Eadie et al. [2] reported that the water-based FM can reduce both squeal and flanging noise. Then, other authors showed by field tests that the water-

based FMs are able to delay or completely avoid the corrugation formation for different wheel-rail systems [3-5]. Tomeoka [6] and Suda [7] reported on-board friction control systems for trains where FMs were sprayed on the top of the inner rail at curves. Their findings have shown that both lateral and tangential forces as well as lateral force fluctuation were reduced after the application of FM [7]. The positive influence of water-based FM on wear and, in particular, on rolling contact fatigue was described in [8] where coal trains were used.

Beside the noise and corrugation reduction, the effect of FMs on adhesion has been studied in recent years [9-11]. Areiza et al. [9] measured

the coefficient of friction (COF) on the rail using a hand-pushed tribometer when oil-based FMs were manually applied on the top of rail. It was observed that FMs can cause a low COF, even lower or the same as in the case of flange lubricants. Similar findings were reported for the laboratory investigations where commercial oil-based FMs and a ball-on-disc apparatus were used [10]. Moreover, Lundberg et al. [11] reported that too much FM results in an unacceptably low friction coefficient (0.13-0.16), also for water-based FMs. All these studies pointed out that FM can be risky in terms of critical adhesion which can result in an unacceptably long braking distance.

An application of FMs seems to be a suitable approach to the reduction of noise, vibrations and corrugation which represent one of the most important problems of railway transportation, especially in urban areas. However, the recently published articles [9-11] indicate that oil-based FMs can have a negative impact on traction or braking. With respect to these articles, the aim of this case study is to clarify the hypothesis that oil-based FMs are able to optimize adhesion and reduce noise emitted by the contact without a serious risk of adhesion loss. For this purpose, the laboratory experiments using twin-disc machine was carried out at first. Subsequently, FM was used in a real track in Brno (Czech Republic). This track is characterized by corrugation and unpleasant noise which represent the typical problems in curves [12]. The conclusions of this article can bring important findings both for safety of rail transportation and for railway owners.

2. MATERIAL AND METHODS

2.1 Twin-disc machine

The used twin-disc machine is schematically depicted in Fig. 1. The wheel-rail contact is simulated using a pair of discs with a diameter of 40 mm. Both discs are made from the bearing steel 100CrMn6 with hardness of 60 HRC and initial roughness of Ra 0.4 μm. The upper disc representing the wheel is cylindrical whereas the lower disc is rounded with a radius of 50 mm. This contact configuration leads to the elliptical contact area (according to the Hertz theory, see Fig. 1b) which is typical for the real

wheel-rail contact. Each disc is independently driven by an AC motor with shaft encoder; thus, the slide-to-roll ratio (SRR) in the contact can be accurately set and controlled according to the following equation:

$$SRR = 2 \cdot \frac{u_1 \cdot r_1 - u_2 \cdot r_2}{u_1 \cdot r_1 + u_2 \cdot r_2} \quad (1)$$

where u_1 and u_2 are the entrainment speeds of discs and r_1 and r_2 are the disc diameters. The mean speed can be controlled over the range of 0 to 2 m/s.

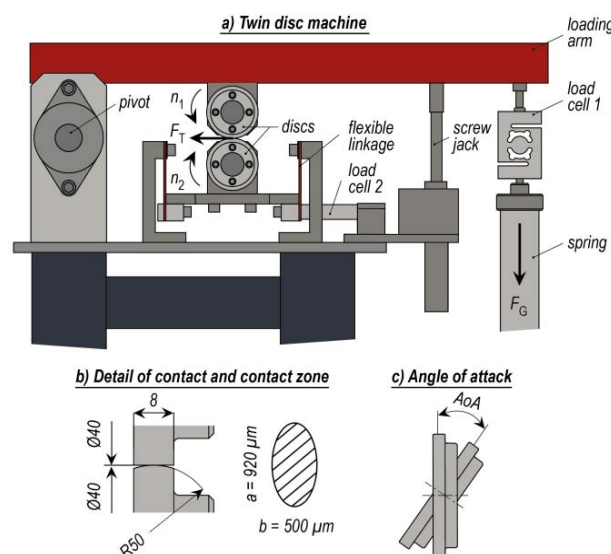


Fig. 1. (a) Twin-disc machine, (b) detail of contact and (c) AoA.

The required contact pressure is realized by the spring-screw loading system which is located, as well as the load cell for normal force, at the end of the loading arm, see Fig. 1a. Quick unloading of the contact is ensured by an AC motor-driven screw jack. The lower disc is mounted on the steel plate which is suspended on the flexible linkages. These linkages allow for a transfer of friction force from the contact to the load cell for friction force. Based on these data, the adhesion coefficient is evaluated:

$$\mu = \frac{F_T}{F_N} \quad (2)$$

where F_T and F_N are the friction and normal force respectively. Beside the friction and normal forces, temperature and air humidity can be measured and controlled using the environmental chamber. Moreover, the support of the lower disc enables to set a different angle of attack (AoA); thus, the passage of a vehicle through a curve is simulated, see Fig. 1c. AoA can be adjusted in the range from -10° to 10° .

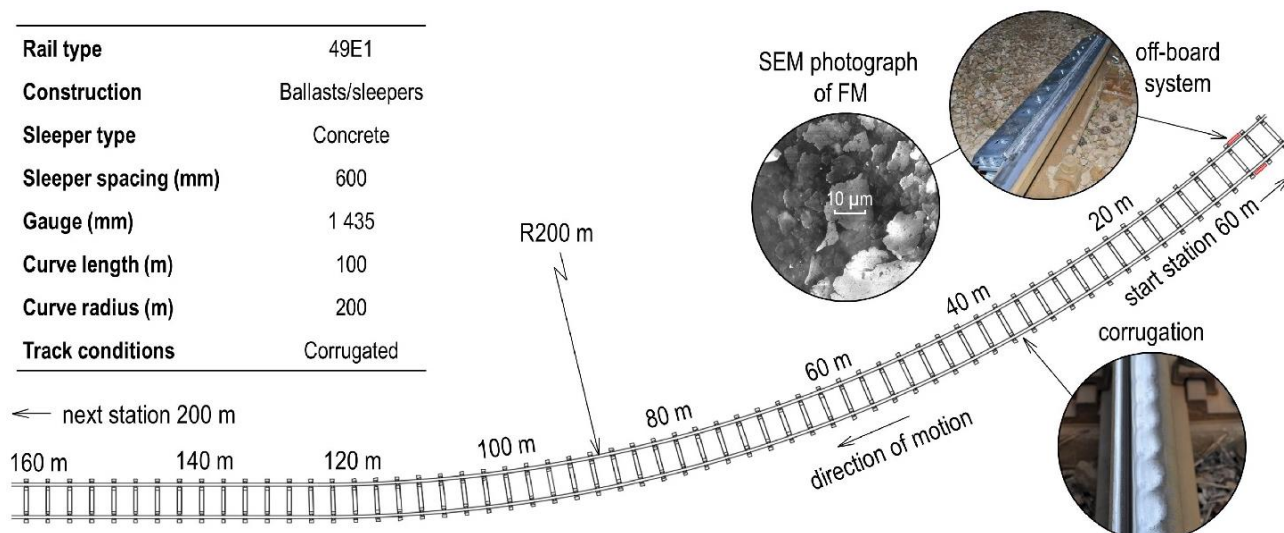


Fig. 2. Testing curve of light rail and technical details.

2.2 Wheel-rail system

The employed wheel-rail system is a light rail in Brno, Czech Republic. For testing purposes, a curve with a radius of 200 m (parallel tracks with rail profile 49E1) was employed because of unpleasant railway noise and corrugation of both rails, see Fig. 2 where the complete track characteristics can be viewed. The off-board system for FM application is located near the curve and simultaneously far enough from the next station where the trams need to decelerate. The tram with four driven and braked wheel axles with axle load of 4 t was used. It should be noted that no adhesion control system was applied during tests.

2.3 Off-board system and friction modifier

The used wayside lubrication system is depicted in Fig. 3. This system allows to apply FM with lubricant viscosity class from NLGI-0 to NLGI-2. FM is applied on the top of the rail using the application strip and the high-pressure pumping device with working pressure of 250 bar. The entire lubrication process is activated by the vehicle-presence sensor which detects the individual tram axles. Based on the signal from this sensor, the control unit applies a dosage of FM. This system enables to set a duration of dosage and also a specific number of axles to pass before the system is activated. It should be emphasized that application bars (strips) are on both rails, see Fig. 3.



Fig. 3. Detail of new-developed off-board system.

In this study, the oil-based FM with NLGI number 1 was utilized. This FM contains plant oil, thickener, and Cu and Zn flakes with the predominant size in the range of 4-10 as was described in [10]. This range of particles is typical for the so-called High Positive Friction modifier (HPF) providing the intermediate level of adhesion and positive friction characteristic. This FM was chosen based on the suitable friction behaviour, particularly N-shape behaviour, which was found in the previous authors' study [10]. Another reason is the fact that this FM is already commonly used in Europe.

2.4 Experimental procedure

Laboratory tests

During laboratory experiments, the adhesion coefficient and level of noise were evaluated. All tests were carried out under the following conditions: contact pressure $p_h = 0.8$ GPa, mean speed $u_m = 1$ m/s, SRR = 0.08 and under ambient temperature $t_a = 23^\circ\text{C}$ and humidity of 40%. FM was applied on the disc using a micropipette which is able to apply liquid substances from minimum of 1 μl (error ± 0.04 μl). In this study, the effect of FM quantity was investigated for four quantities: 1, 2, 3 and 4 μl . The experimental procedure was as follows:

1. To reach the dry level of adhesion the run-in test was carried out.
2. Setup of required AoA. The value of AoA was 4° for all laboratory experiments in this study. This value is typical for reversing loops.
3. Application of given quantity of FM into the contact path on the disc.
4. Start of the main experiment with FM: adhesion and sound level measurements. The experiment was finished when the adhesion coefficient was recovered to the dry level of adhesion.
5. Ultrasonic cleaning of discs.

Field tests

Two different types of field tests were performed in this study. At first, the braking tests with various quantities of FM were conducted to evaluate the appropriate quantity in terms of the braking distance extension. Each braking test started in the station by acceleration of the tram to the required speed of 40 km/h. This speed has to be reached before the tram approaches the off-board system. Subsequently, when the off-board system is reached, the tram driver applies the maximal braking power and the braking distance is recorded. This represents the worst case scenario which can occur in real operation. Each braking test includes the following procedures:

1. Tests under baseline (dry) conditions. These tests were carried out three times in order to investigate the repeatability of experiment.

Based on these tests, an average value of braking distance under baseline conditions was calculated. Subsequently, this average value was used as a reference value for test with FM.

2. Application of given quantity of FM on the top of both rails. In this case, the sensor detecting the vehicle was not used because the tested quantity was always applied prior to the beginning of the experiment.
3. Tests with FM included several passes of the tram in order to determine the changes in braking distance. It should be noted that the tram went to the next station and back after each individual pass in order to spread FM all over the tested track.
4. Comparison of braking performances under baseline and FM conditions as is depicted in Fig. 7.

Once a braking test was completed, the off-board system was turned off for one week. This time period should ensure that almost all FMs were removed from rails by passing trams. After one week, points 1-4 were conducted again for another quantity of FM. In this study, three different quantities of FM were successively tested, specifically 1, 2 and 4 g. Manufacturer's recommended quantity of tested FM is approximately 2 g per 100 axles.

The second type of field tests dealt with the sound level measurements. These measurements were conducted for both baseline conditions (without FM) and the conditions with application of FM. For these measurements, only one quantity of FM was tested with respect to the results of braking tests. These measurements were conducted in real operating conditions.

Sound measurements

Sound level measurements were carried out using a hand-held analyser, Brüel & Kjær type 2270. During the laboratory experiments, the microphone of analyser was mounted 1 m above the floor (10 cm above the contact of discs) and 50 cm from the contact in the horizontal direction. Microphone was oriented towards the contact of discs. The sound level L_{AF} was evaluated from the application point to the

moment when the adhesion coefficient was recovered to the dry conditions.

During field tests, the analyser was placed 7.5 m from the centre of the track with the microphone of analyser 1.2 m above the ground. Each particular sound measurement took 10 seconds. This time period approximately represents the time of train in the curve. The sound measurements were made for 40 trams under both baseline conditions and the conditions with FM. A minimum L_{Aeqmin} , average L_{Aeqavg} and a maximum sound-level L_{Aeqmax} were evaluated during these measurements. With respect to the fact that the testing track is near the urban area, A-weighting was applied for all field and laboratory sound measurements.

3. RESULTS AND DISCUSSION

3.1 Laboratory tests

The adhesion measurements are collected in Fig. 4. During these measurements, the lasting effect and the time period when a critical adhesion occurs were evaluated. In this study, the lasting effect is considered as the time period between the application point and the moment when the adhesion coefficient reaches the value of 0.35 as is depicted in Fig. 4. Above this value, the effect of FM on adhesion as well as on the reduction of sound level is nearly negligible.

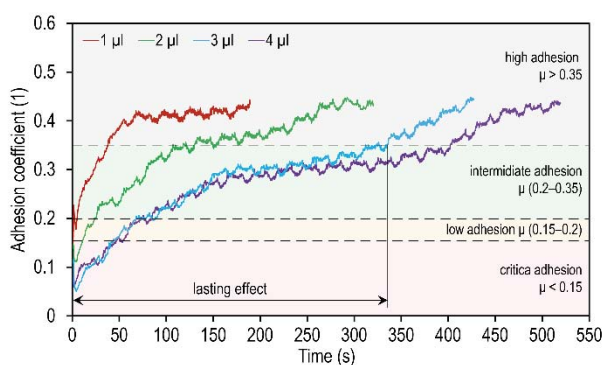


Fig. 4. Friction curves for various quantities of FM.

From Fig. 4, it is obvious that the lasting effect of FM extends with an increasing quantity of FM. A similar trend of friction curves, depending on the applied quantity, was previously found for both oil-based and water-based FM [10, 11]. In the present study, the results showed that the smaller quantities (1 and 2 μl) do not provide

the stable level of adhesion at the intermediate adhesion level, see Fig. 4. In these cases, the performance of FM is markedly affected by starvation of contact, which was described in detail in [14]. In contrast, the quantities 3 and 4 μl can be considered as the suitable quantities because they exhibit the so-called N-shape behaviour which was described in [15]. This behaviour is characterized by the stable part of adhesion after the initial adhesion. This N-shape behaviour extends the lasting effect of FM; thus, also the wear rate is also reduced. However, it should be emphasized that the quantities providing the N-shape behaviour (3 and 4 μl) cause a critical adhesion during the first 50 cycles after the application of FM, see Fig. 4. The tendency to poor adhesion conditions after the application of both water-based and oil-based FM was previously observed in both laboratory and real conditions [10, 11]. These adhesion losses can have a large impact on braking/traction performance; thus, the safety of railway transportation can be affected especially near the station or when climbing a slope.

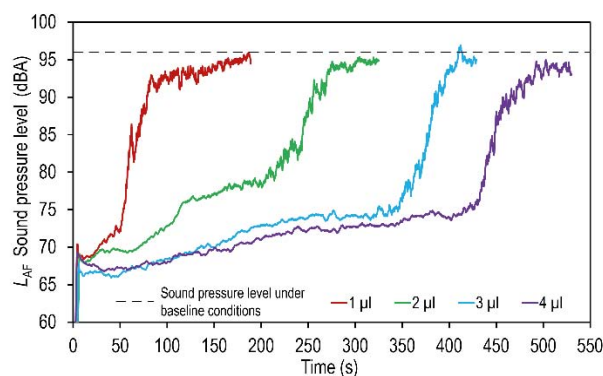


Fig. 5. Effect of FM quantities on sound level.

Sound level measurements showed that all tested quantities of FM reduce noise from 97 dBA (baseline conditions) to 64-68 dBA immediately after the application of FM, see Fig. 5. Subsequently, a gradual increase in adhesion and sound level pressure occurs when the adhesion coefficient reaches the high adhesion level ($\mu > 0.35$), see Fig. 6. Then, the slope of sound and friction curves was changed and a higher scatter of sound data was observed. Based on these experiments, it can be concluded that the quantities 2, 3 and 4 μl provide a significant noise reduction for tested conditions. In contrast, the effect of 1 μl seems to be almost insufficient for noise reduction because of the fast recovery of sound level pressure to baseline conditions.

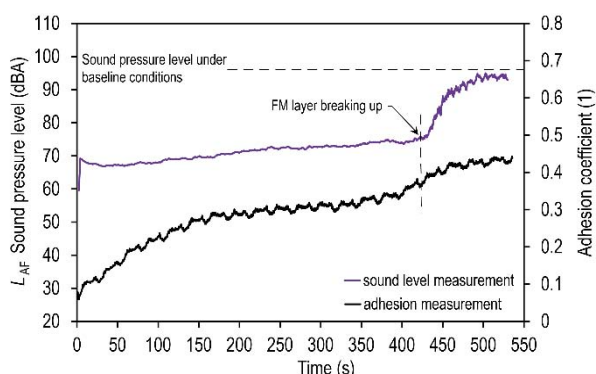


Fig. 6. Comparison of friction and sound pressure measurement.

These laboratory measurements show that the quantities exhibiting advantageous N-shape behaviour ensure a substantial decrease in sound level; moreover, a reduction of wear rate can be expected. On the other hand, the critical adhesion can easily occur during the first passes of the tram.

3.2 Field tests

With respect to the laboratory investigation, the experiments with various quantities (4, 2, 1 g/rail) were performed first to evaluate their impact on braking distance of the tram. The first braking test was conducted with 4 g of FM per single rail, see Fig. 7. This figure shows the change of tram braking distance for several consecutive tram passes. It is evident that the braking distance was considerably extended in all tram passes in comparison with baseline conditions. It should be noted that the longest braking distance was observed in the second and third tram pass while the braking distance closest to baseline conditions was found for the first pass after the application of FM. During the second and third pass, slide of wheel (complete wheels slip) occurred as a result of high quantity of FM on the rails. This slide of wheels has a negative impact on both contact bodies (flat spot, rail joints, etc.) and also on a brakes of vehicle as a result of high temperature between wheel and brake shoes [16, 17]. On the contrary, in the fourth pass, wheels slide was not detected but some wheels were still under slip. In the case of the following passes, no slip was observed; thus, the shorter braking distances were evaluated.

At the end of the braking test No.1, the spreading ability (carry distance) of FM over the rails was evaluated, see Fig. 8. From this figure, it is

evident that FM was found at the distance of 100 m from the application point, observed with naked eye. This observation suggests that if the reasonable quantity of FM is applied, the carry distance is rather limited compared to the previous published results where these distances reached several miles [18]. However, this shorter carry distance can be advantageous to light rail systems or metros because a braking performance of vehicle near the next station should not be already influenced.

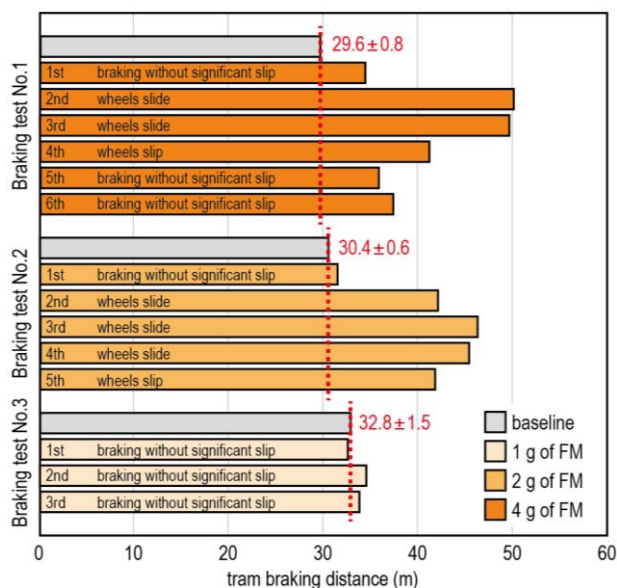


Fig. 7. Testing curve of tramway track and technical details.

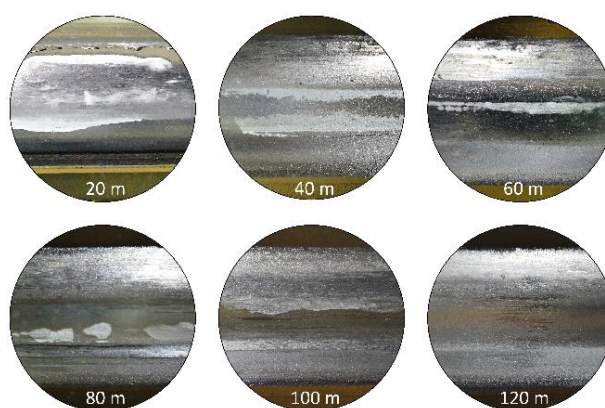


Fig. 8. The spreading ability of FM depending on the distance from the application point.

The braking test No.2 was conducted with 2 g of FM per single rail. The results showed that the trend of the braking distances was almost the same as in the braking test No.1. While the effect of FM on braking distance was almost negligible during the first pass, it became essential for the next three passes. It should be noted that the

braking distance started to decrease after the third pass although the slide of wheels occurred in the following two passes. It can be expected that if the next pass was carried out, the braking distance would be the shortest and simultaneously the slide of wheels would not occur as well as in the case of the braking test No.1.

The last braking test (No.3) was performed with FM quantity of 1 g/rail. The results showed that the extension of braking distances was negligible for all passes. Moreover, no slide of wheels was observed. It is apparent that the trend of braking distances was the same as in the previous braking test. It should be noted that the braking distance was even slightly shorter during the first pass with FM than under baseline conditions.

The above-mentioned braking tests give the evidence that the larger quantity of FM (4 and 2 g/rail) can endanger the safety of rail transportation especially during the second and third passes after the application of FM where inadequate long braking distances were found. On the contrary, in the first pass, the effect of FM on braking performance was not as significant as expected. This behaviour can be explained as follows: the FM film is formed on top-of-rails during the first pass. It means that the braking performance during the first pass is influenced both by FM and the braking ability of dry contact. Regarding the safe braking distance of tram, the quantity of 1 g/rail seems to be the optimal quantity (from among the tested quantities).

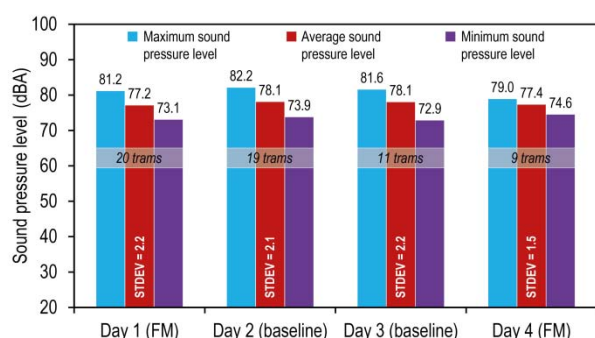


Fig. 9. Sound pressure measurement for contact with FM and for baseline conditions.

With regard to the braking tests, the quantity of 1 g/rail was selected as a suitable quantity in terms of braking distance for investigation of FM effect on noise. The quantity of 1g/rail of FM was

applied every 100 axles. As it is clear from Fig. 9, FM was applied on the day 1 and 4 whereas the experiments during the day 2 and 3 were carried out under baseline conditions (without FM).

Fig. 9 shows that there is no positive effect of FM on noise reduction in spite of the fact that FM was visible on the top-of-rails. These findings showed that the quantity of 1 g/rail appears to be inefficient in terms of noise reduction. This is in accordance with laboratory measurement with 1 μ l where the effect of FM on noise reduction was almost negligible because of rapid increase of sound level to baseline conditions. Other authors reported that water-based FM can reduce a squeal noise about 12 dB for tram/light rail system [2]. However, the effect of FM on adhesion or braking distance was not studied in [2]. It can be reasonably expected that the larger quantities used in this study (e.g. 4 g/rail) are able to considerably reduce noise as in the case of [2] but there is a significant impact on braking distance. Inability of FM to reduce noise can be explained by the absence of squeal noise on the test track. It suggests that FM is probably not able to reduce the other type of wheel/rail noise.

This study suggests that if the wheel-rail contact is overdosed by oil-based FM, the slide of wheels can occur; it results in significant impact on the length of the tram braking distance. Moreover, flat spots can be formed on wheels due to the wheel slide. This conclusion is in a good agreement with the previous field study conducted by Lundberg et al. [11]. They revealed that the adhesion coefficient was strongly dependent on the quantity of FM in the contact, and the application of large quantity of FM led to unacceptably low adhesion coefficients (on average 0.13-0.16). This decrease of adhesion can be catastrophic with respect to the length of braking distances. A similar drop of COF was observed in [9] where a hand-pushed tribometer in real railway system was used. In this case, COF was reduced to 0.15 and 0.13, depending on the contact pressure, when FM was applied. Beside the field tests, the laboratory experiments also show that oil-based FMs can cause adhesion losses after application of FM [10]. In [10], this behaviour was explained as an effort of metal particles to avoid the point contact under fully flooded conditions. However, considering that the width of the real contact area is several times larger compared to the ball-on-disc apparatus employed in [10], it can be

assumed that the metal particles enter the contact. Furthermore, the metal particles were identified on the top-of-rail surfaces after the braking test with high quantity of FM, see Fig. 8. In author's opinion, adhesions, as well as the braking distance, are controlled by the metal particles contained in FM only in the case of small quantity of FM. Provided that the quantity of FM is high, adhesion is controlled especially by the base oil and it results in poor adhesion conditions.

It should be noted that the results mentioned above do not correspond with the field study carried out by Yu et al. [18]. This study reported that FM has no negative impact on the train braking. However, FMs used in this research were water-based and petroleum-based. Moreover, a heavy haul freight train with many wagons was employed, so the operating conditions significantly varied. Based on this, it can be expected that the oil-based FM can cause a poor adhesion and wheels slide in an easier way than the water-based (drying FM) or petroleum-based FM. In addition, commuter trains and trams are probably more prone to wheels slide in comparison with heavy haul freight trains, as was reported in [19]. It should be noted that poor adhesion occurring immediately after the application of oil-based FM may be suppressed using the on-board system. In this case, FM is gradually sprayed over the rails thus avoiding an overdose of contact by FM.

4. CONCLUSION

The laboratory and field investigations focused on the effect of quantities of commercial oil-based FM on sound level and adhesion or tram braking distances have been presented in this paper.

The laboratory measurements showed that the larger quantities provide the significant noise reduction but critical adhesion occurs immediately after the application of FM. In contrast, smaller quantities are able to decrease both sound and adhesion without the risk of braking performance. However, these smaller quantities did not lead to the N-shape behaviour; thus, the lasting effect is rather limited.

In the case of field experiments, it was suggested that if the contact is overdosed by FM, then the braking distance can be significantly extended. The most critical passes were especially the second and third one after the application of FM which was accompanied by wheel slide. It means that under these conditions, the braking performance is significantly limited. It can be assumed that there is a limit for FM quantity below which the adhesion is mainly controlled by metal particles contained in FM, while above this quantity the adhesion is mainly given by the base medium. With regard to both laboratory and field results, the applied quantity appears as a crucial parameter for top-of-rail friction modification.

From laboratory and field investigations it is evident that it is quite difficult to achieve a reduction of sound level without the significant extension of braking distance as a result of critical adhesion.

The sound level measurements under real operating conditions showed that there is no positive effect of FM (1 g/rail) on noise reduction in spite of the fact that FM was visible on the top-of-rails.

Acknowledgement

The authors are sincerely grateful to European Commission for the financial sponsorship of the H2020-MSCA-RISE Project No. 691135 "RISEN: Rail Infrastructure Systems Engineering Network," which enables a global research network that tackles the grand challenge in railway infrastructure resilience and advanced sensing under extreme environments.

Authors would like to appreciate and thank for all the work and experiments done by Bc. Jiří Knápek during his study at the Brno University of Technology.

REFERENCES

- [1] J. Kalousek and K. Johnson, 'An investigation of short pitch wheel and rail corrugations on the Vancouver mass transit system', *Proceedings of the the Institution of Mechanical Engineers, Part F: Journal Of Rail And Rapid Transit*, vol. 206, no. 2, p. 206, 1992.

- [2] D.T. Eadie, M. Santoro and J. Kalousek, 'Railway noise and the effect of top of rail liquid friction modifiers: changes in sound and vibration spectral distributions in curves', *Wear*, vol. 258, no. 7-8, pp. 1148-1155, 2005.
- [3] J.I. Egana, J. Vinolas and N. Gil-Negrete, 'Effect of liquid high positive friction (HPF) modifier on wheel-rail contact and rail corrugation', *Tribology International*, vol. 38, no. 8, pp. 769-774, 2005.
- [4] D.T. Eadie, M. Santoro, K. Oldknow and Y. Oka, 'Field studies of the effect of friction modifiers on short pitch corrugation generation in curves', *Wear*, vol. 265, no. 9-10, pp. 1212-1221, 2008.
- [5] D.T. Eadie and M. Santoro, 'Top-of-rail friction control for curve noise mitigation and corrugation rate reduction', *Journal of Sound and Vibration*, vol. 293, no. 3-5, pp. 747-757, 2006.
- [6] M. Tomeoka, N. Kabe, M. Tanimoto, E. Miyauchi and M. Nakata, 'Friction control between wheel and rail by means of on-board lubrication', *Wear*, vol. 253, no. 1-2, pp. 124-129, 2002.
- [7] Y. Suda et al., 'Development of onboard friction control', *Wear*, vol. 258, no. 7-8, pp. 1109-1114, 2005.
- [8] D. Elvidge, R. Stock, C. Hardwick and K. Oldknow, 'The effect of freight train mounted TOR-FM on wheel life and defects', *The Third International Conference on Railway Technology: Research, Development and Maintenance*, Cagliari, Italy, 2016, p. 174.
- [9] Y.A. Areiza, S. I. Garces, J.F. Santa, G. Vargas and A. Toro, 'Field measurement of coefficient of friction in rails using a hand-pushed tribometer', *Tribology International*, vol. 82, pp. 274-279, 2015.
- [10] R. Galas, M. Omasta, I. Krupka and M. Hartl, 'Laboratory investigation of ability of oil-based friction modifiers to control adhesion at wheel-rail interface', *Wear*, vol. 368-369, pp. 230-238, 2016.
- [11] J. Lundberg, M. Rantatalo, C. Wanhainen, and J. Casselgren, 'Measurements of friction coefficients between rails lubricated with a friction modifier and the wheels of an IORE locomotive during real working conditions', *Wear*, vol. 324, pp. 109-117, 2015.
- [12] S. Kaewunruen, 'Monitoring of rail corrugation growth on sharp curves for track maintenance prioritisation', *The International Journal of Acoustics and Vibration*, in press.
- [13] O. Arias-Cuevas, Z. Li, R. Lewis and E. A. Gallardo-Hernandez, 'Rolling-sliding laboratory tests of friction modifiers in dry and wet wheel-rail contacts', *Wear*, vol. 268, no. 3-4, pp. 543-551, 2010.
- [14] D. Kostal, P. Sperka, I. Krupka and M. Hartl, 'Experimental comparison of the behavior between base oil and grease starvation based on inlet film thickness', *Tribology in Industry*, vol. 39, no. 1, pp. 110-119, 2017.
- [15] X. Lu, J. Cotter and D. T. Eadie, 'Laboratory study of the tribological properties of friction modifier thin films for friction control at the wheel/rail interface', *Wear*, vol. 259, pp. 1262-1269, 2005.
- [16] F. Elshukri and R. Lewis, 'An Experimental Investigation and Improvement of Insulated Rail Joints', *Tribology in Industry*, vol. 38, no. 1, pp. 121-126, 2016.
- [17] A. Tudor, C. Radulescu and I. Petre, 'Thermal Effect of the Brake Shoes Friction on the Wheel /Rail Contact', *Tribology in Industry*, vol. 25, no. 1&2, pp. 27-32, 2003.
- [18] M. Yu and P. Ray, 'Evaluation of two TOR products on river grade track', in *the AREMA Annual Conference*, Minneapolis, USA, 2015, p. 16.
- [19] R. Stock, L. Stanlake, C. Hardwick, M. Yu, D. Eadie and R. Lewis, 'Material concepts for top of rail friction management - Classification, characterisation and application', *Wear*, vol. 366-367, pp. 225-232, 2016.

NOMENCLATURE

Subscripts:

1	Relation to the wheel disc
2	Relation to the rail disc
AoA	Angle of attack
F_N	Normal force in the contact
F_T	Friction force in the contact
L_{AF}	A-weighted, Fast, Sound level
L_{Aeqmin}	A-weighted, Fast, Minimum, Equivalent sound level
L_{Aeqavg}	A-weighted, Fast, Average, Equivalent sound level
L_{Aeqmax}	A-weighted, Fast, Maximum, Equivalent sound level
$n_{1;2}$	Revolutions of discs
p_h	Hertzian pressure in the contact
$r_{1;2}$	Diameters of discs
SRR	Slide-to-roll ratio
t_a	Ambient temperature
$u_{1;2}$	Entrainment speeds of surfaces
u_m	Mean speed; $(u_1 + u_2)/2$
μ	Adhesion coefficient

DESIGN AND DEVELOPMENT OF A TWIN DISC TEST RIG FOR THE STUDY OF SQUEAL NOISE FROM THE WHEEL – RAIL INTERFACE

Original scientific paper

UDC: 629.4.027:534.322.3
<https://doi.org/10.18485/aeletters.2022.7.1.2>

Milan Omasta^{1*}, Václav Navrátil¹, Tomáš Gabriel¹, Radovan Galas¹, Milan Klapka¹

¹Brno University of Technology, Faculty of Mechanical Engineering, Czech Republic

Abstract:

Wheel squeal noise research requires many repeatable experiments under controlled driving conditions. While it is difficult to control those conditions on the real track, test rigs are designed. For the experimental validation of the models describing the wheel-squeal noise and other dynamic-related phenomena, suitable experimental models must be utilized. The aim of this paper is to present the design of the twin-disc test rig for the study of the wheel-squeal phenomena. This test rig utilizes a dynamic model of the track-train interaction and uses real train wheel for a more realistic representation of the emitted noise. This twin-disc test rig is intended for research into the mechanisms of the wheel squeal noise formation and for the development and validation of a prediction model. In particular, the influence of weather conditions and the presence of various friction layers in the contact will be addressed.

ARTICLE HISTORY

Received: 06.12.2021.

Accepted: 14.02.2022.

Available: 31.03.2022.

KEYWORDS

Wheel-rail contact, twin-disc, wheel squeal noise, adhesion characteristic, dynamic model

1. INTRODUCTION

Due to its strong tonal character, wheel squeal noise is one of the most unpleasant noises in railway transport. The problem is mainly in densely populated areas, where, according to Müller [1], wheel squeal affects up to 1,000 inhabitants within a radius of 250 m from the noise source. Therefore, it is necessary to investigate this phenomenon and seek measures against its occurrence. Full-scale testing with real vehicles and on-board diagnostic equipment has the advantage of obtaining the real track data. However, such testing is time consuming and if the research requires many repetitive experiments in a controlled environment, this method is unsuitable. A more appropriate approach is to use test rigs that eliminate these disadvantages.

Various test rigs were developed to study the wheel-rail interface. The devices vary based on their main purpose and scale. While some may take up several floors to achieve a correct shape of the contact patch [2], others take advantage of scaling and can be made e.g., by modifying a lathe [3,4]. An

overview of different approaches and designs was compiled by Naeimi [5]. Six general categories of test rigs were defined: 1) full-size vehicle/ bogie, 2) full-size wheel-on-roller, 3) full-size wheel-on-straight, 4) twin-discs, 5) scaled wheel on rail track ring and 6) scaled wheel on the straight track. Due to the easy slip control and compact dimensions, twin-disc concept can be considered the most common approach to study a single wheel-rail contact. This concept is also utilised to investigate squeal noise.

Hsu et al. [6] utilized a twin-disc test rig with rollers scaled to one-third of a locomotive wheel to simulate the wheel rail contact in relation to curve squeal. The disc profile was adapted so that realistic contact pressure can be reached with reasonable force. Only the rail disc is driven, which makes it impossible to adjust the longitudinal creepage. To vary the lateral creepage, a change of the angle of attack (AoA) of the wheel relative to the rail roller is made. Similar device of the same scale was developed at TNO-TPD Delft and used to study the squeal noise behaviour [7,8]. Especially, the effect of longitudinal creepage together with lateral

creepage was investigated by incorporating the chain and gear wheel transmission to create a fixed longitudinal creepage [8]. Another device was developed at the University of Queensland by Walls to study the rail corrugation as an uneven wear of a railway track due to varying dynamic loads [9]. Later, this device has been extensively used by Meehan and Liu [10-12] for several experiments regarding wheel-squeal noise and friction modifiers. The load is applied through a set of leaf springs. The deflection of the springs is measured to determine the force load and their stiffness is optimized to simulate the stiffness of wheel suspension.

Other twin-disc test rigs exist that are not directly targeted to the noise studies but allow to simulate the effect of the AoA. At the Railway Technical Research Institute in Tokyo, Jin et al. [13] used an atypical twin-disc for testing of material wear. The design of this machine allows both radial and lateral forces to be applied and even the rail inclination to be modified. Researchers at the University of Pardubice and the railway research institute VÚKV in the Czech Republic developed a twin-disc rig using a real tram wheel [14]. The device allows adjustment of AoA and load is applied via a pneumatic system. The device is used to investigate the effect of various contact conditions and contamination as well as on the contact cleaning process [15]. A reduced-scale twin-disc rig was developed at Brno University of Technology by Galas [16]. The experimental machine uses 1:3 scale and enables versatile creepage settings by using mutually independent drives for both discs. The device was used mainly for examining the effect of sanding and development of friction modifiers.

For the experimental validation of the models describing the wheel-squeal noise and other dynamic-related phenomena, suitable test rigs must be utilized. The dynamics of the experimental model is essential to the effects studied. The aim of this paper is to present the design of the twin-disc test rig for the study of wheel-squeal phenomena. This test rig utilizes a dynamic model of the track-train interaction and uses real train wheel for a more realistic representation of the emitted noise. In the following sections the theoretical model will be introduced. Then the relevant parameters will be defined, which sets the objectives of the design. Then the device, its parts and main features will be described. Finally, an outline of possible uses and drawbacks of the test rig will be presented.

2. METHODS

2.1 Mechanisms of the wheel-squeal

Several mathematical models of wheel-squeal noise and its dependence on the contact dynamics have been proposed. An overview of this problematic was composed by Thompson et al. [17]. In the dynamic model derived by Rudd [18], three mechanisms of wheel-squeal noise origin are considered: frictional contact with high creepage between wheel flange and rail, the differential tangential creepage caused by different speeds of inner and outer wheel and finally lateral creepage caused by angle of attack. Experiments showed that wheel-squeal is present even with elimination of the first two causes, therefore the lateral creepage was identified as a source of the noise. Rudd's final equation is as follows (1):

$$SPL = 10 \cdot \log \left\{ v^2 \cdot \frac{\left(\frac{l}{R} - \frac{1}{100} \right)}{\left(\frac{3}{100} - \frac{l}{R} \right)} \right\} + 10 \cdot \log(\phi \cdot A) + 93 \quad (1)$$

where SPL is the sound pressure level of wheel-squeal noise 50 ft from the wheel, v is the train speed, l the distance between axles, R the rail curve radius, A the area of wheel and ϕ a coefficient ≈ 1 . Rudd also proposed that sufficient damping in the wheels should eliminate the problem, but further experiments were inconclusive.

Rudd's model was further examined as a dynamic system shown in Fig. 1(a). The mass representing the wheel oscillates on a moving belt. The belt pulls the mass to the right, but the spring pushes it back. This represents the movement of the wheel due to lateral creepage. The instability of the system is caused by the descending part of adhesion characteristic known as "negative friction", see Fig. 2. The coefficient of adhesion decreases with increasing speed, effectively adding energy to the system and causing the instability. This phenomenon acts as negative damping when implemented into the dynamic model.

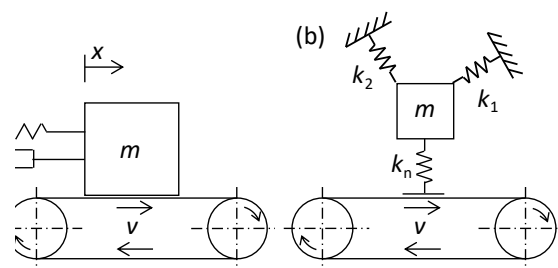


Fig. 1 Scheme of a dynamic model of wheel-rail contact (a) falling-friction; (b) mode-coupling

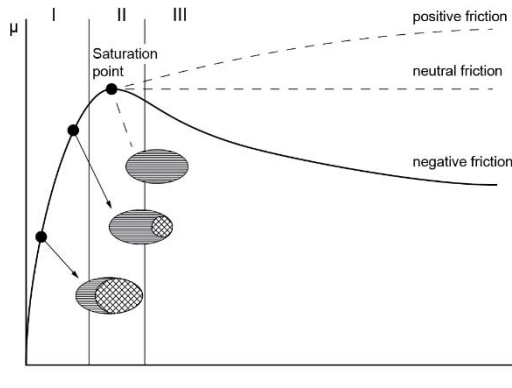


Fig. 2. Traction curve as a function of coefficient of adhesion (μ) on creepage (s)

However, the previous approach cannot explain the origin of squealing noise in positive friction after the saturation of adhesion curve. Therefore, another mechanism of wheel-squeal noise, the so-called “mode-coupling”, has recently been proposed. The schematic of the mode-coupling dynamic model is depicted in Fig. 1(b). This model shows the dependency of frictional force on the normal force. The oscillations in the vertical direction affect the normal force, which changes the frictional force through the coefficient of friction, therefore the oscillations in horizontal direction are affected, effectively “coupling” the two together. This model shows importance of the dynamic properties of wheel suspension and track stiffness. The designed test rig must be able to monitor the adhesion characteristics which provide the basic data for the above models. For extracting the characteristic for lateral creepage it is necessary to measure tangential and lateral frictional force separately. Also, the acoustic emission of the wheel needs to be recorded. These insights act as a foundation to the designed measurement system. This mode was recently investigated by Meehan [19].

2.2 Dynamic concept of the test rig

The mode-coupling dynamic model shows that the wheel suspension and the track stiffness affect contact behaviour. This fact should be considered during the design of the device. A simplified suspension system for the twin-disc was proposed, see Fig. 3. The suspension of the wheel disc in normal and lateral directions is modelled based on the real stiffness of the primary suspension of train wheels. Similarly, the same directions of the rail disc suspension are modelled according to track stiffness. Contact stiffness and damping are controlled by the geometry and materials of the disc.

This system will simulate oscillations in both directions and excite the wheel vibrations.

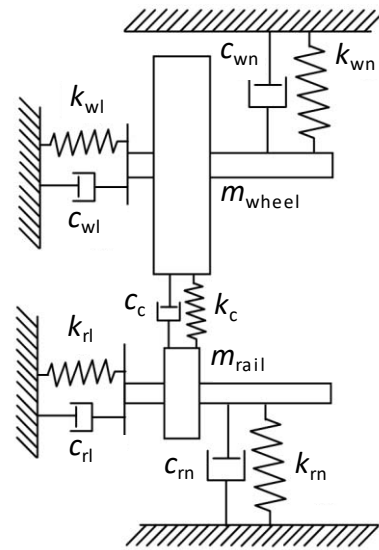


Fig. 3. The dynamic concept of the test rig

2.3 Scaling approach

To determine desired values of design parameters a scaling strategy must be set. As Bosso et al. summarised in their book [20], several approaches are possible. Table 1 offers a comparison of several scaling models with scaling factors of parameters derived from the length scaling factor φ_l . As the rig uses a real scale train wheel, the scaling factors for the wheel are reduced to 1. The rest of the device has to match the scaling of the wheel, meaning all values should be modelled to real scale.

Table 1. Scaling strategy comparison [20]

Scaling factor	Jaschinski	Pascal	Iwnicki
Length	φ_l	φ_l	φ_l
Time	$\varphi_l^{1/2}$	φ_l	1
Velocity	$\varphi_l^{1/2}$	1	φ_l
Acceleration	1	$1/\varphi_l$	φ_l
Angular velocity	$1/\varphi_l^{1/2}$	$1/\varphi_l$	1
Mass	φ_l^3	φ_l^3	φ_l^3
Force	φ_l^3	φ_l^2	φ_l^4
Density	1	1	1
Young’s modulus	1	1	1
Stiffness	φ_l^2	φ_l	φ_l^3
Power	$\varphi_l^3 \cdot \varphi_l^{1/2}$	φ_l^2	φ_l^5

2.4 Concept of the measurement system

Fig. 4 shows the concept of the measurement system. The wheel and the disc are pressed together with normal force F_n . AoA is set and one or both discs are driven with speeds of v_1 and v_2 ,

resulting in creepage s . AoA causes both tangential and lateral friction forces F_{ft} and F_{fl} . Normal and frictional forces are used to calculate immediate coefficient of adhesion, which together with creepage defines the adhesion characteristic. Thanks to the known tangential and lateral components of frictional force, separate characteristics can be created for these directions. SPL is recorded to be compared with the adhesion characteristic and is used to validate wheel-squeal prediction models or the effectivity of applied noise generation countermeasures. Information about the temperature of the contact is noted as a reference value because it can affect the contact behaviour.

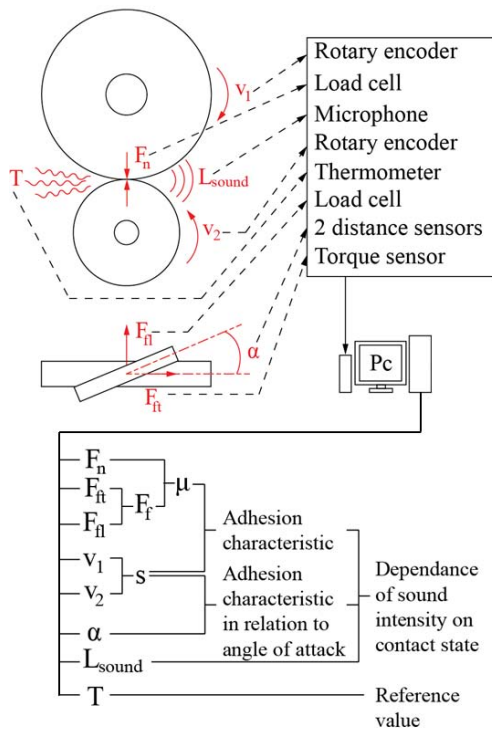


Fig. 4. Concept of the measurement system

3. RESULTS

3.1 Overview of the design

Final model of the device is displayed in Fig. 5, with all the main parameters listed in Table 2. The 800 mm diameter train wheel is placed below the 320 mm diameter rail disc. The wheel (profile ORE S 1002) is mounted on a lever pivoted around one end and supported by the loading mechanism on the other. The loading mechanism consists of a hydraulic cylinder, compression coil spring and a load transducer measuring the normal force on the lever. The rail disc is mounted above the wheel on a support that allows adjustment of the AoA of the

disc assembly. The disc assembly is supported by a pair of linear guideways that allows change in the lateral position and the lateral force measurement using a force transducer. The wheel is driven with 11 kW AC electric drive with a gearbox. Driving shaft includes a constant velocity joint to allow rotation of the loading arm. A torque meter is used to measure the driving torque and to evaluate traction force in longitudinal direction. The device is held together by a frame welded and screwed from profiles, mounted on a base plate. The asynchronous motor driving the wheel is mounted on an independent frame.



Fig. 5. Design of the test rig

Table 2. Overview of main parameters of the test rig

Parameter	Value	Unit
Outer dimensions	1,340 x 3,020 x 1,690	mm
Weight	2,270	Kg
Wheel diameter	800	mm
Wheel profile	ORE S 1002	-
Rail disc diameter	320	mm
Rail disc profile radius	100	mm
Max. contact pressure	900	MPa
Max. normal force	3,507	N
Maximum velocity	4	m/s
Wheel drive torque	1,000	Nm
Wheel drive power	11	kW
Angle of attack range	±5	°

3.2 Implementation of the dynamic model

The dimensions and parameters of the test rig were designed with respect to the required dynamic properties. The dynamic properties of the wheel and the disc suspension are realised by optimization of the stiffness of certain elements in the frame of support. The model implementation is

depicted in Fig. 6. The normal stiffness of the rail disc k_{rn} is controlled by the bridging beams on top of the device. They also influence the lateral stiffness k_{rl} together with the lateral stiffness of the positioning system. Normal stiffness of wheel k_{wn} is set by the stiffness of the compression spring in the loading mechanism and the lateral wheel stiffness k_{wl} is ensured by the beams from which wheel's lever is made.

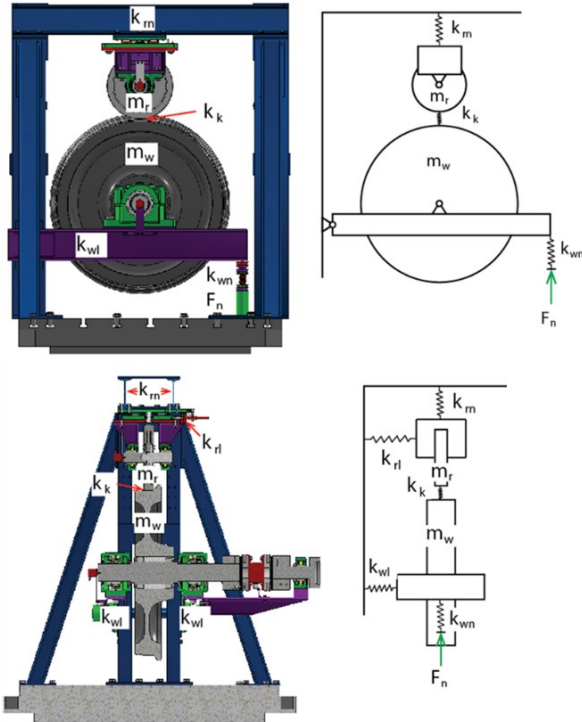


Fig. 6. Implementation of the dynamic model

Stiffness of these elements was designed using FEM software and analytical calculations. Table 3 shows the final values for stiffness for both specimens at the contact point. To determine the correct target stiffness for the rail disc, a preliminary analysis was made on a rail profile 60R2 between two sleepers. The stiffness of the rail housing was simulated as well. The FEM model was created with functional mechanical constraints and subjected to a non-linear calculation to correctly reflect the rig's behaviour. A linear relation between deflection and loading was also examined, maximum diversion of final stiffness along the intended loading range is 0.5 %.

Table 3. Stiffness values of the test rig

Suspension	Stiffness (kN/mm)
Wheel normal	0.172
Wheel lateral	5.21
Rail disc normal	124
Rail disc lateral	6

3.3 Realization of the test rig

The test rig was manufactured and assembled according to the described design, as shown in Fig. 7. An alignment of individual assemblies was made to ensure smooth operation and low internal dynamic effects. The loading mechanism, shafts and the disc and wheel assemblies were equipped with an appropriate sensor according to the measurement system concept. Sound can be recorded by a microphone array that is not a part of the core construction. To ensure accurate measurement of AoA, two ultrasound distance sensors are employed, and the angle can be easily calculated from measured distances.

Although the individual design parameters were achieved as planned, certain limitations and diversions from the real world must be discussed.

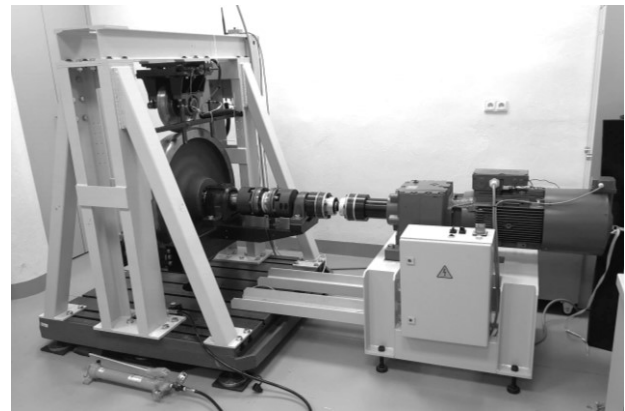


Fig. 7. Realization of the test rig

4. DISCUSSION

4.1 Rail disc geometry

The replacement of the straight rail with a disc changes the contact patch and the contact pressure. Because the contact pressure is considered one of the most important parameters for tribological models of the contact, it is necessary to modify the situation so that correct pressure is achieved. This resulted in lowering the normal loading force to 3.5 kN opposed to 20-30 kN on the real track. Although this means that the exciting forces will be lower than the scale suggests, it will only decrease the amplitude of dynamic processes.

4.2 Rail stiffness

The actual stiffness of the rail changes as the wheel travels along the sleepers. Also, the mass of the rail cannot be precisely modelled. The case

when wheel is between sleepers was selected for its lowest stiffness. If such a need arises, it is possible to modify the machine by further reinforcing the bridging beams and thus effectively reducing the compliance of rail disc. However, the current understanding suggests that the wheel itself plays the main role in wheel-squeal origin and the aim of this study is to find a reliable way to prevent wheel-squeal by applying a friction modifier or by changing the dynamic properties of the wheel, thus modification of the rail stiffness is not expected.

4.3 Damping

Damping of the wheel is preserved thanks to the usage of a real wheel. Damping of rail and the suspension system is not considered at this point and its effect on wheel-squeal is not well known. Simulation of damping in the primary suspension of the wheel could be introduced by modifying the loading system with a damper. However, modulation of the rail damping would be challenging.

4.4 Slip without setting AoA

Currently, rolling of the rail disc is caused by the traction force in the contact and creepage is controlled only by setting the AoA. To control the slip in the longitudinal direction with an aligned disc, a brake would have to be applied to the disc shaft. While such modification is certainly possible, special attention should be paid when selecting the braking system as regular frictional brakes could excite the dynamic system with a stick-slip effect and compromise the overall dynamic behaviour. As the current intention is to study the contact behaviour in lateral direction with applied AoA, a brake is not needed.

5. CONCLUSION

The twin-disc test rig was designed to allow to investigate the squeal noise phenomenon due to unstable frictional behaviour of the contact. The main features of the test rig are as follows:

- The dynamic model has been utilized considering the real stiffness of the wheel suspension and the track;
- Full-scale train wheel provides realistic noise emission;
- Lateral creepage and resulting lateral force can be varied by changing the angle of attack of the upper rail disc;

- Adhesion behaviour in the lateral and longitudinal directions and noise can be investigated;
- The effect of various lubricants, friction modifiers and environmental conditions can be studied.

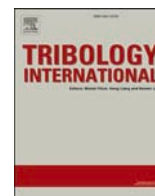
ACKNOWLEDGEMENT

This research was supported by the Czech Science Foundation (Project No. 20-23482S).

REFERENCES

- [1] B. Müller, J. Oertli, Combating Curve Squeal: Monitoring existing applications. *Journal of Sound and Vibration*, 293(3-5), 2006: 728-734. <https://doi.org/10.1016/j.jsv.2005.12.005>
- [2] J.R. Koch, N. Vincent, H. Chollet, O. Chiello, Curve squeal of urban rolling stock — Part 2: Parametric study on a 1/4 scale test rig. *Journal of Sound and Vibration*, 293(3-5), 2006: 701-709. <https://doi.org/10.1016/j.jsv.2005.12.009>
- [3] E.A.G. Hernandez, Wheel and Rail Contact Simulation Using a Twin Disc Tester (Ph.D. thesis). *The University of Sheffield*, Sheffield, 2008.
- [4] W.J. Wang, S.R. Lewis, R. Lewis, A. Beagles, C. G. He, Q. Y. Liu, The role of slip ratio in rolling contact fatigue of rail materials under wet conditions. *Wear*, 376-377, 2017: 1892-1900. <https://doi.org/10.1016/j.wear.2016.12.049>
- [5] M. Naeimi, Z. Li, R.H. Petrov, J. Sietsma, R. Dollevoet, Development of a New Downscale Setup for Wheel-Rail Contact Experiments under Impact Loading Conditions. *Experimental Techniques*, 42(1), 2018: 1–17. <https://doi.org/10.1007/s40799-017-0216-z>
- [6] S. S. Hsu, Z. Huang, S. D. Iwnicki, D. J. Thompson, C. J. C. Jones, G. Xie, P. D. Allen, Experimental and theoretical investigation of railway wheel squeal. *Proceedings of the Institution of Mechanical Engineers, Part F: Journal of Rail and Rapid Transit*, 221(1), 2007: 59–73, <https://doi.org/10.1243/0954409JRRT85>
- [7] F G. de Beer, M.H.A. Janssens, P.P. Kooijman, Squeal noise of rail-bound vehicles influenced by lateral contact position. *Journal of Sound and Vibration*, 267(3), 2003: 497-507. [https://doi.org/10.1016/S0022-460X\(03\)00710-7](https://doi.org/10.1016/S0022-460X(03)00710-7)

- [8] A.D. Monk-Steel, D.J. Thompson, F.G. de Beer, M.H.A. Janssens, An investigation into the influence of longitudinal creepage on railway squeal noise due to lateral creepage. *Journal of Sound and Vibration*, 293(3-5), 2006: 766-776. <https://doi.org/10.1016/j.jsv.2005.12.004>
- [9] L. Walls, Test Rig Design for Simulation and Identification of Rail Corrugation (Ph.D. thesis). *The University of Queensland*, Queensland, 2003.
- [10] P.A. Meehan, X. Liu, Modelling and mitigation of wheel squeal noise amplitude. *Journal of Sound and Vibration*, 413, 2018: 144-158. <https://doi.org/10.1016/j.jsv.2017.10.032>
- [11] P. A. Meehan, X. Liu, Modelling and mitigation of wheel squeal noise under friction modifiers. *Journal of Sound and Vibration*, 440, 2019: 147-160. <https://doi.org/10.1016/j.jsv.2018.10.025>
- [12] P.A. Meehan, X. Liu, Wheel squeal noise control under water-based friction modifiers based on instantaneous rolling contact mechanics. *Wear*, 440-441, 2019: 203052. <https://doi.org/10.1016/j.wear.2019.203052>
- [13] Y. Jin, M. Ishida, A. Namura, Experimental simulation and prediction of wear of wheel flange and rail gauge corner. *Wear*, 271(1-2), 2011: 259-267. <https://doi.org/10.1016/j.wear.2010.10.032>
- [14] P. Voltr, M. Lata, O. Cerny, Measuring of wheel-rail adhesion at a test stand, 8th International Conference Engineering Mechanics, 2012, Svratka, Czech Republic, pp.1543-1553.
- [15] P. Voltr, M. Lata, Transient wheel-rail adhesion characteristics under the cleaning effect of sliding. *Vehicle System Dynamics*, 53(5), 2015: 605-618. <https://doi.org/10.1080/00423114.2014.961488>
- [16] R. Galas, D. Smejkal, M. Omasta, M. Hartl, Twin-disc experimental device for study of adhesion in wheel-rail contact. *Engineering Mechanics*, 21, 2014: 329-334.
- [17] D.J. Thompson, G. Squicciarini, B. Ding, L. Baeza, A State-of-the-Art Review of Curve Squeal Noise: Phenomena, Mechanisms, Modelling and Mitigation. *Notes on Numerical Fluid Mechanics and Multidisciplinary Design*, 139, 2018: 3-41. https://doi.org/10.1007/978-3-319-73411-8_1
- [18] M.J. Rudd, Wheel/rail noise - Part II: Wheel Squeal. *Journal of Sound and Vibration*, 46(3), 1976: 381-394. [https://doi.org/10.1016/0022-460X\(76\)90862-2](https://doi.org/10.1016/0022-460X(76)90862-2)
- [19] P.A. Meehan, Prediction of wheel squeal noise under mode coupling. *Journal of Sound and Vibration*, 465, 2020: 115025. <https://doi.org/10.1016/j.jsv.2019.115025>
- [20] N. Bosso, M. Spirzagin, A. Gugliotta, A. Soma, Mechatronic Modeling of Real-Time Wheel-Rail Contact, *Springer*, Heidelberg, 2013.



An approach for the creep-curve assessment using a new rail tribometer

Martin Valena^{*}, Milan Omasta, Daniel Kvarda, Radovan Galas, Ivan Krupka, Martin Hartl

Faculty of Mechanical Engineering, Brno University of Technology, Technická 2896/2, 616 69 Brno, Czech Republic

ARTICLE INFO

Keywords:

Wheel-rail tribology
Portable tribometer
Creep curve
Coefficient of traction

ABSTRACT

The friction properties of the wheel-rail contact are characterized by a coefficient of traction (CoT), which can be affected by many contaminants. Numerous devices for assessing CoT are available; however, only a small number of them are capable of recording creep curves. This work introduced a rail-mounted tribometer that uses controlled changes in braking torque on a measuring wheel to induce creep in the contact. A methodology for assessing creep curve parameters was proposed, utilizing both analytical and numerical models of the contact. The experiments were performed both in the field and in the laboratory to investigate the effect of railhead conditions under various contact pressures and to track the evolution of the CoT during a measurement.

1. Introduction

A coefficient of traction (CoT) is one of the most important parameters characterizing the conditions in the wheel-rail contact. A high CoT value leads to excessive wear, high rolling resistance and corrugation making the operation more expensive [1]. On the other hand, low value causes problems with traction and braking, such as increased braking distance. The CoT is mainly affected by conditions of a wheel and a rail surface, 3rd body layers, environmental conditions, etc. High humidity, iron oxides, flange lubricants and leaves reduce the CoT, while sanding is used to increase it [2]. In addition to CoT, the wheel-rail contact is characterised by a creep curve, which is a CoT dependency on creep. In the low creep region, CoT rises steeply, then saturates and continues to rise slowly or starts to fall. "Dry" conditions usually show a falling creep curve, leading to stick-slip oscillations that may cause corrugation and generate squeal noise [3–5]. To prevent these phenomena, top-of-rail (TOR) products are applied to the contact to reduce the CoT to an intermediate value (0.2 – 0.4) [6] and provide a positive friction characteristic. Exact values may vary depending on the rail system. These parameters are measured in the laboratory using test rigs or in the field using instrumented trains or tribometers.

The laboratory provides well-controlled conditions for experiments, which is a major advantage over field measurements; however, with lower representativeness. There are many types of laboratory test rigs and tribometers available for studying wheel-rail contact. High-pressure torsion test rig (HPT) allows a simple 3rd body characterisation [7,8], pin-on-disc tribometers provide basic friction and wear data [9,10] and ball-on-disc tribometers like Mini-Traction Machine (MTM) are used to

determine creep curve in the rolling-sliding contact [11,12]. The most widely used is a small-scale twin-disc concept that provides an optimal ratio between contact representativeness and testing costs. Rolling-sliding contact can be achieved with a controlled slip [13–17] or a torque [18,19]. Small-scale test rigs with a disc in rotation on a circular rail are also used [20,21]. The most realistic configuration is provided by full-scale tribometers using a train wheel and another disc representing the rail [22,23] or the rail itself [24–26].

There are several ways to determine the friction level on a railway. The simplest way is to measure the coefficient of friction using a simple sliding tribometer such as the Pendulum that is based on the energy loss measuring principle [27,28]. On the other side, the most representative is the measurement of the CoT with a locomotive equipped with a measuring system that records the traction forces and sliding velocities of all the bogies when the sliding occur [29,30]. These experiments are very expensive. A less expensive option is to use rolling-stock brake testing, especially together with low adhesion simulants [25,31] or TOR products [14].

A compromise is to use field tribometers inducing a rolling-sliding contact between a measuring wheel and the rail. Several generations of such devices were developed during the last decades. One of them is a car-pushed tribometer TriboRailer [32], where the creep is induced by rotating the measuring wheel around the yaw axis. A widely used device is the hand-pushed tribometer from Salient Systems [29,32,33]. This device utilizes an application of ramping braking force to the measuring wheel by an electromagnetic brake to determine when the measuring wheel begins to slip. The corresponding braking torque is then used to determine the coefficient of friction. The TriboMetro FR 101 hand-pushed tribometer works on a similar principle, but provides the

^{*} Corresponding author.

E-mail address: Martin.Valena@vut.cz (M. Valena).

Nomenclature			
A	Ratio of CoT at zero and infinity slip velocity	M_B	Braking torque
a, b	half-axes of the contact ellipse	p	Contact pressure
B	Coefficient of exponential friction decrease	Q	Wheel load
C	Proportionality coefficient characterising the contact shear stiffness	s	Rigid slip
CoT	Coefficient of traction	T	Traction force
CoT _e	Effective CoT	u	Surface displacement
D	Diameter of measuring wheel	v	Rolling velocity
F	Tangential contact force	v_L	Longitudinal speed of measuring module
I	Momentum of inertia	v_R	Tangential speed of measuring wheel
k_A	Reduction factor in the area of adhesion	w	Total creep (slip) velocity
k_S	Reduction factor in the area of slip	α	Angular acceleration
L_1	Kalker's contact flexibility	ε	Gradient of the tangential stress in the area of adhesion
L_e	Elastic flexibility of 3rd body layer	μ_0	Maximum CoT at zero slip velocity
L_p	Plasticity parameter	μ_{c1}	Elasticity limiting coefficient of friction
		μ_{c2}	Plasticity limiting coefficient of friction
		τ	Shear stress
		τ'	Shear stress in the previous calculation step

entire creep curve [34]. Hand-pushed tribometers give an average value of friction coefficient from a longer section of the track (e.g. 30 m in the case of TriboMetro FR 101 [34]) and generally overestimate the coefficient of friction [29]. Because of the averaging, the results are rather rough and these devices are not suitable for determining the traction curve at a specific place on the rail.

The latest generation of field tribometers includes the Hand-operated (HO) tribometer [35–37], also called OnTrak [38]. In this device, creep is induced in the lateral direction by rotating the measuring wheel with a certain angle of attack (AoA), i.e. in a similar way to the TriboRailer. The measurement can be performed with a constant or a changing AoA that can be set to achieve approx. 16% creep according to [37,38], so the HO tribometer operates in a low-creep regime. Changing AoA allows the creep curve to be evaluated in one pass, but this mode is not reliable. Use of controlled slip in a lateral direction to build a traction curve may be considered less representative.

Various lab-scale contact simulators, field tribometers and instrumented wheels differ from each other in the way they simulate the rolling-sliding contact, in the measurement principle, in the contact geometry and materials and in the representativeness of the friction layer studied. Typically, lab-scale measurements give higher friction under dry conditions due to a stronger formation of wear and oxide particles. Rail tribometers tend to give lower values depending on the conditioning of the counter body. In all the scaled tests, the formation of the friction layer is of a transient nature, which should be considered when interpreting the results under dry conditions. Moreover, the results vary greatly depending on the cleaning procedure, a common part of laboratory tribological tests.

Time-consuming and costly measurements using the instrumented train, the difficult use of complex track tribometers and the low representativeness of simple portable devices make a fast assessment of frictional properties on the rail head challenging. Since it is nearly impossible to simulate the formation of a real friction layer in the laboratory, an experimental device with rolling-sliding contact enabling measurement on the rail in both field and laboratory conditions is required. Comparison of results using the same methodology in the field and in the laboratory will provide a better understanding of the real friction layer formation.

This work aims to introduce an approach utilizing a new portable rail tribometer with a controlled traction force to evaluate the creep curve. Fitting a creep force model to the experimental data allows for a simple and fast assessment of the tribological properties of the 3rd body layer formed on the rail. This approach can be used in both laboratory and field research into the wheel-rail interface and in the implementation of friction-management techniques etc.

2. Material and methods

2.1. Experimental device

A new tribometer (BUT rail tribometer), shown in Fig. 1, has been developed to study adhesion conditions on a rail in the field or in the laboratory. The main part of the tribometer is a horizontal linear unit with a timing-belt drive and a carriage. The ends of the unit are embedded in bases equipped magnets to fix the device to the rail. A stepper motor is used to drive the linear unit and to move the carriage with a measuring module along the rail. Its linear position is determined using a rotary encoder on the drive. The device is powered by a battery.

The measuring module, shown in Fig. 1, is attached to the carriage by a linear guide allowing free movement in the vertical direction to allow

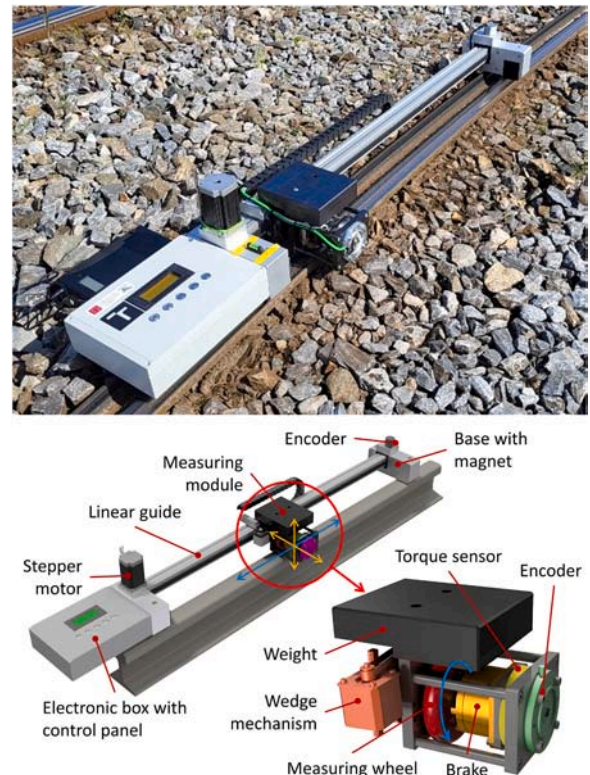


Fig. 1. BUT rail tribometer and the measuring module detail.

loading using a dead weight. Moreover, there is a wedge mechanism with a stepper motor to provide automatic positioning of the module in lateral direction, allowing measurements to be made on different contact paths. The measuring wheel is fixed on a shaft and attached to the rotor of the electromagnetic brake. Braking torque is measured with a torque transducer and shaft speed is recorded by the encoder. The measuring wheel is made of bearing steel and has a diameter of 100 mm and a transverse radius of 10 mm. The dimensions correspond to a scale of the contact width in the lateral direction of 1:10. The normal contact force is developed by the mass of the measuring module and additional weights, resulting in the theoretical Hertzian contact pressure of 0.8, 0.9 or 1 GPa. All parameters of the BUT rail tribometer are summarised in Table 1.

2.2. Data acquiring and processing

The relationship between the traction coefficient and creep is analysed by processing multiple signals to obtain a typical creep curve. The traction coefficient is calculated using data from the torque transducer attached to the brake, while the creep value is computed based on the values of the longitudinal module speed and the tangential wheel speed. Both these speeds are determined using rotary shaft encoders (see Fig. 1). Based on this data, a typical creep curve is plotted, as depicted in Fig. 2b. The stepper motor of the linear unit drives the measuring module along the rail. After reaching a constant speed of 260 mm/s, the brake starts to apply a braking torque according to the measuring mode described below. During a measurement, the wheel is rolling due to the traction force in the contact. When the brake develops sufficient torque, the creep starts to increase rapidly resulting in a blocking of the wheel and pure sliding in the contact. At the end of each measurement pass the data from the encoders and the torque transducer are post-processed automatically and the position-creep and position-braking torque curves (Fig. 2a) and the corresponding creep curve (b) are plotted.

The tribometer can operate in three measuring modes controlled by the three following parameters – initial and final braking torques and a number of steps. In the first mode, "Constant" (Fig. 3a), the measuring module runs over a rail section with constant braking torque. It is useful when some rail head sections have significantly different CoT and are too short to be investigated separately (e.g. TOR product spots) or when low-adhesion occurs as a transition phenomenon (e.g. during water evaporation). In the second one called "Step ramp" (b-c) the torque is gradually increased or decreased according to the set values and the steps are evenly distributed along the pass. Its main characteristic is the ability to make a creep curve in a single pass, while assuming adhesion conditions to be equal along the pass. The last mode (d) is called "Pulse" and alternates between two braking torques. The number of steps indicates the number of braking torque changes. It can be used when several transitions between rolling and sliding are required. In this study, only the Step ramp mode was used for all measurements.

The Gaussian filter is applied to a record of positions from the wheel and drive encoders, from which the velocities are calculated by using

Table 1
Parameters of the BUT rail tribometer.

Dimensions (mm)	1635 × 270 × 210
Weight (without battery and laptop) (kg)	21
Maximal evaluated distance (mm)	700
Minimal evaluated distance (mm)	200
Total stroke length (mm)	800
Range of lateral position (mm)	8
Speed of measuring module (mm/s)	260
Maximal Hertz pressures (GPa)	0.8, 0.9, 1
Normal force (N)	76, 110, 152
Measuring modes	Constant, step ramp, pulse
Contact	Elliptical
Main and transverse radii (mm)	50 and 10
CoT range (1)	0.02 – 0.7

numerical derivation. Creep is given by Eq. (1) and pure sliding conditions correspond to 100%. The tangential force in the contact is obtained from an equilibrium of momentum (Eq. 2). The normal force is not measured directly; it is assumed to be a constant that was determined from the actual mass of the measuring module and weights. The CoT is defined as the ratio of the tangential and the normal forces (Eq. 3).

$$creep = \frac{v_L - v_R}{v_L} \cdot 100\% \quad (1)$$

$$T = \frac{2}{D}(I\alpha + M_B) \quad (2)$$

$$CoT = \frac{T}{Q} \quad (3)$$

2.3. Assessment of creep curve parameters

The raw data from the measurement is a point cloud, as shown in Fig. 2b, that is further processed. Three methods have been proposed to properly compare the traction curves and quantify their parameters.

The first one is the simplest and it only determines the effective CoT (CoT_e), i.e. a value at which the initial steep curve part transforms into the flat part that can slightly rise, fall or stay neutral. The braking torque is the controlled parameter and is used to calculate the CoT, so it can be said that the CoT is indirectly controlled; therefore, it must be evaluated in relation to the creep. The data from the passes are combined and only those that are within 5–15 per cent of the creep are selected to calculate a median CoT value. The 5% reliably separates points in the initial steep part of the curve, while the 15% provides enough points to calculate the median CoT.

The second method is based on the data approximation by Polach's model [39]. The tangential force in the contact F is calculated using Eqs. 4–7, where μ_0, A, B, k_A, k_S are sought parameters. The fit of the unadjusted data cannot achieve the same steepness in the low creep region as the measured data, so the following procedure has been proposed. The points are divided into three regions: – 10–5, 5–8 and 8–100 (Fig. 4a). The points in region I are approximated by the linear function passing through the origin (the black solid line in region I). This function is used to calculate new points (red points) that are equally distributed from the CoT minimum to the median. The median is computed from points in region II. The new dataset (Fig. 4b), which is subsequently fitted by Polach's model, consists of the calculated points in region I and the original points in regions II and III.

$$\mu = \mu_0 [(1 - A)e^{-Bw} + A] \quad (4)$$

$$\varepsilon = \frac{2}{3} \frac{C\pi a^2 b}{Q\mu} \quad (5)$$

$$F = \frac{2Q\mu}{\pi} \left(\frac{k_A \varepsilon}{1 + (k_A \varepsilon)^2} + \arctan(k_S \varepsilon) \right) \quad (6)$$

$$C = 3.2893 + \frac{0.975}{\frac{b}{a}} - \frac{0.012}{\left(\frac{b}{a}\right)^2} \quad (7)$$

The third method uses the modified FASTSIM model based on publication [40]. The model calculates shear stresses across a discretized contact area. This model assumes an elasto-plastic 3rd body layer on contacting surfaces, that affects the initial slope of the creep curve and limits CoT. The initial slope is reduced by adding the 3rd body layer flexibility coefficient L_e to Kalker's flexibility coefficient L_1 into FASTSIM calculation, as seen in Eq. 8. The τ' represents shear stress from the previous calculation step that is located with a step difference Δa across the longitudinal strip. When the calculation exceeds the elastic limit $\mu_{c1}P$ a pseudo-plastic material model published by Voce [41] is used. Shear

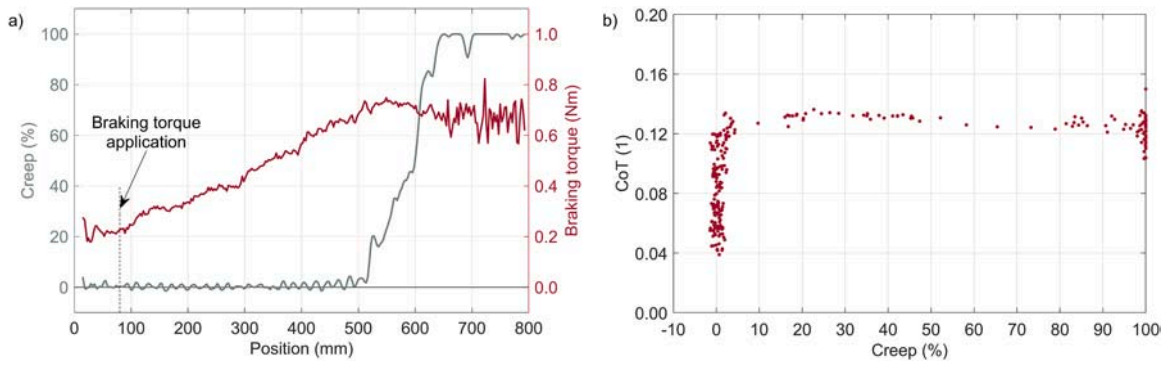


Fig. 2. a) Position-creep and position-braking torque curves of one pass obtained under step ramp measuring mode, b) corresponding creep curve.

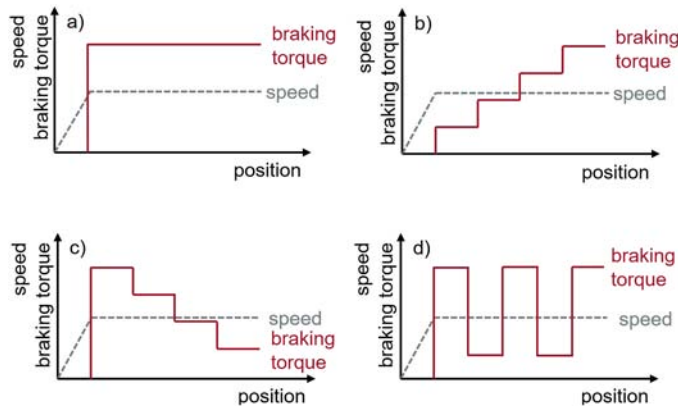


Fig. 3. Measuring modes: a) Constant, b) Step ramp - increasing c) Step ramp - decreasing, d) Pulse.

stresses in the pseudo-plastic region are defined by Eq. (9). The displacement value u is calculated using the equation from the elastic region. In these equations, the normal stress p is calculated in each discretized point using Hertzian contact theory. The resulting CoT is a ratio between shear stresses and normal stresses.

$$\tau = \tau' - \frac{2\Delta a}{v} \frac{s}{L_1 + L_e} \quad (8)$$

$$\tau = \mu_{c1}P + (\mu_{c2}P - \mu_{c1}P)(1 - e^{(-u + \mu_{c1}PL_e)/L_p}) \quad (9)$$

2.4. Conditions of experiments

The tests in this study were carried out in the laboratory on UIC60 rail under ambient temperature and relative humidity of 25 °C and 38%,

respectively, and in field on the rail of a light rail transit at the temperature and relative humidity of 6 °C and 50%, respectively. The measuring wheel was cleaned with acetone before each series of passes to normalise its conditions and to make the results comparable. Three series of tests were carried out as follows and as indicated in Table 2.

The aim of the first test series consisting of 12 measurements was to investigate the effect of railhead conditions under various contact pressure on the CoT and a creep curve shape in laboratory-controlled conditions. The individual measurements involved a certain number of passes of the measuring module on the same contact path, while the resulting creep curves were derived from all the passes. The measurements were made for Hertzian contact pressure of 0.8, 0.9 and 1.0 GPa. The following contact conditions were simulated:

- The “clean” conditions are considered to represent the initial state of the rail after the cleaning. The rail was cleaned with acetone to remove any dirt and lubricant residues, but the presence of naturally occurring oxide layers has been assumed. During the measurement, the number of passes was limited to one or two due to the rapid increase in friction on repeated passes.
- The “run-in” conditions represent a 3rd body layer produced by a normal traffic. This layer was simulated using a wheel-rail contact device consisting of a cylindrical disc rolling along the tested rail with 2% slip and 0.8 GPa contact pressure. The run-in process has included 100 passes of the “conditioning” disc conducted before each test. After the run-in the rail surface was not cleaned to keep oxides and wear particles in place for the test.
- The water condition simulates heavy rain. The rail was cleaned with a solvent followed by a run-in process. Subsequently, the contact path was wiped with a dry cloth to remove excessive wear debris. Before the test, 20 ml of water was applied evenly along the length of the tested part of the rail.
- The TORL conditions correspond to the presence of a TOR lubricant (TORL) residual layer on a rail after several overruns. The tested part

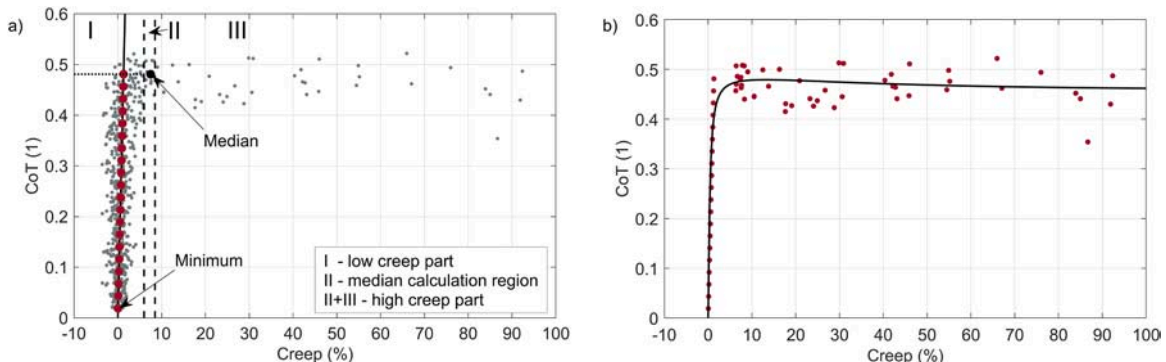


Fig. 4. Data adjustment for fitting (a) the original dataset and new point in the region I, b) a new dataset fitted by Polach's model.

Table 2
Conditions of tests.

Test series	Rail conditions	Contact pressure (GPa)	Number of passes	Rail run-in	Rail cleaning	
1	Clean	0.8	2	no	yes	
		0.9	1	no	yes	
		1	2	no	yes	
	Run-in	0.8	13	yes	no	
		0.9	7	yes	no	
		1	9	yes	no	
	Water	0.8	12	yes	yes	
		0.9	11	yes	yes	
		1	14	yes	yes	
	TORL	0.8	7	yes	no	
		0.9	11	yes	no	
		1	11	yes	no	
	2	Oil-based lubricant	0.9	30	no	no
	3	laboratory	0.9	37	no	yes
field		0.9	20	no	yes	
field		0.9	20	no	no	

of the rail was evenly covered with 100 μ l of conventional grease-based TORL, which was then wiped out with a paper towel as much as possible to create a thin layer that corresponds to the condition of the rail in real operation when TORL is used.

The second test series was aimed to demonstrate the repeatability of measurements. For this purpose, the rail was coated with a conventional oil-based lubricant (WD-40) to ensure stable friction conditions during individual passes. The measuring wheel was cleaned as for the previous measurements. The tribometer parameters were set so that the entire creep curve could be recorded during one pass, allowing the CoT_e to be evaluated and compared for each pass. A total of 30 passes were made at 0.9 GPa contact pressure.

The last set of measurements was carried out in the laboratory and in the field to investigate the effect of evolution of CoT . The contact pressure of 0.9 GPa was selected and the tribometer parameters were set to record the entire creep curve in one pass. In the laboratory, the rail was cleaned with a solvent to remove contaminants, while a run-in process was not included. In the field, a visibly clean section of the track, free of contaminants, was chosen. The intention was to observe the CoT evolution under real conditions, therefore the rail was not cleaned with a solvent and a run-in process was not performed.

3. Results and discussion

3.1. Effect of railhead conditions and contact pressure

Fig. 5 shows creep curves recorded under three contact pressures and four rail conditions. Each graph contains points from all measuring passes, further fitted by Polach's model (solid yellow) and modified FASTSIM model (dashed black). The parameters of the modified FASTSIM model are listed in Table 3. The agreement between the models is very good in almost all cases, only the run-in conditions show larger differences around the saturation point and at higher creep values but still show the same curve trend. The traction curves determined using the tribometer are relatively steep in the elastic area. The intersection of the linear region with the friction coefficient occurs at a creep of 1–2%, which is much closer to a prediction compared to other field tribometer [37].

The creep curves (Fig. 5) show a relatively low scatter that depends mainly on the number of measuring passes. The lowest scatter of the points is reported for the clean conditions (graph a-c), where only one or two passes were made. On the other hand, the run-in conditions (graph d-f) show the highest scatter of the points due to the device dynamics at higher CoT and creep. Slight variability in frictional conditions along the

pass may also play a role, as further discussed.

The creep curves in Fig. 5a-c were recorded after the rail had been cleaned to remove all contaminants and residual grease. The curve trends change from slightly increasing to slightly decreasing with increasing the contact pressure, but the CoT_e values vary between 0.20 and 0.23, which is an intermediate friction value [6]. The run-in process shifts the CoT_e values to 0.4–0.5 (graph d-f) and the curves show a decreasing tendency for all contact pressures.

Water reduces the CoT_e to 0.35 – 0.4 and maintains the same curve trend (graph g-i) but the slope of the high creep part is not as steep as for the run-in conditions. The last three creep curves (graph j-l) represent the measurement after the application of TORL. The CoT_e reaches the lowest values, between 0.13 and 0.16. The trends of the curves at high creep are slightly increasing in two cases and slightly decreasing in the third (l).

The clean and the run-in conditions are considered as “dry” because no artificial contaminants are present, but they result in totally different creep curves in terms of the CoT and shape. It is assumed that the rail surface is covered with a thin oxide layer that reduces adhesion under the clean conditions. This layer is very easy to remove, so when more passes were made, the creep curve has a strong upward tendency in the high creep region as a result of energy dissipation due to the frictional work. This phenomenon will be discussed below. The run-in process has a cleaning effect removing the oxide layer. On the other hand, it promotes the formation of another layer consisting mainly of Magnetite (Fe_3O_4). This oxide tends to increase CoT [42].

In the case of water contamination, the CoT value is strongly dependent on the actual state of the resulting 3rd body layer. Relatively high values obtained in this study are consistent with previous data measured on MTM with samples made from the same material [43]. Lower values occur mainly in the field due to the interaction with other naturally occurring contaminants. Prolonged exposure to water also leads to the formation of hydrates [44], which usually reduce adhesion.

TORL should maintain an intermediate level of friction and ensure positive friction characteristics [5,6]. This statement cannot be fully approved because the trends of the curves are slightly increasing in two cases (Fig. 5j, k) and slightly decreasing in the third case (l). Although the residual layer containing a small amount of TORL was measured, the CoT values fall within the low friction band where lubricant should act, but TOR products should result in higher CoT . Studies [29,34] carried out in the field with the hand-pushed tribometer report similar CoT values, but a larger amount of TOR product was applied with a brush. On the other hand, different contact sizes affect the absolute CoT value compared to full-scale [24]. More TOR product ends up in a small contact, while less TOR product ends up in the actual contact because the excess is pushed away.

Fig. 6 shows the effect of the Hertzian contact pressure on the CoT under different conditions on the top of the rail head. The median (first) method was chosen for the evaluation, so the bars and error whiskers indicate the median of the selected points and the standard deviations, respectively.

The CoT decreases with increasing contact pressure for all conditions, while it is most evident for the run-in and the water conditions. The largest decrease was observed between 0.8 and 0.9 GPa in all cases, namely 10%, 12%, 8% and 13% for the clean, the run-in, the water and the TORL conditions, respectively. The results are consistent with other laboratory and field studies [18,32,34,45]. Studies using rail tribometers also report a significant decrease in the CoT for dry conditions, approximately 12% and 9% for a 0.1 GPa increase in contact pressure in the case of [34] and [45], respectively. The reduction depends on the conditions in contact as well as on the curvatures of the measuring wheel, roughness, and speed.

3.2. Comparison of evaluating methods

Three methods of evaluating the creep curve parameters have been

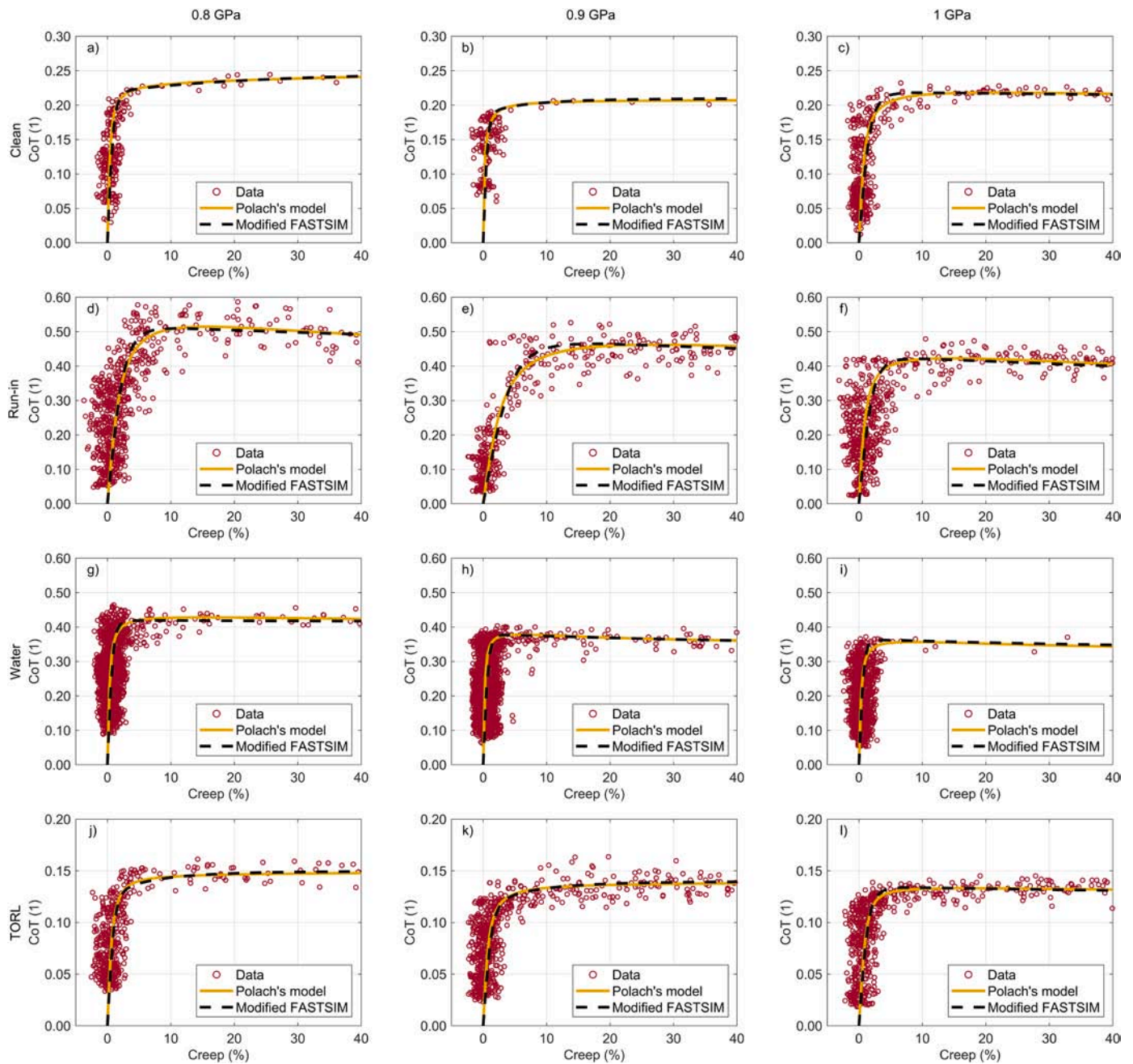


Fig. 5. Creep curves for clean, run-in, water and TORL conditions under contact pressure of 0.8, 0.9 and 1 GPa.

Table 3
Modified FASTSIM model parameters.

Conditions	Clean			Run-in			Water			TORL		
	0.8	0.9	1	0.8	0.9	1	0.8	0.9	1	0.8	0.9	1
μ_1 (1)	0.22	0.19	0.22	0.52	0.48	0.43	0.42	0.38	0.365	0.13	0.12	0.135
μ_2 (1)	0.25	0.21	0.21	0.45	0.35	0.3	0.41	0.34	0.33	0.15	0.14	0.125
L_e ($\times 10^{-6}$)	250	200	500	300	600	300	100	100	100	500	700	700
L_p ($\times 10^{-3}$)	1.8	0.5	4	5	10	10	8	4	4	0.5	0.5	5

proposed. To compare the median method with the other two, the 10% creep was chosen to calculate the CoT values using Polach's and the modified FASTSIM models. The comparison of these methods for 0.9 GPa contact pressure is shown in Fig. 7. Despite the different complexity of the methods, the results are almost identical for all

conditions except the run-in conditions, where the modified FASTSIM model gives a higher value of 0.033, which is 7%. The difference between the maximum and minimum values for the clean, water and the TORL conditions is 0.5%, 1.5% and 3.4% respectively. The median method gives good results, so it can be used for quick estimation of CoT_e,

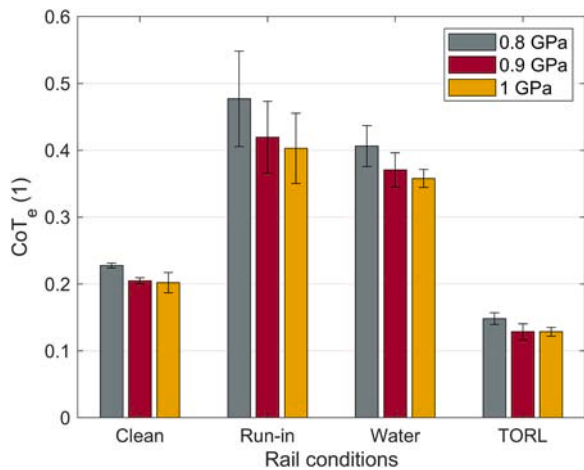


Fig. 6. Influence of contact pressure under clean, run-in, water and TORL conditions.

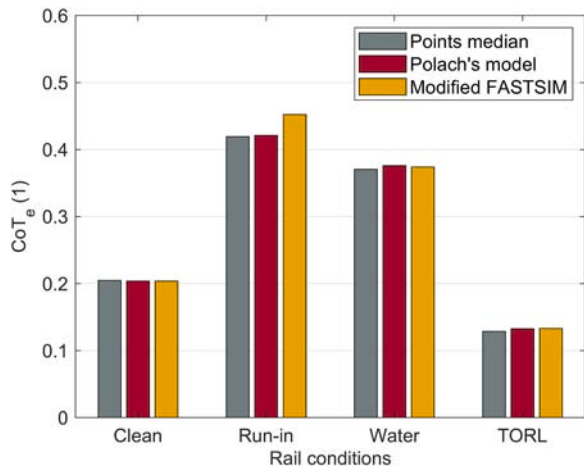


Fig. 7. Comparison of evaluation methods.

but it does not characterise the whole creep curve.

3.3. Repeatability of measurement

One of the important parameters of tribometers is the repeatability of the measurement, therefore a test under the stable friction conditions

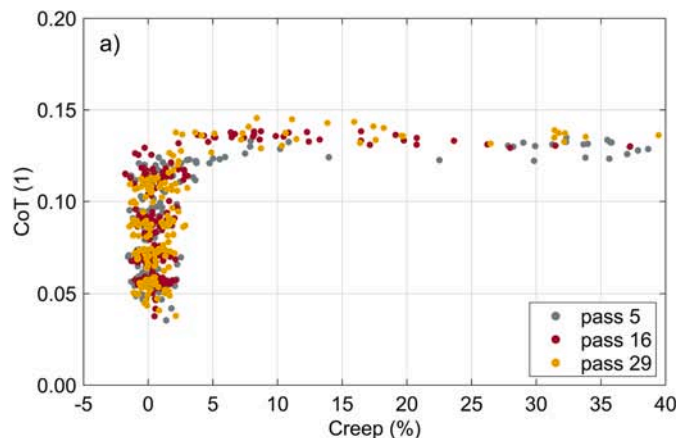


Fig. 8. a) Creep curves of repeatability test, b) CoT development with an increasing number of passes.

was carried out to define it. For better clarity, only some of the 30 passes are shown in Fig. 8a). The passes together form a creep curve without any large deviations caused by subsequent passes because the rail was coated with a conventional lubricant to maintain stable, unchanging conditions. The CoT_e values of all 30 passes with standard deviations are shown in Fig. 8b).

The mean CoT_e value is 0.1352 and the standard deviation is 0.0039 calculated for all passes. The maximum difference between individual passes and the mean is 0.0052 for the fifth and sixth passes. The most of further passes are slightly shifted higher thus the differences are smaller, around 0.0032, but there are still passes with a lower CoT_e.

3.4. The effect of subsequent passes

The final test series was carried out to define the effect of repeating passes along the same contact path when an evolution in friction conditions is assumed. The first measurement was made in the laboratory under clean conditions. It shows a strong upward trend with an increasing number of passes (Fig. 9). For the first 20 passes, the maximum braking torque applied was increased before each pass to record the entire creep curve. In some of the passes, the measuring wheel was blocked at the end of the pass resulting in 100% creep. Between passes 21 and 26 the maximum braking torque was not high enough, so the number of points in the high creep region was lower but the CoT_e remained similar. The maximum braking torque was gradually increased in the last ten passes, otherwise the entire creep curve would not be recorded. The last pass reached 0.55 CoT_e which corresponds to the creep curve in Fig. 5e).

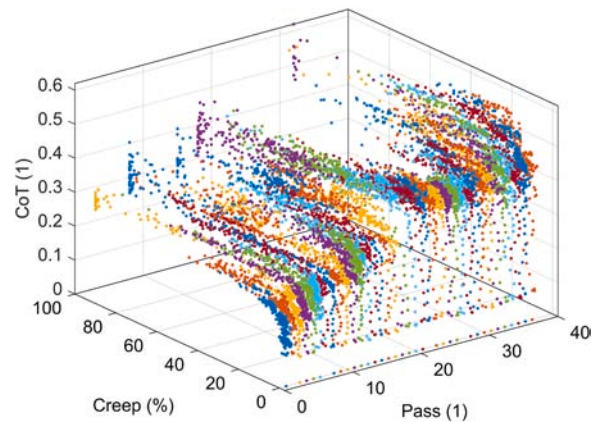


Fig. 9. Creep curve development with a rising number of passes.

A similar measurement was carried out in the field to compare the laboratory results with the real conditions. The comparison is shown in Fig. 10. In the case of the solvent-cleaned rail, the same trend and CoT_e gradient as in the laboratory was achieved, while the value of CoT_e was about 0.04 lower in the field. Once the solvent was not used for rail cleaning, a stable CoT_e of 0.25 occurred even after 20 passes. This indicates the presence of a durable 3rd body layer. The layer is made up of substances capable of absorbing the frictional work without changing the contact conditions despite the high creep achieved in each pass. However, the substances are easily soluble in acetone, resulting in much weaker 3rd body layer. It can be concluded, that although the solvent is often used in a laboratory to obtain reference conditions, it is not suitable when a real layer is studied. The cleaning process has significant effect not only to the instantaneous value of CoT but also on the durability of the 3rd body layer.

The previous study [46] reported an increasing CoT during a braking test. The following wheelsets reach a higher CoT than the previous one, which is caused by the cleaning effect. The following wheelsets can be represented by successive measuring passes [47]; therefore, the CoT should increase within the passes, but this did not happen in our case when the rail was not cleaned. A possible explanation is that the BUT rail tribometer does not deliver sufficient energy to the contact to induce the cleaning effect. This phenomenon should be further investigated.

The number of passes is a critical parameter with the ability to alter the results, so it should be respected during a measurement. A small number of passes should be selected to measure the current condition of the rail, e.g. oxide layer or easily removable layers. This will ensure that there is no degradation of the layer. On the other hand, a large number should be selected to evaluate wear resistance of the friction layer, which can be an important parameter e.g. for lubricants and TOR products.

3.5. Limitation in the study

The main uncertainties have been assessed (Table 4) to define a deviation of the measurement using the tribometer. Uncertainties such as the non-repeatability of the torque transducer and bearing losses are independent of the exact CoT value and they are two orders of magnitude smaller. A further uncertainty arises from the error between the actual and set diameters of the measuring wheel. This error is linearly dependent on the diameter deviation (e.g. a deviation of 0.2 mm corresponds to 0.2% of CoT). The largest uncertainty is caused by the normal force variation due to friction losses in vertical linear guides. The losses occur as the measuring wheel moves vertically and reacts to irregularities on the rail. It has been estimated to be up to 4% at a contact pressure of 0.9 GPa.

Another possible uncertainty lies in the clearances in the measuring

Table 4
Uncertainties of measurement.

Non-repeatability of torque transducer	0.00091 CoT
Bearing losses	0.00023 CoT
Diameter deviation	0.2 mm corresponds to 0.2% of CoT
Losses in vertical guides	Up to 4% of CoT

module and its guide. The traction force may cause a slight inclination of the module due to the clearances. The non-zero angle of attack creates a lateral creep which influences and reduces the longitudinal creep being evaluated [32]. Based on the investigations carried out, this deviation can be considered negligible.

In the addition to these uncertainties affecting CoT, there is also an error in creep measurement. This error is caused by the finite resolution of the encoders and it is directly responsible for the scatter of points in the low creep region (e.g. Fig. 8a), where the difference between the longitudinal and circumferential velocities is very small. It is also the reason for the negative creep values, as can be seen in the position data (Fig. 2a). This problem is overcome by the proposed fitting methods described in chapter 2.3.

The results may be affected by the material of the measuring wheel that is made of bearing steel with a higher hardness compared to regular wheel steel. Bearing steel was chosen for technological reasons, particularly because it provides much stable conditions. Moreover, lower wear of the measuring wheel has less effect on the real contact conditions.

3.6. Comparison with other tribometers

Several tribometers have been developed for assessing the CoT in the field, some of them are also suitable for laboratory use, see Fig. 11. These results indicate that all devices provide the highest traction coefficients under dry conditions. In the case of TOR products, the results cannot be directly compared because different TOR products were used, and the applied amounts were not the same. The effect of water also varies, which may be attributed to the amount or duration of water on the specimen surfaces. Furthermore, significant differences exist among these devices, including variations in contact body size, material, and roughness. It's also important to note that these devices differ significantly in terms of kinematics. While the BUT tribometer achieves typical rolling-sliding conditions, the pendulum tribometer operates under pure sliding conditions. Other devices, such as the HO tribometer, employ an angle of attack to simulate rolling-sliding conditions. Simultaneously, it is necessary to mention that the measurements were conducted at various locations and in different environments. Therefore, a straightforward comparison of values between tribometers can be misleading. Similarly, it is quite challenging to compare these values with data collected by an instrumented train if the measurements did not take

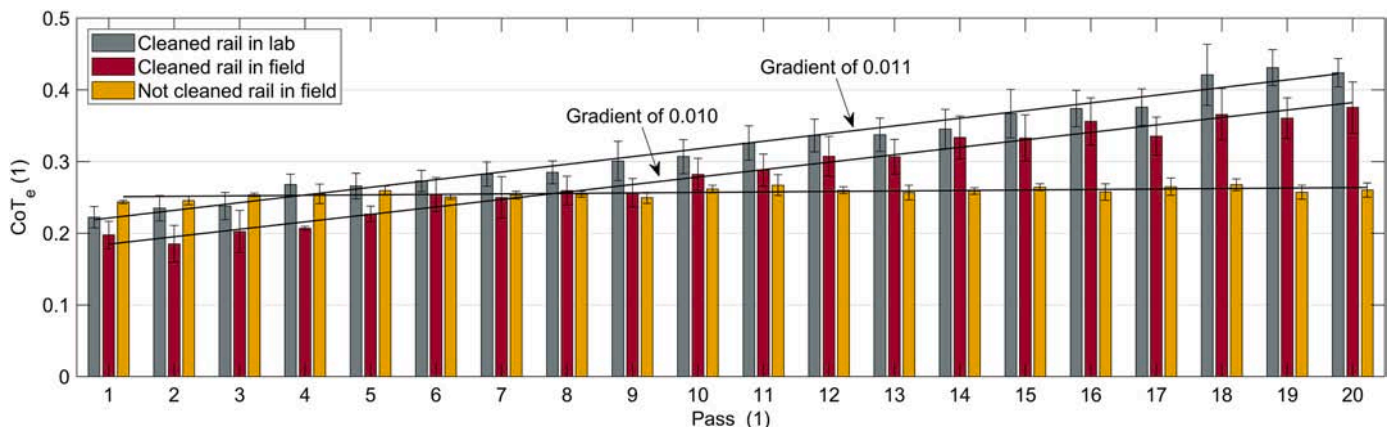


Fig. 10. CoT development in the field and in the laboratory.

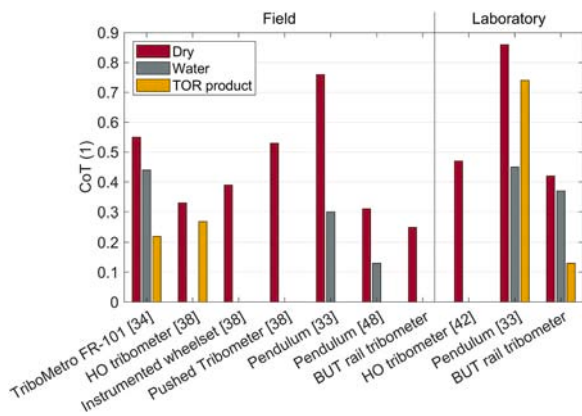


Fig. 11. The comparison of tribometers [33,34,38,42,48].

place simultaneously, on the same track, and under the same environmental conditions. Despite these limitations, these tribometers still enable comparative measurements, which can be very useful prior to testing using an instrumented train. Individual tribometers and their benefits are discussed below.

The Hand-pushed Tribometer [32], TriboMetro FR 101 [34] and HO tribometer [35] can measure the friction also at the gauge corner of the rail, whereas the Pendulum [33,48] and the BUT rail tribometer can only measure the CoT at the top of the rail. The extension of BUT rail tribometer will be made in future work.

TriboMetro FR 101, HO tribometer and BUT rail tribometer allow to assess the entire creep curve. The TriboMetro FR 101 and the BUT rail tribometer record the creep while the measuring wheel is braked, meanwhile, the HO tribometer yaws the wheel to induce lateral creep. The first method is closer to the actual wheel-rail contact. With the TriboMetro FR 101, measurements are taken over several metres of the rail, which can distort the resulting creep curve due to varying friction conditions along the measured section. The HO tribometer and the BUT rail tribometer are fixed to the rail and measure a shorter section of the rail, so the resulting creep curve is not as affected by changing friction conditions. These devices can also be advantageously used in a laboratory environment. When set up appropriately, the entire traction curve can be measured in one pass, so the negative effect of friction changes during repeated passes can be suppressed.

4. Conclusion

The new approach to the creep curve assessment using the new rail tribometer was presented. The measurement on the fixed part of the rail allows to study tribology of the wheel-rail interface in both, the laboratory and field. The controlled traction force approach has been chosen to simulate conditions of the real wheel-rail contact. Several approaches were implemented to evaluate the creep curve parameters. The creep curve measurement usually consists of several passes of the measuring module; nevertheless, if the control parameters are set correctly, the entire creep curve may be evaluated in one pass. The approach provides a useful tool to evaluate parameters of TOR products such as redistribution, carry distance, retentivity and others. Thanks to the high creep induced by the tribometer, and the ability to measure the entire traction curve in one pass, the tribometer can be used to investigate the wear resistance of the friction layer. This is especially important when developing friction layer models, implementing friction management techniques, etc.

The specific findings and conclusions from the application of the methodology are as follows:

- Effective coefficient of traction (CoT_e) decreases with increasing contact pressure.

- Traction curves were fitted by Polach's analytical model and modified FASTSIM model. Despite the different complexity of the methods, the results of CoT_e vary within 2% compared to the models describing the entire creep curve.
- The running-in of the rail increases CoT significantly and provides negative creep-curve characteristics. This conditioning technique is suitable to provide "reference" conditions in the laboratory.
- Using a solvent to clean the rail in the field significantly reduces the durability of the real 3rd body layer.

Statement of originality

As a corresponding author, I Martin Valena, hereby confirm on behalf of all authors that:

- 1) The authors have obtained the necessary authority for publication.
- 2) The paper has not been published previously, that it is not under consideration for publication elsewhere, and that if accepted it will not be published elsewhere in the same form, in English or in any other language, without the written consent of the publisher.
- 3) The paper does not contain material which has been published previously, by the current authors or by others, of which the source is not explicitly cited in the paper.

Upon acceptance of an article by the journal, the author(s) will be asked to transfer the copyright of the article to the publisher. This transfer will ensure the widest possible dissemination of information.

Declaration of Competing Interest

The authors declare that they have no known competing financial interests or personal relationships that could have appeared to influence the work reported in this paper.

Data availability

Data will be made available on request.

Acknowledgements

This work was carried out in the framework of the projects "Josef Bozek National Center of Competence for Surface Vehicles" (TN01000026) and "Bozek Vehicle Engineering National Center of Competence" (TN02000054) that were co-financed from the state budget by the Technology Agency of the Czech Republic within the programme "National Centres of Competence".

References

- [1] Harmon M, Lewis R. Review of top of rail friction modifier tribology. *Tribol - Mater Surf Interfaces* 2016;10:150–62. <https://doi.org/10.1080/17515831.2016.1216265>.
- [2] Olofsson U, Lyu Y. Open system tribology in the wheel-rail contact—a literature review. *Appl Mech Rev* 2017;69:1–10. <https://doi.org/10.1115/1.4038229>.
- [3] Eadie DT, Santoro M. Top-of-rail friction control for curve noise mitigation and corrugation rate reduction. *J Sound Vib* 2006;293:747–57. <https://doi.org/10.1016/j.jsv.2005.12.007>.
- [4] Eadie DT, Elvidge D, Oldknow K, Stock R, Pointner P, Kalousek J, et al. The effects of top of rail friction modifier on wear and rolling contact fatigue: Full-scale rail-wheel test rig evaluation, analysis and modelling. *Wear* 2008;265:1222–30. <https://doi.org/10.1016/j.wear.2008.02.029>.
- [5] Stock R, Stanlake L, Hardwick C, Yu M, Eadie D, Lewis R. Material concepts for top of rail friction management – classification, characterisation and application. *Wear* 2016;366–367:225–32. <https://doi.org/10.1016/j.wear.2016.05.028>.
- [6] White B, Lee ZS, Lewis R. Towards a standard approach for the twin disc testing of top-of rail friction management products. *Lubricants* 2022;10:124. <https://doi.org/10.3390/lubricants10060124>.
- [7] Evans M, Skipper WA, Buckley-Johnstone L, Meierhofer A, Six K, Lewis R. The development of a high pressure torsion test methodology for simulating wheel/rail contacts. *Tribol Int* 2021;156:106842. <https://doi.org/10.1016/j.triboint.2020.106842>.

- [8] Kvarda D, Skurka S, Galas R, Omasta M, Shi L, Ding H, et al. The effect of top of rail lubricant composition on adhesion and rheological behaviour. *Eng Sci Technol Int J* 2022;35:101100. <https://doi.org/10.1016/j.jestch.2022.101100>.
- [9] Lewis SR, Lewis R, Olofsson U, Eadie DT, Cotter J, Lu X. Effect of humidity, temperature and railhead contamination on the performance of friction modifiers: pin-on-disk study. *Proc Inst Mech Eng Part F J Rail Rapid Transit* 2013;227:115–27. <https://doi.org/10.1177/0954409712452239>.
- [10] Khalladi A, Elleuch K. Tribological behavior of wheel-rail contact under different contaminants using pin-on-disk methodology. *J Tribol ASME* 2017;139. <https://doi.org/10.1115/1.4033051>.
- [11] Galas R, Omasta M, Krupka I, Hartl M. Laboratory investigation of ability of oil-based friction modifiers to control adhesion at wheel-rail interface. *Wear* 2016;368–369:230–8. <https://doi.org/10.1016/j.wear.2016.09.015>.
- [12] Cann PM. The “leaves on the line” problem - a study of leaf residue film formation and lubricity under laboratory test conditions. *Tribol Lett* 2006;24:151–8. <https://doi.org/10.1007/s11249-006-9152-2>.
- [13] Arias-Cuevas O, Li Z, Lewis R, Gallardo-Hernandez EA, Gallardo-Hernández EA. Rolling-sliding laboratory tests of friction modifiers in dry and wet wheel-rail contacts. *Wear* 2010;268:543–51. <https://doi.org/10.1016/j.wear.2009.09.015>.
- [14] Galas R, Omasta M, Klapka M, Kaewunruen S, Krupka I, Hartl M. Case study: the influence of oil-based friction modifier quantity on tram braking distance and noise. *Tribol Int* 2017;39:198–206. <https://doi.org/10.24874/ti.2017.39.02.06>.
- [15] Zhu Y, Chen X, Wang W, Yang H. A study on iron oxides and surface roughness in dry and wet wheel-rail contacts. *Wear* 2015;328–329:241–8. <https://doi.org/10.1016/j.wear.2015.02.025>.
- [16] Shrestha S, Spiryagin M, Harisson H, Persson I, Meehan P, Wu Q, et al. Introduction of rail cleaning effect into locomotive traction study based on tribometer measurements. ICRT 2021 - Proc. 2nd Int. Conf. Rail Transp, vol. 15. Reston, VA: American Society of Civil Engineers; 2022. p. 41–51. <https://doi.org/10.1061/9780784483886.006>.
- [17] Chen H, Kimura S, Ikoma K, Ishizaka K, Suzumura J, Hibino S. Evaluation test of tangential force coefficient under different types of fallen leaves. *Wear* 2023;205072. <https://doi.org/10.1016/j.wear.2023.205072>.
- [18] Chen H, Namura A, Ishida M, Nakahara T. Influence of axle load on wheel/rail adhesion under wet conditions in consideration of running speed and surface roughness. *Wear* 2016;366–367:303–9. <https://doi.org/10.1016/j.wear.2016.05.012>.
- [19] Bosso N, Magelli M, Zampieri N. Investigation of adhesion recovery phenomenon using a scaled roller-rig. *Veh Syst Dyn* 2021;59:295–312. <https://doi.org/10.1080/00423114.2019.1677922>.
- [20] Guidoum S, Merino P, Saulot A, Berthier Y, Hervieu S. Experimental study of the influence of the relative humidity of leaves and their link to adhesion losses in the wheel-rail contact. *Mech Ind* 2022;23:23. <https://doi.org/10.1051/meca/2022017>.
- [21] Zhang P, Li Z. Experimental study on the development mechanism of short pitch corrugation using a downscale V-Track test rig. *Tribol Int* 2023;180:108293. <https://doi.org/10.1016/j.triboint.2023.108293>.
- [22] Voltr P, Lata M. Transient wheel-rail adhesion characteristics under the cleaning effect of sliding. *Veh Syst Dyn* 2015;53:605–18. <https://doi.org/10.1080/00423114.2014.961488>.
- [23] Zhang W, Chen J, Wu X, Jin X. Wheel/rail adhesion and analysis by using full scale roller rig. *Wear* 2002;253:82–8. [https://doi.org/10.1016/S0043-1648\(02\)00086-8](https://doi.org/10.1016/S0043-1648(02)00086-8).
- [24] Buckley-Johnstone L, Harmon M, Lewis R, Hardwick C, Stock R. A comparison of friction modifier performance using two laboratory test scales. *Proc Inst Mech Eng Part F J Rail Rapid Transit* 2019;233:201–10. <https://doi.org/10.1177/0954409718787045>.
- [25] White B, Hyland-Knight J, Lewis R. Assessing the effectiveness of traction gels using full-scale and field testing. *Proc Inst Mech Eng Part F J Rail Rapid Transit* 2021;235:690–9. <https://doi.org/10.1177/0954409720953943>.
- [26] Lewis SR, Riley S, Fletcher DI, Lewis R. Optimisation of a railway sanding system: adhesion tests. *Int J Railw Technol* 2017;6:87–98. <https://doi.org/10.4203/ijrt.6.2.5>.
- [27] Lewis SR, Lewis R, Olofsson U. An alternative method for the assessment of railhead traction. *Wear* 2011;271:62–70. <https://doi.org/10.1016/j.wear.2010.10.035>.
- [28] Lewis R, Lewis SR, Zhu Y, Abbasi S, Olofsson U. The modification of a slip resistance meter for measurement of railhead adhesion. *Proc Inst Mech Eng Part F J Rail Rapid Transit* 2013;227:196–200. <https://doi.org/10.1177/0954409712455147>.
- [29] Lundberg J, Rantatalo M, Wanhainen C, Casselgren J. Measurements of friction coefficients between rails lubricated with a friction modifier and the wheels of an IORE locomotive during real working conditions. *Wear* 2015;324–325:109–17. <https://doi.org/10.1016/j.wear.2014.12.002>.
- [30] Meierhofer A, Trummer G, Bernsteiner C, Six K. Vehicle tests showing how the weather in autumn influences the wheel-rail traction characteristics. *Proc Inst Mech Eng Part F J Rail Rapid Transit* 2020;234:426–35. <https://doi.org/10.1177/0954409719863643>.
- [31] Lanigan JL, Krier P, Johnstone LB, White B, Ferriday P, Lewis R. Field trials of a methodology for locomotive brake testing to assess friction enhancement in the wheel/rail interface using a representative leaf layer. *Proc Inst Mech Eng Part F J Rail Rapid Transit* 2021;235:1053–64. <https://doi.org/10.1177/0954409720973135>.
- [32] Harrison H, McCanney T, Cotter J. Recent developments in coefficient of friction measurements at the rail/wheel interface. *Wear* 2002;253:114–23. [https://doi.org/10.1016/S0043-1648\(02\)00090-X](https://doi.org/10.1016/S0043-1648(02)00090-X).
- [33] Harmon M, Santa JF, Jaramillo JA, Toro A, Beagles A, Lewis R. Evaluation of the coefficient of friction of rail in the field and laboratory using several devices. *Tribol - Mater Surf Interfaces* 2020;14:119–29. <https://doi.org/10.1080/17515831.2020.1712111>.
- [34] Areiza YA, Garcés SI, Santa JF, Vargas G, Toro A. Field measurement of coefficient of friction in rails using a hand-pushed tribometer. *Tribol Int* 2015;82:274–9. <https://doi.org/10.1016/j.triboint.2014.08.009>.
- [35] Harrison H. Development of a Third Generation Tribometer. CM2015–0130 2015; September.
- [36] Spiryagin M, Persson I, Hayman M, Wu Q, Sun YQ, Nielsen D, et al. Friction measurement and creep force modelling methodology for locomotive track damage studies. *Wear* 2019;432–433:202932. <https://doi.org/10.1016/j.wear.2019.202932>.
- [37] Persson I, Spiryagin M, Casanueva C. Influence of non-dry condition creep curves in switch negotiation. *Veh Syst Dyn* 2023;61:892–904. <https://doi.org/10.1080/00423114.2022.2037668>.
- [38] Eadie DT, Harrison H, Kempka R, Lewis R, Keylin A, Wilson N. Field assessment of friction and creepage with a new tribometer. 2018 Proc 11th Int Conf Contact Mech Wear Rail/Wheel Syst C 2018;vol. 17:208–17.
- [39] Polach O. Creep forces in simulations of traction vehicles running on adhesion limit. *Wear* 2005;258:992–1000. <https://doi.org/10.1016/j.wear.2004.03.046>.
- [40] Kvarda D, Galas R, Omasta M, Shi L, Ding H, Wang W, et al. Asperity-based model for prediction of traction in water-contaminated wheel-rail contact. *Tribol Int* 2021;157:106900. <https://doi.org/10.1016/j.triboint.2021.106900>.
- [41] Voce E. The relationship between stress and strain for homogeneous deformation. *J Inst Met* 1948;74:537–62.
- [42] Harrison H. Producing and measuring the 3rd body layer. *Jt. Rail Conf*, 2020. American Society of Mechanical Engineers; 2020. p. 1–7. <https://doi.org/10.1115/JRC2020-8095>.
- [43] Galas R, Omasta M, Shi L, Ding H, Wang W, Krupka I, et al. The low adhesion problem: the effect of environmental conditions on adhesion in rolling-sliding contact. *Tribol Int* 2020;151. <https://doi.org/10.1016/j.triboint.2020.106521>.
- [44] White BT, Lewis R, Olofsson U, Lyu Y. The contribution of iron oxides to the wet-rail phenomenon. *Civ-Comp Proc* 2016;vol. 110. <https://doi.org/10.4203/ccp.110.154>.
- [45] Harrison H. The development of a low creep regime, hand-operated tribometer. *Wear* 2008;265:1526–31. <https://doi.org/10.1016/j.wear.2008.03.028>.
- [46] Bosso N, Gugliotta A, Magelli M, Oresta IF, Zampieri N. Study of wheel-rail adhesion during braking maneuvers. *Procedia Struct Integr* 2019;24:680–91. <https://doi.org/10.1016/j.prostr.2020.02.060>.
- [47] Shrestha S, Spiryagin M, Harisson H, Persson I, Meehan P, Wu Q, et al. Introduction of rail cleaning effect into locomotive traction study based on tribometer measurements. ICRT 2021 - Proc 2nd Int Conf Rail Transp 2022:41–51. <https://doi.org/10.1061/9780784483886.006>.
- [48] Folorunso MO, Lewis R, Lanigan JL. Effects of temperature and humidity on railhead friction levels. *Proc Inst Mech Eng Part F J Rail Rapid Transit* 2022. https://doi.org/10.1177/09544097221148236/ASSET/IMAGES/LARGE/10.1177_09544097221148236-FIG8.JPEG.